

Alma Mater Studiorum - Università di Bologna

DOTTORATO DI RICERCA

IN

SCIENZE CHIMICHE

Ciclo XXVI

Settore Concorsuale di afferenza: CHIM/04

Settore Scientifico Disciplinare: 03/C2

**FIBER-REINFORCED CERAMICS
FOR THERMOSTRUCTURAL APPLICATIONS,
PRODUCED BY POLYMER IMPREGNATION PYROLYSIS**

Presented by:

Dott. Claudio Mingazzini

Tutor

Prof. Daniele Caretti

Co-Tutor

Prof. Daniele Nanni

Ing. Sergio Sangiorgi

Final examination: 2014

INDEX

INTRODUCTION, AIM AND DEFINITIONS

CHAPTER 1. CERAMIC FIBERS AND FABRICS

1.1 Fiber Reinforced Composite structural materials	15
1.2 Toughening mechanism in ceramics and CFCCs	18
1.3 Carbon, glass, basalt and oxide ceramic fibers	22
1.4 Silicon non-oxide ceramic fibers	32
1.5 Types of fabrics	39
1.6 Typical ceramic matrixes for CFCCs	40
1.7 Processes to obtain non oxides CFCCs	42
1.8 Characterization techniques for the ceramics development	53

CHAPTER 2. PRECERAMIC POLYMERS

2.1 State of the Art	59
2.2 The Polymer Infiltration and Pyrolysis (PIP) process	62
2.3. The development of a PIP pilot plant	67
2.4. Development of the synthesis of a polymeric precursor for ZrC	71
2.4.1 Testing of a patented synthesis procedure	72
2.4.2 Pyrolysis experiments and characterization of the residue	72
2.4.3 Conclusion from the synthesis experiments	76

CHAPTER 3. PIP OF POLYCARBOSILANES

3.1 First assessment of performances of PIP pilot plant with PCS	
3.1.1 Materials and methods.	77
3.1.2 Thermogravimetric analysis	78
3.1.3 Microstructural and morphological characterisation	81
3.1.4 Mechanical characterisation	84
3.1.5 Preliminary conclusions	86
3.2 Further development of the PCS pyrolysis in the ENEA pilot plant	86
3.3 Views and prospects	89

CHAPTER 4. PIP OF POLY-SILOXANES

4.1 State of the Art	90
4.1.1 Basalt reinforced Silicon OxyCarbides	93
4.1.2 Curing of poly-siloxane resins	96
4.1.3 Blackglas TM - Nextel TM	97
4.2 Study of the pyrolysis of Poly Methyl Siloxane	99
4.2.1 Materials and Methods	99
4.2.2 Thermogravimetric and mineralogical investigations	100
4.2.3 Design of the PIP composites	102
4.3 Study of the PIP process of poly-methylsiloxane on SiC fibers	104
4.3.1 PIP process of poly-methylsiloxane on pressed SiC felts	104
4.3.2 PIP process on unidirectional SiC plies	111

4.4 Study of the PIP process of poly-methylsiloxane on basalt fibers	114
4.4.1 One PIP step with poly-methylsiloxane	115
4.4.2 Two PIP steps with poly-methylsiloxane, in N ₂ flow	118
4.4.3 Two PIP steps with poly-methylsiloxane, in vacuum	122
4.4.4 Two PIP steps with poly-siloxane, 2D fabric plies	129
4.4.5 Densification data for the various solutions	137
4.4.6 Further optimization of the process	139
4.4.7 Stability towards oxidation and completion of pyrolysis	151
4.4.8 Fracture toughness optimization	162
4.4.9 PIP with poly-methylsiloxane on oxide fibers	163

CHAPTER 5. CBC COMPOSITES

5.1 Introduction	164
5.2 New phosphate cements	167
5.3 Characterization of a commercially available phosphate cement	172
5.3.1 Mineralogical investigations on the setting reaction	173
5.3.2 Thermogravimetric investigations	181
5.3.3 Mechanical and thermomechanical compression tests	184
5.3.4 Mechanical bending tests	186
5.3.5 Evaluation of suitable maturation time	190
5.4 Development of fibre-reinforced phosphate material	191

CONCLUSIONS	199
--------------------	------------

LIST OF TABLES

Table 1.2.1 - Main properties of commercially available fibers	19
Table 1.2.2 - Typical properties of monolithic ceramics	20
Table 1.3.1 - Classification of carbon fibers	22
Table 1.3.2 - Chemical compositions and characteristics of glass fibers	24
Table 1.3.3 - Characteristics of e-glass, basalt and silica fibers	26
Table 1.3.4 - Nextel 312, 440 and 550 fibers characteristics	27
Table 1.3.5 - Nextel 610 and 720 fibers characteristics	28
Table 1.3.6 - Indicative costs of oxide fibers	29
Table 1.4.1 - Tyranno fibers main characteristics	34
Table 1.4.2 - Nicalon and Silramic fibers characteristics	37
Table 1.4.3 - Indicative costs of commercially available SiC fibers	38
Table 1.5.1 - Typical properties of weave styles.	40
Table 1.6.1 - Typical properties of ceramic matrixes for CFCCs	41
Table 1.7.1 - Common processes for C_f / SiC and SiC _f / SiC CFCCs	48
Table 2.2.1 - Properties of Starfire preceramic polymers	63
Table 4.1.1 - Literature data about some of Lukosil products	95
Table 4.4.1 - Mechanical parameters for PIP derived CFCC	122
Table 4.4.2 - Mechanical parameters after PIP in vacuum and N ₂	123
Table 4.4.3 - Mechanical parameters after PIP in vacuum at various T	124
Table 4.4.4 - Densification data on the various solution considered	136
Table 4.4.5 - MOR values for the various solution considered	138
Table 4.4.6 - Densification, E and MOR values after one PIP step	145
Table 5.1.1 - Typical PiroSiC properties	166
Table 5.1.2 - EDS chemical analysis on a basalt reinforced composite	168
Table 5.3.1 - DTG peaks and the corresponding mass losses	182
Table 5.3.2 - Summary table of Grancrete specimens tested at 25°C	185
Table 5.3.4 - Flexural strength and E, at 25°C, of as-set grancrete	187
Table 5.3.5 - Flexural strength and E, at 25°C, of dried grancrete	188
Table 5.3.6 - Flexural strength and E, at 25°C, of grancrete fired at 500°C	189
Table 5.4.1 - MOR results on basalt-reinforced grancrete at 25°C	193
Table 5.4.2 - MOR results on samples after drying and heat treatment	194
Table 5.4.3 - MOR and E values (at 25°C) on basalt-reinforced grancrete	195
Table 5.4.4 - MOR and E values (at 25°C) after vacuum drying	196
Table 5.4.5 - MOR and E values (at 25°C) after heating at 500°C	197
Table 6.1.1 - Conclusions and perspectives of CFCCs	204

LIST OF FIGURES

Figure 1.1.1 - Typical mechanical behavior of FRP	15
Figure 1.1.2 - Tensile strength and elongation to break of typical PMC fibers	16
Figure 1.1.3 - Ideal stress-strain curve for a PMC	17
Figure 1.2.1 - Crack deflection mechanism in CFCCs	18
Figure 1.2.2 - Fiber "pull-out" and "crack bridging" toughening mechanisms	21
Figure 1.3.1 - Forecasted carbon fiber demand	22
Figure 1.3.2 - Continuous glass fibers and glass yarns manufacturing process	23
Figure 1.3.3 - Tensile strength of Nextel fibers, as a function of temperature	30
Figure 1.3.4 - Fiber performances in oxidative environments	31
Figure 1.3.5 - Normalized strength vs temperature for some common fibers	31
Figure 1.4.1 - UBE and the Nicalon process for producing SiC fibers	33
Figure 1.4.2 - Tensile strength of Tyranno and Nicalon fibers, vs temperature	33
Figure 1.4.3 - Tyranno fibers main characteristics	35
Figure 1.4.4 - Possible structure for Yarn (or Tows)	36
Figure 1.5.1 - Plain, Twill and Satin weave	39
Figure 1.5.2 - Basket, Leno and Mock Leno weave	39
Figure 1.5.3 - Example of 3D-woven fiber preform	40
Figure 1.7.1 - Overview of ENEA Faenza CVI pilot plant	43
Figure 1.7.2 - Pull-out mechanism in the developed SiC _f / SiC composites	43
Figure 1.7.3 - UBE SA Tyranno HEX CFCCs after Hot-Pressing	44
Figure 1.7.4 - Typical PIP production process of SiC _f / SiC, according to UBE	45
Figure 1.7.5 - Typical PIP densification curve of a SiC _f / SiC	46
Figure 1.7.6 - CFCCs developed by CVI and PIP: differences	47
Figure 1.7.7 - Automotive braking rotors produced by PIP	49
Figure 1.7.8 - CVI/PIP processes developed by NASA for G.T. engines	50
Figure 1.7.9 - Specific strength comparison vs temperature	51
Figure 1.7.10 - EBC on a fiber reinforced CMC, for hypersonic vehicles	52
Figure 1.8.1 - SEM probed depth of secondary and backscattered e ⁻ and EDS signal	53
Figure 1.8.2 - SEM (Cambridge 438VP) - EDS (Link Isis 300)	54
Figure 1.8.3 - XRD goniometer for powder diffraction	55

Figure 1.8.4 - TG-DTA Netzsch 409S	56
Figure 1.8.5 - Helium pycnometer	56
Figure 1.8.6 – Four-point bending apparatus scheme.	57
Figure 1.8.7 - MTS testing machine equipped with a furnace for a high T flexural tests	58
Figure 1.8.8 - SiC four-point bending apparatus for a high T flexural tests	58
Figure 2.1.1 - Some interesting preceramic polymers	60
Figure 2.1.2 - An overview of the PDC possible applications	61
Figure 2.2.1 - Microstructure and mechanical properties of a Starfire CFCC	63
Figure 2.2.2 - Scheme of the PIP process	64
Figure 2.2.3 - RTM equipment, working on the principle of vacuum infiltration	65
Figure 2.2.4 -Wet lay-up composite production	66
Figure 2.3.1 - ENEA PIP pilot plant	68
Figure 2.3.2 - AISI 310S pyrolysis chamber	69
Figure 2.3.3 - Vacuum infiltration of fiber preforms	70
Figure 2.3.4 - Scheme representing PIP steps and subsequent microstructure	70
Figure 2.4.1 - Targets for a synthesis of organosilicon polymers	71
Figure 2.4.2 - TG-DTA under nitrogen of ZrC preceramic	73
Figure 2.4.3 - XRD of the inorganic residue after pyrolysis	74
Figure 2.4.4 - SEM micrograph and EDS spectra	75
Figure 2.4.5 - SEM micrograph taken into an area rich of Mg	75
Figure 3.1.1 - TG of the polymeric precursor	78
Figure 3.1.2 - TG of the residual ceramic obtained after 2h pyrolysis at 900°C	79
Figure 3.1.3 - XRD on P900, before and after the TG at 1200°C	80
Figure 3.1.4 - XRD on P1000, before and after the TG at 1200°C	80
Figure 3.1.5 - XRD of crushed CMCs after treatment at 1200°C under N ₂	81
Figure 3.1.6 - Weight change of the CMCs during the 11 PIP infiltrations	82
Figure 3.1.7 - Microstructure of the PIP CMC produced at 900°C	83
Figure 3.1.8 - Microstructure of the PIP CMC produced at 1000°C	83
Figure 3.1.9 - Standard samples used for four-points bending tests	84
Figure 3.1.10 - Four-points bending tests apparatus	85
Figure 3.1.11 - Graphite furnace for the final consolidation step	85
Figure 3.2.1 - Second series of impregnated SiC felts	87

Figure 3.2.2 - Densification curves on pressed and non-pressed SiC felts	87
Figure 3.2.3 - Microstructure obtained by 2 PIP steps at 900°C	88
Figure 3.2.4 - MOR experiments at RT on the pressed SiC felts, after 2 PIP	88
Figure 4.1.1 - Thermal gradient for cure and pyrolysis of poly-siloxanes	93
Figure 4.1.2 - Thermal and pressure gradient for curing of poly-methylsiloxanes	97
Figure 4.1.3 - SiOC Nextel 312 BN Tailcone	98
Figure 4.2.1 - Overview of HG-GBF basalt products and applications	99
Figure 4.2.2 - TG after curing or after simple drying	100
Figure 4.2.3 - XRD on poly-methylsiloxane after drying and after curing	101
Figure 4.2.4 - XRD on pyrolysed M130, before and after oxidation	101
Figure 4.3.1 - Steel apparatus used to press the SiC felts	105
Figure 4.3.2 - Steel mould for CFCC with predetermined height	105
Figure 4.3.3 - Folded carbon paper containers	105
Figure 4.3.4 - Stress-strain curves and MOR values (vs T) on the 6 pressed SiC felts	106
Figure 4.3.5 - Microstructure obtained by 2 PIP steps (3 felts) at 900°C	107
Figure 4.3.6 - Microstructure obtained by 2 PIP steps (6 felts) at 900°C	107
Figure 4.3.7 - Microstructure obtained by 4 PIP steps at 900°C, on unpressed felts	108
Figure 4.3.8 - MOR values (vs T) on unpressed SiC felt (4 PIP steps with SiCO)	109
Figure 4.3.9 - Macroscopic morphology of SCS-6 SiC unidirectional fabric	111
Figure 4.3.10 - SEM of the SiC _f / SiCO composite	112
Figure 4.3.11 - SEM of the SiC _f / SiCO composite	113
Figure 4.3.12 - Residue of a metallic fiber, originally present	114
Figure 4.4.1 - Preparation of the uniaxial basal fibers	115
Figure 4.4.2 - Basalt reinforced composite after one PIP step at 650°C	116
Figure 4.4.3 - Microstructure obtained by one PIP steps at 650°C	116
Figure 4.4.4 - MOR values at rt on the basalt reinforced composite, after one PIP step	117
Figure 4.4.5 - MOR values (vs T) on the basalt reinforced composite, after one PIP	117
Figure 4.4.6 - HG-GBF employed bidirectional fabric	119
Figure 4.4.7 - Morphology of bidirectional HG-GBF fabric	119
Figure 4.4.8 - Standard samples for the thermomechanical characterization	120
Figure 4.4.9 - Stress strain curves at 25°C (bidirectional basalt plies, 2PIPs)	121
Figure 4.4.10 - MOR and E values at 400°C (bidirectional plies, 2PIPs)	122
Figure 4.4.11 - Stress-strain curves at various t (bidirectional plies, 2PIPs)	123

Figure 4.4.12 - Stress-strain curves at 400°C (from PIP in vacuum and N ₂)	123
Figure 4.4.13 - SiCO-basalt composites produced at 700°C under vacuum	125
Figure 4.4.14 - SiCO-basalt composites produced at 700°C under nitrogen flow	126
Figure 4.4.15 - SiCO-basalt microstructure obtained under vacuum	127
Figure 4.4.16 - SiCO-basalt microstructure obtained under nitrogen flow	128
Figure 4.4.17 - 2D basalt fabric derived from preregs	129
Figure 4.4.18 - Morphology of the CFCC obtained using 2D basalt fabric plies	130
Figures 4.4.19 - 4.4.22: Microstructure of the CFCCs obtained using 2D basalt fabric	131
Figure 4.4.23 - Stress strain curves at various T (6 2D-basalt plies, 2 PIPs)	135
Figure 4.4.24 - Improved steel mould	139
Figure 4.4.25 - Stress strain curve at 400°C after one PIP at 700°C(N ₂)	140
Figure 4.4.26 - Stress strain curve at 400°C up to rupture	140
Figure 4.4.27 - 4.4.29 HG-GBF unidirectional basalt fabric	141
Figure 4.4.30 - 4.4.31 EDS and microstructure of HG-GBF unidirectional basalt fabric	143
Figure 4.4.32 - Stress strain curve on composites produced with 8 unidirectional plies	145
Figures 4.4.33 - 4.4.34: Microstructure obtained using unidirectional basalt fabric	146
Figure 4.4.35 - Microstructure obtained using unidirectional basalt fabric in vacuum	148
Figure 4.4.36 - Stress strain curve obtained using unidirectional basalt fabric	149
Figure 4.4.37 - Stress vs piston stroke obtained using unidirectional basalt fabric	149
Figure 4.4.38 - Microstructure obtained using unidirectional basalt fabric, mould 2	150
Figure 4.4.39 - Stress strain curve obtained using unidirectional basalt fabric, mould 2	151
Figure 4.4.40 - Stress vs piston stroke obtained using unidir basalt fabric, mould 2	151
Figure 4.4.41 - TG in argon on SiCO produced in vacuum	153
Figure 4.4.42 - TG on SiCO before and after boiling with water	154
Figure 4.4.43 - TG in air on SiCO (produced in vacuum, 700°C, 15h)	155
Figure 4.4.44 - TG in Ar on SiCO upon different xylene drying procedures	156
Figure 4.4.45 - TG in air on SiCO upon different xylene drying procedures	157
Figures 4.4.46 - 4.4.53: XRD on various SiCO produced in the PIP plant, before and after TGs	
Figure 4.4.54 - Optical microscopy observation on basalt _f /SiCO produced at 700°C	162
Figure 4.4.55 - CFCC obtained using oxide rock wool	163
Figure 5.1.1 - PyroSic Formula 1 racing car exhaust system	165
Figure 5.1.2 - PyroSic main characteristics and thermomechanical properties	166
Figure 5.1.3 - Microstructure of a basalt reinforced Pyromeral composite	167

Figure 5.2.1 - Working principle of the Self Compacting Impregnator	170
Figure 5.2.2 - Working principle of the SCI, from WO 2009/030710	171
Figure 5.3.1 - Grancrete after molding into various shapes	174
Figure 5.3.2 - XRD on Grancrete starting powder	175
Figure 5.3.3 - XRD after the setting	176
Figure 5.3.4 - XRD on Grancrete before and after the setting	177
Figure 5.3.5 - XRD on set Grancrete and white efflorescences	179
Figure 5.3.6 - TG-DTA on Grancrete precursor	180
Figure 5.3.7 - TG-DTA on set Grancrete (compared to precursor)	181
Figure 5.3.8 - TG-DTA on "white efflorescences"	181
Figure 5.3.9 - TG on set Grancrete in fluent air, up to 600°C and up to 1000°C	182
Figure 5.3.10 - XRD on Grancrete calcinated 10 hours at 600 and 1000°C	182
Figure 5.3.11 - Compressive test assembly	184
Figure 5.3.12 - Stress vs Apparent Strain: compressive tests at room temperature	185
Figure 5.3.13 - Stress strain curves, at 25°C, on as-set grancrete	187
Figure 5.3.14 - Stress strain curves, at 25°C, on vacuum dried grancrete	188
Figure 5.3.15 - Stress strain curves, at 25°C, on grancrete fired at 500°C	189
Figure 5.3.16 - Schematic representation of "impact excitation technique"	190
Figure 5.3.17 - Young modulus vs maturation time (days) at 25°C	191
Figure 5.4.1 - Example of basalt reinforced CBC composite produced	191
Figure 5.4.2 - Wet lay-up procedure for the CBCC composite	192
Figure 5.4.3 - Fiber reinforced CBC for MOR measurements	193
Figure 5.4.4a - Stress strain curves (at 25°C) on basalt-reinforced grancrete	195
Figure 5.4.4b - Basalt-reinforced grancrete samples after the bending tests (at 25°C)	195
Figure 5.4.5a - Stress strain curves (at 25°C) after vacuum drying	196
Figure 5.4.5b - Dried basalt-reinforced grancrete amples after the bending tests	196
Figure 5.4.6a - Stress strain curves (at 25°C) after heating at 500°C	197
Figure 5.4.6b - Heat treated basalt-reinforced grancrete samples after the bending tests	197
Figure 5.4.7 - Teflon mould used to produce thin CBC samples	198

INTRODUCTION, AIM AND DEFINITIONS

The use of fossil fuels is changing the composition of the atmosphere, introducing carbon dioxide and other greenhouse gases (like methane, nitrous oxide), with unpredictable negative consequences on climate change and global warming. In order to reduce the impact of human activities it is important to develop more sustainable technologies. One way of reducing emissions and natural resources consumption is developing more efficient and durable thermostructural materials. These new materials will permit the increase of the thermodynamic efficiency by increasing the working temperature of engines and industrial plants. New approaches and technologies will be possible both in the field of energy production (e.g. plants for nuclear fusion, steam reforming, biomass pyrolysis/gasification) and in the energy-demanding industrial productions (e.g. glass and ceramic industry). Along with that there will be benefits also for transports and constructions, especially in terms of increased security, fire and antiballistic protection and decreased weights.

This thesis is about the development of **Continuous Fiber Ceramic Composites** (CFCC), focusing on the less expensive and more appealing procedures for an industrial application, especially for the automotive (both for structural parts and as friction materials) and the construction fields. CFCCs are Fiber-Reinforced **Ceramic Matrix Composites** (CMC) specifically developed for thermostructural applications at high temperature, to exploit the advantages of ceramics (high thermodynamical stability, high melting temperature, corrosion and erosion resistance) without a fragile (brittle) mechanical behavior. Thanks to the addition of fibers, both strength and fracture toughness of the ceramics are increased, and (with a suitable interphase between the fibers and the matrix) pull-out mechanism provide pseudo-plastic non-brittle behavior, since (as the ceramic matrix cracks) the load is transferred to the reinforcing fibers, which are significantly stronger. Therefore CFCCs provide superior long-term mechanical properties, retained under high temperature, high pressure, prohibitive and chemically aggressive conditions (like steam and oxidizing environments). Currently major applications of CFCCs are in metallurgy (nozzles, crucibles etc) and small size land-based power-turbines, but

CFCCs are also used for the Army Aircraft Engines, hypersonic missiles, rockets and advanced reusable space launch vehicles.

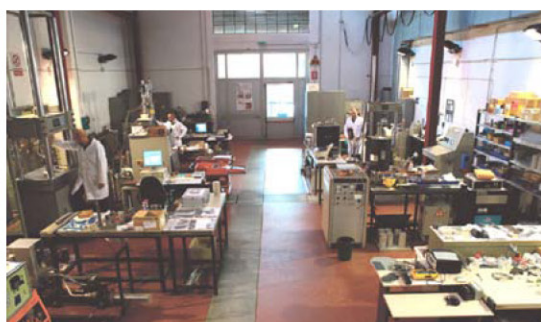
Regarding the process technologies for introducing a ceramic matrix into a fiber-preform, several approaches were considered and tested during this thesis work, starting from the most well known **Chemical Vapour Infiltration (CVI)**. Even if the production of a CFCC component by CVI is expensive and very time consuming (about one month to achieve high densification, that is residual porosity less than 10%) it is the production technique currently preferred in the aerospace industry because it is highly automated, reproducible and (producing a ceramic matrix from the thermal decomposition of a precursor gas) virtually independent from component geometry. Anyway for a mass production aiming at conventional transports and construction fields, infiltration with **Chemically Bonded Ceramics (CBC)** and **Polymer Infiltration (or Impregnation) Pyrolysis (PIP)** seem much more promising in term of lowering the production costs.

For thermostructural applications at temperature between 800°C and 1350°C, preceramic polymers together with ceramic fibers (both silicon carbide and oxide ceramic) seem the best solution. The higher temperature performance is achievable using high pure polycarbosilane precursors, that are however very expensive, and high quality SiC fibers. Several Polymer Impregnation Pyrolysis (PIP) steps are necessary in order to get suitable density and mechanical performance.

For fire resistant panels to be used for reinforcement/thermal insulation in the construction field, much less expensive polymers, like silicones, and much less expensive fibers, like basalt fibers, may be used. Basalt fibers don't melt up to 1200°C, offering mechanical reinforcement up to 600°C. In the present work it will be demonstrated that, in some case, one or two PIP steps are enough to give a suitable consolidation to the panel, with processing time of a few days. Basalt fibers could potentially be an optimum reinforcement also for CBC, even if the processes and the technologies for producing CFCCs, with few exceptions, are still far from being properly developed. In the construction field, Fiber Reinforced Polymers (FRP) have been being used for some time, mainly for restoring historical buildings (due to lower volumes, lower time and costs needed to achieve high mechanical reinforcement). They can also be useful for

reinforcement in seismic areas of new constructions. In more recent times also FRCM (Fiber Reinforced Cementitious Matrix), and TRM (Textile Reinforced Mortars) have been started to be introduced, thanks to higher fire resistance and increased adhesion to humid substrates. The fire resistance and the mechanical properties can be optimised in order not only to achieve better performance in the construction field, but also to find useful new application for increasing efficiency and security for collective transports (trains, ships, lorries), even if the maximum specific strength achievable is significantly lower than in the case of PIP derived composites.

This thesis work was mainly performed within the laboratories of ENEA Faenza [1], the institution to which the candidate belongs since 1999. ENEA has a Technical Unit (UTTMATF) dedicated to ceramic materials and composites, operating in Faenza since 1994. Currently in ENEA Faenza works about 30 employees, on about 3000 m² of laboratories, equipped with a remarkable instrumental capability, including the biggest CVI plant operating in Italy. The aim of this thesis work was to develop PIP processes and also a PIP pilot plant of the same size of the CVI pilot plant, to study combination of PIP and CVI for producing CFCCs with better performances and lower costs. These so called "hybrid techniques" are very interesting also because PIP represents a flexible way to introduce matrix modifiers, while the same result by CVI would require, every time, a complete rethinking and hardware modification of the instrumental apparatus.



Keywords: Polymer Impregnation Pyrolysis (PIP), Ceramic Matrix Composites (CMCs), Preceramic polymers, Continuous Fiber Ceramic Composites (CFCCs).

[1] http://www.enea.it/it/documenti/BrochureUTTMATF_2011EN.pdf

CHAPTER 1. CERAMIC FIBERS AND FABRICS

1.1 Fiber Reinforced Composite structural materials

Typically a fiber-reinforced composite structural material is one in which short or long fibers are combined to a bulk material (the ‘matrix’), added as a reinforcement, primarily to increase the original strength and stiffness of the matrix. Materials such as glass and carbon in the form of fibers have extremely high tensile strength which in ‘solid form’ would not be readily apparent. This is due to the fact that when stressed, random surface flaws will cause the bulk material to crack and fail well below its theoretical ‘breaking point’. On the other hand, when the material is produced in the fiber form, the same number of random flaws will occur but the failure will be restricted to a small number of fibers with the remainder exhibiting the theoretical strength typical of the material. Therefore a bundle of fibers will reflect more accurately the optimum performance of the material. As a consequence, it is possible to achieve exceptional mechanical performances by using fiber-reinforcement (figure 1.1.1).

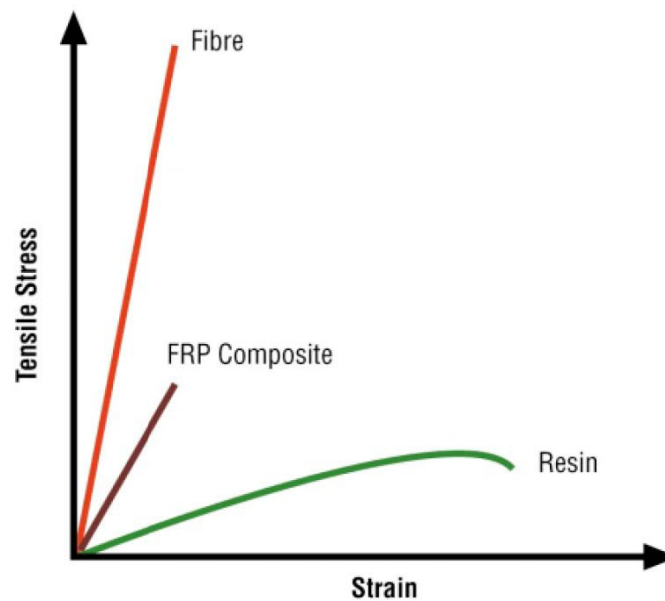


Figure 1.1.1 - Typical mechanical behavior of Fiber-Reinforced Plastics (FRP) [2]

[2] SP Systems - Composite Engineering Materials,
www.bolton.ac.uk/codate/spguidetocomposites.pdf.

The most common fiber-reinforced composites can be divided into three main groups:

- **Polymer Matrix Composites (PMC)**, also known as **FRP** - Fiber Reinforced Polymers), in which the matrix is a polymer and the fibers are made of other polymers (e.g aramid), carbon, glass or basalt;
- **Metal Matrix Composites (MMC)**, in which the matrix is a metal, and the fibers are usually non-metallic inorganic compounds (like silicon carbide) which can withstand the temperature needed for metal processing;
- **Ceramic Matrix Composites (CMC's)** - particularly suitable for high temperature environments, especially when in conjunction with aggressive environments.

Generally short fibers provide less mechanical reinforcement than long fibers and fabrics, however their introduction is quite easier, while long fiber reinforcements required specific instrumentation and processes. The effort however is quite rewarding in term of performance and, because of that, in the last century, fiber and composite production has become more and more important, especially for transports, where reducing weights and increasing mechanical performances are crucial. Carbon and aramid fibers are particularly appreciated, also because of their high specific strength, compared to glass and basalt.

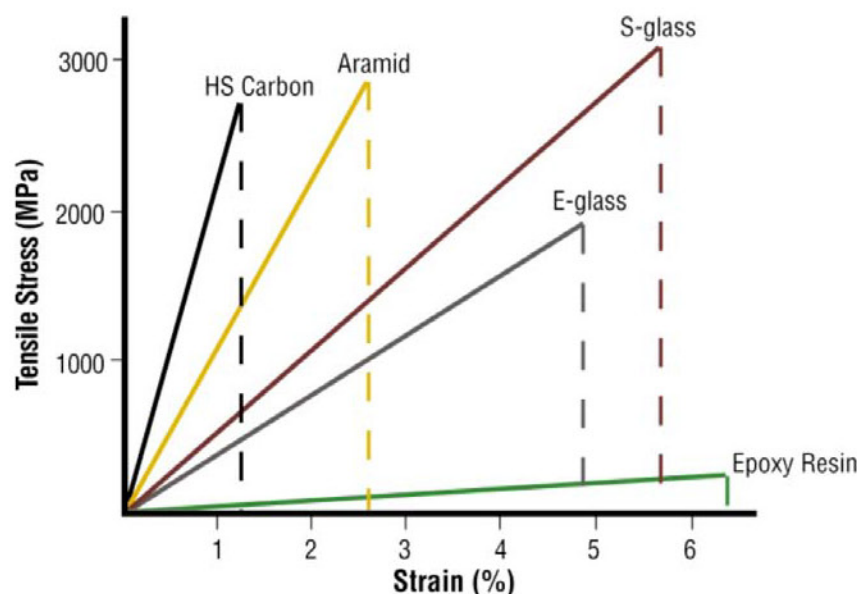


Figure 1.1.2 - Tensile strength and elongation to break of typical PMC fibers.

A typical mechanical behavior of a PMC is shown in figure 1.1.3. The stress-strain curve shows initially high stiffness (indicated by the high initial gradient) followed by a plastic deformation region and a high strain to failure. In this case the polymeric matrix has the ability to deform more than the fiber. On the contrary, in the case of a ceramic or a cementitious matrix (that is a brittle matrix), the matrix will crack before the fibers, but nevertheless the stress-strain curve will be similar, except for discontinuities due to progressive cracking. Beyond the elastic range (that is when first cracking occurs), there will be a pseudo-plastic region before failure, that is possible due to the fact that a suitable interphase between fiber and matrix will permit fiber pull-out, crack bridging, crack deflection and microcracking, the typical CFCC toughening mechanisms [3,4].

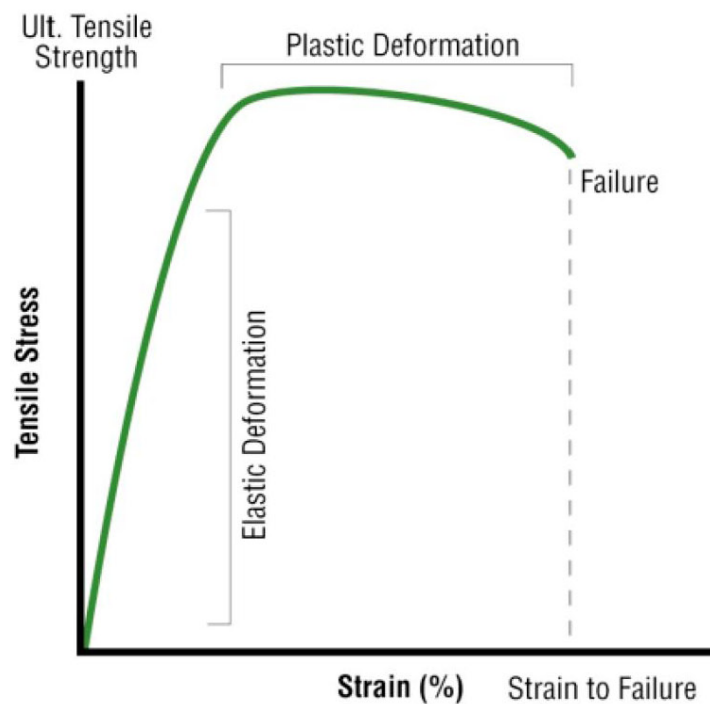


Figure 1.1.3 - Ideal stress-strain curve for a PMC.

[3] A. Bentur and S. Mindess, "Fibre Reinforced Cementitious Composites", Modern Concrete Technology Series, First published 1990, by E & FN Spon; Second edition published 2007, by Taylor & Francis, New York.

[4] V. Kostopoulos. Z. Pappas, Capitolo 4.05 "Toughening Mechanisms in Long Fiber Ceramic Matrix Composites", pages 95-114 Comprehensive Composite Materials, 2000, Elsevier, New York, ISBN 0-08 0429939.

1.2 Toughening mechanism in ceramics and CFCCs

The main limitation of mechanical applications of ceramics is low fracture toughness and brittleness. This limitation may be overcome by reinforcing with fibers. Some mechanisms which the presence of fibers make possible are the same that make possible enhancing strength using whiskers or particle reinforcement, but there are some more. The overall result is that, by adding whiskers/particulate or short fibers, the maximum fracture toughness that can be reached is $10 \text{ MPa}\cdot\text{m}^{0.5}$, whereas a monolithic ceramic could not exceed a value of $5 \text{ MPa}\cdot\text{m}^{0.5}$. In the case of CFCCs, thanks to "fiber pull-out" and exploiting the very high tensile strength of fibers, causing "crack bridging", fracture toughness can reach $20 \text{ MPa}\cdot\text{m}^{0.5}$. In brief, main toughening mechanisms for ceramic materials are:

- Crack Bowing

Brittle materials containing secondary phase dispersions (or dispersed voids) can possess higher strength than if they were homogeneous because the crack front is pinned by the dispersed particles and voids, increasing the crack length, and reducing the fracture energy.

- Crack Deflection

Crack deflection can also enhance the fracture toughness, as theoretical models demonstrate. The most effective morphology of added grains is rod-shaped, with a high aspect ratio. Obviously long fibers fully take advantage of this mechanism also, but a "weak interphase" is needed.

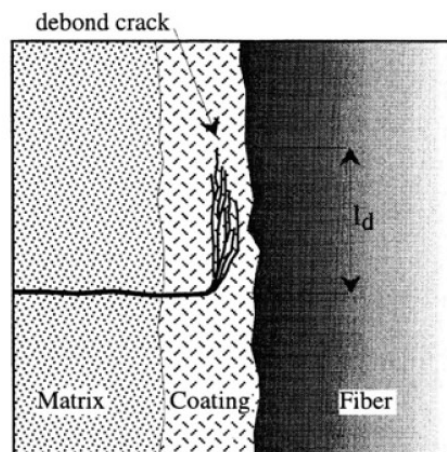


Figure 1.2.1 - Crack deflection mechanism in CFCCs.

- Microcracking

Toughening due to microcracking is expected to occur because the incorporation of the microcracking zone into the crack, as crack extends, distribute the fracture energy to a larger volume.

- Transformation Toughening

It is typical of certain ceramic phases, partially stabilized Zirconia (PSZ) in particular. The volume and morphology of the particles ahead of the crack tip change due to a phase transformation (e.g. from tetragonal to monoclinic zirconia), and this modifies the stress distribution. Generally it is not a mechanism exploited in CFCCs, which are generally based on non oxide ceramics.

The main long ceramic fibers which have become recently available, based on oxide and non oxide compositions, together with the producers and the main characteristics are summarized in the table 1.2.1 and will be discussed in detail in the next two paragraphs. It should be noted that the tensile strength of the fibers is one order of magnitude higher than that of the corresponding ceramics (table 1.2.2), as a consequence of the already mentioned "volume effect" on the crack propagation in brittle materials.

Material	Ceramic fibers properties	trade name	Tensile strength (GPa)	Tensile modulus (GPa)	Elongation to break (%)	Diameter (μm)	Density (g/cm^3)
Carbon	PAN-based	—	3–7	200–700	0.5–2	4–7	1.8
	Pitch-based	—	3–4	600–900	0.50	7–10	2.2
SiC	56.6Si–31.7C–11.7O	Nicalon	3.0	220	1.40	14	2.55
	62.4Si–37.1C–0.5O	Hi-Nicalon	2.8	270	1.00	14	2.74
	68.9Si–30.9C–0.2O	Hi-Nicalon S	2.6	420	0.60	12	3.1
	51.0Si–27.9C–17.7O–3.1Ti	Tyranno	3.3	195	—	8.5–15	—
	66.6Si–28.5C–0.8O–2.1Ti–2.3B–0.4N	Sylramic	3.4	386	—	10	3.1
Alumina	99.5% $\alpha\text{-Al}_2\text{O}_3$	Almax	1.8	330	—	10	3.6
	>99% Al_2O_3	Nextel 610	2.93	373	—	10–12	3.96
Oxides	85% Al_2O_3 –15% SiO_2	Nextel 720	2.1	260	—	10–12	3.4

Table 1.2.1 - Main properties of commercially available ceramic fibers [5].

[5] "Handbook of Advanced Ceramics", volume 2, chapter 15, "Ceramic-Matrix Composites" by Akira Okada. Elsevier, New York, 2003, ISBN 0-12-654640-1.

In table 1.2.2 also coefficient of thermal expansion are reported, since the difference between the CTE of the matrix and the fibers needs also to be considered, when developing composites for thermostructural application, otherwise tension and stress would develop on heating, before applying any external loading. Moreover CMC production involves generally high temperature itself.

Ceramics properties:	Al ₂ O ₃	SiC	Si ₃ N ₄	Y-ZrO ₂	SiO ₂ -MgO
Density, g/cm ³	4.0	3.1	3.2	6,1	2.2-2.8
Fracture toughness, MPa m ^{0.5}	4	4		8-10	-
Flexural strength, MPa	500	350	750	1000	110-180
Young's modulus, GPa	380	350	305	210	70-120
Vicker's Hardness, GPa	18	25	16	13	-
Max operating temp., °C	1500	1800	1600	1000	1000
Coeff. Of Therm. Exp., 10 ⁻⁶ K ⁻¹	8.5	4.3	3.2	8	

Table 1.2.2 - Typical properties of monolithic ceramics [6].

Even if the tensile strength of ceramic fibers is really high, the toughening mechanisms in CFCCs like the above mentioned crack deflection, but also the other two most typical CFCCs toughening mechanism, "fiber pull-out" and "crack bridging", shown in figure 1.2.2, are not fully effective without a "weak interphase" on the fibers, meaning a thin coating able to delaminate. Toughening results essentially from sliding friction along the debonds, a completely different situation from polymeric composites, where a strong bonding between the fibers and the matrix generally represents the target [7,8]. The main limitation of ceramic composites is having a low ultimate tensile elongation, limited the ceramic matrix cracking and failure.

[6] www.ceramtec.com/e-mail/downloads/tag/ceramic-manual/

[7] "Engineered interfaces in fiber reinforced composites", Jang-Kyo Kim, Elsevier Science Ltd, Oxford UK, 1998.

[8] "Mechanics and analysis of composite materials", Valery V. Vasiliev, Evgeny V. Morozov, Elsevier Science Ltd, Oxford, UK, 2001.

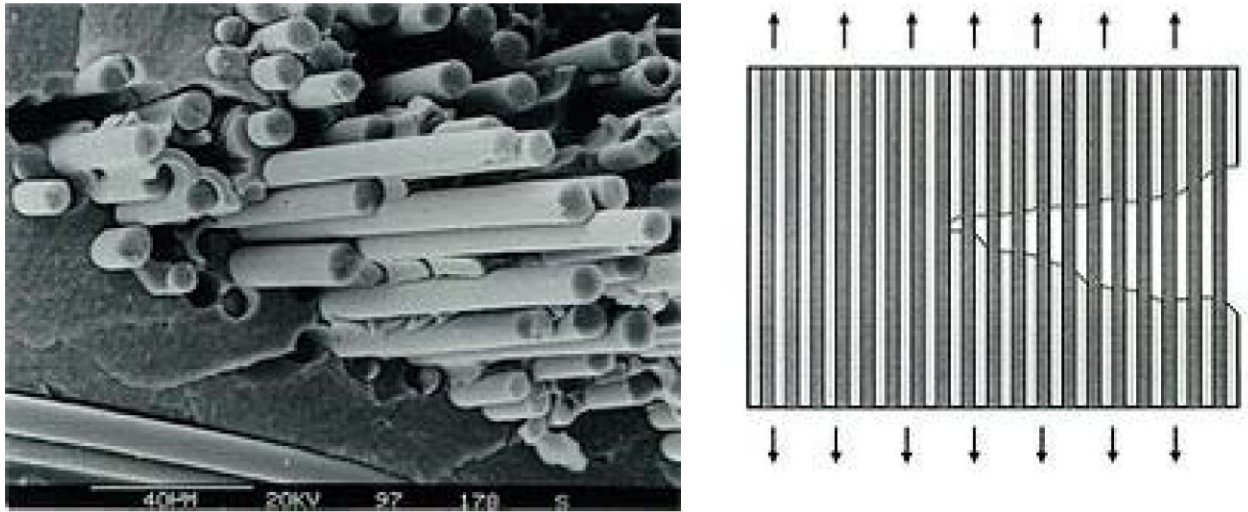


Figure 1.2.2 - Fiber "pull-out" (left) and "crack bridging" (right) toughening mechanisms.

In CMCs, the cracks develop first in the matrix than in the fibers, because of matrix lower strength. Consequently fiber acts as bridges which oppose to crack propagation (figure 1.2.2-right), providing higher toughness (resistance to crack propagation) and strength, compared to monolithic ceramics. In order to act in such way, the characteristics the interphase must possess are:

- chemical inertia especially towards the matrix;
- multilayered structure.

Another characteristic which is generally required to the interphase is the ability to keep these two conditions over long times, in the expected operating conditions. Typical examples of interphases used for SiC-fiber reinforced SiC ($\text{SiC}_f / \text{SiC}$) are pyrolytic Carbon (Py-C) and hexagonal boron nitride (H-BN). The weakness of Py-C interphases is generally the poor oxidation resistance, especially in certain temperature ranges, 800-1000°C, where SiC autopassivation is less effective.

1.3 Carbon, glass, basalt and oxide ceramic fibers

Many information about fibers are freely available in internet, given directly by the vendors and by National Committees [9]. Currently there is a huge market for **carbon fibers** and prepreg fabrics for PMC. Carbon fibers are produced generally from polymeric precursors, PAN in particular. Prices are about 30€/kg, typical mechanical properties and classification are reported in table 1.3.1.

Classification	Tensile modulus (GPa)	Tensile strength (MPa)	Elongation at break (%)
UHM (ultra high modulus)	>600	–	–
HM (high modulus)	>300	–	<1
IM (intermediate modulus)	275–350	–	>1
LM (low modulus)	<100	low	–
HT (high tensile)	200–300	>3000	1.5–2

Table 1.3.1 Classification of carbon fibers.

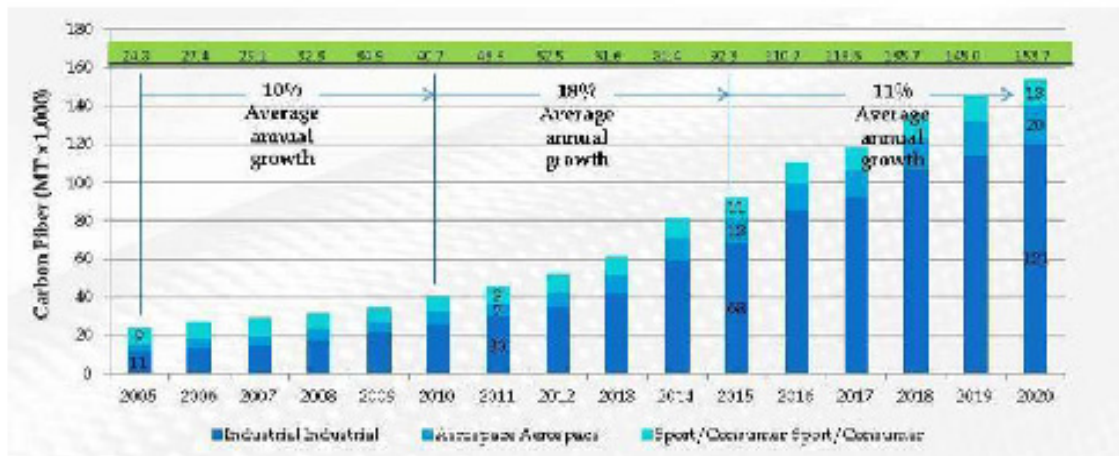


Figure 1.3.1 - Forecasted carbon fiber demand [10].

[9] Committee on Advanced Fibers for High-Temperature Ceramic Composites, "Ceramic Fibers and coatings" Publication NMA-B-494, National Academic Press 1998.

https://download.nap.edu/login.php?record_id=6042&page=/download.php?record_id=6042

[10] <http://compositesforecasts.com>

Today there is also a huge offer and consumption of **glass fibers**, of different types and characteristics (table 1.3.2) produced in continuous industrial plants, like that shown in figure 1.3.2. The most common types are type S (with high stiffness and strength, but expensive) type E (less expensive and widely used) and type C (with higher corrosion resistance).

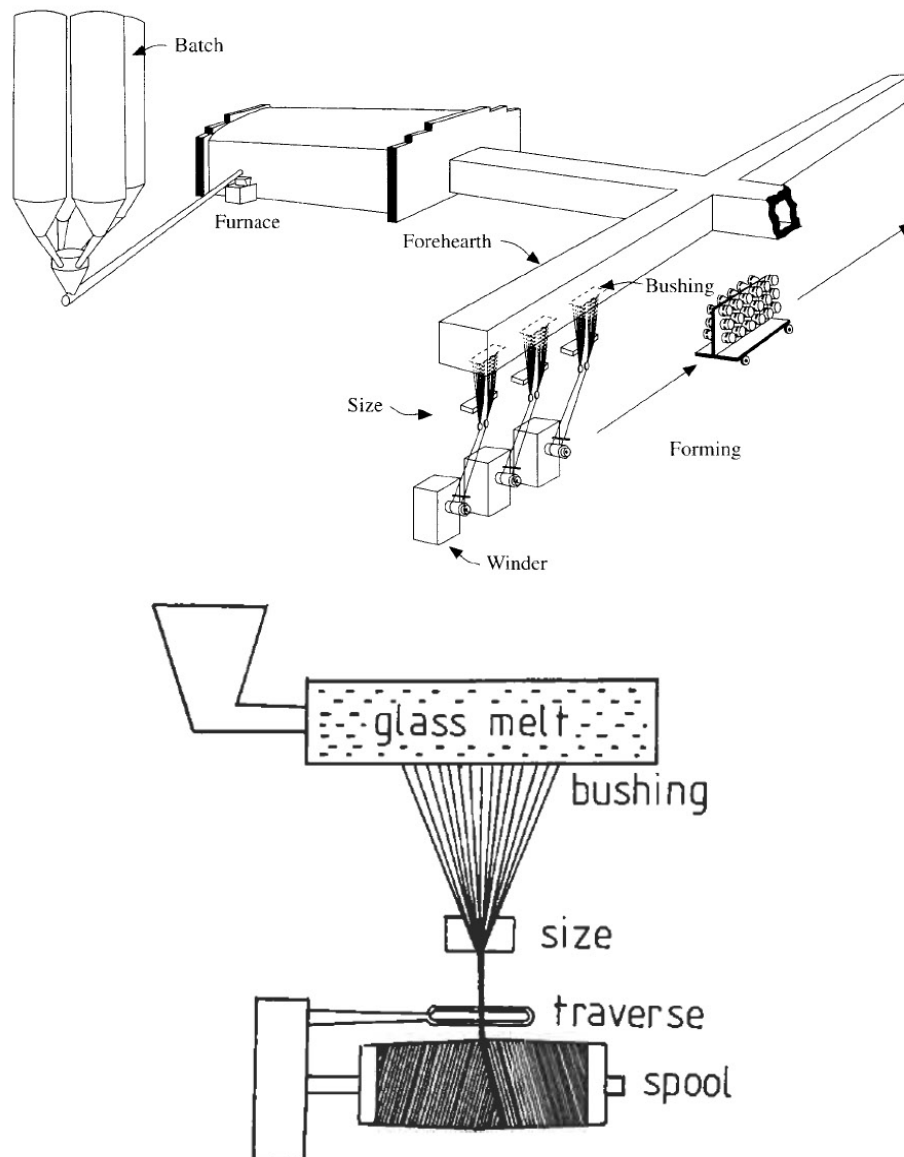


Figure 1.3.2 - Continuous glass fibers (up) and glass yarns (down) manufacturing process.

	A GLASS	C GLASS	D GLASS	E GLASS	ECRGlas®	AR GLASS	R GLASS	S-2 GLASS®
Oxide	%	%	%	%	%	%	%	%
SiO ₂	63-72	64-68	72-75	52-56	54-62	55-75	55-60	64-66
Al ₂ O ₃	0-6	3-5	0-1	12-16	9-15	0-5	23-28	24-25
B ₂ O ₃	0-6	4-6	21-24	5-10		0-8	0-0.35	
CaO	6-10	11-15	0-1	16-25	17-25	1-10	8-15	0-0.2
MgO	0-4	2-4		0-5	0-4		4-7	9.5-10
ZnO					2-5			
BaO		0-1						
Li ₂ O						0-1.5		
Na ₂ O + K ₂ O	14-16	7-10	0-4	0-2	0-2	11-21	0-1	0-0.2
TiO ₂	0-0.6			0-1.5	0-4	0-12		
ZrO ₂						1-18		
Fe ₂ O ₃	0-0.5	0-0.8	0-0.3	0-0.8	0-0.8	0-5	0-0.5	0-0.1
F ₂	0-0.4			0-1		0-5	0-0.3	

PHYSICAL PROPERTIES								
	A GLASS	C GLASS	D GLASS	E GLASS	ECRGlas®	AR GLASS	R GLASS	S-2 GLASS®
Density, gm/cc	2.44	2.52	2.11-2.14	2.58	2.72	2.70	2.54	2.46
Refractive Index	1.538	1.533	1.465	1.558	1.579	1.562	1.546	1.521
Softening Point, °C (°F)	705 (1300)	750 (1382)	771 (1420)	846 (1555)	882 (1619)	773 (1424)	952 (1745)	1056 (1932)
Annealing Point, °C (°F)		588 (1090)	521 (970)	657 (1215)				816 (1500)
Strain Point, °C (°F)		522 (1025)	477 (890)	615 (1140)			736 (1357)	766 (1410)
Tensile Strength, MPa								
-196°C		5380		5310	5310			8275
23°C	3310	3310	2415	3445	3445	3241	4135	4890
371°C				2620	2165		2930	4445
538°C				1725	1725		2140	2415
Young's Modulus, GPa								
23°C	68.9	68.9	51.7	72.3	80.3	73.1	85.5	86.9
538°C				81.3	81.3			88.9
Elongation %	4.8	4.8	4.6	4.8	4.8	4.4	4.8	5.7

Table 1.3.2 - Chemical compositions and technical characteristics of glass fibers [11].

[11] www.agy.com/technical_info/graphics_PDFs/HighStrengthTechPaperEng.pdf

In the recent years also **basalt fibers** have become being available at low prices, thanks to the development of the producing technologies [12]. The price of basalt fabrics is generally between 5 and 20 €/kg, which is quite reasonable compared to ceramic fibers, thanks to the fact they can be directly spun from abundant natural sources. They have been tested and proved to be non-carcinogenic and non-toxic. The major international producers are in Russia and China, but the raw materials are abundant almost everywhere, including Italy, where a production pilot plant was financed and tested in Diatech srl, within Italian National Research Programmes. The mechanical and thermomechanical properties are superior to glass, in particular basalt show higher tensile strength and a higher chemical and temperature resistance.

Going on towards more expensive fibers, **quartz fibers** can be considered, even if are still is far too expensive for most industrial applications. ASTROQUARTZ is the commercial name of pure silica fibers (99.95%), produced by JPS Industries Inc. Company, with very high tensile strength (6 GPa) and a maximum working temperature of 1070°C. A peculiar characteristic of these fibers is having a Thermal Expansion Coefficient (CTE) near to zero [13], a quite peculiar property even if for composites it is more important the CTE difference of fibers and the matrix, than the value of CTE itself. Prepreg silica fabrics are also provided, mainly for space and other advanced applications where the price is not a limiting factor. Glass, basalt and silica fibers are compared in table 1.3.3.

One of the major producers and developers of polycrystalline **ceramic oxide fibers** is "3M Ceramic Textiles and Composites", which produces the **Nextel fibers**, which are alumina fibers, with the main characteristics reported in tables 1.3.3 and 1.3.4. Certainly the performances are interesting, but the costs are two order of magnitude higher than basalt, due to the complexity of the industrial production, still too high for transports or the construction field. An overview of prices and vendors, updated at 2008, was found in literature [14] and is reported in table 1.3.6.

[12] S. N. Gushchin, M. D. Kazyaev, B. N. Arseev, D. M. Kazyaev "A plant for high-speed melting of basalt rocks", *Refractories and Industrial Ceramics*, 50, 2 (2009) 112.

[13] www.jpsglass.com/jps_databook.pdf

[14] "Ceramic Matrix Composites", Edited by Walter Krenkel, 2008 WILEY-VCH Verlag GmbH & Co., ISBN: 978-3-527-31361-7, page 11.

Properties	SI Units	Basalt Filaments	Fiberglass	Silica Filament
Thermal				
Maximum application temperature	(°C)	982	650	1100
Sustained operating temperature	(°C)	820	480	1000
Minimum operating temperature	(°C)	-260	-60	-170
Thermal conductivity	(W/m K)	0.031-0.038	0.034-0.040	0.035-0.040
Melting temperature	(°C)	1450	1120	1550
Thermal expansion coefficient	(ppm/°C)	8.0	5.4	0.05
Physical/Mechanical				
Density	(g/cm ³)	2.75	2.60	2.15
Filament diameter	μm	9-23	9-13	9-15
Tensile strength	(M Pa)	4840	3450	4750
Compression	(psi)	550,000	440,000	510,000
Elastic modulus	(G Pa)	89	77	66
Linear expansion coefficient	(x10 /K)	5.5	5	0.5
Elongation at break	(%)	3.15	4.7	1.2
Absorbtion of humidity (65%RAH)	(%)	<0.1	<0.1	<0.1
Stability at tension (20 C°)	(%)	100	100	100

Table 1.3.3 - Comparative technical characteristics of fibers made from e-glass, basalt and silica [15].

[15] <http://www.smarter-building-systems.com/smarter-building-basalt-faqs.html>

3M™ Nextel™ Ceramic Fiber 312, 440, and 550

Property	Units	Nextel™ 312	Nextel™ 440	Nextel™ 550
Sizing Color	color	white	coral	blue
Chemical Composition	wt. %	62.5 Al ₂ O ₃ 24.5 SiO ₂ 13 B ₂ O ₃	70 Al ₂ O ₃ 28 SiO ₂ 2 B ₂ O ₃	73 Al ₂ O ₃ 27 SiO ₂
Melting Point	°F (°C)	3272 (1800)	3272 (1800)	3272 (1800)
Filament Diameter	µm	10 – 12	10 - 12	10 – 12
Denier / Nominal Filament Count	g/9000 m	600 / 400 900 / 400 1800 / 750	700 / 400 1000 / 400 2000 / 750	1000 / 400 2000 / 750
Tex / Nominal Filament Count	g/1000 m	67 / 400 100 / 400 200 / 750	78 / 400 111 / 400 222 / 750	111 / 400 222 / 750
Crystal Size	nm	<500	<500	<500
Crystal Phase		Mullite + amorphous (or 100% amorphous)	γ-Al ₂ O ₃ + Mullite + amorphous SiO ₂	γ-Al ₂ O ₃ + amorphous SiO ₂
Density	g/cc	2.70	3.05	3.03
Refractive Index		1.568	1.614	1.602
Surface Area	m ² /g	<0.2	<0.2	<0.2
Filament Tensile Strength (25.4 mm gauge)	MPa ksi	1700 250	2000 290	2000 300
Filament Tensile Modulus	GPa msi	150 22	190 27	193 28
Thermal Expansion (100-1100°C)	ppm/°C	3 (25-500°C)	5.3	5.3
Dielectric Constant	(@ 9.375 GHz)	5.2	5.7	~5.8
Loss Tangent	(@ 9.375 GHz)	0.018	0.015	NA
Specific Heat @500°C (932°F)	cal/g/°C or BTU/lb/°F	0.25	0.27	NA

Table 1.3.4 - Nextel fibers main characteristics: 312, 440 and 550 types [16].

[16] http://www.3m.com/market/industrial/ceramics/pdfs/Nextel_Tech_Notebook_11.04.pdf

3M™ Nextel™ Ceramic Fiber 610 and 720

Property	Units	Nextel™ 610	Nextel™ 720
Sizing Color	color	off-white	green
Chemical Composition	wt. %	>99 Al ₂ O ₃	85 Al ₂ O ₃ 15 SiO ₂
Melting Point	°F (°C)	3632 (2000)	3272 (1800)
Filament Diameter	μm	10 - 12	10 - 12
Denier / Nominal Filament Count	g/9000 m	1500/400 3000/750 10000/2550	1500/400 3000/750
Tex / Nominal Filament Count	g/1000 m	167/400 333/750 1111/2550	167/400 333/750
Crystal Size	nm	<500	<500
Crystal Phase		α-Al ₂ O ₃	α-Al ₂ O ₃ + Mullite
Density	g/cc	3.9	3.40
Refractive Index		1.74	1.67
Surface Area	m ² /g	<0.2	<0.2
Filament Tensile Strength (25.4 mm gauge)	MPa ksi	3100 450	2100 300
Filament Tensile Modulus	GPa msi	380 55	260 36
Thermal Expansion (100-1100°C)	ppm/°C	8.0	6.0
Dielectric Constant	(@ 9.375 GHz)	~9.0	~5.8
Loss Tangent	(@ 9.375 GHz)	NA	NA
Specific Heat @500°C (932°F)	cal/g/°C or BTU/lb/°F	TBD	TBD

Table 1.3.5 - Nextel fibers main characteristics: 610 and 720 types.

Producer Fiber	Composition (Wt.-%)	Diameter (μm)	Density (g/cm^3)	Tensile strength/ modulus (MPa/GPa)	Production technique/ structure	Approx. price
3M <i>Nexiel 720</i>	Al_2O_3 : 85 SiO_2 : 15	10–12	3.4	2100/260	Sol-Gel/ 59 vol.% $\alpha\text{-Al}_2\text{O}_3$ + 41 vol.% Mullite	€790/kg (1500 den) €600/kg (3000 den)
3M <i>Nexiel 610</i>	Al_2O_3 : >99	10–12	3.9	3100/380	Sol-Gel/ $\alpha\text{-Al}_2\text{O}_3$	€790/kg (1500 den) €600/kg (3000 den) €440/kg (10 000 den)
3M <i>Nexiel 550</i>	Al_2O_3 : 73 SiO_2 : 27	10–12	3.03	2000/193	Sol-Gel/ $\gamma\text{-Al}_2\text{O}_3$ + SiO_2 amorph.	€590/kg (2000 den)
3M <i>Nexiel 440</i>	Al_2O_3 : 70 SiO_2 : 28 B_2O_3 : 2	10–12	3.05	2000/190	Sol-Gel/ $\gamma\text{-Al}_2\text{O}_3$ + Mullite + SiO_2 amorph.	€500/kg (2000 den)
3M <i>Nexiel 312</i>	Al_2O_3 : 62.5 SiO_2 : 24.5 B_2O_3 : 13	10–12	2.7	1700/150	Sol-Gel/Mullite + amorph. or 100% amorph	€260/kg (1800 den)
Sumitomo <i>Altex</i>	Al_2O_3 : 85 SiO_2 : 15	10/15	3.3	1800/210	Polyaluminoxane/ $\gamma\text{-Al}_2\text{O}_3$	€640–720/kg
Nitivy <i>Nitivy</i> <i>ALF</i>	Al_2O_3 : 72 SiO_2 : 28	7	2.9	2000/170	Sol-Gel/ $\gamma\text{-Al}_2\text{O}_3$	€390/kg (twisted yarn, twists: 10–15)
Mitsui <i>Almax-B</i>	Al_2O_3 : 60–80 SiO_2 : 40–20	7–10	2.9	Not available	Unknown/ $\delta\text{-Al}_2\text{O}_3$	Price not available

Table 1.3.6 - Overview of indicative costs of various oxide fibers.

Nextel fibers are being effectively used for thermostructural parts in oxidative and chemically aggressive environments, generally up to 1200°C [17]. CMC can be produced by infiltrating preforms with ceramic slurries. One of the problems to be solved is producing a suitable interphase between the ceramic oxide matrix and the ceramic oxide fibers, in order to avoid a brittle behavior.

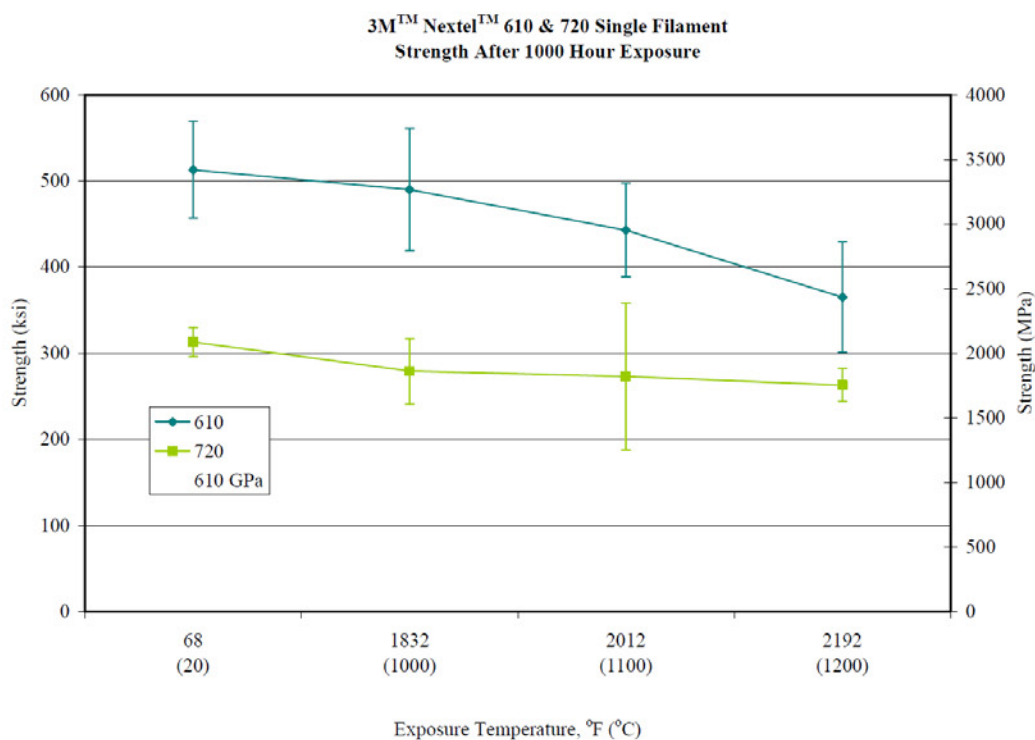


Figure 1.3.3 - Tensile strength of Nextel fibers, as a function of temperature.

Other producers of **alumina fibers** are:

- Sumitomo (producing “Altex”, Al_2O_3 99.5%, see table 1.3.6) [18]
- Saffil (www.saffil.com)
- Du Pont, where types “FP” and “PRD 166” were developed.

They can be high purity oxide fibers, or polycrystalline oxide fibers in which the incorporation of secondary phases yields benefits in term of high-temperature creep and strength. Nevertheless considering both strength and creep, in many cases the only fiber material with suitable thermomechanical properties for continuous operation at temperature above 1200°C in oxidative environments

[17] www.aerospacelab-journal.org/al3/Potential-and-Perspectives-for-Oxide-Oxide-Composites

[18] <http://sumitomocorp.en.chemnet.com/suppliers/product/173179/Alumina-Fiber-Altex.html>

results to be silicon carbide since polycrystalline oxide fibers are chemically stable to the oxidative environments, but, in these conditions, undergo creep up to failure. On the other hand, thank to the formation of a protective SiO_2 layer, silicon carbide fibers can tolerate oxidative environments, withstanding the higher specific load without failure. This maybe be clearly demonstrated also with a very simple (yet effective) experiment, involving a Bunsen, a weight and a fiber yarn, figure 1.3.4 [19]. The result of this experiment is a consequence of the different decadence law of the fiber strength with temperature, which is higher for alumina than for SiC (figure 1.3.5).

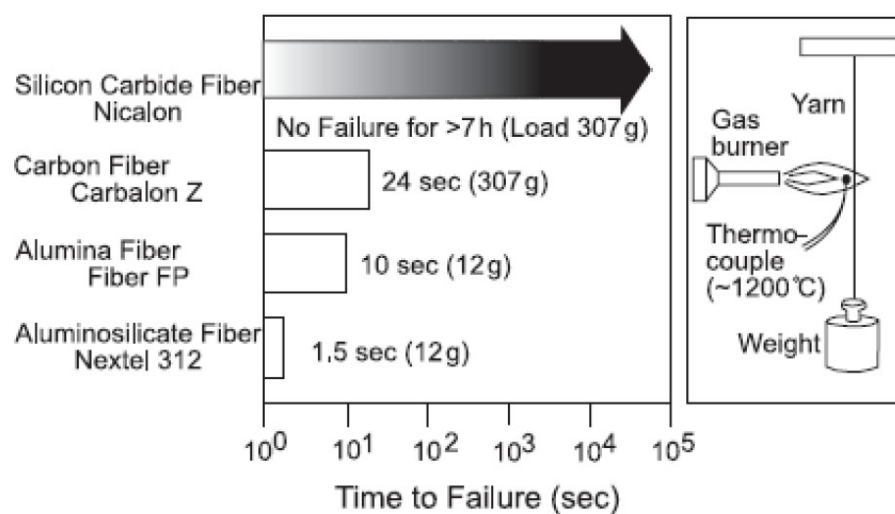


Figure 1.3.4 - Simple experiment to demonstrate the higher performances that SiC fibers may offer also in oxidative environments.

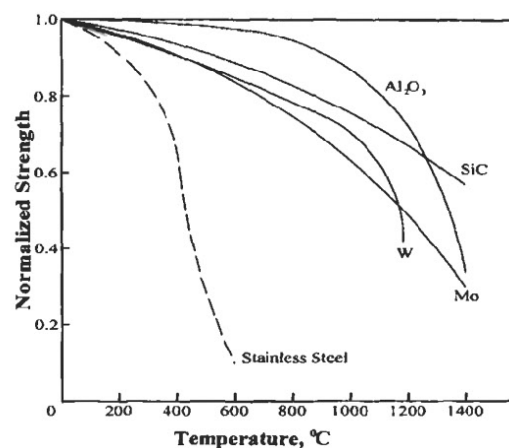


Figure 1.3.5 - Normalized strength vs temperature for some common fibers.

[19] H. Ichikawa, T. Ishikawa, Volume 1, Chapter 1.04 "Silicon Carbide Fibers (Organometallic Pyrolysis)", pages 107-145, *Comprehensive Composite Materials*, 2000, Elsevier, New York.

1.4 Silicon non-oxide ceramic fibers

Since the 1970s it has been demonstrated the possibility of converting polyorganosilicon, and in particular polycarbosilanes, into silicon non-oxide ceramics, by pyrolysis in controlled atmosphere. Based on this approach, the typical process for producing silicon non-oxide ceramic fibers can be summarized into three main steps:

- Synthesis and forming into fibers of a suitable organo-silicon preceramic;
- cross-linking of the polymer fiber;
- pyrolysis of the cross-linked polymer, and conversion into a ceramic fiber.

The crosslinking step is of crucial importance in determining the ceramic structure, properties and composition and can be thermally, physically or chemically activated. During this step, covalent bonds are formed among the low molecular weight chains, increasing **ceramic yield** (ceramic mass residue on pyrolysis) and lowering defects formation, because early gas formation is avoided.

Currently there are three main industrial producers of SiC fibers, two of which are in Japan (UBE Industries LTD and Nippon Carbon) and one in the USA (Coi Ceramics). An interesting overview about prices and producers in 2008 was found in literature [20]. The commercial name of UBE Industries product is "Tyranno fibers", available into several types, whose characteristics and compositions are resumed in table 1.4.1 and figure 1.4.3. Tyranno fibers are obtained from modified polycarbosilanes, modified with titanium, zirconium or aluminium alkoxides. The resulting fibers provides very good mechanical performances, even at high temperature and in oxidative environments. The lower oxygen content fibers, recently developed, are more stable at high temperature, table 1.4.1. Nippon Carbon produce the Nicalon fibers, starting from polycarbosilanes and exploiting electron beam irradiation for curing (instead of using a thermal oxidation, as in the UBE process, see figure 1.4.1). The fibers are constituted of SiC microparticles, together with SiO₂ and C (table 1.4.2). A comparison of thermomechanical performance of Nicalon and Tyranno (UBE) fibers is shown in figure 1.4.2, while indicative prices of various types are reported in table 1.4.3.

[20] "Ceramic Matrix Composites", Edited by Walter Krenkel, 2008 WILEY-VCH Verlag GmbH & Co., ISBN: 978-3-527-31361-7, page 13.

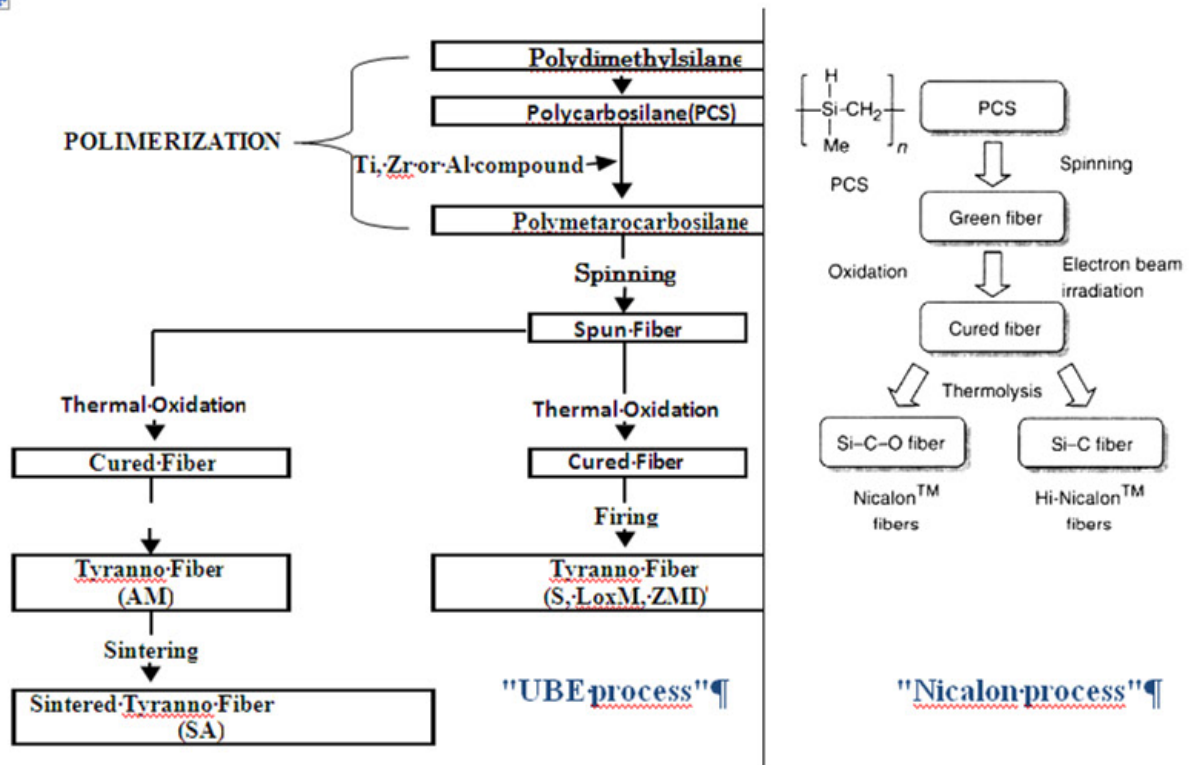


Figure 1.4.1 - UBE and Nicalon processes for producing SiC fibers.

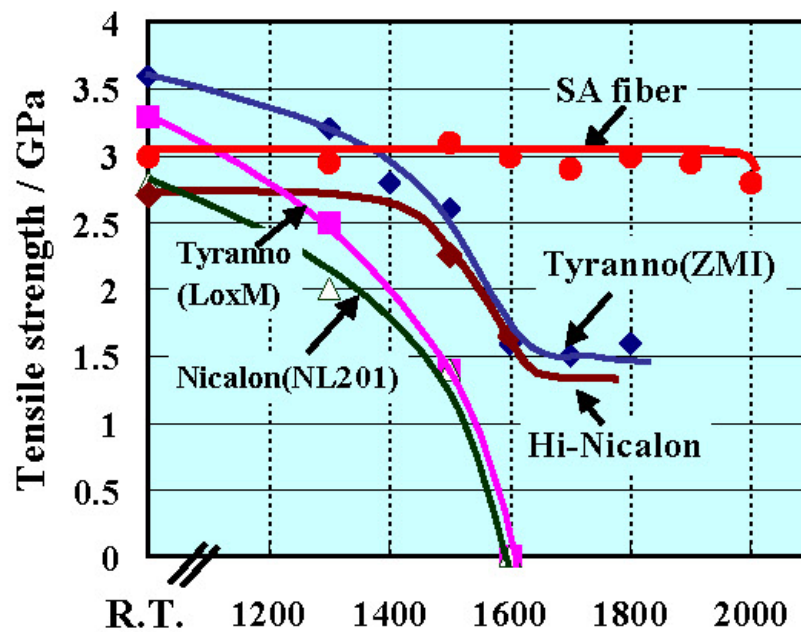


Figure 1.4.2 - Comparison of tensile strength of Tyranno and Nicalon fibers, as a function of temperature.

TYRANNO FIBERS		S	LoxM	ZMI	SA3
Fiber Diameter	μm	11-8.5	11	11	10-7.5
Number of filaments	fil./yarn	800-1600	800	800	800-600
Tex	g/1000 m	200-220	200	200	180-190
Tensile strength	GPa	3.2	3.3	3.4	2.8
Tensile Modulus	GPa	170	180	190	380
Elongation at break	%	1.9	1.8	1.7	0.7
Density	g/cm³	2.35	2.48	2.48	3.10
Thermal conductivity	W/mK	1.0	1.4	2.5	6.5
Coefficient of thermal expansion	10⁻⁶/K	3.1 (25-500°C)	-	4.0 (25- 1000°C)	4.5 (25- 1000°C)
Chemical composition	Si	50	55	56	67
wt%	C	30	32	34	31
	O	18	11	9	1
	Ti	2	2	-	-
	Zr	-	-	1	-
	Al	-	-	-	<2

Table 1.4.1 - Tyranno fibers main characteristics [21].

[21] www.upilex.jp/catalog/pdf/tyranno_fiber_e.pdf

Grade	S (85)	G,F,A (88)	<u>LoxM</u> (90)	<u>LoxE</u> (92)	ZMI (96)	ZE (96)	SA (97)
Properties							
Composition	Containing Ti				Containing Zr		Containing Al
Structure	Amorphous						polycrystal
Strength /GPa	2.6 ~ 3.5						
Oxygen content /wt %	18	11	5	8	2	0	
Heat-resistance /°C	1200	1300	1400	1500	1600	2000	400
modulus /GPa	170	190	200	200	230		
Alkali-resistance (1000°C<)	×	×	×	×	△~○	△~○	◎

Figure 1.4.3 - Tyranno fibers main characteristics.

Sylramic fibers are produced by Coi Ceramics (USA) and are constituted of stoichiometric silicon carbide (95%) together with titanium diboride (3%) and small quantities of boron carbide and nitride. They are currently the more expensive and more performing fibers currently available (last column table 1.4.2). Superior mechanical properties make it possible using conventional weaving apparatus for preparing the fiber preforms, while the termomechanical performance at high temperature and oxidative environments is better than any other ceramic fiber (no degradation after 10 hours at 1550°C in argon) thanks to high stoichiometry and the presence of B₄C. Obviously such fibers are of no interest for transports, they are used only for space, nuclear and military applications.

While some properties reported in the previous tables, like diameter, density or

composition, are simple to be understood, other need some words of explanation. The diameters of the fibers/filaments are generally between 5 and 15 μm , too thin to be weaved as themselves. So filaments, generally in a number between 500 and 2000, are twisted together to form "yarns" or "tows", which can be weaved. The two terms are synonymous and refer to strands or bundles of continuous filaments or fibers, usually twisted and suitable for making textile fabric or structure. In the figure 1.4.4, an overview of possible yarn structures is presented.

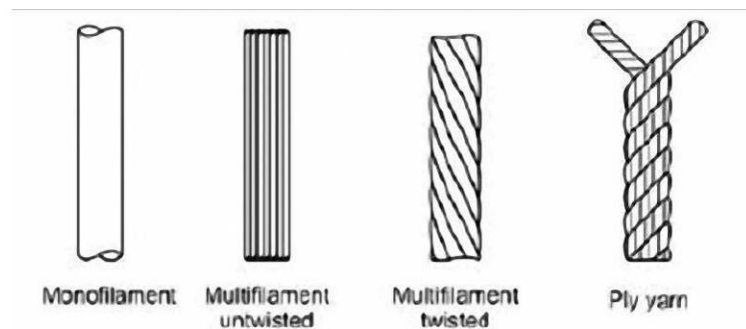


Figure 1.4.4 - Possible structure for Yarn (or Tows).

The fiber vendor generally has to specify the "number of filaments per yarn". Another important parameter is linear density, measure as "Tex units", $\text{g} / 1000 \text{ m}$, or "Denier units", $\text{g} / 9000 \text{ m}$. Tensile strength, tensile modulus and elongation at break at room temperature and at high temperature are obviously the most important parameters for a thermostructural application, but also thermal conductivity and CTE are important, since, for example, a mismatch of CTE between matrix and fibers can make the material fail upon heating, while thermal conductivity is related to thermal shock resistance. Costs are strongly linked to the complexity of the industrial processes, but they could be greatly reduced if the market would really develop.

		Nicalon NL-200	Hi-Nicalon	Hi-Nicalon S	SYLRAMIC
Fiber Diameter	μm	14	14	12	10
Number of filaments	fil./yarn	500	500	500	800
Tex	g/1000 m	210	200	180	180
Tensile strength	GPa	3.0	2.8	2.6	2.8-3.4
Tensile Modulus	GPa	220	270	420	390-400
Elongation at break	%	1.4	1.0	0.6	-
Density	g/cm³	2.55	2.74	3.10	3.0-3.1
Specific heat (25°C)	J/g K	0.71	0.67	0.70	-
Specific heat (500°C)	J/g K	1.17	1.17	1.15	-
Thermal conductivity	W/m K	2.97 (25°C) 2.20(500°C)	7.77(25°C) 10.1(500°C)	18.4 (25°C) 16.3(500°C)	40-45
Coefficient of thermal expansion	10⁻⁶/K	3.2	3.5	-	5.4
Chemical composition	Si	56.6	52.4	68.9	66.6
wt%	C	31.7	37.1	30.9	28.5
	O	11.7	0.5	0.2	Traces
	B	-	-	-	2.3
	Ti	-	-	-	2.1
	C/Si	1.31	1.39	1.05	-

Table 1.4.2 - Nicalon [22] and sylramic [23] fibers main characteristics.

[22] www.coicceramics.com/pdfs/Hi-nicalon_1-17-06.pdf; www.coicceramics.com/pdfs/Hi-nicalon-typeS_1-17-06.pdf

[23] www.coicceramics.com/pdfs/Sylramic_1-17-06.pdf

Producer <i>Fiber</i>	Composition (Wt.-%)	Diameter (μm)	Density (g/cm ³)	Tensile strength/modulus (MPa/GPa)	Production technique/structure	Approx. price
Nippon Carbon Hi-Nicalon "S"	Si: 68.9 C: 30.9 O: 0.2	12	3.10	2600/420	Polycarbosilane/ β-SiC	€7000/kg >10 kg
Nippon Carbon Hi-Nicalon	Si: 63.7 C: 35.8 O: 0.5	14	2.74	2800/270	Polycarbosilane/ β-SiC + C	€3250/kg >10 kg
Nippon Carbon Nicalon NL-200/201	Si: 56.5 C: 31.2 O: 12.3	14	2.55	3000/220	Polycarbosilane/ β-SiC + SiO ₂ + C	€1000/kg >10 kg
UBE Industries Tyranno Fiber SA 3	Si: 67.8 C: 31.3 O: 0.3 Al: <2	10/7.5	3.10	2800/380	Polycarbosilane/ β-SiC _{cryst.} + ...	€6500/kg >10 kg
UBE Industries Tyranno Fiber ZMI	Si: 56.1 C: 34.2 O: 8.7 Zr: 1.0	11	2.48	3400/200	Polycarbosilane/ β-SiC + ...	€1400/kg >10 kg
UBE Industries Tyranno Fiber LoxM	Si: 55.4 C: 32.4 O: 10.2 Ti: 2.0	11	2.48	3300/187	Polycarbosilane/ β-SiC _{amorph.} + ...	€1200/kg >10 kg
UBE Industries Tyranno Fiber S	Si: 50.4 C: 29.7 O: 17.9 Ti: 2.0	8.5/11	2.35	3300/170	Polycarbosilane/ β-SiC _{amorph.} + ...	€1000/kg >10 kg
COI Ceramics Sylramic-iBN	SiC/BN	10	3.00	3000/400	Precursor-polymer/ SiC/BN and other phases	€10500/kg >10 kg
COI Ceramics Sylramic	SiC: 96.0 TiB ₂ : 3.0 B ₄ C: 1.0 O: 0.3	10	2.95	2700/310	Precursor-polymer/ SiC and other phases	€8500/kg >10 kg
Specialty Materials SCS-Ultra	SiC on C	140 (with carbon fiber core)	3.0	5865/415	CVD on C-filament/β-SiC on C	€16 400/kg
Specialty Materials SCS-9A	SiC on C	78 (with carbon fiber core)	2.8	3450/307	CVD on C-filament/β-SiC on C	€19 600/kg
Specialty Materials SCS-6	SiC on C	140 (with carbon fiber core)	3.0	3450/380	CVD on C-filament/β-SiC on C	€4850/kg
Tisics Signa	SiC on W	100/140 (with tungsten wire core)	3.4	4000/400	CVD on W-filament/SiC on W	Price not available

Table 1.4.3 - Indicative costs of commercially available SiC fibers [20].

1.5 Types of fabrics

In the case of carbon and polymer fibers, it is easy to find several kinds of 2D knitting, in particular "twill-weave" and "satin-weave". Other common weaving types are Basket, Leno and Mock Leno. These types are shown in the figures below [24]. Plain weave is symmetrical, with good stability and porosity. Twill and Satin are less stable, but less porous and provide a higher mechanical strength. Basket weave is fundamentally the same as plain weave, except that two or more warp fibers alternately interlace with two or more weft fibers, providing less crimping. Leno weave improves the stability in 'open' fabrics with a low fiber count, with can be helpful, for example, in case of difficult infiltration with a CBC matrix. Mock Leno provides a fabric with increased thickness and rougher surface.

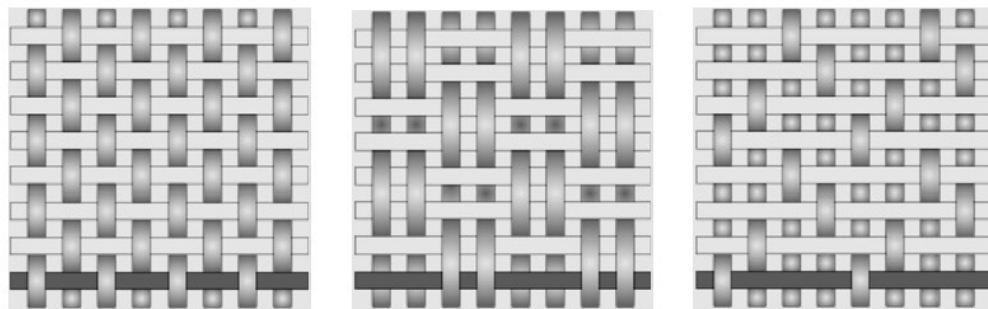


Figure 1.5.1 - Plain, Twill and Satin weave.

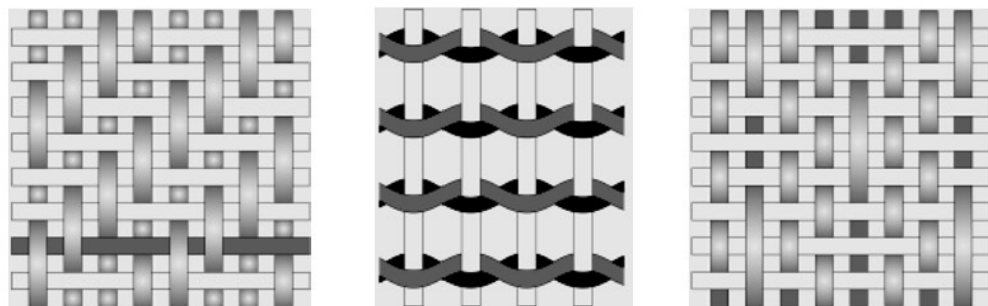


Figure 1.5.2 - Plain, Twill and Satin weave.

[24] "SP Systems - Composite Engineering Materials: Guide to Composites"
www.bolton.ac.uk/CODATE/SPGuidetoComposites.pdf

Property	Plain	Twill	Satin	Basket	Leno	Mock leno
Good stability	****	***	**	**	*****	***
Good drape	**	****	*****	***	*	**
Low porosity	***	****	*****	**	*	***
Smoothness	**	***	*****	**	*	**
Balance	****	****	**	****	**	****
Symmetrical	*****	***	*	***	*	****
Low crimp	**	***	*****	**	**/*****	**

***** = excellent, **** = good, *** = acceptable, ** = poor, * = very poor

Table 1.5.1 - Typical properties of weave styles.

Together with fabric weight, usually measured as gsm, grams per square meter, the knitting type is crucial in determining mechanical performances, being 3D fabrics the most performing, reducing delamination problems which generally affect 2D architectures. In the current thesis work we considered only felts, unidirectional fabrics and 2D twill-weave fabrics, producing panels in the simpler way possible, that is by stacking several layers (plies) of felts or fabrics with alternative orthogonal orientation (0-90°), but it should be remembered that major mechanical and thermomechanical improvements are expected through optimization of weaving a preform structure for a specific geometry and application. However the problem is that as far as ceramic fabrics will be niche products, some fabrics types may be very expensive and difficult to find.

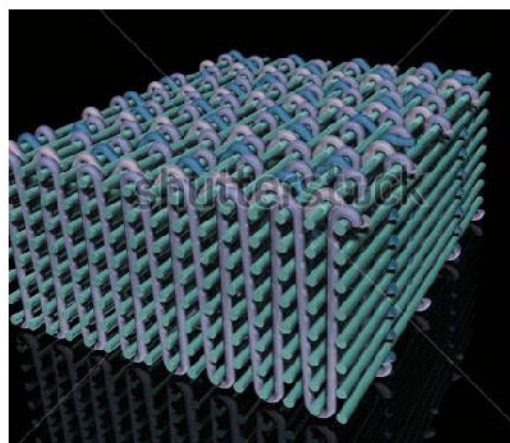


Figure 1.5.3 - Example of 3D-woven fiber preform.

1.6 Typical ceramic matrixes for CFCCs

Since the difference between the coefficient of thermal expansion cannot differ too much from that of the fiber, also the choice of the ceramic matrix has to be carefully considered when designing a composite ceramic material. The following table [25] gives an overview of the main characteristics of the typical ceramic matrixes.

<i>Matrix</i>	<i>Crystal structure</i>	<i>Melting point in pure form (°C)</i>	<i>Onset of active oxidation (°C)</i>	<i>Theoretical density (Mg m⁻³)</i>
SiC	α : hexagonal β : cubic	> 2200 (sublimes)	900 ^b	3.19
Si ₃ N ₄	α , β : hexagonal	\approx 1750 (sublimes)	900 ^b	3.20
MoSi ₂	tetragonal	2030	1000 ^b	6.25
B ₄ C	rhombohedral	2420	800	2.52
BN	hexagonal	> 2500 (sublimes)	800	2.27
CVD // deposition CVD \perp deposition AlN	hexagonal (wurtzite)	> 2000 (decomposes)	900 ^c	3.26
TiB ₂	hexagonal	2870	700	4.50
TiN	cubic	2950 (sublimes in vacuum at > 1450)	700	5.44
TiC	cubic	3065	700	4.92

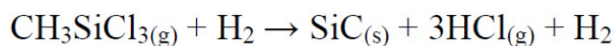
<i>Matrix</i>	<i>Elastic modulus (GPa)</i>	<i>Typical flexural strength (MPa)</i>	<i>Thermal expansion coefficient, 10⁻⁶ K⁻¹ (25–1000 °C)</i>	<i>Thermal conductivity W m⁻¹ K⁻¹ (25 °C)</i>	<i>Electrical conduction ^a</i>
SiC	440	300	4	30	Insulator
Si ₃ N ₄	320	300–800	3	100	Insulator/ semiconductor
MoSi ₂		380	8	60	Conductor
B ₄ C	450	350	5	30	Insulator
BN	40–60	40–60	7	20	Insulator
CVD // deposition CVD \perp deposition AlN	– 150 350	– 150 400	25 0.4 5.6	150 2 > 150	Insulator
TiB ₂	500	600	6	–	Conductor
TiN	450	–	8	–	Conductor
TiC	460	800	8	30	Conductor

Table 1.6.1 - Typical properties of ceramic matrixes for CFCCs.

[25] R. Morrell, Chapter 4.01, "Matrix Materials", pages 1-22, "Comprehensive Composite Materials", 2000, Elsevier, New-York, ISBN 0-08 0429939.

1.7 Processes to obtain non oxides CFCCs

Probably the most used technique for the industrial productions of SiC_f/ SiC, C_f/ SiC and C_f/ C composites for thermostructural applications is **Chemical Vapor Infiltration**. With this technique the production of a component require about one month of continuous infiltration, with a matrix deposition rate around 1 μm per hour. The ceramic matrix is produced by thermal decomposition of a gaseous precursor. Many interesting ceramic matrixes can be produced in this way, carbides (like SiC, ZrC, HfC, TiC, B₄C, TaC, Cr₃C₂, C etc) nitrides (Si₃N₄, BN), borides (TiB₂), oxides (Al₂O₃, ZrO₂), exploiting the same reactions considered in Chemical Vapour Deposition (CVD). Even if the process is slow, it has the advantage that it can be applied to virtually any geometry, keeping in mind that the thickness and the porosity distribution are the crucial parameters to obtain densification. In figure 1.7.1 it is shown the CVI pilot plant developed in ENEA Faenza. It is based on a graphite furnace, where the gaseous precursors are decomposed to produce SiC or C matrix into a fiber preform. The furnace, thanks to graphite heating elements, can operate up to 1600°C in order to be used also for the deposition of different ceramic matrixes. The internal available volume is a cylinder 300 mm wide and 800 mm high. The reaction which is exploited to produce SiC is the decomposition of methyl trichlorosilane (MTS) at 1000°C:



while the Pyrolytic Carbon interphase is obtained by the decomposition of methane, at 1200°C.

With this facility it is possible to deposit SiC on SiC_f preforms, obtaining good densities and near-net-shape parts. Moreover, deposited SiC has high purity and a well-controlled microstructure and different shapes and size can be treated simultaneously. However deposition rate is low (in order to avoid too rapid sealing of the pore entrance by the deposit) and consequently production costs very high. In the CVI process, both the interphase and the matrix are successively deposited from gaseous precursors. In some cases, also the external coating is

deposited with the same technique. The starting material is generally a 2D-fiber preform, fixing the shape using a graphite tooling.

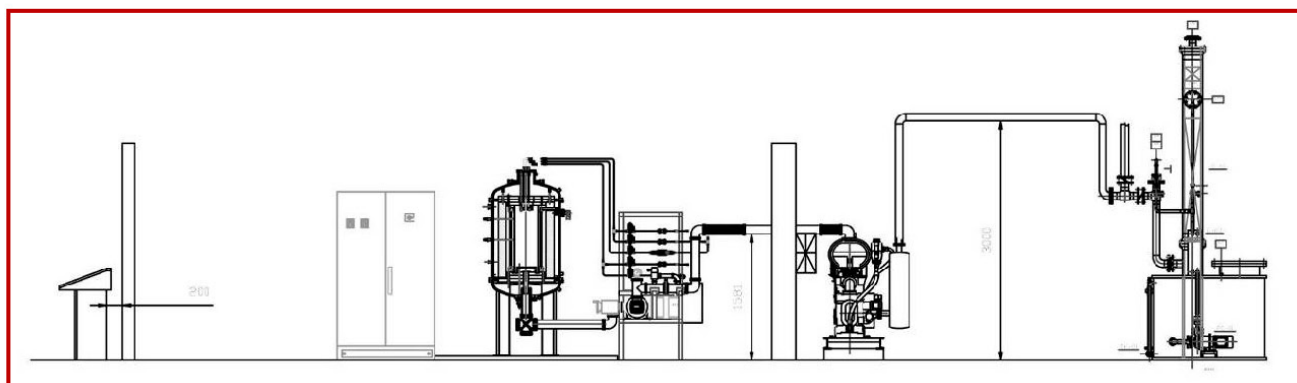


Figure 1.7.1 - Overview of ENEA Faenza CVI pilot plant.



Figure 1.7.2 - Other views of ENEA Faenza CVI pilot plant and microstructure of the developed SiC_f/ SiC composites.

In an attempt to reduce production time, but keeping performances unchanged, UBE SiC-fiber producer proposed **Hot-Pressing**, since it was demonstrated that it is possible to obtain fiber reinforced material with interesting pseudo-plastic thermomechanical characteristics [26] due to the formation of a carbon interphase. Components prepared with this technique are commercialised by UBE under the name of Tyranno HexTM and SA Tyranno HexTM. The name was given to underline the hexagonal shape that fibers take, when hot-pressed. This technique is generally limited to simple geometries and there is some inevitable deformation during sintering.

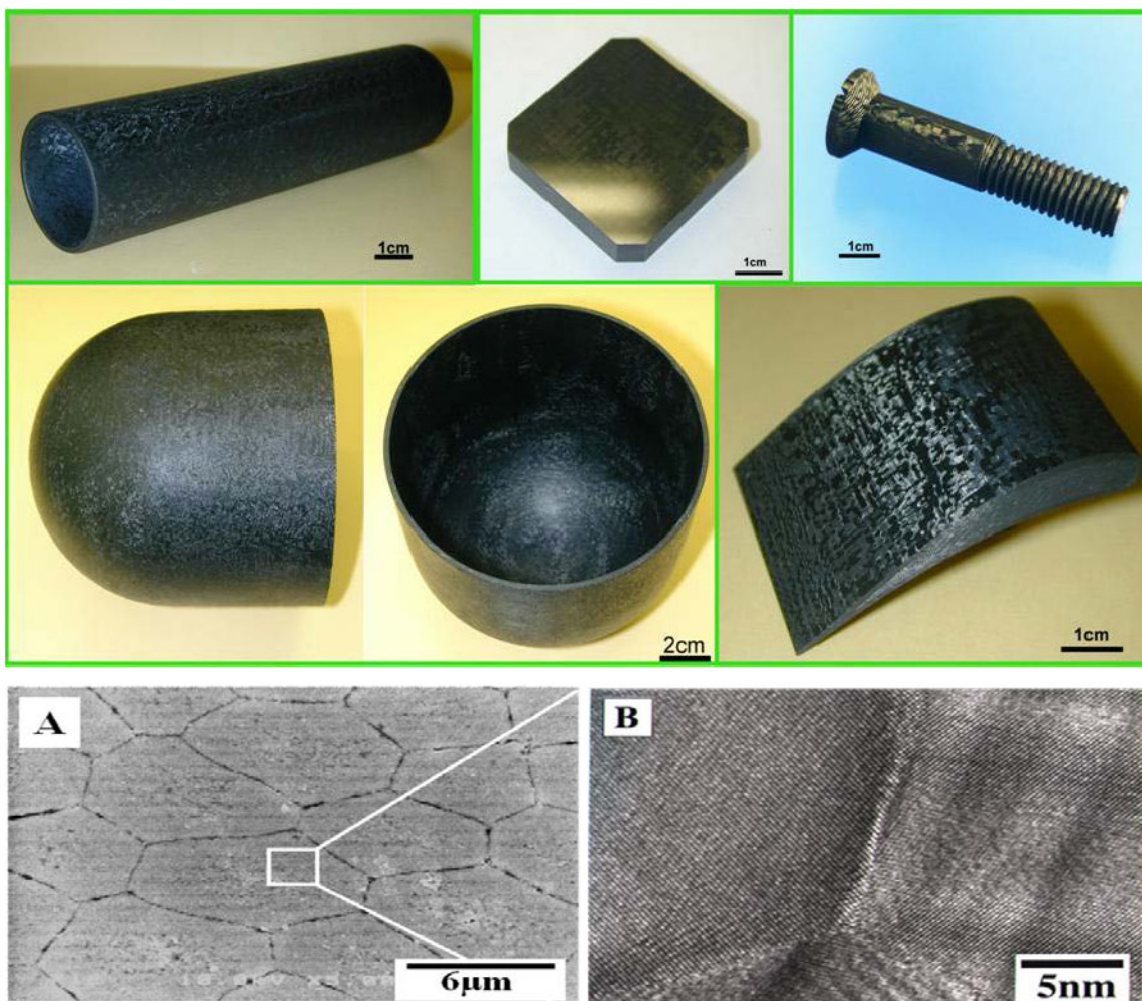


Figure 1.7.3 - UBE SA Tyranno HEX CFCCs and hexagonal microstructure after Hot-Pressing.

[26] Shaoming Dong, Yutai Katoh, Akira Kohyama "Processing optimization and mechanical evaluation of hot pressed 2D Tyranno-SA/SiC composites", Journal of the European Ceramic Society, 23 (2003) 1223–1231.

While CVI infiltrates the fiber preform using a gas, **Polymer Impregnation Pyrolysis** uses a polymer. For example the pyrolysis of polycarbosilanes (PCS) produces SiC. In particular the same polymer which UBE uses to produce fibers can be purchased to infiltrate fiber preforms [27]. According to UBE, a complete densification could be achieved by repeating 10 time the process described in figures 1.7.4 and 1.7.5. The completion of this process requires about one month to be performed (about 3 days for each PIP), so the advantage over CVI is not in the production time, but only in the minor initial investment needed for the instrumentation.

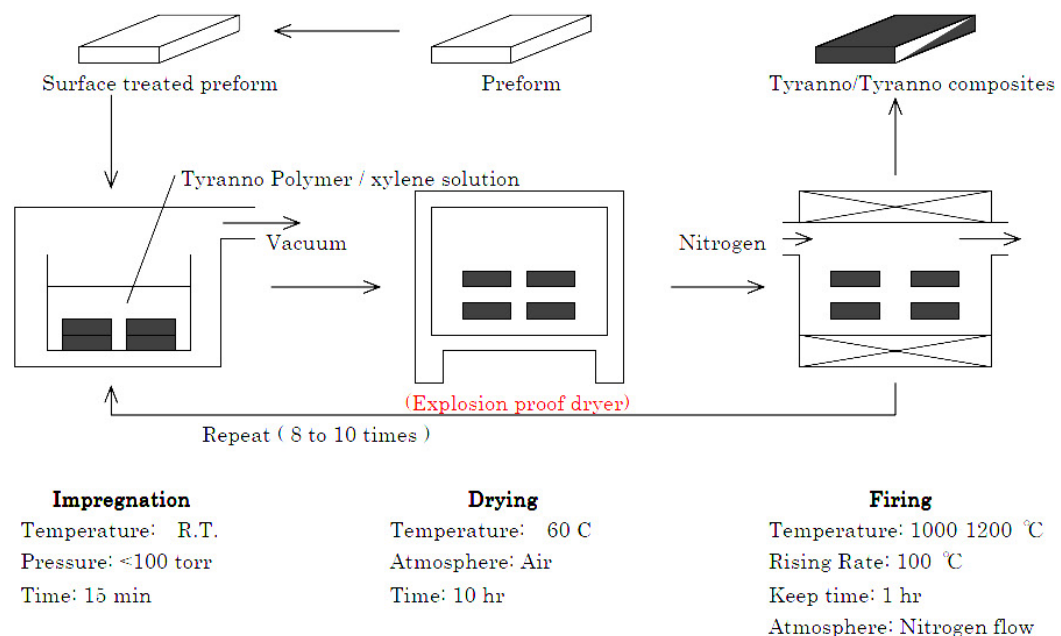


Figure 1.7.4 - Typical PIP production process of SiC_f/SiC, using UBE precursors.

[27] T. Mamiya, Y. Kagawa, "Tensile Fracture Behavior and Strength of Surface-Modified SiTiCO Fiber SiC-Matrix Minicomposites Fabricated by the PIP Process", J. Am. Ceram. Soc., 83 [2] (2000) 433–35.

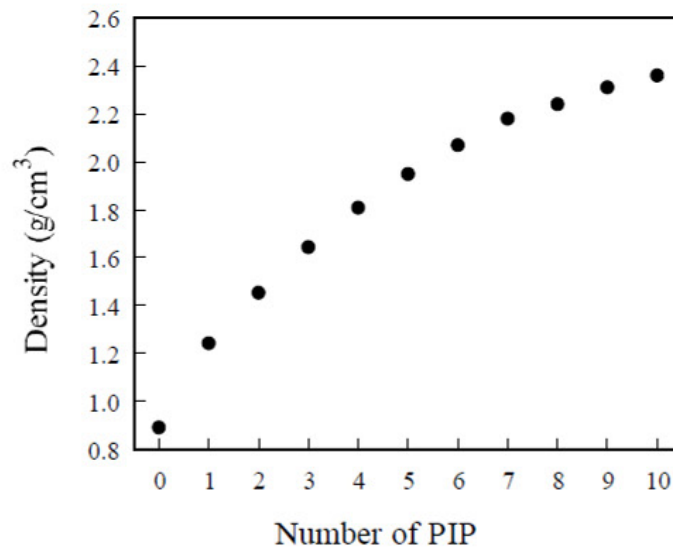


Figure 1.7.5 - Typical densification curve of a SiC_f/ SiC, using UBE precursors.

Regarding microstructure, in the figure 1.7.6 it is shown the typical microstructure of a composite produced by CVI and PIP. The different distributions of pore size generate differences also in the mechanical behavior (stress-strain curve), and generally CVI technique produces materials with higher strength and higher reliability, both because of lower porosity and lower porosity diameter. Moreover PIP materials porosity have much broader distributions.

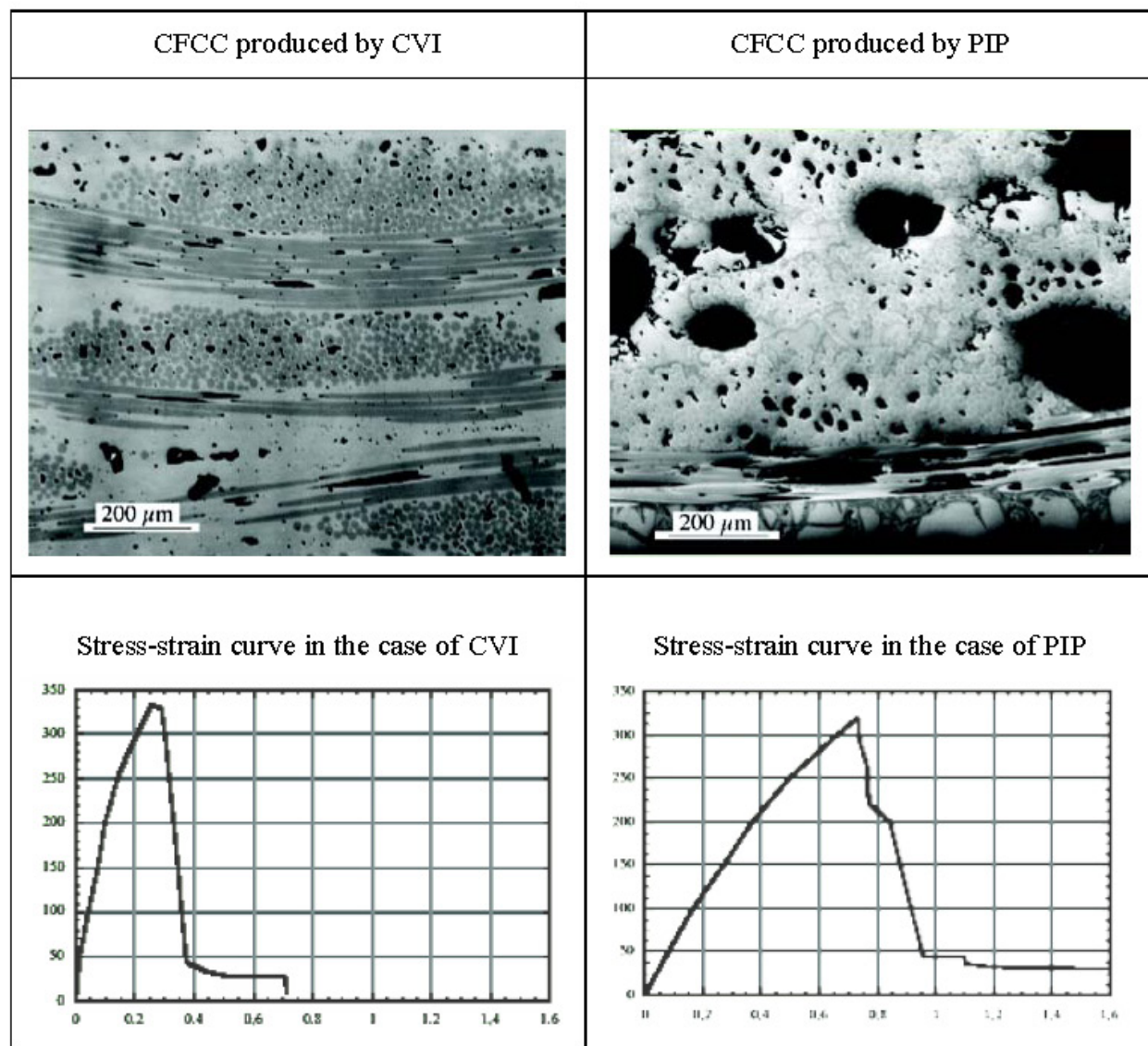


Figure 1.7.6 - Comparison of typical microstructure and Stress-Strain curves for CFCCs developed by CVI and PIP respectively.

Another technology which can be used for producing CMC is based on the reaction of C fibers preforms with liquid silicon. Some silicon reacts with carbon to produce silicon carbide reinforced with carbon fibers (C_f / SiC). This process, known as **Liquid Silicon Infiltration** (LSI), is affected by the fact that some silicon remain, limiting the thermostructural performances up to its softening point (around 1400°C). To use a definition that reminds similarities to LSI, PIP technology is sometimes called **LPI, Liquid Polymer Infiltration**. Summarizing the CVI and Hot-press processes are the most expensive technologies, but provide the most performing materials. Liquid Polymer Infiltration (PIP) is the cheapest, particularly interesting for frictional applications. Motorcycle, automobile, heavy vehicles and aircraft brakes made from LPI short fiber reinforced composite materials are one of the most efficient solution due to high thermal capability, high strength and toughness, and low weight of these material compared to metal alternatives. For example Starfire developed automotive braking rotors, engineered with drill holes and ventilation, for high end performance cars, developed using a chopped fiber reinforced molding compound and subsequent pyrolysis to a CMC (figure 1.7.7).

Material Type	Reinforcement Type	Cost	Technical Maturity	Temperature Capability (°C)	Thermal Conductivity – Z-direction	Toughness	Strength
LPI – Liquid Polymer Infiltration Technology	<ul style="list-style-type: none"> •Continuous Fiber/Fabric •Chopped Fiber •Non-Woven 	\$	Moderate	>1,400°C	Low	High	High
LSI – Liquid Siliconization Technology	<ul style="list-style-type: none"> •Chopped Fiber •Non-Woven 	\$\$	High	1,400°C Max	Medium / High	Low	Moderate
CVI – Chemical Vapor Infiltration Technology	<ul style="list-style-type: none"> •Continuous Fiber/Fabric •Non-Woven 	\$\$\$\$	Moderate	>1,600°C	Medium	High	High

Table 1.7.1 - Most used processes for preparing C_f / SiC and SiC_f / SiC CFCCs.



Figure 1.7.7 - Automotive braking rotors, produced by LPI.

Many different smart combinations of all the before mentioned principles and processes are employed for thermostructural application in extreme environments, including nuclear fusion [28] and aerospace (e.g. multistage nozzles for rocket motors). NASA, in particular, develops CMC technologies also for gas turbine engine components with higher temperature capability which will require less cooling compared to current metallic turbine components [29]. Ceramic materials have no problems to withstand high temperature, but without a suitable fiber reinforcement the fracture toughness and reliability wouldn't be high enough. Besides developing the materials and processes, NASA puts a great effort in the engineering and reliability assessment issues, including the problem of joining and integrating ceramic parts.

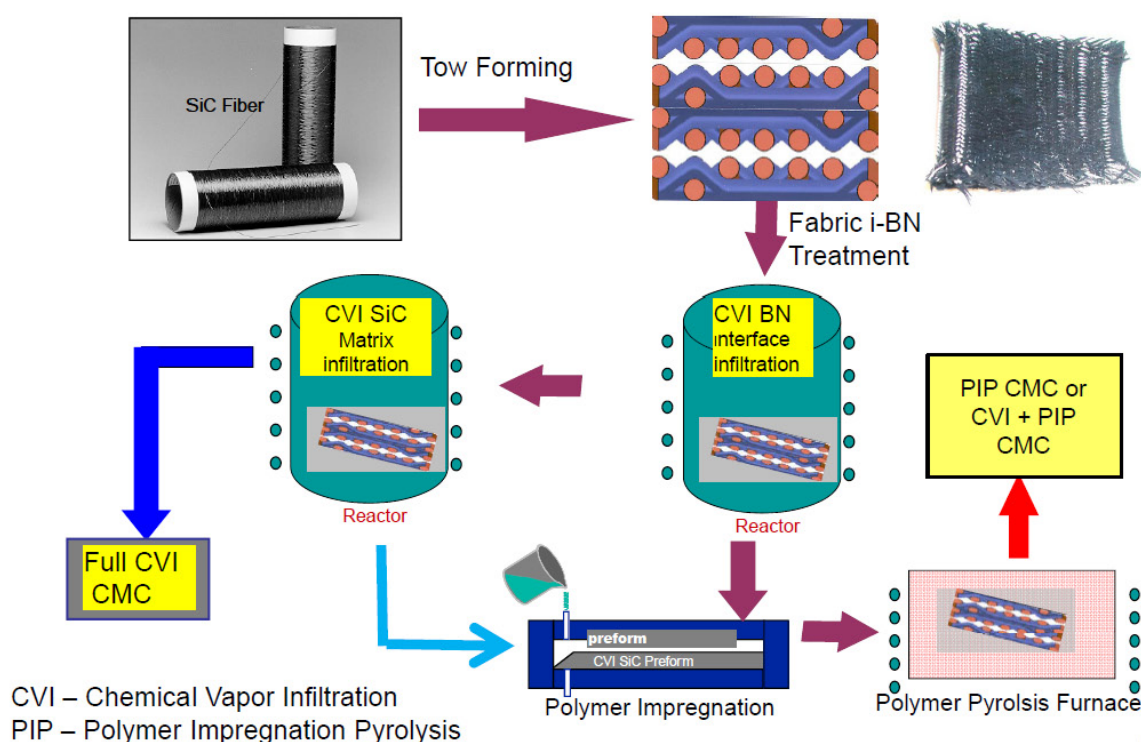


Figure 1.7.8 - CVI and PIP processes developed by NASA for Gas Turbine Engines.

[28] http://web.ornl.gov/sci/physical_sciences_directorate/mst/fusionreactor/pdf/june2000/youngblood4.pdf
 [29] http://www.ntsr.nasa.gov/archive/nasa/casi.ntsr.nasa.gov/20110011258_2011011958.pdf

Currently turbine blades in aerojet engines are fabricated using superalloys, that is the most performing metallic materials at high temperature. However superalloys cannot withstand continuous operation at temperature above 1000°C, and therefore they need internal air-cooling and an external ceramic Thermal Barrier Coating (TBC) which makes the realization of these components really challenging. SiC CFCCs represent a promising future alternative, since are light, though, refractory and creep-resistant materials and would permit a significant increase of service temperature and engine efficiency. Moreover weight saving (30-50%) and lowering toxic emission are expected. As a first step, the application of SiC-matrix composites will probably be limited to non rotating parts (Leading Edge and Trailing Edge inserts). Even if they are far from being fully developed, high strength density for the aerospace may be reached also by ACC (Advanced Carbon Composites, figure 1.7.9), developing very good Environmental Barrier Coating (EBC) for their oxidation protection.

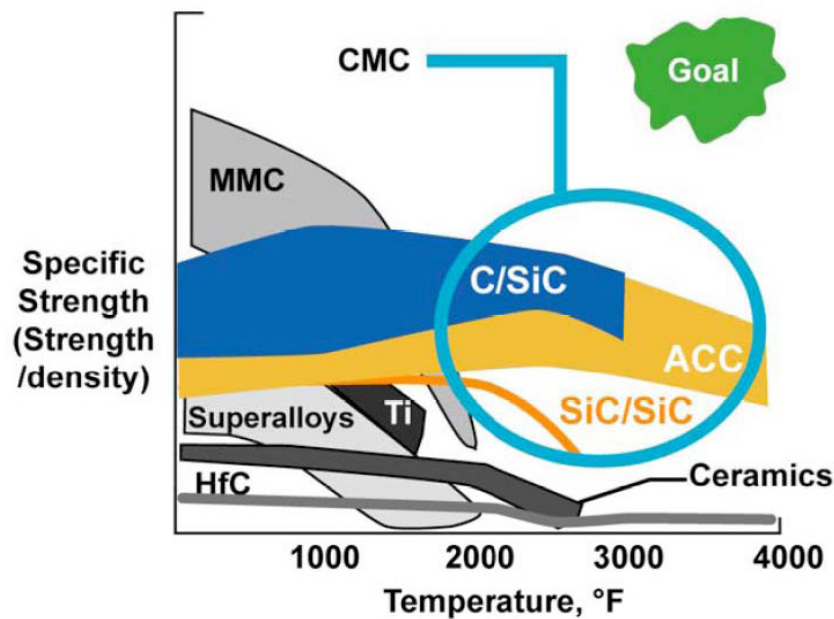


Figure 1.7.9 - Specific strength comparison as a function of temperature [30].

[30] David E. Glass, "Ceramic Matrix Composite (CMC) Thermal Protection Systems (TPS) and Hot Structures for Hypersonic Vehicles", 15th AIAA Space Planes and Hypersonic Systems and Technologies Conference.

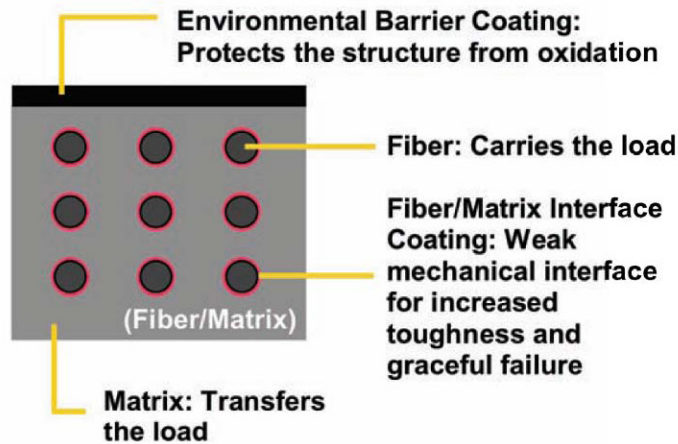


Figure 1.7.10 - EBC on a CFCC, for hypersonic vehicles [AIAA 2008].

Beyond aerospace, SiC_f/SiC composites are already widely used for military and nuclear applications because of the unique combination of high temperature strength, high toughness, low weight, reliability, creep resistance and resistance to shocks and fatigue. Because of these properties, CFCCs and CMCs could be interesting candidates for the replacement of metal in many other thermomechanical applications (above 1000°C), for example for energy demanding industries, and power generation in particular. Like it is done in aerospace, chemically-aggressive and oxidative environments could be withstood by CFCCs using appropriate Environmental Barrier Coatings (EBCs), generally based on highly stable ceramic oxides. Together with reliability and reproducibility issues, it is certainly true that the main limitation to the introduction of these new materials is linked to the high cost, but mass production should overcome all these problems.

Compared to traditional materials, CMC and CFCC components are characterized by higher strength density, improved durability at high temperature, corrosion and erosion resistance, so process efficiency can be increased and emissions reduced. Mechanical properties depend strongly on microstructure, being CFCCs the most performing. However, in many cases, particulate or chopped-fibers reinforcements will be satisfying solutions.

1.8 Characterization techniques for the ceramics development

The development of a new ceramic materials requires a combination of specific characterization techniques. A profound knowledge of these technique is also necessary to correctly evaluate the literature results. All these techniques are available in ENEA Faenza and are following described.

SEM-EDS

SEM-EDS observations give information about the microstructure and local elemental analyses, crucial for determining ceramic phases characteristics. SEM observations are based on an electron gun, and imaging exploits two kinds of detectors, for secondary and backscattered electrons respectively, giving information slightly different, being backscattered electrons signal more dependent on atomic weight and being characterized by a deeper probe depth (figure 1.8.1). EDS technique are based on X-ray fluorescence microanalysis, to determine semiquantitative chemical composition on spot sizes of about 1-2 μm . In ENEA they are performed using a Cambridge LEO 438 VP, equipped with a Oxford Link Isis 300 EDS (figure 1.8.2). It can operate in "partial vacuum" meaning that ceramic materials can be analyzed without any prior treatment.

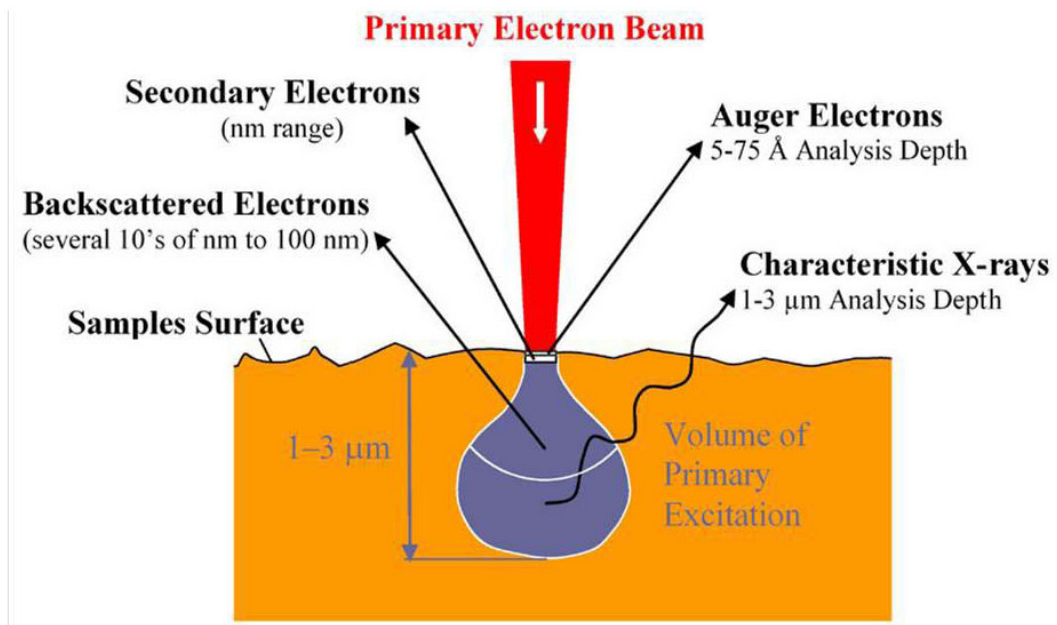


Figure 1.8.1 - SEM probed depth of secondary and backscattered electrons and EDS signal.



Figure 1.8.2 - SEM (Cambridge 438VP) - EDS (Link Isis 300).

Mineralogical evaluations

XRD powder diffraction analyses are necessary to identify the mineralogical phases present in a ceramic material. The technique exploits Bragg's Law ($2d \sin \theta = n \lambda$) and a monochromatic X-ray source to determine crystalline interplanar distances. The most typical use is for qualitative analysis, comparing the XRD spectra with the ICDD database. Quantitative analyses can also be performed. The easiest way is based on the RIR method, based on the calculation of a sort of emissivity ratio of each phase, compared to a reference material (generally Al_2O_3) [31,32].

$$X_i = \frac{X_c \cdot I_i}{k_i \cdot I_c}$$

X = weight percentages (of the analyte, i, and the standard, c)

I = area of the chosen peak (for the analyte, i, and the standard, c)

k_i = RIR del picco considerato

In ENEA Faenza the XRD analyses are performed using Philips PW1820 powder diffractometer, equipped with a Cu K α tube and a dedicated software.

[31] F.H. Chung, Quantitative interpretation of X-ray diffraction patterns. I. Matrix-flushing method of quantitative multicomponent analysis. *Jour. of Applied Crystallography*, 7, (1974) 519-525.

[32] D.L. Bish, S.J. Chipera, "Accuracy in quantitative x-ray powder diffraction analyses" *Advances in X-ray Analysis* 38, (1995) 47-57.

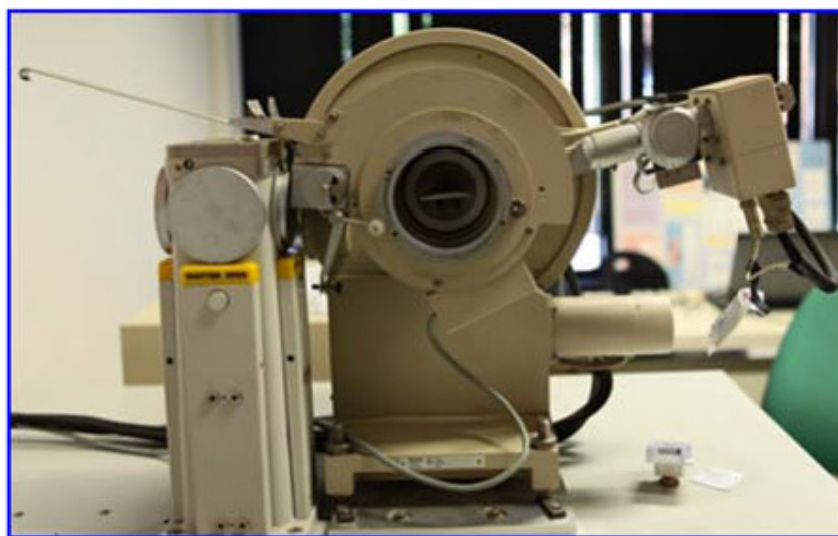


Figure 1.8.3 - XRD goniometer for powder diffraction.

Thermogravimetry

The study of weight changes (TG, thermogravimetry) and heat exchanges (DTA, Differential Thermal Analysis) during high temperature ceramic processing is essential in order to optimize the materials. In ENEA Faenza TG-DTA were performed using a Netzsch 409S. DTA is based on the temperature difference which develops between the sample and a reference material, while an heating ramp is applied to both. Since the oxidation of non oxide ceramics is also associated to weight changes, TG may represent a very simple but sensitive technique to assess thermodynamical stability in simulated working conditions.



Figure 1.8.4 - TG-DTA Netzsch 409S.

Density measurements

Archimede and geometric density measurements are maybe the most easy, but nevertheless essential, evaluation. About the density definitions and procedures, we referred to the relevant standard [33,34,35]. Helium Pycnometry was performed using a AccuPyc 1330 Pycnometer - Micromeritics. The technique can be applied to solid of irregular and irregular forms, and powders, determining the occupied volume, and then density is calculated as weight to volume ratio. Since the processing gas is Helium, all pores larger than Helium diameter are filled with the processing gas and don't contribute the volume measurement. In the case of composites theoretical density was calculated from fiber and matrix density, or by making a pycnometer evaluation, neglecting the presence of closed porosity, which is indeed a rather good approximation for low densified composites obtained by PIP.



Figure 1.8.5 - Helium pycnometer.

Thermomechanical characterization

The mechanical and thermomechanical characterization, were performed on a MTS 880 electro-hydraulic testing machine, equipped with an Instron furnace. According to the standards ASTM C 1341 [36] and UNI EN 12789-2003 [37],

[33] UNI ISO 10545-3 Determination of water absorption apparent porosity, apparent relative density and bulk density, 1993.

[34] ASTM C373 - 88(2006). Standard Test Method for Water Absorption, Bulk Density, Apparent Porosity, and Apparent Specific Gravity of Fired Whiteware Products"

[35] ISO 18753:2004, Fine ceramics (advanced ceramics, advanced technical ceramics). Determination of absolute density of ceramic powders by pycnometer

[36] ASTM C1341 (2013), "Standard Test Method for Flexural Properties of Continuous Fiber-Reinforced Advanced Ceramic Composites".

[37] EN 12789:2003 "Advanced technical ceramics - Mechanical properties of ceramic composites at high temperature under air at atmospheric pressure - Determination of flexural strength".

four-point flexural tests were performed with a test jig, with a support (outer) span of 75 mm, and a load (inner) span of 25 mm (figure 1.8.6).

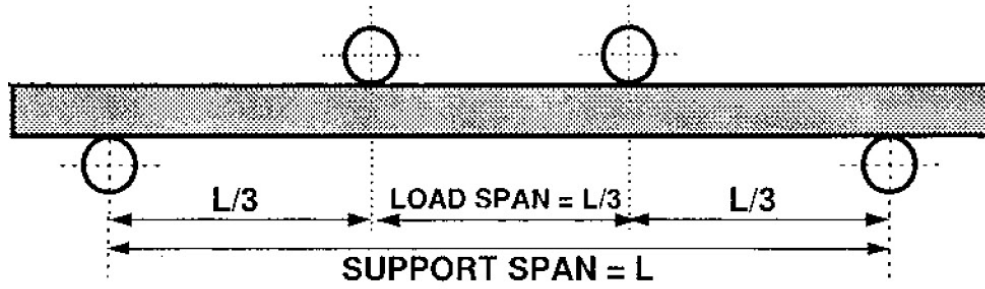


Figure 1.8.6 - Four-point bending apparatus scheme.

The flexural strength, in MegaPascal (MPa) is calculated using the formula:

$$\sigma_{f,m} = \frac{3F_m(L - L_i)}{2bh^2}$$

where F_m is the maximum flexural force (in newton, N), L and L_i the outer and the inner span in millimeter (mm), b the mean width of the test specimen (in mm), h the mean thickness (in mm). The Young modulus can be estimated from the slope of the stress strain curves ($E = \sigma/\epsilon$). The precise determination of E would require ultrasonic techniques, which are not available in ENEA Faenza. For Young module evaluations for cements, the "Impact excitation method" using a Grindo-Sonic System Mk5 frequency analyzer (JW Lemmens NV, Belgium) was used.

For experiments at high temperature, a furnace (figure 1.8.7) and silicon carbide apparatus (figure 1.8.8) were employed: this kind of combined equipment can be used to tests up to 1500°C in oxidative environment. As cross-head speed, 2 mm/min was chosen. MOR (Modulus Of Rupture) values are calculated from the stress-strain curves. The data gathered during the test and recorded in a basic MTS ASCII file were processed by a specific Excel table that collects and plots all the numeric results. It should be noted that in many cases, due to high deformation-to failure, the LVDT (Linear Variable Differential Transformer) used for the measure the strain reached the limit of the range of measure before the sample broke, and the measure was repeated without LVDT, using the first measure to evaluate the Young modulus. All tests have been done "in control of displacement".

Fatigue and creep measures may also be performed with the same equipment.

Fatigue tests imply the periodic application of loads comparatively low compared to the strength of the material, but which can anyway produce significant damage, being well documented that the majority of structural failures of composite orthotropic materials occur due to fatigue-related mechanisms [38].



Figure 1.8.7 - MTS testing machine equipped with a furnace for a high T tests.

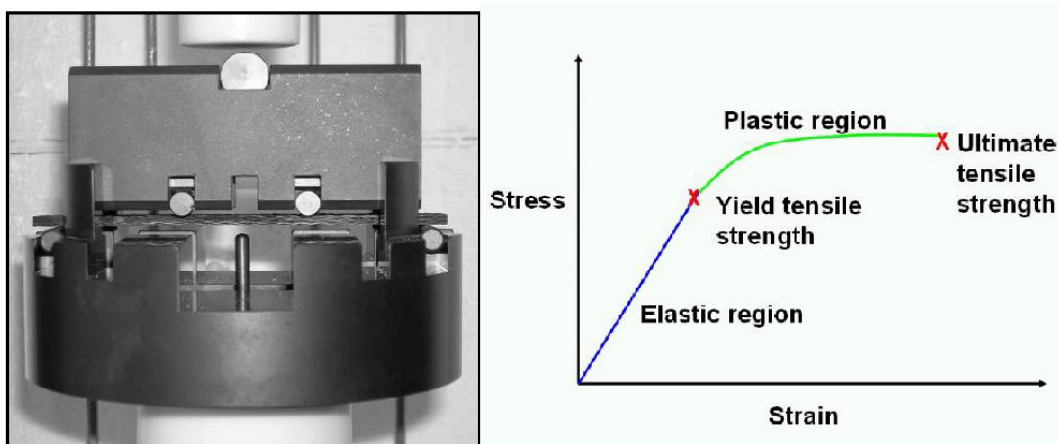


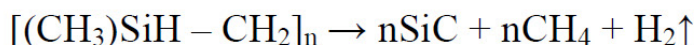
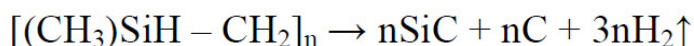
Figure 1.8.8 - SiC four-point bending apparatus for a high T flexural tests and a typical curve for a fiber reinforced ceramic composite material.

[38] Fatigue of Fiber-reinforced Composites, Anastasios P. Vassilopoulos, Thomas Keller. Springer, New York, 2011, ISBN 978-1-84996-180-6.

CHAPTER 2. PRECERAMIC POLYMERS

2.1 State of the Art

Traditionally ceramics are produced starting from powder, by pressing and sintering. During sintering ceramic grains grow and porosity between grains reduces near to zero, with a volume reduction generally higher than 20%. However with this conventional processing route it is impossible to produce fiber-reinforced materials. Another disadvantage of this procedure is that it is impossible to produce "near-net shape" components, due to volume reduction and deformation during sintering. Among non-conventional ceramic production techniques the one which seems more suitable to the low-cost production of CFCCs, is based on Pre-Ceramic Polymers. This process was first proposed for producing ceramic fibers in 1970s by Yajima [39] developing previous fundamental work of Fritz [40]. The process consists in the conversion of a polymer in a solid ceramic through a pyrolysis, with gaseous by products, at about 1000°C under inert atmosphere. A typical chemical reaction which it is exploited is poly-carbosilane (PCS) decomposition:



The volume change is higher than 50%, which results normally in a cracking, however production of monoliths in some cases is also possible, especially if shrinkage is reduced using "Passive" or "Active Fillers". Active fillers are those which react with the preceramic polymer, while passive fillers (including fibers) do not, but both can help in lowering volume reduction and cracking during the pyrolysis. A careful examination of the various synthetic routes of Preceramic Polymers is outside the aim of this Doctorate, but a very comprehensive and updated discussion may be found in literature, and some very good monographs

[39] S. Yajima, J. Hayashi, and M. Imori, "Continuous Silicon Carbide Fiber of High Tensile Strength," Chem. Lett., 4 [9] (1975) 931–4.

[40] G. Fritz, B. Raabe, "Bildung siliciumorganischer Verbindungen. V. Die Thermische Zersetzung von $\text{Si}(\text{CH}_3)_4$ und $\text{Si}(\text{C}_2\text{H}_5)_4$," Z. Anorg. Allg. Chem., 286 (1956) 149–67.

are available [41,42].

Even if the most common case of preceramic polymer is an organo-silicon compound used to produce a silicon based ceramic is pretty well known, there are many other possibilities still to be developed including other metals and non-metals, and many interesting applications, especially in the field of membranes and nanocomposite functional materials [43].

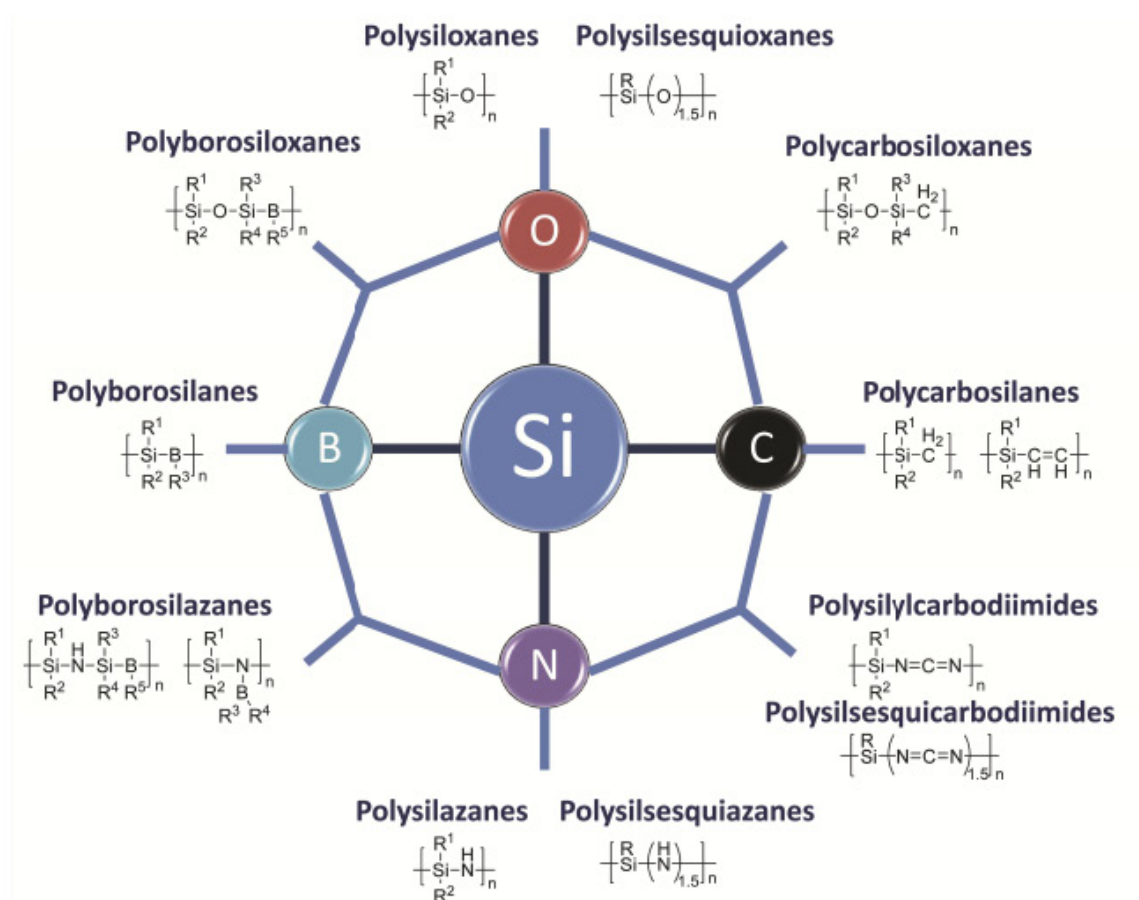


Figure 2.1.1 - Some interesting preceramic polymers based on organo-silicon compounds, taken from 2010 Colombo fundamental review on PDC.

Another very interesting field is that of fire resistant coatings, being possible the applications of PDC on steel, thanks to the low temperature of pyrolysis necessary

[41] "Handbook of Advanced Ceramics", volume 1 and 2, Elsevier, New York, 2003, ISBN 0-12-654640-1.

[42] "Polymer Derived Ceramics", DEStech Pub.2010, ISBN 978-1-60595-000-6.

[43] P. Colombo, G. Mera, R. Riedel, G. D. Soraru, "Polymer-Derived Ceramics: 40 Years of Research and Innovation in Advanced Ceramics" J. Am. Ceram. Soc., 93 [7] (2010) 1805–1837.

to produce SiC or other refractory ceramics [44], refractory here meaning very thermodynamically stable compounds.

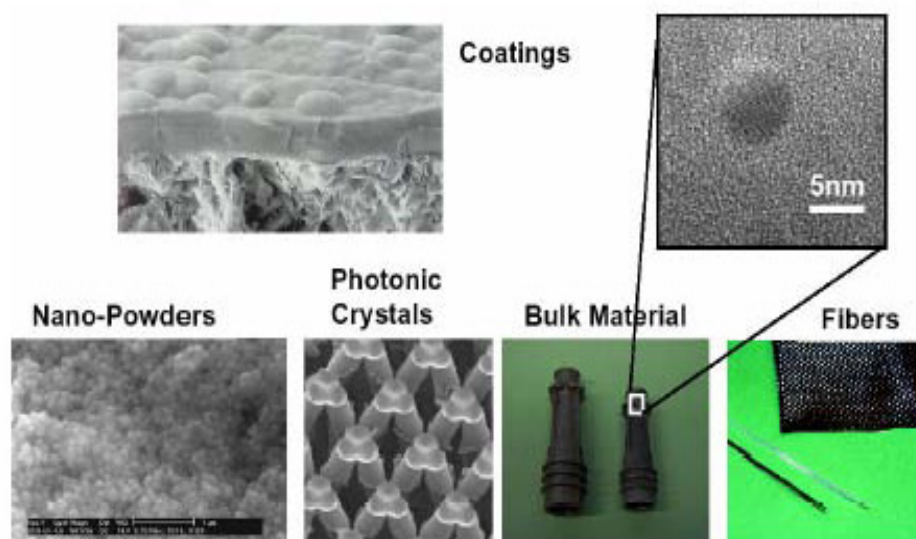


Figure 2.1.2 - An overview of the PDC possible applications in the field of nanotechnologies [45].

Preceramic polymers, besides having made possible the industrial production of ceramic fibers and besides the huge future potential applications in the field of nanotechnologies, can be exploited for densification of ceramic fiber preforms (PIP process) [46]. Among the already discussed advantages of the PIP process, it should be stressed versatility: for example it is much easier to test new self-healing matrixes or additives than would be using CVI [47]. However it is also true that some very effective (in term of mechanical properties) laminated microstructures could be achievable only by CVI [48].

-
- [44] M. Günthner, A. Schütz, U. Glatzel, K. Wang R. K. Bordia, O. Greißl, W. Krenkel, G. Motz, "High performance environmental barrier coatings, Part I: Passive filler loaded SiCN system for steel", *Journal of the European Ceramic Society*, 31 (2011) 3003–3010.
 [45] Lisa Biasetto, PhD thesis, Padova University (Prof. Paolo Colombo).
 [46] S. Yajima, Y. Hasegawa, K. Okamura, I. Matsuzawa, "Development of High Tensile Strength SiC Fibre Using an Organosilicon Polymer Precursor", *Nature (London)*, 273 (1978) 525-7
 [47] Bin Wu Shaoming Dong Zhen Wang Yanmei Kan Liangrun Zhang Fan Zhou "Properties of C/SiC composites modified by a boron- containing phase", *Ceramics International*, 39, 4 (2013) 4729-4734.
 [48] Liu, Yongsheng, Zhang Litong; Cheng Laifei; Yang Xin'gang Luan Wenbin; Zhang Weihua "Preparation and oxidation resistance of 2D C/SiC composites modified by partial boron carbide self-sealing matrix", *Materials Science & Engineering A*, 498, 1-2 (2008) 430-436.

Regarding PIP processes, PCS is usually applied in solution (e.g. 50%w/w xylene) on the fiber preform. However also liquid polycarbosilane, or polymer processing could help in increasing efficiency. Also in the case of composite production, active and passive fillers may be very effective tools to change the characteristics or the composition of the ceramic matrix [49,50]. There is a strong dependence of "ceramic yield" on PCS structure, so the research in this field is always ongoing [51], like research about new applications and functionalities [52].

One of the conditions for future large-scale industrial application of the process is, however, the reduction of the polymer industrial production costs. The first company in succeeding in the aim of optimizing a mass production of a preceramic polymer was Starfire Inc. [53] which is still a reference vendor and producer of PIP polymeric precursors. Starfire Inc. offers pre-ceramic polymers in a range of viscosities and compositions to allow tailoring and processing flexibility to fit with component property targets. These polymers can be used to produce carbon fiber reinforced composites for frictional, structural and thermostructural applications. Typical mechanical performance are shown in figure 2.1.1, which remarkably reminds mechanical plastic behavior of polymeric matrix composites of figure 1.1.3, and it is referred as "pseudo-plastic" or "pseudo-ductile" behavior of fiber reinforced CMCs.

2.2 The Polymer Infiltration and Pyrolysis (PIP) process

To summarize again, the starting point of the PIP process for producing a CFCC is the forming of the object using preceramic polymers, using traditional polymer forming processes. Pyrolysis is typically performed in an inert environment to a minimum of 850°C, causing the polymer to transform from a polymer into an engineered ceramic. After the first pyrolysis, the preform shape is mechanically

[49] Luo Yongming, Zheng Zhimin, Xu Caihong, Mei Xuening "Polycarbosilane derived Ti_3SiC_2 ", Materials Letters, 62, 20 (2008) 3570-3572.

[50] Yuxi Yu Xueyuan Tang, "Ceramic Precursor Aluminum-Containing Polycarbosilane: Preparation and Structure" Journal of Inorganic and Organometallic Polymers and Materials, 19, 3 (2009) 389-394.

[51] Houbu Li, Litong Zhang, Laifei Cheng, Yiguang Wang, Zhaoju Yu, Muhe Huang, Huibin Tu, Haiping Xia, "Effect of the polycarbosilane structure on its final ceramic yield", Journal of the European Ceramic Society, 28, 4 (2008) 887-891.

[52] Manabu Fukushima Paolo Colombo "Silicon carbide-based foams from direct blowing of polycarbosilane", Journal of the European Ceramic Society, 32, 2 (2012) 503-510.

[53] <http://www.starfiresystems.com/docs/Starfire-Brochure.pdf>

stabilized, but porosity is formed due to polymer-to-ceramic volume change, which is generally higher than 50%, so that new polymer can be vacuum infiltrated. The shape of the object is retained during the various steps, meaning that PIP process is a near-net-shape process, requiring generally minor or no mechanical machining before use. In figure 2.2.1, CFCCs label use the convention of specifying, in order, the fibers type/nature, sometimes with the prefix "f", and then the matrix type/nature (e.g. SiC_f/SiC).

Property	SMP-10	SPR-688	SPR-212
Ceramic Formed	SiC	SiOC	SiOC
Viscosity (cP)	40-100	300-2,000	12-26
Pyrolysis Yield (%)	72-78	65-68	50-65
Liquid Density (g/cm ³)	1.0	1.1	1.0
Ceramic Density (g/cm ³)	2.20	1.99	1.95

Table 2.2.1 - Typical properties of Starfire preceramic polymers, precursors of SiC and SiOC.

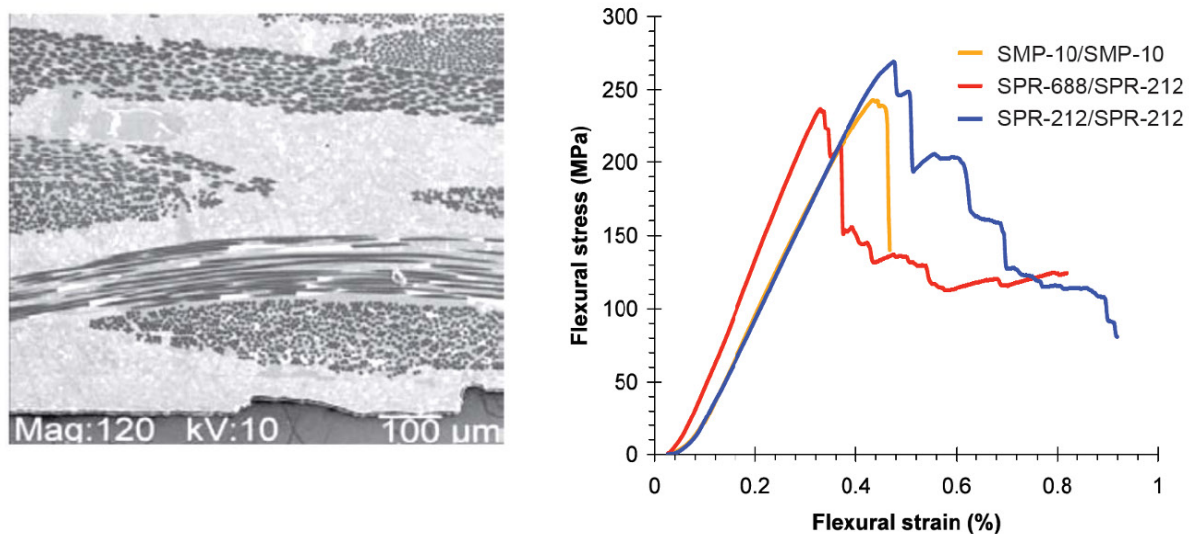


Figure 2.2.1 - Typical microstructure and mechanical performance of Starfire CFCCs.

The PIP process is based on several steps (typically between 6 and 10) of infiltration of a fiber preform with a preceramic polymer (maybe which with an inorganic filler), and the subsequent conversion into a ceramic matrix by pyrolysis, repeated up to the desired degree of densification (figure 2.2.2).

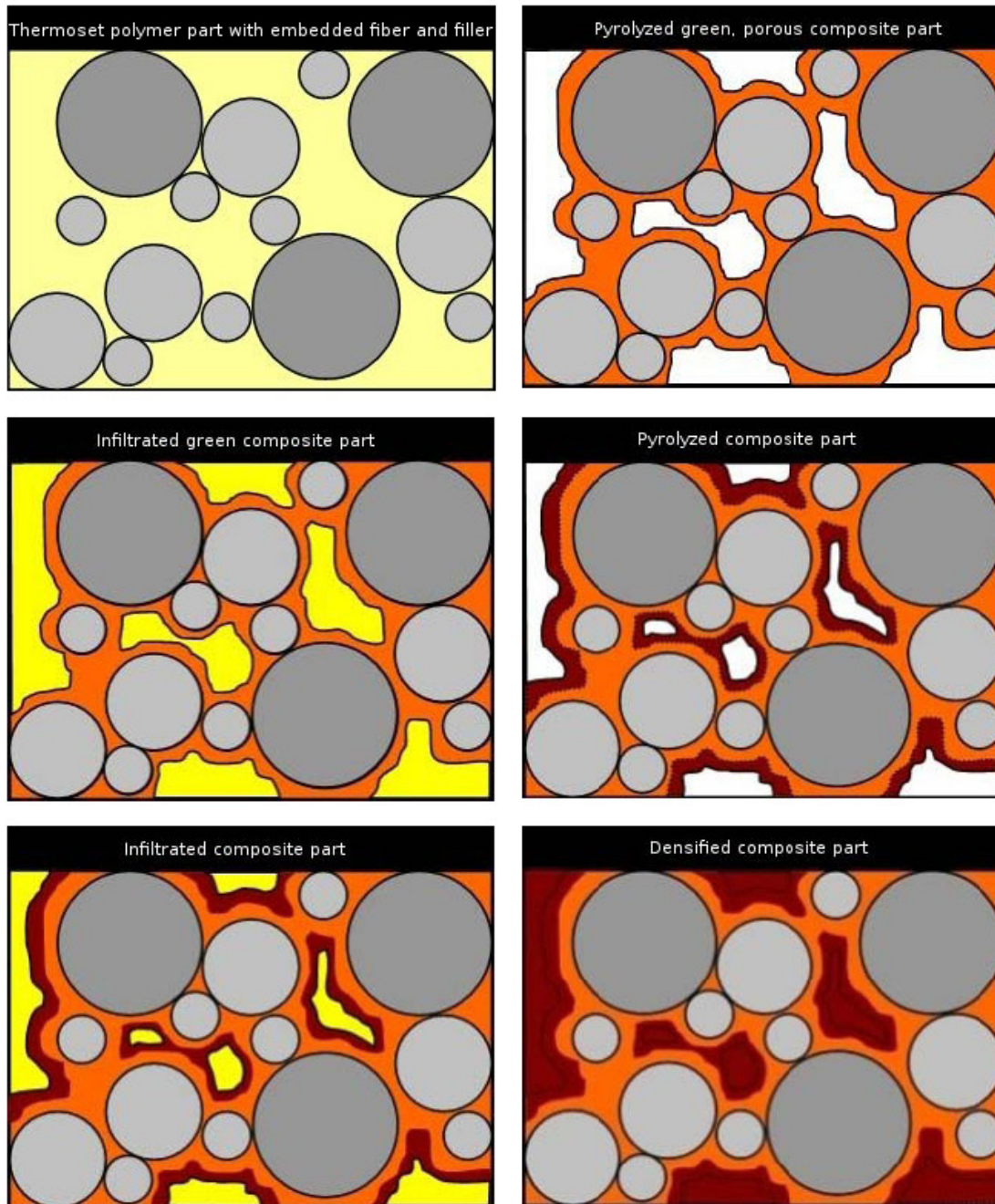


Figure 2.2.2 - Scheme of the PIP process. In "yellow" it is indicated the polymer, in "ocre" the obtained ceramic, and in "gray" the fibers/fillers.

The vacuum infiltration step is accomplished in a simple three step process, and can take approximately 30 minutes each. First vacuum is applied to the porous body, then the polymer is introduced through vacuum infusion, and finally the porous body is allowed to equilibrate to atmospheric pressure conditions. A typical vacuum infiltration station consists of a vacuum vessel and a vacuum pump capable of achieving vacuum below 1 mbar. Generally dry pumps are the best choice, but conventional rotary pumps can be used, better if equipped with

cold trap, to protect oil from solvents and other low molecular weight species. The vacuum vessel used for infiltration should have three valves, one to make vacuum, one for polymer infusion and one for the final backfilling with air. The principle of "vacuum infiltration" is exploited also by RTM equipments (figure 2.2.3), but here also heating is exploited.

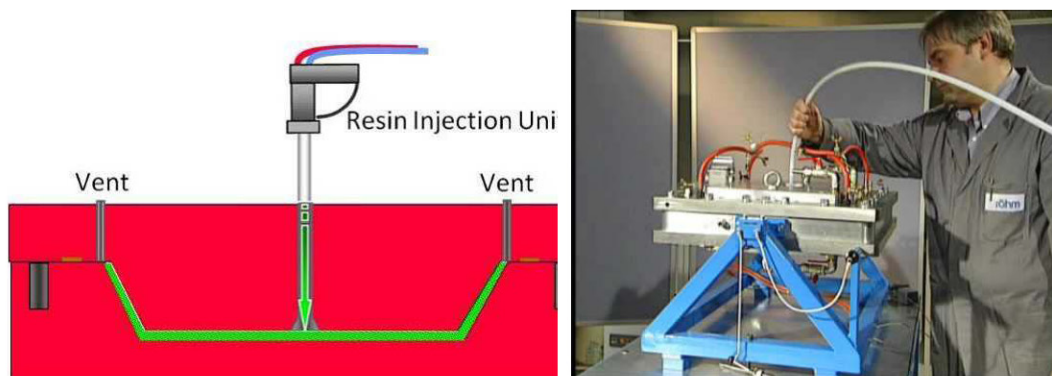


Figure 2.2.3- RTM equipment, working on the principle of vacuum infiltration.

After that, it is generally advisable to clean off the parts of any excess polymer using a smooth spatula, recovering any unused polymer. Then the pyrolysis is performed in an inert environment, better wrapping carbon cloth around the components, to ensure that no oxygen can reach the polymer.

An approach alternative to vacuum infiltration is known as "wet lay-up" (figure 2.2.4) and employs liquid slurries and nude fabrics. Wet lay-up systems (also called Hand Lay-Up, HLU) consist in applying a preceramic polymer onto the ceramic fabric, using assembling tools like rollers on both sides to remove air bubbles and residual polymer. After curing, the single plies are stacked together and the first pyrolysis is performed. Alternatively, all the fabrics layers can be stacked together on a mold before curing, and degassing may be obtained by applying vibrations or by vacuum.

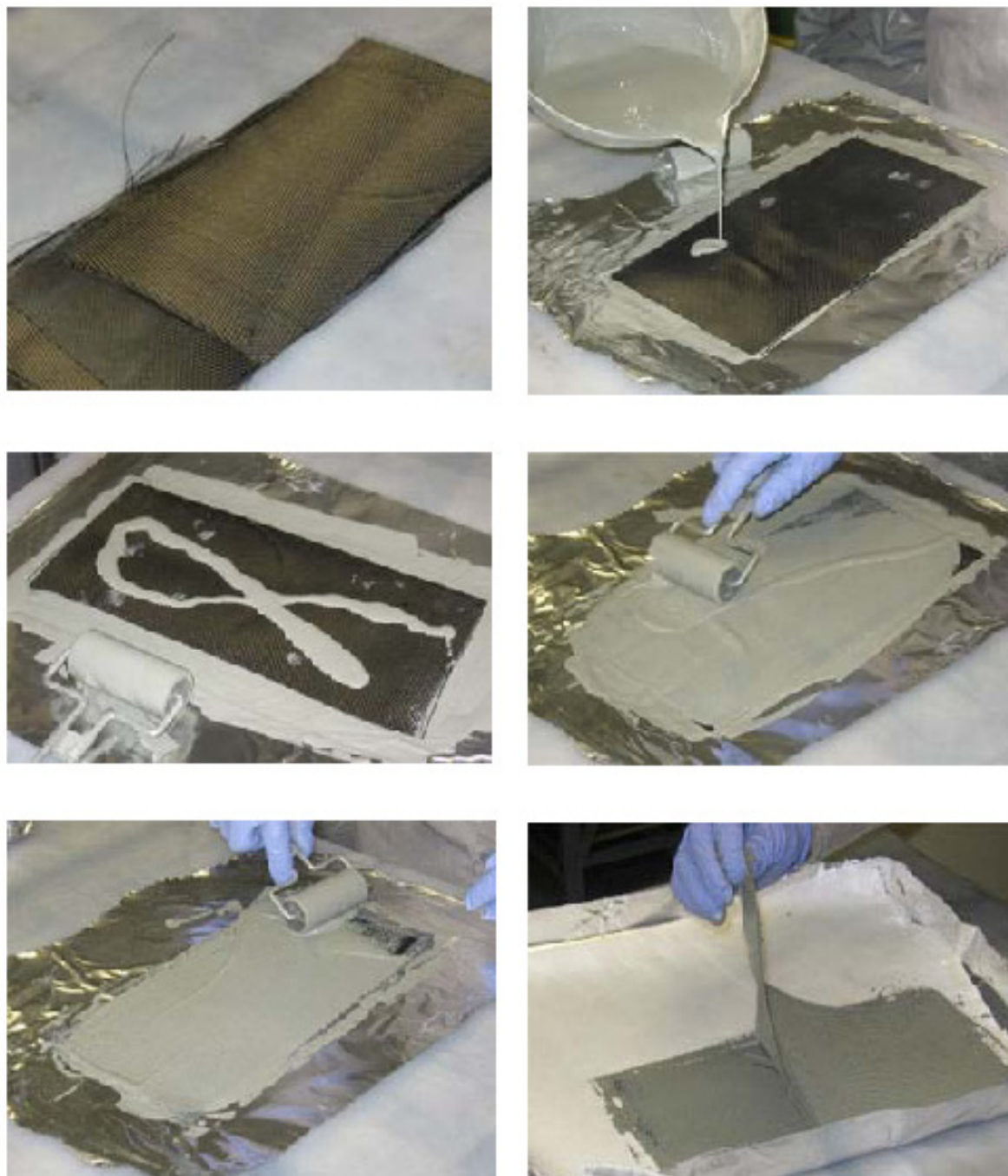


Figure 2.2.4 - Wet lay-up composite production.

Quite recently another Chinese industrial producer has begun his production of PCS, offering apparently cheaper and more stable polycarbosilanes [54] which seem particularly interesting, since it is mainly the price of the raw materials that is currently limiting the potential applications of PIP technology. In this case the PCS is sold in its solid form, stable more than 6 months, and soluble in common

[54] <http://www.nabond.com/Polycarbosilane%20from%20NaBond.html>

organic solvents like xylene, toluene, and THF. According to the vendor, this PCS, has a low oxygen levels, an average molecular weight of 1500-2000 g/mol, provides a ceramic yield at 900°C of 55%, after a thermally induced self curing.

2.3. The development of a PIP pilot plant

The development of a PIP pilot plant was probably one of the main achievement of this thesis work. The hardware starting point was a steel autoclave, generally used for debonding ceramics produced by injection molding. The furnace had not been used for a long time, and originally had a maximum working temperature of 600°C. It had been necessary a complete revision of the apparatus in order to make possible its application to PIP processes. It was possible to keep only the structure outer vacuum vessel and the internal one, in AISI 310S, the heating elements and the thermocouples. First of all, it was necessary to introduce ceramic insulation fibers between the outer and the inner vessel, to revise completely the gas feeds, introducing the possibility to work both in inert atmosphere (fluent nitrogen) and in fluent air, the outlets valves and also the vacuum system. Flowing air and flowing nitrogen were considered almost of equal importance, since it was expected the PIP plant would need periodical clean-up in air, especially if working with untested preceramic polymers. A cold trap for low molecular weight organics was also introduced, and the power unit was completely revised, in order to follow the current legislation and regulations. Particular attention was required to guarantee achievement of good vacuum sealing, since originally the furnace was built to work at high pressure (up to 10 bars) but not in good vacuum. The optimization of all the procedures was made while performing the first pyrolysis tests, and the manual was written together with the company who had to certify the instrumentation.

This kind of furnace is very similar to those used to produce PMC, from which could be obtained by upgrading the power unit and the resistors, which could make the technology transfer of PIP process cheaper and easier.



Figure 2.3.1 - An overview of the PIP pilot plant, developed for thermal treatments up to 950°C in flowing air, flowing nitrogen and vacuum.



Figure 2.3.2 - Other views of the AISI 310S pyrolysis chamber (diameter 0.40 m, length 0.75 m).

During the thesis work, one of the worries was about the formation of liquid and solid residues in the furnace, with a possible locking of the exhaust pipes. The autoclave system was originally built to tolerate pressures up to 10 bar (even if no more allowed to from current security standards and legislations) but we preferred to put an emergency valve, which, in emergency conditions, would also act as an alternative exhaust pipe. The furnace was equipped with seven thermocouples, to check the temperature on the sample and temperature uniformity, which indeed is within 10-20°C also when operating in vacuum ($4 \cdot 10^{-1}$ mbar, during the pyrolysis step).

Regarding the vacuum infiltration apparatus, it was employed a conventional vacuum oven, equipped with a Teflon rotary pump. The SiC felts were put onto graphite paper throughout all the process, including pyrolysis. Both polycarbosilane and poly-siloxane preceramic polymers were used as low viscosity solutions (50% w/w xylene).

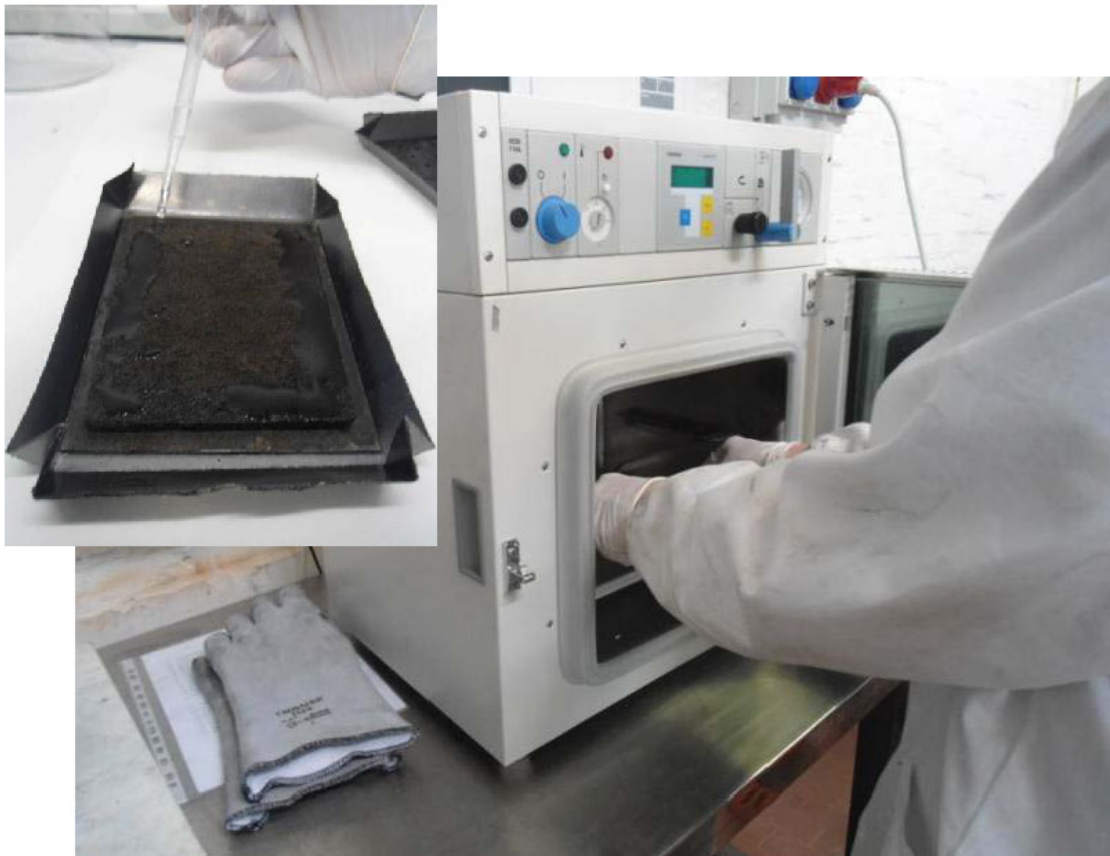


Figure 2.3.3 - A view of vacuum infiltration of fiber preforms with the polymer solution.

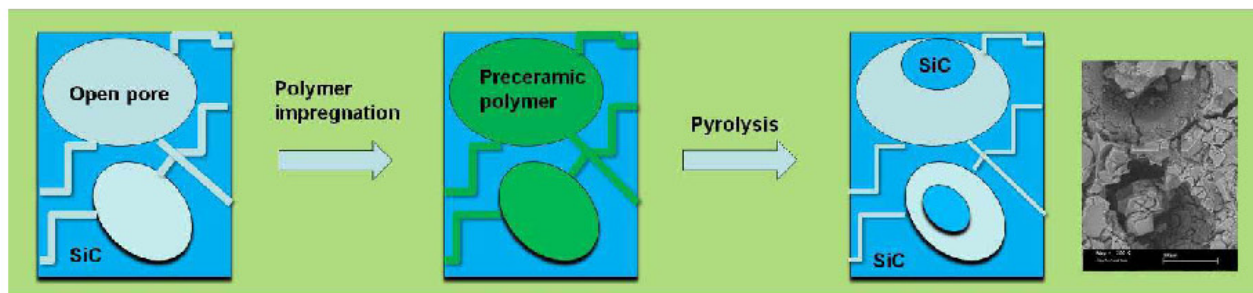


Figure 2.3.4 - Scheme representing PIP steps and subsequent microstructure.

2.4. Development of the synthesis of a polymeric precursor for ZrC

Aiming at going beyond current performances of CFCCs, it would be necessary to develop new synthesis of preceramic polymers. Again the already mentioned review of Colombo [55] is very clear in identifying the possible synthetic strategies and the characteristic that the resulting preceramic polymer must possess to be interesting for the applications. Preceramic polymers should guarantee favorable rheological properties for making possible the infiltration of the mould or, in the case of CFCCs production, of the fiber preforms. Curing should be complete, without leaving low molecular fractions, which could produce gas and porosity.

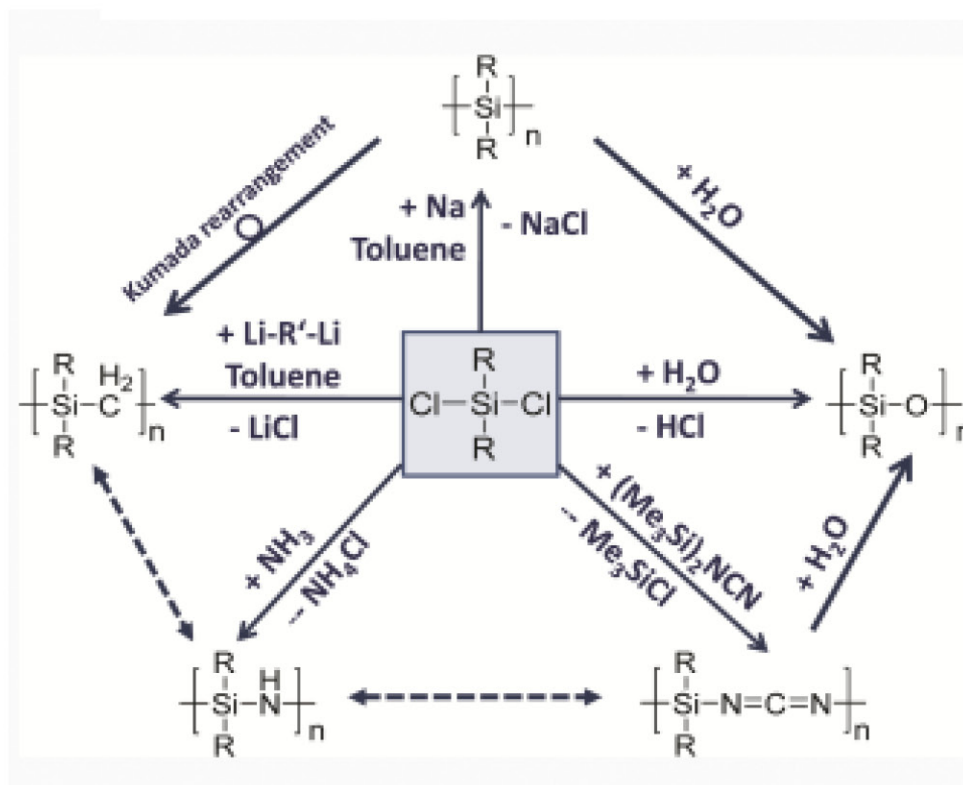


Figure 2.4.1 - Typical synthesis routes of organosilicon polymers.

The main problem in setting up such experimental synthetic activity in relation to

[55] P. Colombo, G. Mera, R. Riedel, G. D. Soraru, "Polymer-Derived Ceramics: 40 Years of Research and Innovation in Advanced Ceramics", J. Am. Ceram. Soc., 93, 7 (2010) 1805–1837.

thermostructural applications is related to quantities, being 1kg the minimum quantity of polymer which makes possible to test a preceramic polymer and being 1 kg far beyond the preparation capability limits of traditional chemical research laboratories. However an high performing preceramic polymer could be beneficial also in low quantities if used not as a matrix, but as a coating. Aiming at this application, we tested the preparation of a polymeric precursor of ZrC, being ZrC (which is an Ultrahigh-Temperature Ceramic, UHTC) superior to SiC in terms of various critical characteristics, thermodynamic stability and fusion temperature in particular.

2.4.1 Testing of a patented synthesis procedure

The interest for producing polymeric precursor of ZrC can be deduced also from several recent articles [56]. We applied the results shown in the patent US 6395840-B1 (2002), which is about Grignard reactions to produce preceramic polymers. To test this procedure, 100 ml of anhydrous THF (treated with sodium) were put into a 3-neck flask together with 1g di ZrCl₄ anhydrous ($1/233.03=4.29$ mmol) with a 20% stoichiometric excess of magnesium vinyl chloride, adding slowly a THF solution 1.7 M of the Grignard reagent. Nitrogen was flown throughout the all experiment and the temperature was kept around -80°C, using a bath of alcohol, cooled with liquid nitrogen. Upon completion of the addition of the Grignard reagent, the solution color changed from yellow to ochre. The solution was kept under stirring for 7 hours, measuring a final temperature of about -70°C, before filtering, in air, the resulting solid polymer on paper. The dried polymer was stored under vacuum, before pyrolysis experiments.

2.4.2 Pyrolysis experiments and characterization of the residue

Pyrolysis experiments were done using a TG-DTA, operating in flowing nitrogen. A weight loss of about 32% was measured before 800°C, and another 12% was lost between 800 and 1200°C. DTA curve is generally less significant for this kind

[56] Qinggang Li, Shaoming Dong, Zhi Wang, Guopu Shi, Yan Ma, Haijun Zhou, Zhen Wang, Ping He, " Microstructures and mechanical properties of 3D 4-directional, C_f/ZrC–SiC composites using ZrC precursor and polycarbosilane", Materials Science and Engineering B, 178 (2013) 1186-1190.

of processes, however it is usually registered simultaneously, in order to help identifying exothermic and endothermic processes.

The resulting ceramic yield (inorganic mass residue upon pyrolysis) would be of about 56%, while the maximum yield expected according to the patent should be of no more than 22%. This means that the solid contains MgO residue, besides the preceramic polymer. The presence of MgO is probably due to the degradation, caused by the humid air, of the excess of Grignard reagent, during the filtration. After pyrolysis of the polymer for three hours under nitrogen, a white solid residue was obtained. XRD powder diffraction is the most useful technique for semiquantitative mineralogical investigations on unknown inorganic/ceramic phases. The technique is based on the comparison of the experimental spectra with the ICDD database [57]. In this case (figure 2.4.3) the pyrolysis of the synthesized polymer lead to the formation of ZrC, the product of interest in this case, but also ZrO₂ and MgO, impurities.

The result was confirmed using SEM-EDS, were the ZrO₂ and MgO aggregates with a specific morphology, different from other area where ZrC prevailed. EDS was used for elemental analysis (an example of the spectra in figure 2.4.4).

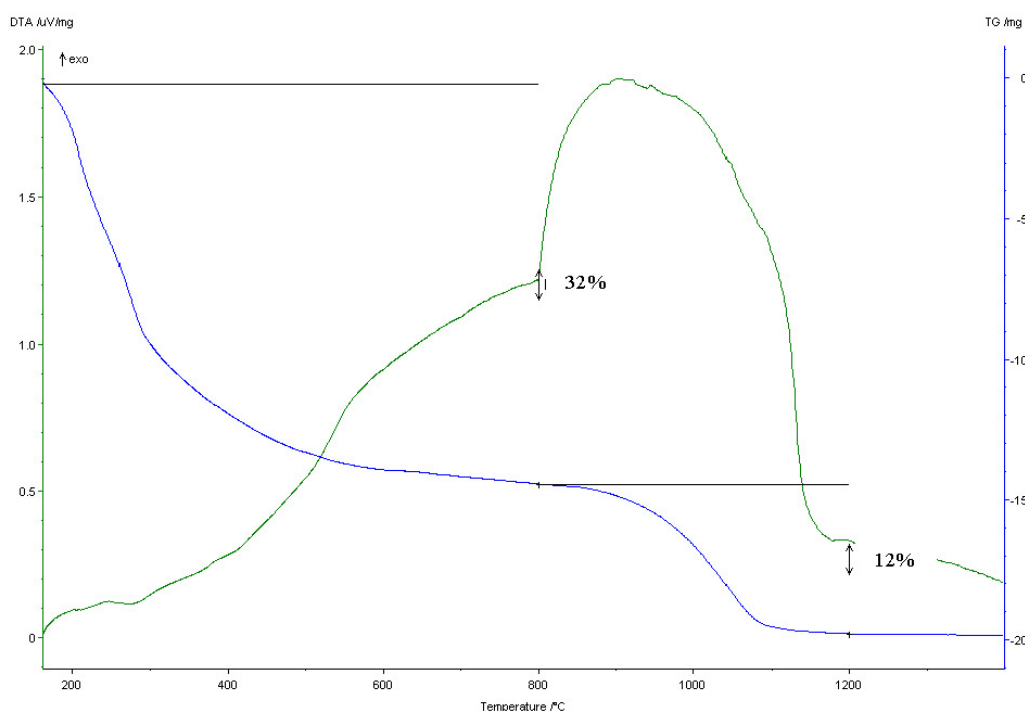


Figure 2.4.2 - TG-DTA under nitrogen of the ZrC preceramic polymer.

[57] <http://www.icdd.com>

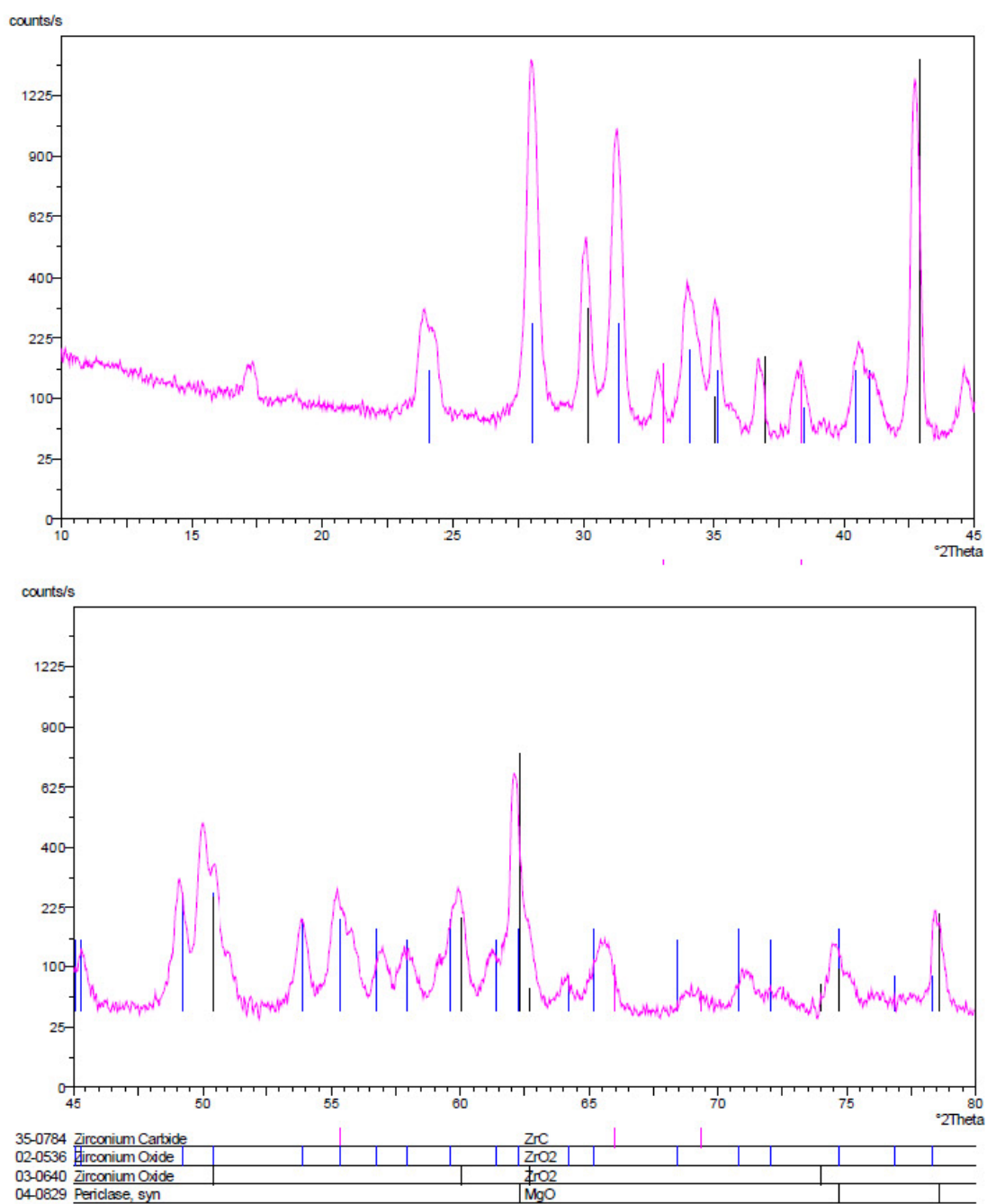


Figure 2.4.3 - XRD on the inorganic residue after pyrolysis at 1200°C under N₂.

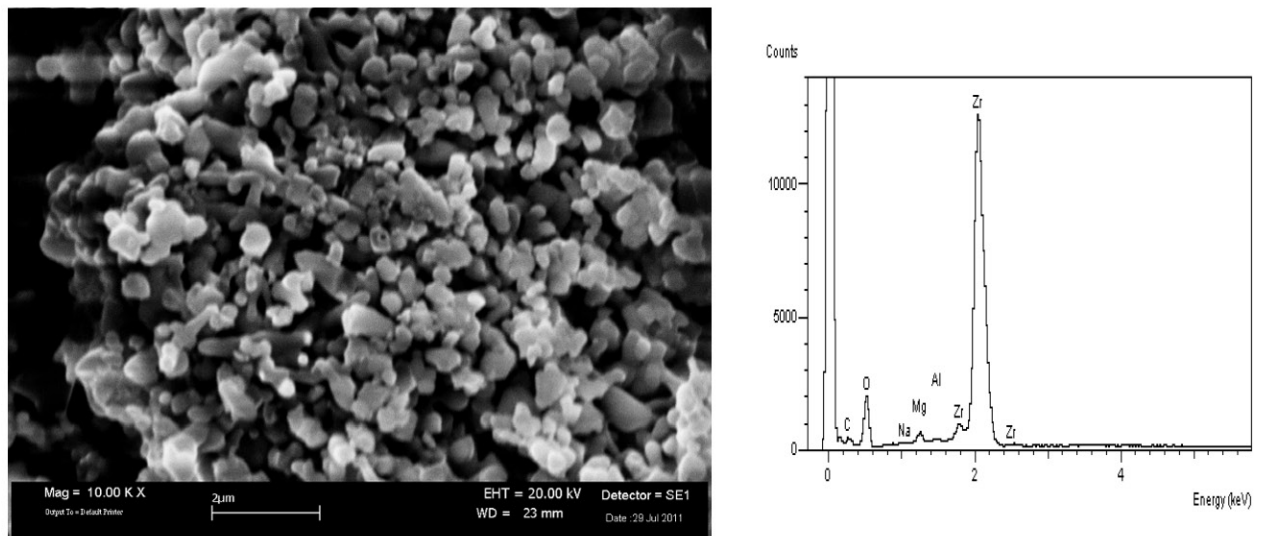


Figure 2.4.4 - SEM micrograph and EDS spectra, taken into an area rich of Zr.

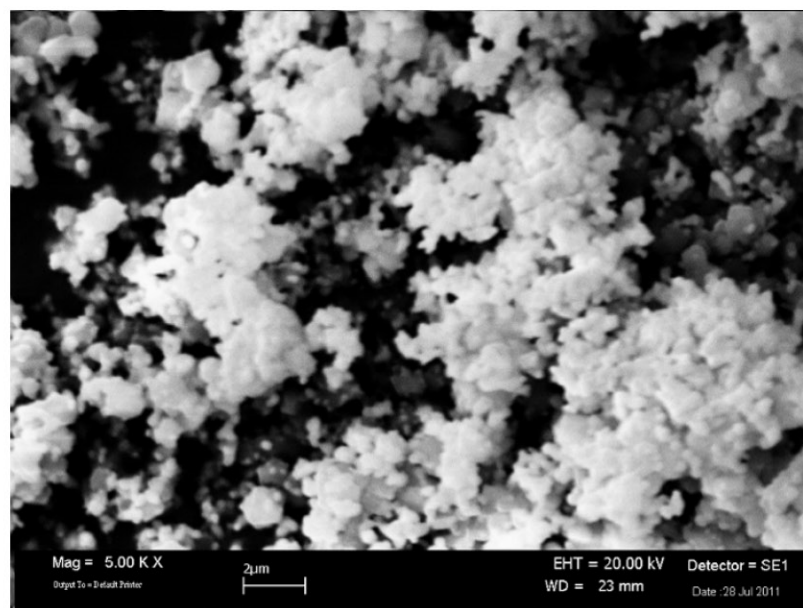


Figure 2.4.5 - SEM micrograph taken into an area of the residue rich of Mg.

2.4.3 Conclusion from the synthesis experiments

The experiment demonstrated the possibility of obtaining preceramic polymers with Grignard reactions, but with low purity and in small quantity. Aiming at developing processes of industrial interest, it was preferred to go on with the study of commercially available polymers, which, by the way, can be effectively modified using active and passive fillers.

In particular this last study would be particularly interesting to obtain innovative (but nevertheless low cost) formulations, without starting the challenging development of new synthetic routes for new preceramic polymers.

CHAPTER 3. PIP OF POLYCARBOSILANES

3.1 First assessment of performances of PIP pilot plant with PCS

Since the pyrolysis temperature in our PIP pilot plant is limited, by the AISI stability, to an operational temperature of about 925°C, the performance with polycarbosilanes (PCS), which are normally pyrolysed above 1000°C, had to be assessed [58]. As a first study, we compared the thermostructural properties and microstructures obtained using UBE polymeric precursors as a function of pyrolysis temperature. The two pyrolysis conditions which were compared were 900°C in the AISI furnace, and 1000°C in a graphite furnace, both under nitrogen flow.

3.1.1 Materials and methods.

Commercial UBE preceramic precursor (Tyranno polymer VL-100, diluted in xylene) of a SiC ceramic matrix (with 11 wt% O and 2 wt% Ti) was used to infiltrate 100 x 85 x 3 mm³ SiC felts (Tyranno ZM fibers, diameter 14 microns, 270 g/m², with 9 wt% O and 1 wt% Zr).

The above SiC felts (100x85x2 mm³) were pretreated by CVI (Chemical Vapour Infiltration) in order to deposit a pyrolytic carbon interphase (about 0.1 microns), necessary for increasing the composite toughness.

The felts were then submitted to 11 PIP cycles. Vacuum impregnation was obtained by dipping the preform into the polymer solution and by degassing the preform under vacuum. Drying of the solvent (xylene) was carried out by heating between 60°C and 90°C, first under vacuum and then in an explosion-proof heating oven.

Pyrolysis was performed, under nitrogen flow, in two different conditions:

- 1) at 1000 °C for 60 min;
- 2) at 900 °C for 120 min.

Pyrolysis at 1000°C was performed in a graphite furnace. Pyrolysis at 900 °C was performed in a AISI 310S austenitic steel furnace. A 2h-final thermal treatment at

[58] C Mingazzini, A. Brentari, E. Buresi, F. Burgio, M. Scafè, L. Pilloni, D. Caretti, D. Nanni, "Optimization of a pyrolysis procedure for obtaining SiC-SiCf CMC by PIP for thermostructural applications CIMTEC 2012 - 4th International Conference "Smart Materials, Structures and Systems" Montecatini Terme, Tuscany, Italy, June 10 - 14, 2012.

1200°C under inert atmosphere in a graphite furnace was done in both cases. Geometric density was monitored during the densification. Mechanical characterisation (bending tests at room temperature) and helium pycnometry were performed after 11 PIP cycles. The results were used to compare the influence of pyrolysis temperature on densification.

3.1.2 Thermogravimetric analysis

Thermogravimetric investigations were performed on the preceramic polymer in order to verify suitable pyrolysis temperature and procedure. In the following figure, TG registered at different ramp rates are reported (ramp 10°C/min, black, and 20°C/min, red). The results indicated that at 900°C pyrolysis should be complete (figure 3.1.1) and that the ceramic residual solid (i.e. the ceramic yield) decreases significantly with increasing ramp rate. Literature suggests slow pyrolysis rates, e.g. 100°C/h. However, as a compromise between efficiency and production time, a ramp rate of 300°C/h (the maximum value possible with the AISI furnace) was chosen. This choice was made also because 300°C/h was the minimum ramp rate that could be applied with the graphite furnace in order to avoid unsupervised overnight operation, which, in the case of graphite, water-cooled furnaces, may involve some safety problems.

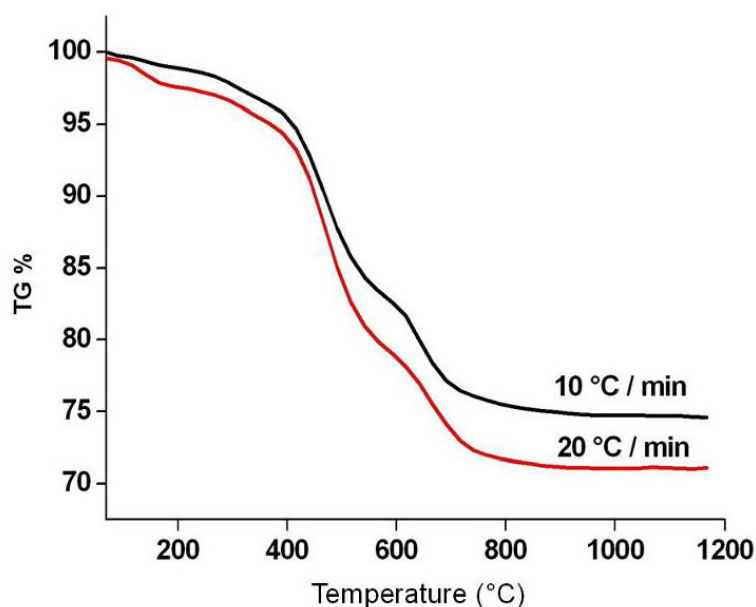


Figure 3.1.1 - TG of the polymeric precursor. Ramp rate of 10°C/min (black) and 20°C/min (red), under argon atmosphere.

In order to determine if there is un-pyrolysed polymer after the two adopted pyrolysis procedures, powdered samples of the resulting ceramic matrix were treated under inert atmosphere (Ar) up to 1200°C, and then kept 30 min in air at 1200°C, to study oxidation resistance. Residual unpyrolysed phase was around 0.1 wt% after 1h pyrolysis at 1000°C, and around 1wt% after 2h pyrolysis at 900°C (figure 3.1.2). Subsequent oxidation in air at 1200°C produces a slight weight gain due to conversion of SiC to SiO₂ (0.1-0.2 wt% in the case of a pyrolysis temperature of 900°C). XRD was performed on the ceramic matrix obtained at 900°C (P900) and 1000°C (P1000), before and after the TGs at 1200°C, establishing that (figures 3.1.3 and 3.1.4) a thermal treatment at 1200°C is needed in order to convert the ceramic matrix to β -SiC. In addition, the ceramic matrix obtained at lower temperature appears to have a lower oxidation resistance, as the broad peak at $2\theta = 20^\circ$ indicates, not being present on P1000 after the same thermal treatment at 1200°C in air [59].

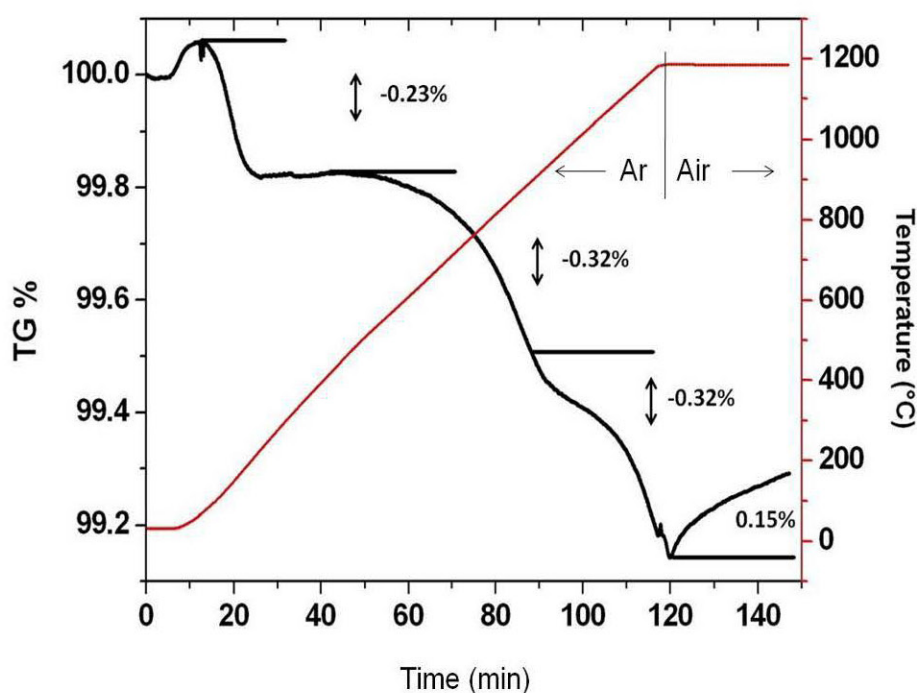


Figure 3.1.2 - TG of the residual ceramic obtained after 2h pyrolysis at 900°C (P900). Ramp rate 10°C/min in argon up to 1200°C, followed by a 30 min isotherm at 1200°C in air.

[59] Ming Luo, Yawei Li, Shengli Jin, Shaobai Sang, Lei Zhao, "Oxidation resistance of multi-walled carbon nanotubes coated with polycarbosilane-derived SiC_xO_y ceramic", *Ceramics International*, 37 (2011) 3055–3062.

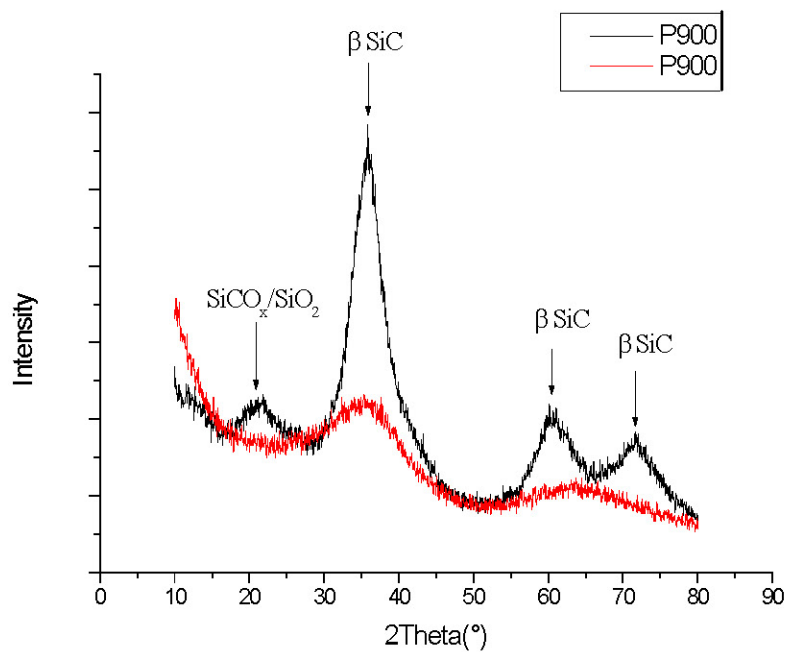


Figure 3.1.3 -XRD on P900, before (red) and after (black) the TG at 1200°C (Ar/Air).

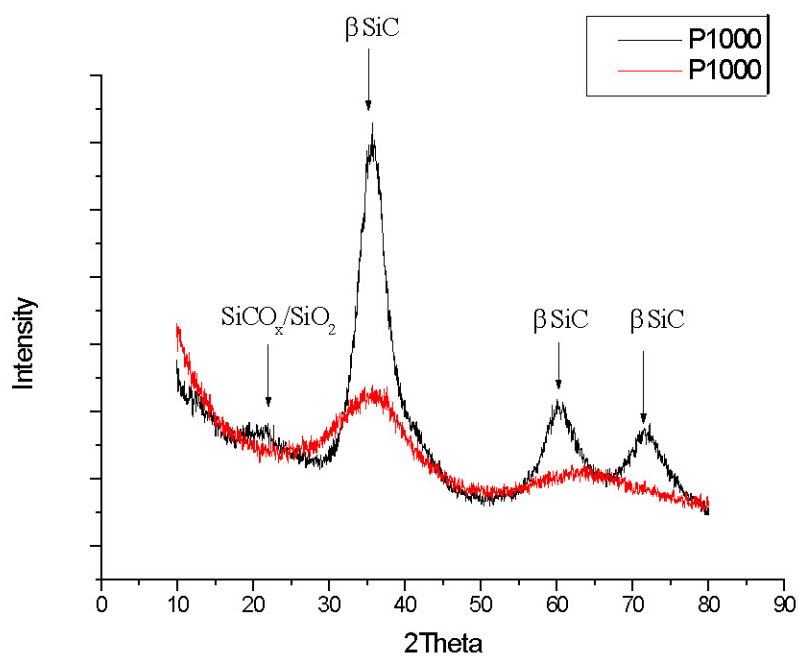


Figure 3.1.4 - XRD on P1000, before (red) and after (black) the TG at 1200°C Ar/Air).

XRD was also registered on crushed CMCs produced by PIPs at 900°C and 1000°C, after the final consolidation treatment at 1200°C under nitrogen (figure 3.1.5), confirming the previous observations.

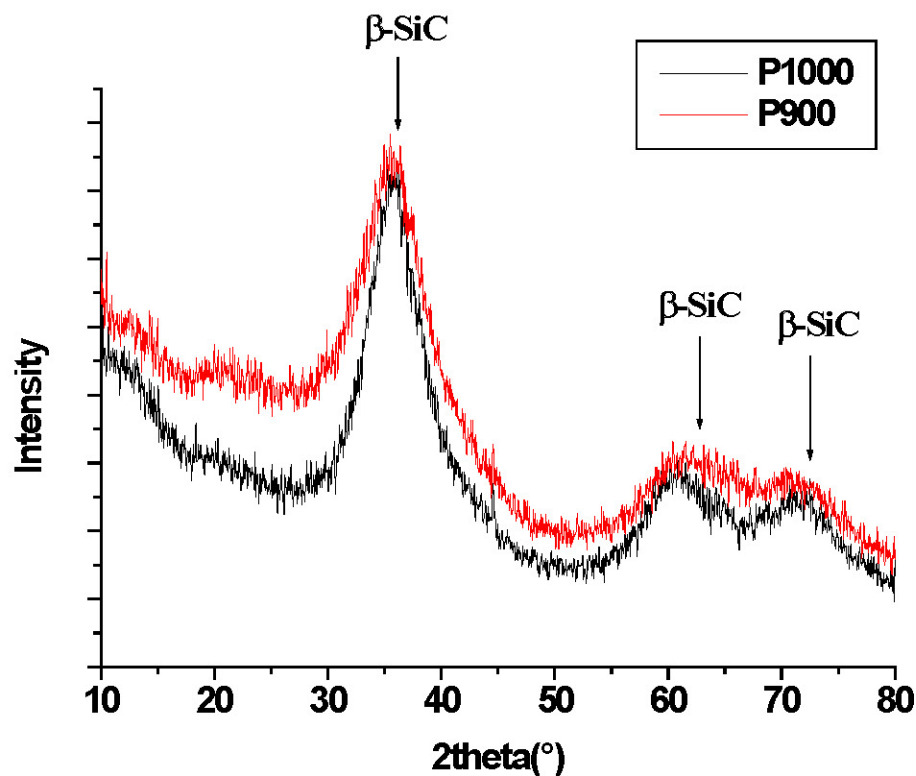


Figure 3.1.5 - XRD of crushed CMCs produced by PIPs at 900°C and 1000°C, after the final consolidation treatment at 1200°C under nitrogen.

3.1.3 Microstructural and morphological characterisation

Weight gain during PIP densification is reported in the figure 3.1.6. The initial weight of the felts was around 2 g, so fibers represent only 4.5 wt% of the final CMC (since it weighs less than 45 g). The yield for ceramic formation was around 30 wt% of the initial polymer mass, at both temperatures. After 11 PIP cycles, standard samples for the mechanical characterisation were cut, using a diamond wire saw. Geometric density and total porosity were determined: geometric density is significantly lower for the CMC produced at 900°C: 1.23 g/cm³ against

1.38 g/cm³. Theoretical density for this matrix is 2.48 g/cm³ [60], so relative density obtained was, respectively, 50% and 56%. These results were confirmed by helium pycnometry, which indicates that the porosity is almost completely open. SEM investigations (figures 3.1.7 and 3.1.8) were performed in partial vacuum conditions, because the high porosity value affects negatively the “charging effects” also on a SiC matrix, which is one of the ceramic phases with higher electronic conductivity. The observations on P900 (figure 3.1.7) and on P1000 (figure 3.1.8) didn’t show significant morphological or microstructural differences, being the homogenously distributed presence of cracks the most unexpected characteristic. Macropores are distributed homogenously across the 3 mm-thick sample section, with a pore size which is generally between 300 and 400 μm. The pyrolytic carbon interphase appears to be effective in making the fiber pull-out possible, essential for the desired “pull-out mechanism”.

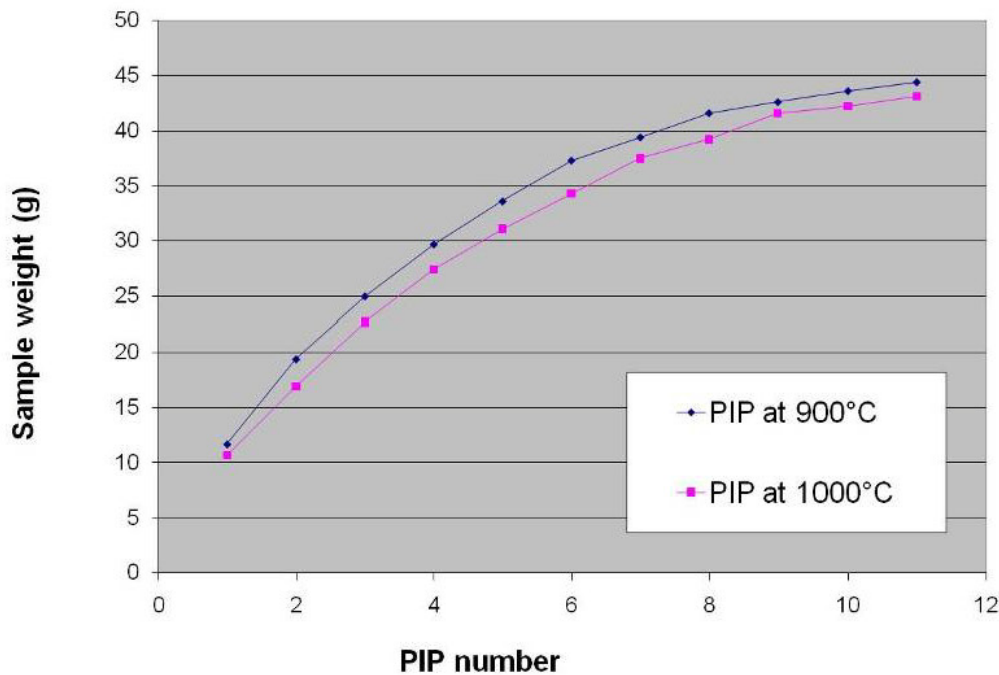


Figure 3.1.6 - Weight change of the CMCs during the 11 PIP infiltrations.

[60] T. Mamiya, Y. Kagawa, Y. Shioji, M. Sato, T. Yamamura, “Tensile Fracture Behavior and Strength of Surface-Modified SiTiCO Fiber SiC-Matrix Minicomposites Fabricated by PIP Process”, J. American Ceramic Society, 83, 2 (2000) 433–435.

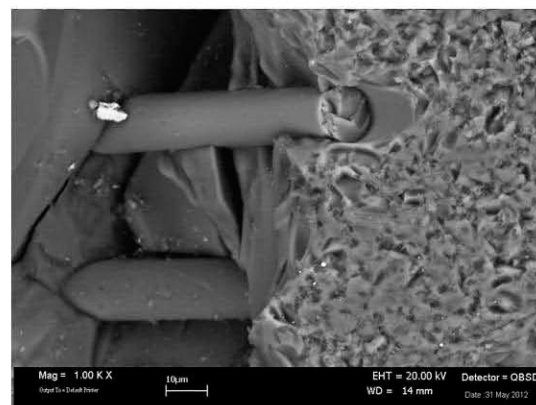
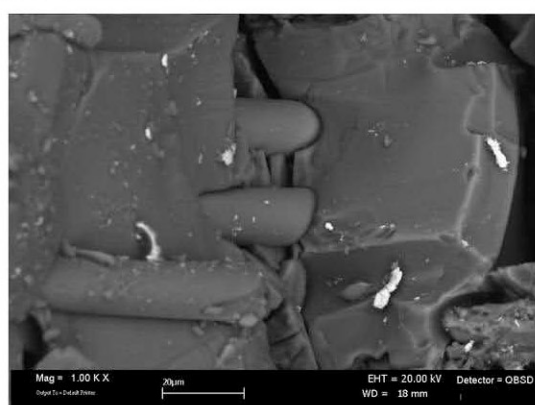
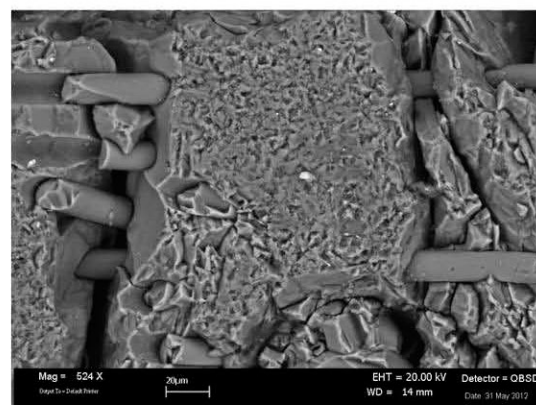
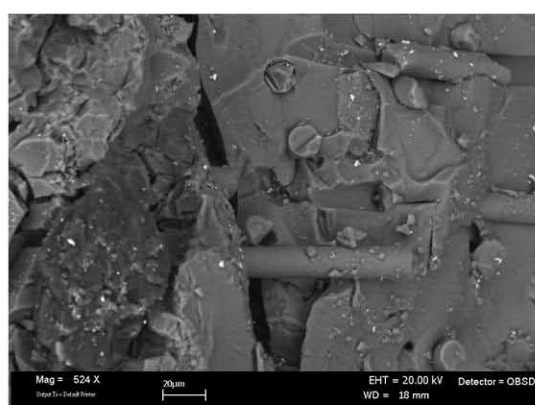
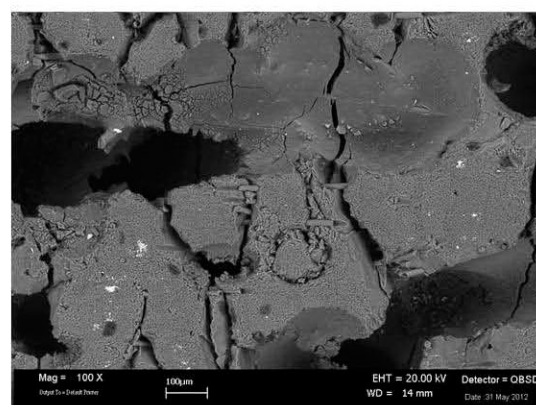
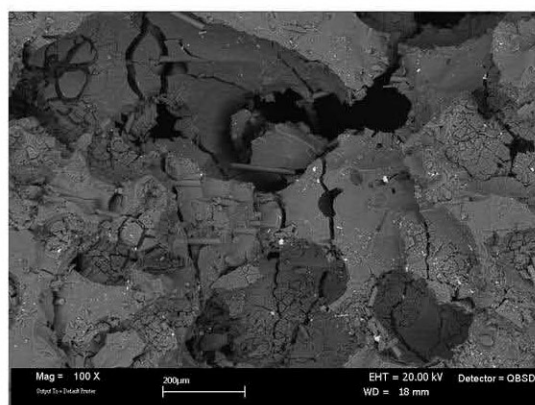
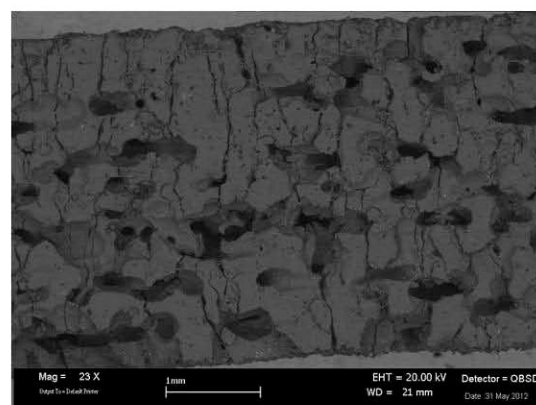
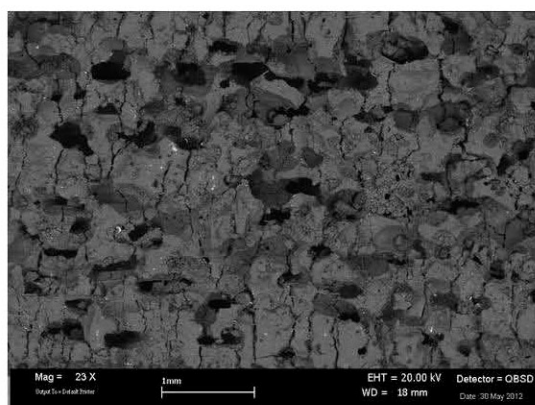


Fig. 3.1.7 - Morphology and microstructure of the PIP CMC produced at 900°C.

Fig. 3.1.8 - Morphology and microstructure of the PIP CMC produced at 1000°C.

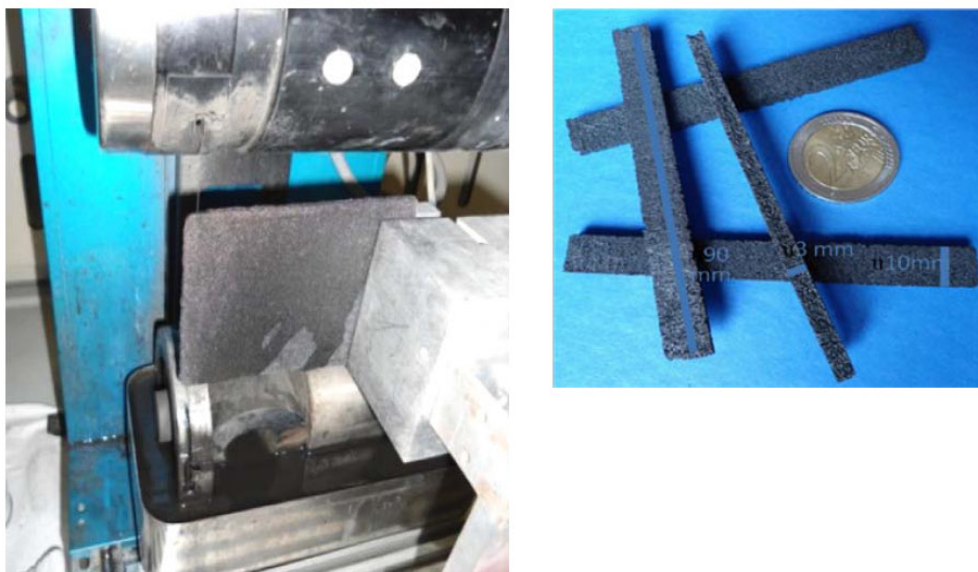


Figure 3.1.9 - Standard samples used for four-points bending tests prepared using a diamond wire saw.

3.1.4 Mechanical characterisation

As stated before, the bending strength tests were performed after cutting standard samples with a diamond wire saw (figures 3.1.9 and 3.1.10). The obtained results were the following: 4.5 MPa for the CMC produced at 900°C and less than 3 MPa for the CMC produced at 1000°C. Considering the difference of relative density, CMC produced at 1000°C would have been expected to have an higher bending strength, because, generally, CMC bending strength is favoured by higher densification. Probably microcracking that can be seen all across the matrix plays a very important role in determining these mechanical results. Cracks in the matrix are probably produced during PIP process as a consequence of the strong volume reduction, which accompanies the conversion of the preceramic polymer into the ceramic matrix, and, possibly, because of a too high pyrolysis ramp rate. In order to verify the critical role of these cracks, they should be sealed using the CVI technique and then the bending tests repeated. This can be obtained by performing a CVI deposition at a very low deposition rate. In this way, the macropores would be practically unaffected.

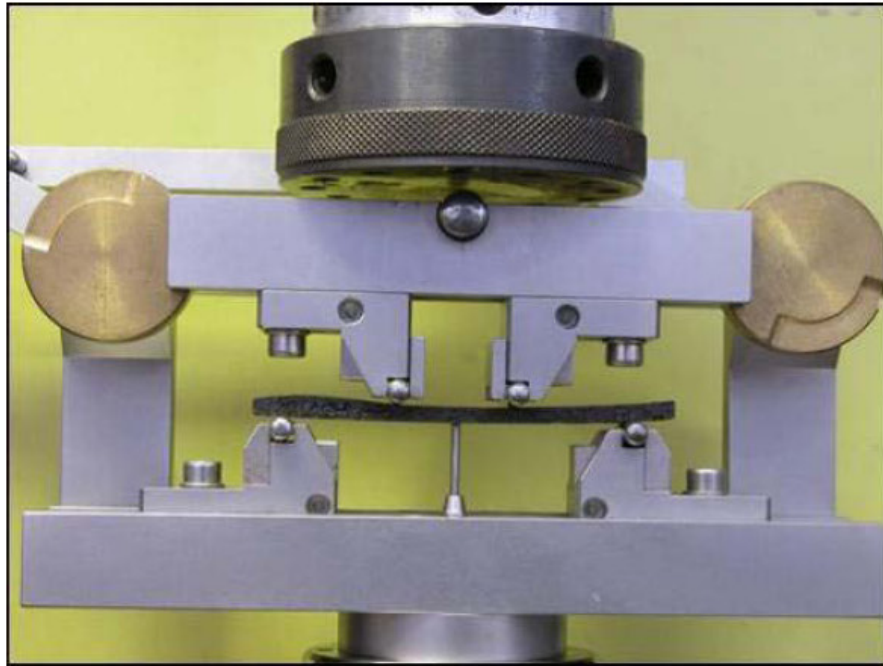


Figure 3.1.10 - Four-point bending tests apparatus, used for MOR (modulus of rupture) evaluations.



Figure 3.1.11 - Graphite furnace used for the final consolidation step at 1200°C, before the mechanical characterization.

3.1.5 Preliminary conclusions

The produced SiC_f / SiC Ceramic Matrix Composite (CMC) showed low mechanical properties, probably due to matrix microcracking and high residual porosity. However there were not unfavorable consequences of a pyrolysis temperature of 900°C, which could be more interesting for an industrial production. In fact, CMC obtained with a lower pyrolysis temperature has a lower relative density but higher bending strength. Since bending strength should be higher for higher values of relative density, the results depend probably on matrix microcracking. The origin of the observed microcracking could be the high pyrolysis ramp rate chosen.

However the obtained relative density of the produced CMC was far lower than the expected in both cases (50 and 56% respectively at 900°C and 1000°C) and further investigations are needed. Large pores (around 300-400 µm) can be seen across the 3 mm-thick sample section. Besides, to obtain higher densities, preforms must necessarily be evacuated before adding the polymer solution, an operation which cannot be easily done and automated for the production of large objects and on complex shapes. The polymer consumption and its costs were higher than expected.

3.2 Further development of the PCS pyrolysis in the ENEA pilot plant

In a further attempt to overcome the serious problems shown by the first experiments, the process was further investigated during the first months of the third year. In particular it resulted that the polymeric precursor was affected by a problem of foaming, which occurs at low temperature (below 400°C) making really difficult to achieve high densification. To summarize, in order to increase the densification rates it was tested (useless)

- changing pyrolysis temperature (900-1000°C)
- changing pyrolysis rate (30-600°C/h)
- the use of antifoaming and inorganic additives

but, again, after 11 PIP steps still the relative density was around 50%. The only effective way which it was found capable of improving this very unsatisfying results was increasing the fiber density, by pressing together several SiC felts. In this way it was possible to obtain a similar relative density (44%) but with only 2

PIP steps. Moreover the mechanical properties were significantly improved (see figure 3.2.4) [61]. The microstructure is shown in figure 3.2.3.

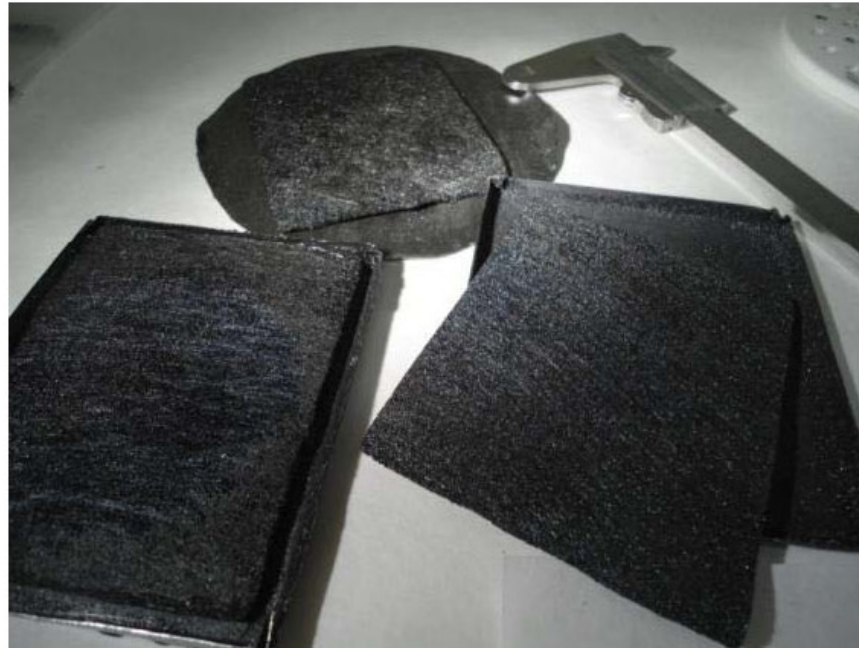


Figure 3.2.1 - Second series of impregnated SiC felts, with UBE SiC precursor.

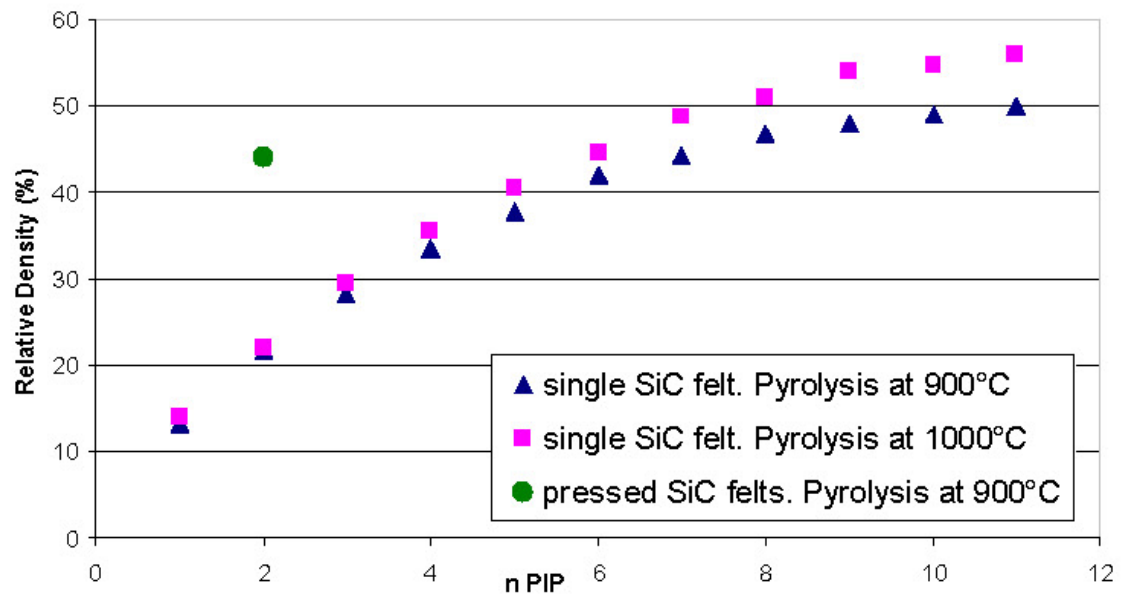


Figure 3.2.2 - Densification curves on pressed and non-pressed SiC felts.

[61] C. Mingazzini, A. Brentari, E. Burrelli, F. Burgio, E. Salernitano, M. Scafe, L. Pilloni, D. Caretti, D. Nanni, ECERS 2013, Limoges (France) 23-28 June 2013. Oral presentation. "Polymer Impregnation Pyrolysis for the cost-effective production of temperature resistant CFCCs".

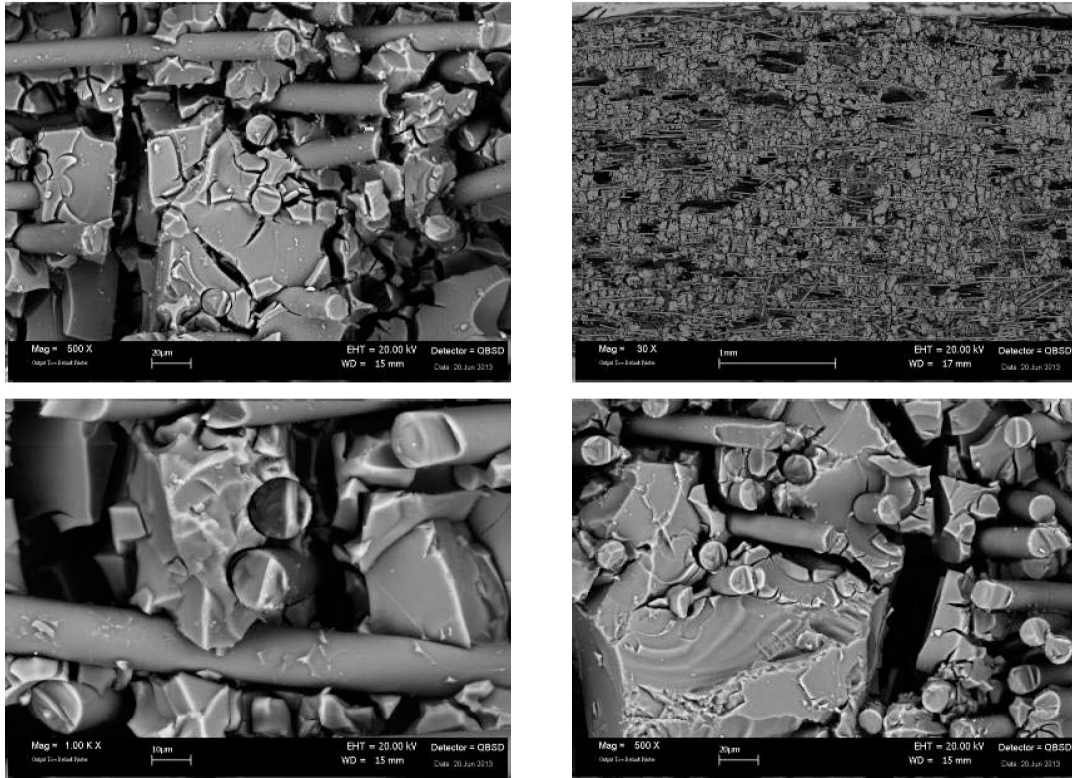


Figure 3.2.3 - Microstructure obtained by 2 PIP steps at 900°C, on pressed felts.

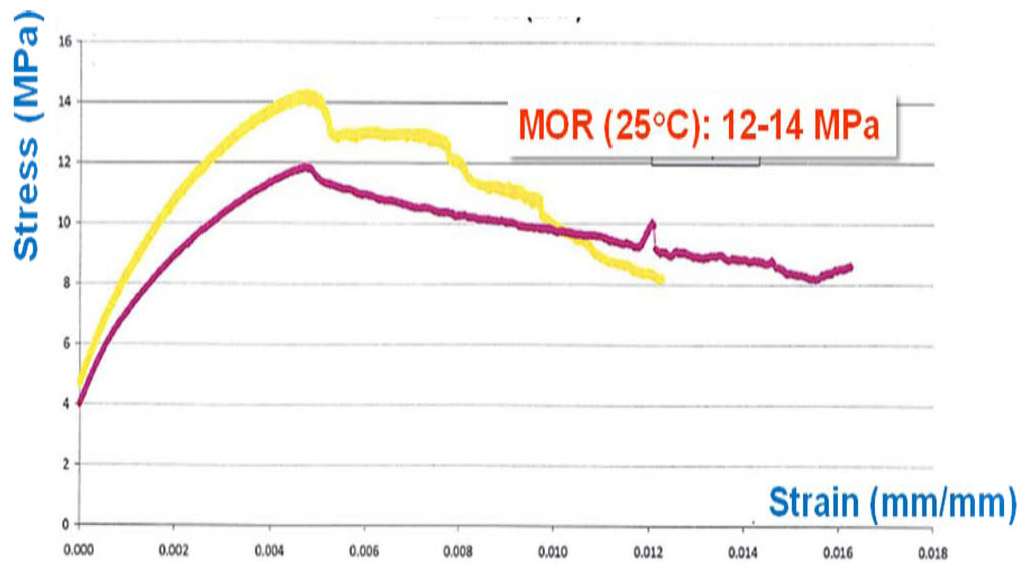


Figure 3.2.4 - MOR experiments at 25°C on the pressed SiC felts, after 2 PIPs.

Even if the mechanical performance is still far than being at the desired level, the improvement is evident: in figure 3.2.4, the four-point stress strain curves are reported for two standard samples, obtained with 2 PIP on 3 pressed SiC felts. The MOR values (modulus of rupture, that is the stress value at which the breaking of the composite starts) was of 12 and 14 MPa for the two samples considered, while

on non-pressed felts, after 11 PIP the maximum recorded MOR value was 4 MPa, even if the level of densification was roughly the same (around 50%). Also the behavior is pseudo-plastic, even if it is not sure this result is a consequence of CVI pyrolytic carbon interphase, or of the still too high porosity level.

3.3 Views and prospects

On the basis of these observations, the difference between the expected density evolution of SiC_f / SiC during PIP process and the experimental data make sense. Using SiC fabrics (like UBE did) would probably permit to reproduce their densification curve, but nevertheless the composite production costs would be too high for the automotive and construction field. So it was preferred to stop the investigation and move to a more suitable preceramic polymer, that is inexpensive silicones, easy to find and yet, according to literature and confirmed by our first experiments, really promising.

CHAPTER 4. PIP OF POLY SILOXANES

4.1 State of the Art

Silicon oxycarbide (SiOC) is another interesting and stable ceramic phase that it is easily produced by pyrolysis of preceramic polymers. Compared to silicon carbide, silicon oxycarbide (SiOC) is characterized by:

- superior oxidation resistance, thanks to a more efficient surface passivation [62-68];
- interesting mechanical properties at elevated temperature, even if lower than SiC [69-73];
- very much lower cost of the preceramic precursor.

As a bulk material, SiCO is a hard glassy material sometimes called "black glass" [74], because generally black, even if not necessarily [75], with properties intermediate between those of silica (SiO_2) and silicon carbide (SiC) [76]. It is

-
- [62] G.D Sorarù, D. Suttor, "High temperature stability of sol-gel-derived SiOC glasses", *J Sol-Gel Sci Technol.*, 14 (1999) 69-74.
- [63] M. Narisawa, R. Sumimoto, K. Kita, " Evaluation of oxidation resistance of thin continuous silicon oxycarbide fiber derived from silicone resin with low carbon content", *J. Mater. Sci.*, 45 (2010) 5642–5648.
- [64] J. Brus, F. Kolar, V. Machovic, J. Svitilova, " Structure of silicon oxycarbide glasses derived from poly(methylsiloxane) and poly[methyl(phenyl)siloxane] precursors ", *J. Non-Cryst. Solids*, 289 (2001) 62–74.
- [65] T.H. Xu, Q.S. Ma, Z.H. Chen, "High-temperature behavior of silicon oxycarbide glasses in air environment" *Ceram. Int.*, 37 (2011) 2555–2559.
- [66] G.M. Renlund, S. Prochazka, R.H. Doremus, *J. Mater. Res.*, 6 (1991) 2716–2734.
- [67] F. Kolar, V. Machovic, J. Svitilova, L. Borecka, *Mater. Chem. Phys.*, 86 (2004) 88–98.
- [68] Xu, T.H., Ma, Q.S., Chen, Z.H., "The effect of environment pressure on high temperature stability of silicon oxycarbide glasses derived from poly-siloxane", *Mater Lett.*, 65 (2011) 1538-1541.
- [69] H.J. Kleebe, Y.D. Blum, *J. Eur. Ceram. Soc.*, 28 (2008) 1037–1042.
- [70] P. Du, X.N. Wang, I.K. Lin, X. Zhang, *Sens. Actuators, A*, 176 (2012) 90–98.
- [71] Moysan, C., Riedel, R., Harshe, R., Rouxel, T., Augereau, F., "Mechanical characterization of a poly-siloxane-derived SiOC glass", *J Eur Ceram Soc*, 27 (2007) 397-403.
- [72] Xu, T.H. & Ma, Q.S. & Chen, Z.H., "Mechanical property and microstructure evolutions of C_f /SiOC composites with increasing annealing temperature in reduced pressure environment", *Ceram Int.*, 38, 1 (2012) 605-611.
- [73] Scarmi, A., Sorarù, G.D., Raj, G.D.R., "The role of carbon in unexpected visco(an)elastic behavior of amorphous silicon oxycarbide above 1273K", *J Non-Cryst Solids*, 351 (2005) 2238-2243.
- [74] Renlund GM, Prochazka S and Doremus RH. "Silicon oxycarbide glasses: part II. Structure and properties" *J Mater. Res.*, 6(12) (1991) 2723–2734.
- [75] Kim, K.J., Lee, S., Lee, J.H., Roh, M.H., Lim, K.Y., Kim Y.W., "Optical characteristics of crystalline silicon carbide nanoparticles synthesized by carbothermal reduction", *J Am Ceram Soc.*, 92 (2009) 424-428.
- [76] Burns, G.T., Taylor, R.B. & Xu, Y., Zangvil, A., Zank, G.A. "High-temperature chemistry of the conversion of siloxanes to silicon carbide", *Chem Mater.*, 4 (1992) 1313-1323.

widely studied both as a fiber material for CFCCs [77-80] and as a precursor for membranes [81,82], energy [83] and biomedical applications [84]. In addition to the basic formula SiCO, there are many similar compound within the formula SiMOC, with M corresponding to boron [85-88], aluminium [89], zirconium, etc., and the formula SiMOCN, easily obtained adding poly-silazane to poly-siloxanes [90-92]. One of the most used preceramic material is poly-dimethyl-siloxane, which is particularly interesting as a matrix material, in association with carbon [93] or silicon carbide fibers, for CFCC because of high ceramic yield (mass residue upon pyrolysis 87%, with a volume shrinkage less than 50%) and minimal

-
- [77] Kita, Kenichiro; Narisawa, Masaki; Nakahira, Atsushi; Mabuchi, Hiroshi; Sugimoto, Masaki; et. al., "Synthesis and properties of ceramic fibers from polycarbosilane/poly-methylphenylsiloxane polymer blends" *Journal of Materials Science*, 45, 13 (2010) 3397-3404.
- [78] Kita, Kenichiro; Narisawa, Masaki; Mabuchi, Hiroshi; Itoh, Masayoshi; Sugimoto, Masaki; et. al., "Formation of Continuous Pore Structures in Si-C-O Fibers by Adjusting the Melt Spinning Condition of a Polycarbosilane-Poly-siloxane Polymer Blend" *Journal of the American Ceramic Society*, 92, 6 (2009) 1192-1197.
- [79] L. F. Chen Z. H. Cai L. Zhang L. Lan X. J. Chen Jun Zeng, "Preparation and properties of silicon oxycarbide fibers", *Journal of Materials Science*, 42, 3 (2007) 1004-1009
- [80] E. L. Vishnyakova V. A. Lavrenko " Composition and structure of silicon oxycarbide fibers", *Powder Metallurgy and Metal Ceramics*, 45, 7-8, (2006) 301-303.
- [81] Biasetto, L., Francis, A., Palade, P., Principi, G., Colombo, P., "Polymer-derived microcellular SiOC foams with magnetic functionality", *J Mater Sci.*, 43 (2008) 4119-4126.
- [82] Duan, L.Q., Ma, Q.S., "Effect of pyrolysis temperature on the pore structure evolution of poly-siloxane-derived ceramics", *Ceram Int.*, 38 (2012) 2667-2671.
- [83] Konno, H., Morishita, T., Wan, C.Y., Kasashima, T., Habazaki, H., Inagaki, M., "SiCO glass-like compound/exfoliated graphite composites for negative electrode of lithium ion battery", *Carbon*, 45 (2007) 477-483.
- [84] Zhuo, R., Colombo, P., Pantano, C., Vogler, E.A., "Silicon oxycarbide glasses for blood-contact applications", *Acta Biomater*, 1 (2005) 583-589.
- [85] Schiavon, Marco A.; Armelin, Nádia A.; Yoshida, I. Valéria Pagotto, "Novel poly(borosiloxane) precursors to amorphous SiBCO ceramics", *Materials Chemistry & Physics*, 112, 3 (2008) 1047-1054.
- [86] Schiavon, M.A., Gervais, C., Babonneau, F., Soraru, G.D., "Crystallization behavior of novel silicon boron oxycarbide glasses", *J Am Ceram Soc.*, 87, 1 (2004) 203-208.
- [87] Sorarù, G.D., Pena-Alonso, R., Kleebe, H.J., "The effect of annealing at 1400°C on the structural evolution of porous C-rich silicon (boron) oxycarbide glass", *J Eur Ceram Soc.* 32 (2012) 1751-1757.
- [88] A. Tamayo R. Peña-Alonso F. Rubio J. Rubio J.L. Oteo "Synthesis and characterization of boron silicon oxycarbide glass fibers", *Journal of Non-Crystalline Solids*, 358, 2, (2012)155-162
- [89] Xu, T.H., Ma, Q.S., Chen, Z.H., "Structural evolution of Al-doped SiAlOC polymer in inert atmosphere", *Mater Lett.* 66, 1, (2012) 364-366
- [90] Schiavon, Marco A., Ciuffi, Katia J., Yoshida, I. Valéria Pagotto, "Glasses in the SiOCN system produced by pyrolysis of polycyclic silazane/siloxane networks" *Journal of Non-Crystalline Solids*, 353, 22-23, (2007) 2280-2288.
- [91] Schiavon, Marco A.; Domenico Sorarù, Gian; Yoshida, I. Valéria Pagotto, "Synthesis of a polycyclic silazane network and its evolution to silicon carbonitride glass", *Journal of Non-Crystalline Solids*, 304, 1-3, (2002) 76-83.
- [92] Schiavon, Marco Antônio; Sorarù, Gian Domenico; Yoshida, Inez Valéria Pagotto "Poly(borosilazanes) as precursors of SiBCN glasses: synthesis and high temperature properties" *Journal of Non-Crystalline Solids*, 348 (2004) 156-161.
- [93] Xu, T.H., Ma, Q.S., Chen, Z.H., "High-temperature behavior of C_f/SiOC composites in inert atmosphere", *Mater Sci Eng A*, 530 (2011) 266-270.

tendency to bubble formation. Even if also very simple and cheap commercial poly-siloxane precursors work really well, there is a huge research work done to decrease weight losses during cure and pyrolysis and to favor oxidative stability [94] and/or the formation of more compact ceramics morphology [95] or favorable stoichiometry [96-99]. A wide range of active fillers, from carbon and SiC [100] to metals [101] and silicides [102], may be used to modify the resulting ceramic [103]. For example it has been demonstrated that the incorporation of 5% boric acid to a mixture of vinyl-triethoxysilane and dimethyl-diethoxysilane to reduce the weight loss during cure and pyrolysis at 1000°C, following the typical thermal gradient for cure and pyrolysis shown in figure 4.1.1, decreasing from 19 to 14% weight loss [104].

-
- [94] F.I. Hurwitz M.A.B. Meador, "Tailoring Silicon Oxycarbide Glasses for Oxidative Stability", *Journal of Sol-Gel Science and Technology*, 14, 1 (1999) 75-86.
- [95] Parmentier, J., Sorarù, G.D., Babonneau, F., "Influence of microstructure on the high temperature behavior of gel-derived SiOC glasses", *J Eur Ceram Soc.*, 21 (2001) 817-824.
- [96] Liqun Duan, Qingsong Ma, Zhaohui Chen, " Preparation and characterization of mesoporous silicon oxycarbide ceramics without free carbon from poly-siloxane", *Journal of the European Ceramic Society* 33, 4 (2013) 841-846.
- [97] Belot, V., Corriu, R.J.P. & Leclercq, D., Mutin, P.H., Vioux, A., "Silicon oxycarbide glasses with low O/Si ratio from organosilicon precursors", *J Non-Cryst Solids*, 176 (1994) 33-44.
- [98] Xu, T.H., Ma, Q.S., Chen, Z.H., "The effect of aluminum additive on structure evolution of silicon oxycarbide derived from poly-siloxane", *Mater Lett*, 65, 3, (2011) 433-435
- [99] Pena-Alonso, R., Mariotto, G., Gervais, C., Babonneau, F., Sorarù, G.D., "New insights on the high-temperature nanostructure evolution of SiOC and B-doped SiBOC polymer-derived glasses", *Chem Mater.*, 19 (2007) 5694-5702.
- [100] Schiavon, Marco Antônio; Radovanovic, Eduardo; Yoshida, Inez Valéria Pagotto "Microstructural characterisation of monolithic ceramic matrix composites from poly-siloxane and SiC powder" *Powder Technology*, 123, 2-3, (2002) 232-241.
- [101] Tianheng Xu Qingsong Ma Zhaohui Chen, "The effect of aluminum additive on structure evolution of silicon oxycarbide derived from poly-siloxane", *Materials Letters*, 65, 3 (2011) 433-435.
- [102] Schiavon, M. A.; Yoshida, I. V. P., "Ceramic matrix composites derived from CrSi₂-filled silicone polycyclic network" *Journal of Materials Science*, 39, 14, (2004) 4507-4514.
- [103] Schiavon, M.A., Radovanovic, E., Yoshida, I.V.P., "Microstructural characterization of monolithic ceramic matrix composites from poly-siloxane and SiC powder", *Powder Technol.*, 123 (2002) 232-241.
- [104] Adam Strachota, Martin Černý, Zdeněk Chlup, Miroslav Šlouf, Jiřina Hromádková, Josef Pleštil, Hana Šandová, Petr Glogar, Zbyněk Sucharda, Martina Havelcová, Jana Schweigstillová, Ivo Dlouhý, Vladislav Kozák, "Optimization of sol-gel/pyrolysis routes to silicon oxycarbide glasses", *Journal of Non-Crystalline Solids*, 358 (2012) 2771-2782.

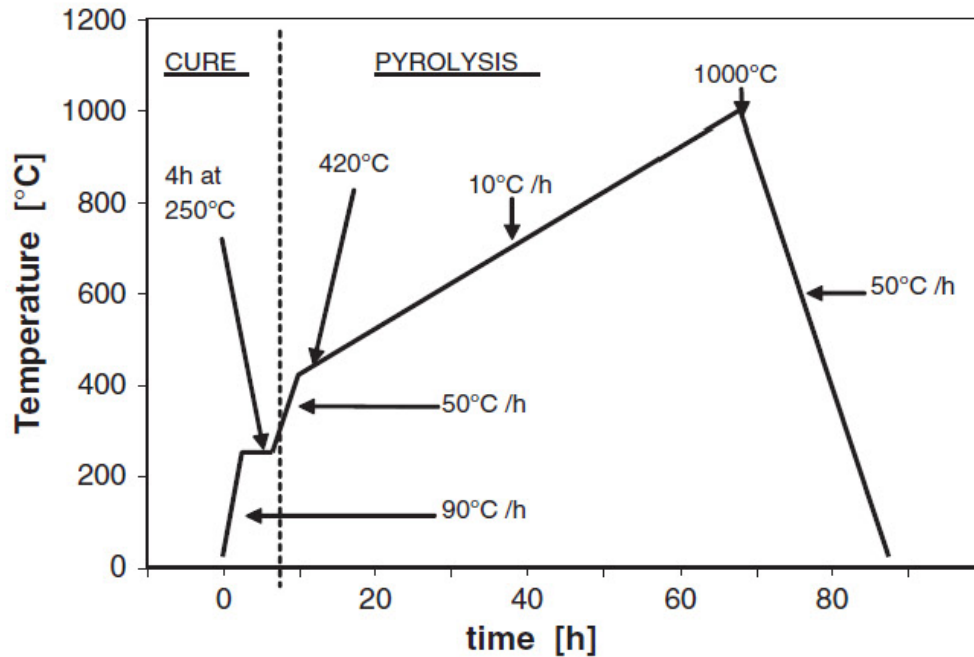


Figure 4.1.1 - Typical thermal gradient for cure and pyrolysis of poly-siloxanes.

Very interesting for the purpose of the current thesis are the articles in which poly-siloxanes is used for PIP on glass [105] and basalt [106-108] that it will be discussed in detail in the next paragraph. Ceramic oxide fibers could be too expensive for the application to automotive, being the cost at least 200 times higher than basalt fibers.

4.1.1 Basalt reinforced Silicon OxyCarbides

The association of SiOC matrix with silicate fibers could be particularly interesting for the automotive, thanks to the low cost of the fibers, their high oxidation resistance and their good thermostructural characteristics [109]. The literature demonstrates that the presence of iron oxide in basalt fibers leads to

[105] Cerny M, Glogar P, Sucharda Z, et al. "Properties and performance of poly-siloxane-derived ceramic matrix in heat resistant composites reinforced with R-glass or fineceramic fibres." *Ceram. Silikaty*, 49, 3 (2005) 145–152.

[106] M. Cerny, P. Glogar, Z. Sucharda, Z. Chlup, J. Kotek, "Partially pyrolyzed composites with basalt fibres - Mechanical properties at laboratory and elevated temperatures", *Composites Part A*, 40 (2009) 1650-1659.

[107] P. Glogar, M. Cerny, Z. Tolde, *Acta Geodyn. Geomater.*, 4 (2007) 27–37.

[108] M. Cerny, P. Glogar, Z. Sucharda, *J. Compos. Mater.*, 43 (2009) 1109–1120.

[109] Martina Halasova, Zdenek Chlup, Adam Strachota, Martin Cerny, Ivo Dlouhy "Mechanical response of novel SiOC glasses to high temperature exposition" *Journal of the European Ceramic Society*, 32, 16 (2012) 4489-4495.

their favorable pull-out behavior [110], which increases fracture toughness and makes such composites highly attractive for mechanical applications.

Compared to basalt fibers, the association with Nextel oxide fibers is interesting for increasing maximum working temperature (good endurance in an oxidizing environment up to 1500°C) and mechanical performances [111]. Flexural strength of the pyrolyzed composites is between 150 and 250 MPa, and after 3 hours of annealing at 1200-1300°C the value slightly decreases, while it increases for annealing at 1500°C, as microstructural changes occurs. It is interesting that the relatively low Young's modulus of SiCO, enables the ceramic fibrous reinforcement to take over the prevailing part of the mechanical stress applied to the composite part under load [112]. One of the problems, however is the tendency to excessively strong fiber-matrix bonding, which should be reduced via the application of a coating [113] not to lose the advantageous pull-out effect, necessary to get high fracture toughness values [114].

Regarding the consideration that were made to choose the raw materials, in table 4.1.1 some interesting literature data (taken from Cerny et al works) are reported [115] about the pyrolysis of Lukosil products. On the basis of these data, Lukosil M130 (from Lučební závody Kolín) was chosen to be tested, because of high ceramic pyrolysis yield and low volume shrinkage (below 50%) together with the lowest price. It is sold diluted in a 50% w/w xylene solution at a price around 8 €/kg, even for quantities below 20 kg, that sounded quite reasonable. In the same article, the experimental values of basalt fiber tensile modulus degradation with temperature are reported.

[110] M. Cerny, Z. Sucharda, A. Strachota, Z. Chlup, P. Glogar, *Ceram. Silik.*, 54 (2010) 345–351.

[111] Martin Cerny, Adam Strachota, Zdenek Chlup, Zbynek Sucharda1, Margit Zaloudkova, Petr Glogar1, Ivo Kubena, "Strength, elasticity and failure of composites with pyrolyzed matrices based on poly-methylsiloxane resins with optimized ratio of D and T components" *Journal of Composite Materials*, 47, 8 (2013) 1055–1066.

[112] M. Černý, P. Glogar, "Young's modulus of ceramic matrix composites with poly-siloxane based matrix at elevated temperatures", *Journal of Materials Science*, 39, 6 (2004) 2239-2242.

[113] Carrere N, Martin E and Lamon J. "The influence of the interphase and associated interfaces on the deflection of matrix cracks in ceramic matrix composites", *Compos. Part A - Appl Sci Manuf.*, 31, 11 (2000) 1179–1190.

[114] Kerans RJ and Parthasarathy TA. Theoretical analysis of the fiber pull-out and push-out tests. *J Am Ceram Soc.*, 74, 7 (1991) 1585–1596.

[115] J. Militký, M. Černý, P. Jakš, V. Kovačič, Z. Sucharda, P. Glogar, "Composite materials with basalt fibre reinforcement and pyrolysed poly-siloxane matrix" *Acta Research Reports*, 17 (2008) 31-36.

Resin name and type	Before pyrolysis 1000°C		After pyrolysis 1000°C		Mass residue after pyrolysis	Volume shrinkage after pyrolysis
	Density (g/cm ³)	Young's modulus (GPa)	Density (g/cm ³)	Young's modulus (GPa)		
Lukosil M130; Poly-methylsiloxane	1.22	2.3	2.02	80	87%	47%
Lukosil L901; Poly- methylphenylsiloxane	1.19	2.6	1.95	80	82%	50%

Table 4.1.1 - Literature data about pyrolysis at 1000°C of some of Lukosil products.

The volume shrinkage, last column of the table, which appears to be a rather significant data for PIP experiments (even if it cannot be changed for a specific polymer) can be deduced from the formula:

$$\frac{\Delta V}{V_1} = 1 - \frac{\rho_1}{\rho_2} \left(1 - \frac{\Delta m}{m_1} \right)$$

where 1 refers to the starting state, after curing, and 2 to the finale state, after pyrolysis at 1000°C.

The choice of poly-methylsiloxane instead of poly-methylphenyl siloxane is supported by another work [116] where a higher oxidation resistance is reported for the M130 derived material, compared to that obtained from the L901 one. The same group, in another work, report some creep data [117], establishing that basalt fibers undergo creep above 600-650°C, which should be considered a limit temperature for thermostructural application with this type of fibers.

They also report many other interesting observations:

- at temperature below 1000°C the pyrolysis of poly-siloxane is not complete, nevertheless "partial pyrolysis" is enough for thermostructural performances;
- the pyrolysis ramp rate should be kept slow to avoid degradation of mechanical

[116] P. Glogar, Z. Sucharda, M. Cerný, S. Puchegger, H. Peterlik "Microstructure and mechanical properties of heat resistant composites reinforced with basalt fibres" *Ceramics-Silikáty*, 51, 4 (2007) 190-197.

[117] Martin Cerny, Petr Glogar, Zbynek Sucharda, Zdenek Chlup, Jiri Kotek, "Partially pyrolyzed composites with basalt fibres - Mechanical properties at laboratory and elevated temperatures", *Composites: Part A*, 40 (2009) 1650-1659.

- characteristics, due to cracking of the matrix, as consequence of tensile stresses;
- fracture toughness of the composite produced at 650°C is about $20 \text{ MPa}\cdot\text{m}^{0.5}$, which is indeed the highest value one should expect for a fiber reinforced CMC;
- flexural strength undergoes some degradation on exposure to high temperature, but some thermomechanical characteristics are kept;
- weight loss upon oxidation is moderate (1.2% after 240 h at 550°C).

Aiming at low production costs, generally the authors considered one PIP step, sometimes two [118]. Fracture toughness measures are reported also in other works of the same group [119] together with microstructural investigations of fiber pull-out, after treatment in hot air (650-750°C).

4.1.2 Curing of poly-siloxane resins

Other important information that can be deduced from the last cited work, and others [120], is that the curing (at 225-250°C, for 1-5h) doesn't require a protective atmosphere. Thermal curing guarantee the highest ceramic yield [121] and curing, like for PCS, is needed to minimise shrinkage, weight loss and crack formation during subsequent pyrolysis. The process has been monitored also using rather sophisticated and accurate techniques, so the proposed procedure for the thermal curing can be considered not to need further optimisation [122]. Some other authors use divinylbenzene as a cross linker [123], other tested photocuring [124], while more exotic methods (like lasers or ionizing radiations) are generally used only for particular applications, like obtaining fibers [125]. According to

[118] Černý, M., Glogar, P., Sucharda, Z. and Machovič, V. "Properties and performance of poly-siloxane derived ceramic matrix in heat resistant composites reinforced with R-glass or fine ceramic fibres, *Ceramics - Silikáty*, 49, 3, (2005) 145–152.

[119] P. Glogar, M. Cerny, Z. Tolde "Fracture behaviour of the basalt fibre reinforced composites with poly-siloxane-derived matrix" *Acta Geodyn. Geomater.*, 4 (2) (146) (2007) 27-37.

[120] L. Duan, Q. Ma, "Effect of Pyrolysis temperature on the pore structure evolution of polysiloxane-derived ceramics" *Ceramics International*, 38 (2012) 2667-2671

[121] Iseki T., Narisawa M., Katase Y., Oka K., Dohmaru T., Okamura K., *Chem. materials*, 13 (2001) 4163.

[122] P. Hron, M. Burian, S. Hytychova, A. Inneman, Z. Sucharda "Monitoring of curing process of siloxane resin by dielectric analysis" *Acta Geodyn. Geomater.*, 3(2) (142) (2006) 69-74.

[123] Q.-S. MA, Z.-H. Chen, W.-W. Zheng, H.-F. Hu, " Effect of pyrolysis processes on microstructure and mechanical properties of $\text{C}_f/\text{Si-O-C}$ composites fabricated by preceramic polymer pyrolysis" *Ceramics International*, 31 (2005) 305-314.

[124] S. Martínez-Crespiera, E. Ionescu, H.-J. Kleebe, R. Riedel, Pressureless synthesis of fully dense and crack-free SiOC bulk ceramics via photo-crosslinking and pyrolysis of a polysiloxane, *Journal of the European Ceramic Society*, 31 (2011) 913–919.

[125] B.V. Manoj Kumar, Young-Wook Kim, " Processing of polysiloxane-derived porous ceramics: a review" *Science and Technology of Advance Materials*, 11 (2010) 1-16.

Cerny's latest work [126], slowness and pressure application appear helpful during curing, but we could not apply pressure, we applied a slow ramp rate up to 250°C.

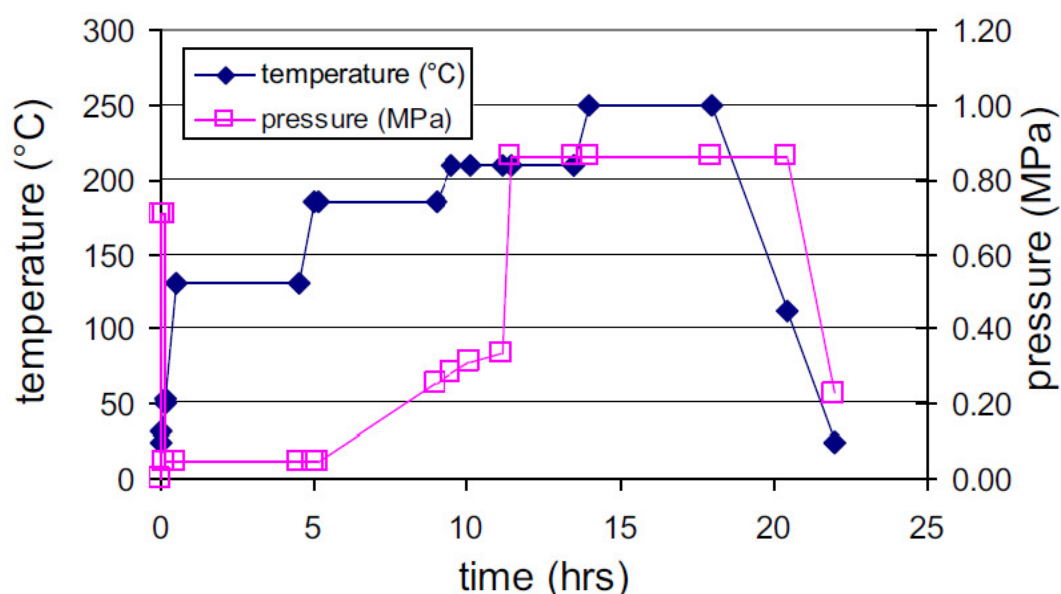


Figure 4.1.2 - Thermal and pressure gradient for curing of poly-methylsiloxanes.

4.1.3 Blackglas™ - Nextel™

In literature it was also found a patent of 1994 [127] in which the Silicon Oxycarbide matrix is used to infiltrate carbon preforms, and a lot of studies and applications about the association with Nextel fibers [128], with a $< 0.1\mu\text{m}$ boron nitride interphase (produced by heating at high temperature the Nextel fabrics in ammonia and hydrogen) to induce fiber pull-out. "Blackglas™" is registered trademark and is commercialized by Honeywell. A lot of accurate studies (by NMR) were done to study pyrolysis kinetics and resulting microstructure [129]. Anyway these solutions were developed for the space, military and aerospace

[126] M. Cerny, H. Halasova, S. Schwaigstilova, Z. Chlup, Z. Sucharda, P. Glogar, J. Svitilova, A. Strachota, R. Ryglova, "Mechanical properties of partially pyrolysed composites with plain weave basalt fibre reinforcement", DOI: <http://dx.doi.org/10.1016/j.ceramint.2013.12.102>, PII: S0272-8842(13)01718-5, to appear in: Ceramics International, 2014.

[127] Leung, R. Y., S. T. Gonczy, M. S. Shum, and J. J. Zupancic, "Carbon Containing Black Glass Monoliths," US 5328976 (1994).

[128] Stephen T. Gonczy, John G. Sikonia "Nextel™ 312/Silicon Oxycarbide Ceramic Composites", chap. 15, Handbook of Ceramic Composites. Edited by Narottam P. Bansal, Kluwer, 2005, ISBN 1420-8 133-2, pages 347-375.

[129] Joel L. Plawsky, Feng Wang, and William N. Gill, "Kinetic Model for the Pyrolysis of Polysiloxane Polymers to Ceramic Composites" Metallurgical and Materials Transactions A, 31 (2000) 911.

industry, and indeed they have a completely different targets, aiming at the highest performances, generally regardless the costs [130-132]. The composite system was successfully tested as a tail cone prototype in a jet engine test for over 1500 hours of cycle time, with a 30% weight reduction over the baseline metal design (Figure 4.1.3). This CMC system has potential applications in secondary structural components that require 600°C durability but also other similar, but more performing solution are being studied [133], in particular exploiting Nextel 610TM with fugitive coatings, for a working temperature which can reach 1000°C (UmoXTM).



Figure 4.1.3 - SiOC/Nextel 312 tailcone.

In conclusion, the number of works relevant to "Poly-siloxane Derived Ceramics" is really huge, much more than expected and, apparently, much more than about polycarbosilane. Moreover poly-siloxane derived matrix appears much more interesting aiming at the low cost production of composites for thermostructural applications in air, at temperature below 1000°C.

[130] Ali Youssefpoor, Mehrdad N. Ghasemi Nejjad, "Processing and performance of Nicalon/Blackglas and Nextel/ Blackglas using cure-on-the-fly filament winding and preceramic polymer pyrolysis with inactive fillers", *Composites Science and Technology*, 61 (2001) 1813–1820.

[131] Sriram Rangarajan, Ronald Belardinelli, Pranesh B. Aswath "Processing, physical and thermal properties of BlackglasTM matrix composites reinforced with NextelTM fabric" *Journal of Materials Science*, 34 (1999) 515–533

[132] W. Zhao, P.K. Liaw, R. Belardinelli, D.C. Joy, C.R. Brooks, C.J. Mchargue " Damage Mechanisms and Fiber Orientation Effects on the Load-Bearing Capabilities of a NEXTEL/BLACKGLAS Low-Cost Ceramic Composite", *Composites Science and Technology*, 61 (2001) 1813–1820.

[133] E. Volkmann, L. Lima Evangelista, K. Tushev, D. Koch, C. Wilhelmi, K. Rezwan, "Oxidation-induced microstructural changes of a polymer-derived NextelTM 610 ceramic composite and impact on the mechanical performance", *J Mater Sci.*, 49 (2014) 710–719.

4.2 Study of the pyrolysis of Poly-methylsiloxane

4.2.1 Materials and Methods

Following the above mentioned papers we chose to employ polymethylsiloxane resin, M 130 (Lučební závody Kolín), that is sold diluted in xylene, 50 wt% of polymer content, viscosity 30-50 mPa·s at 20°C; density 1.00-1.02 g/ml.

We used unidirectional fabrics from HG-GBF Basalt Fiber Co. LTD (<http://www.hg-gbfbasalt.com/it>), a company which collaborates with the ENEA in developing new basalt fiber applications, and from Mapei. However none of these companies provide 2D-basalt fabrics in quantities below 50 m², so we prepared some 2D-basalt fabrics by calcination of prepreg fabrics (courtesy of a local company, Riba Composites srl).

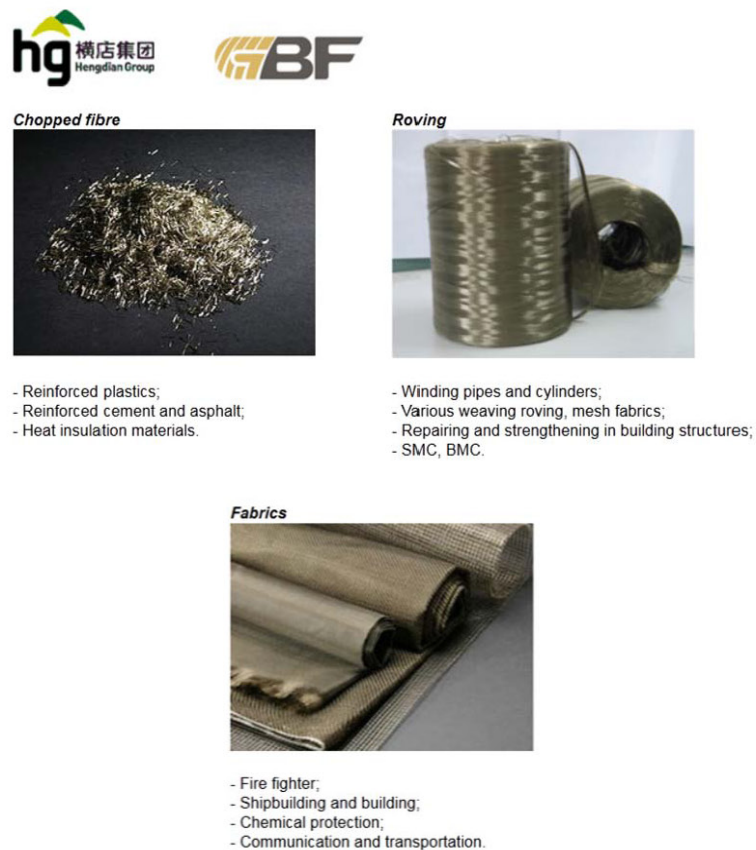


Figure 4.2.1 - Overview of HG-GBF basalt products and applications.

4.2.2 Thermogravimetric and mineralogical investigations

As usual, TG-DTA analysis were used to establish pyrolysis efficiency and pyrolysis temperature, and XRD to investigate ceramic phase formation and phase purity. One important result of the thermogravimetric study is the necessity of an appropriate curing, in order to get a good ceramic yield. As it is shown in figure 4.2.2, without a curing step, the ceramic yield drops from 85% to 76%. Different curing procedures were tested, applying different heating rates, both in air and in inert atmosphere, since, depending on the sample geometry, the easier and more practical procedure maybe different. The result of the optimum curing procedure requires a slow heating ramp (which can be performed indifferently in air or in inert atmosphere) and an isothermal step at 250°C of at least 10 hours. XRD on poly-siloxane M130 after drying, at temperature between 60°C and 90°C, and after curing (at 250°C) demonstrates a change in crystallinity (figure 4.2.3).

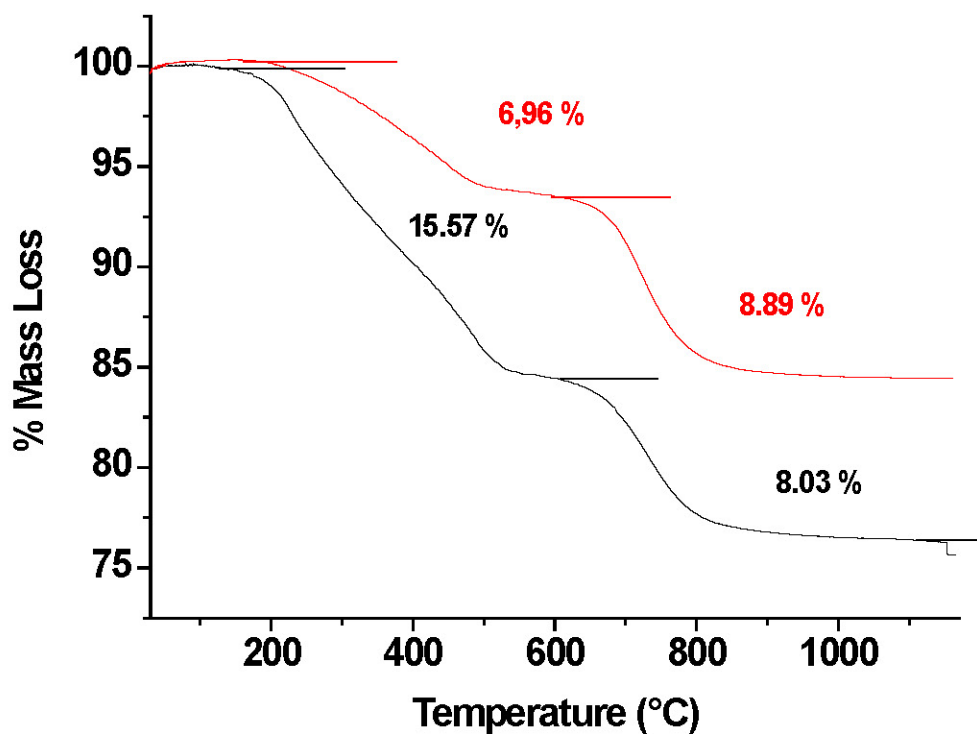


Figure 4.2.2 - TG after curing (red line) or after simple drying (black line).

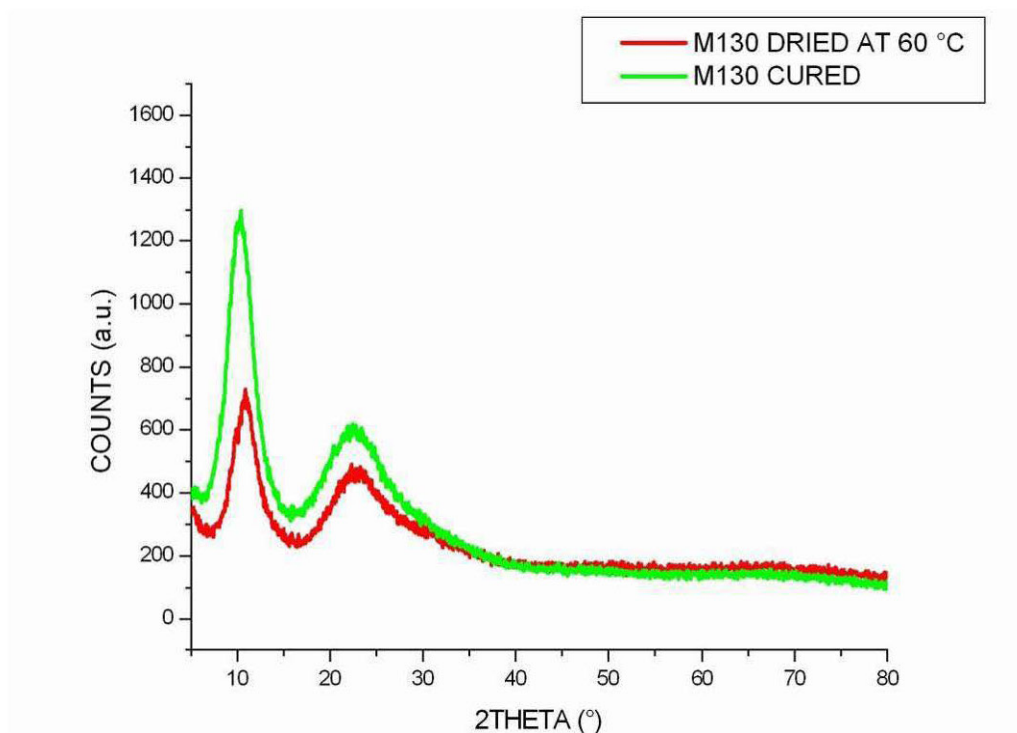


Figure 4.2.3 - XRD on poly-methylsiloxane after drying and after curing.

XRD of the "black glass" after pyrolysis at 1200°C and subsequent oxidation at 1200°C is almost identical, demonstrating high oxidation stability. The same result can be demonstrated by the weight change, which is very low for every pyrolysis temperature above 700°C.

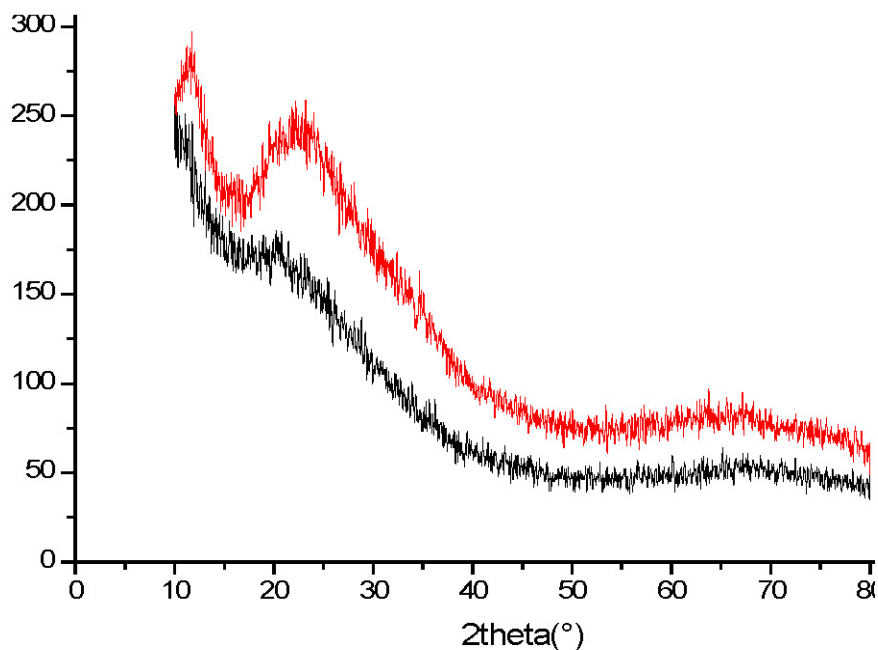


Figure 4.2.4 - XRD on pyrolysed M130, before (black line) and after (red line) oxidation treatment at 1200°C.

4.2.3 Design of the PIP composites

Based on the preliminary observations on the selected preceramic poly-methylsiloxane (Lukosil M130) and previous experimentations on polycarbosilane, regarding the design of the composites, three main "solutions" were investigated:

a) 2D carbon "plain" fabrics: 3, 6 and 15 plies. It was applied a process with 2 PIP steps at 900°C, into the PIP pilot plant, followed by a consolidation step at 1300°C.

b) Pressed SiC felts, 3 and 6 plies. In this case Py-C deposition was sometimes employed to fix the ply geometry, since it would be useless in the current case because of the reaction with SiCO to give SiC. 2 PIP steps were performed at 900°C in the PIP pilot plant, followed by a consolidation step at 1300°C. Similarly to previous experience on PCS, SiC felts potentially were even more interesting than fabrics, because much cheaper (being produced by UBE by electron spinning and being sold at about 2€ for a felt 10x10cm) and with a 3D structure. The results are discussed in the paragraph 4.3.

c) Basalt fiber reinforced CFCCs were prepared employing unidirectional and 2D fabrics. Pyrolysis was performed under nitrogen flow and under vacuum, at 700°C. The results are discussed in the paragraph 4.4.

Regarding solution a), the system was tested to get some preliminary experience on fabrics before going on to (very expensive) SiC fabrics, even if it was expected to produce a composite with fragile mechanical behaviour because of reaction, and subsequent strong adhesion, between the SiCO matrix and the carbon fabric. No mechanical data were collected, but the results were very interesting (thinking to a development with SiC fibers) because of:

- very much simpler processing, compared with unidirectional fabrics or pressed felts, due to the 2D fabrics mechanical stability;
- very high strength density (even if fragile) because of high density of fibers;
- very good aesthetic results (almost identical to typical PMC aspect).

Going on with solution a) would have been useless, because we were aiming at thermostructural application in air above 400°C, condition which couldn't be easily tolerated by carbon fabrics. However many works on these kind of composites are reported in literature [134] because of many interesting applications, for example in the field of space and aeronautics.

In all the above case, clenched steel moulds were used to press the felts or fabrics plies during the first pyrolysis step (both at 900 and 700°C). The moulds are needed to reduce deformation, increase fiber density and make it possible to obtain reproducible geometries since, according to literature, considerable shrinkage (up to 10%) and deformation (twisting and bending) could otherwise occur. In the subsequent steps the use of a steel mould was avoided, except as a support, because steel prevent the reaction between SiCO and the carbon paper.

The consolidation step at 1200°C was performed in a graphite furnace, only in the case of SiC fiber reinforcement. That would not be a problem even for an industrial production, since it is a rather "clean" step, involving only a little weight loss and gas evolution, which can be easily tolerated by graphite furnaces.

[134] Q.-S. MA, Z.-H. Chen, W.-W. Zheng, H.-F. Hu, " Effect of pyrolysis processes on microstructure and mechanical properties of C_f /Si-O-C composites fabricated by preceramic polymer pyrolysis" *Ceramics International*, 31 (2005) 305-314.

4.3 Study of the PIP process of poly-methylsiloxane on SiC pressed felts and fabric

4.3.1 PIP process of poly-methylsiloxane on pressed SiC felts

Two different solutions were considered in the case of PIP process of SiC felts with poly-methylsiloxane: 3 pressed felts and 6 pressed felts. The selected procedure was to infiltrate the felts, and then to squeeze out the excess of polymer with a steel device, equipped with four screws (figures 4.3.1 and 4.3.2).

The holes in the metallic plates make it possible the gas evolution during the pyrolysis and so the device can be kept during the composite processing at 900°C. After several exposition to temperature, the steel components shows only moderate evidence of degradation. The steel mould were used in carbon paper containers, which can be prepared very easily by paper folding and can withstand several PIP steps without damage (figure 4.3.3).

Regarding thermomechanical tests, the use of three pressed felts brought to composite sample 1-2 mm high, too thin and too flexible to be used for flexural tests. The relative density in this case was of 47%. This value of relative density was calculated as the ratio of the theoretical density, measured with the pycnometer, 2.62 g/cm³, and the geometrical density, 1.25 g/cm³. The fiber weight percentage in the CFCC was around 32% w/w.

On the other hand, the results that were obtained on solution using 6 pressed felts were quite interesting. Similarly to previous results with polycarbosilane, after 2 PIP steps at 900°C, it was obtained a relative density of 55%, calculated as the ratio of the theoretical density, measured with the pycnometer, 2.44 g/cm³, and the geometrical density, 1.35 g/cm³. The weight fiber density in the CFCC was around 16% w/w.



Figure 4.3.1 - Steel apparatus used to press the SiC felts, for the PIP process.



Figure 4.3.2- Steel moulds used for the production of CFCC with predetermined height.



Figure 4.3.3 - Folded carbon paper containers, used to avoid furnace contamination.

The MOR of this composite, which is 6 mm high, at room temperature and temperature up to 1000°C was evaluated, using bending tests. In the figure 4.3.4, two stress strain curves registered at room temperature and one at 1000°C are reported. Between 25 and 500°C the stress strain curves are almost the same, corresponding to MOR values between 15 and 18 MPa. The MOR values dropped at half of this value (8-9MPa) at 1000°C. As before, these flexural tests were performed after a consolidation step at 1200°C. In this case, the SiC felts had not

been pretreated with pyrolytic carbon, since it would be useless since C would react with the SiCO to give silicon carbide. However the mechanical behaviour is pseudo-plastic.

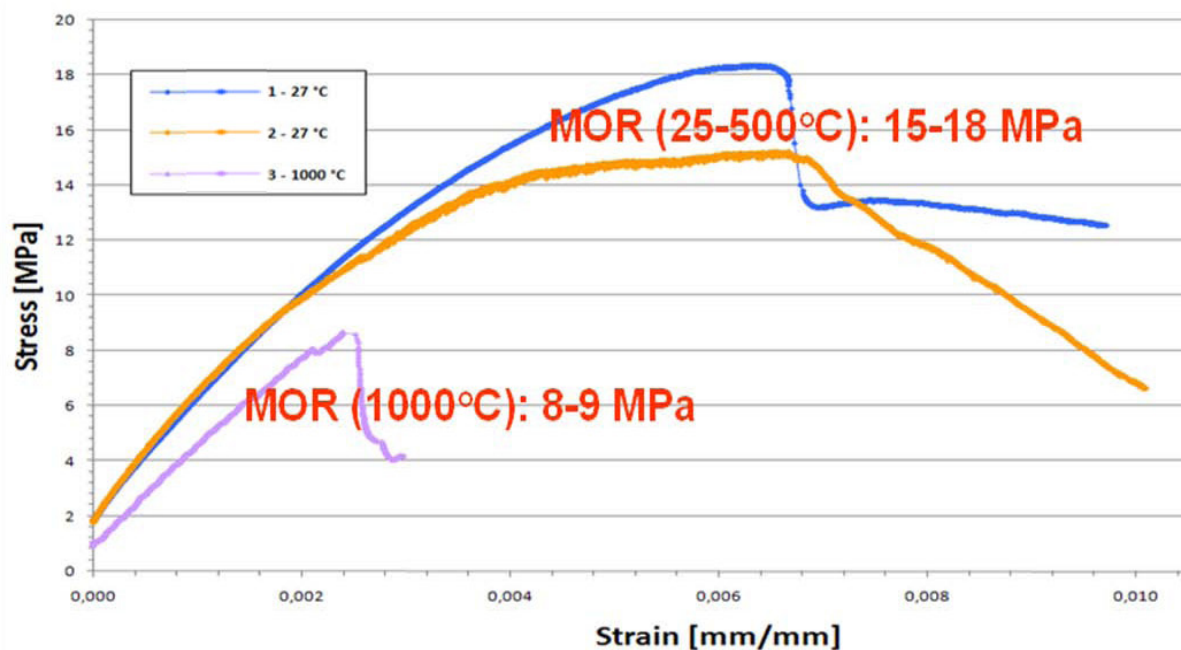


Figure 4.3.4 - Stress strain curves and MOR values (vs T) on the 6 pressed SiC felts, after 2 PIP steps with poly-siloxane.

In figures 4.3.5 and 4.3.6 the microstructure of the composite in the two cases is shown, and some pull-out indications can be seen, which is coherent with the mechanical behaviour.

These results are very promising (pseudo-plastic behaviour and only 50% MOR decrease between 25° and 1000°C) especially considering that the polymer is unexpensive and very fluid. Further increasing fiber density (which is possible using fabrics instead of felts) will certainly increase the absolute values of MOR, producing thermostructural composites which can be used up to 1200°C. These experimental work will be done as soon as possible.

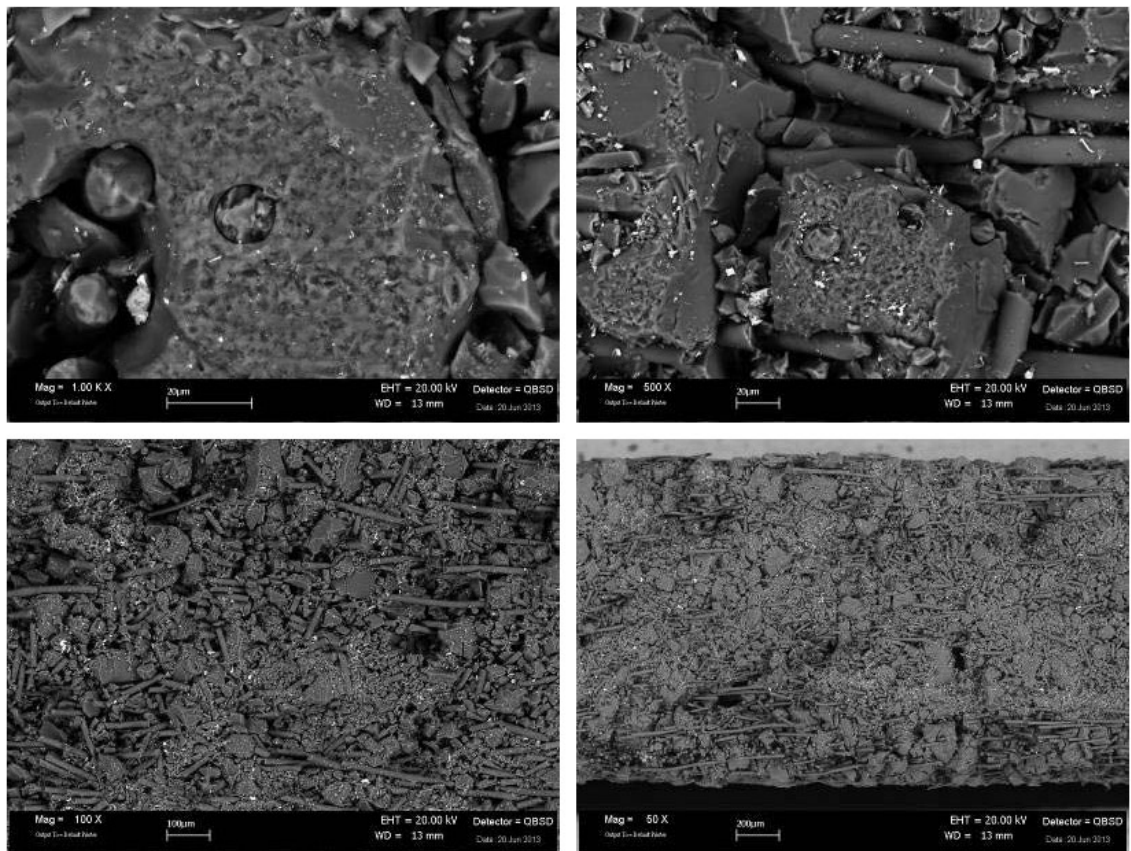


Figure 4.3.5 - Microstructure obtained by 2 PIP steps at 900°C, on 3 pressed felts.

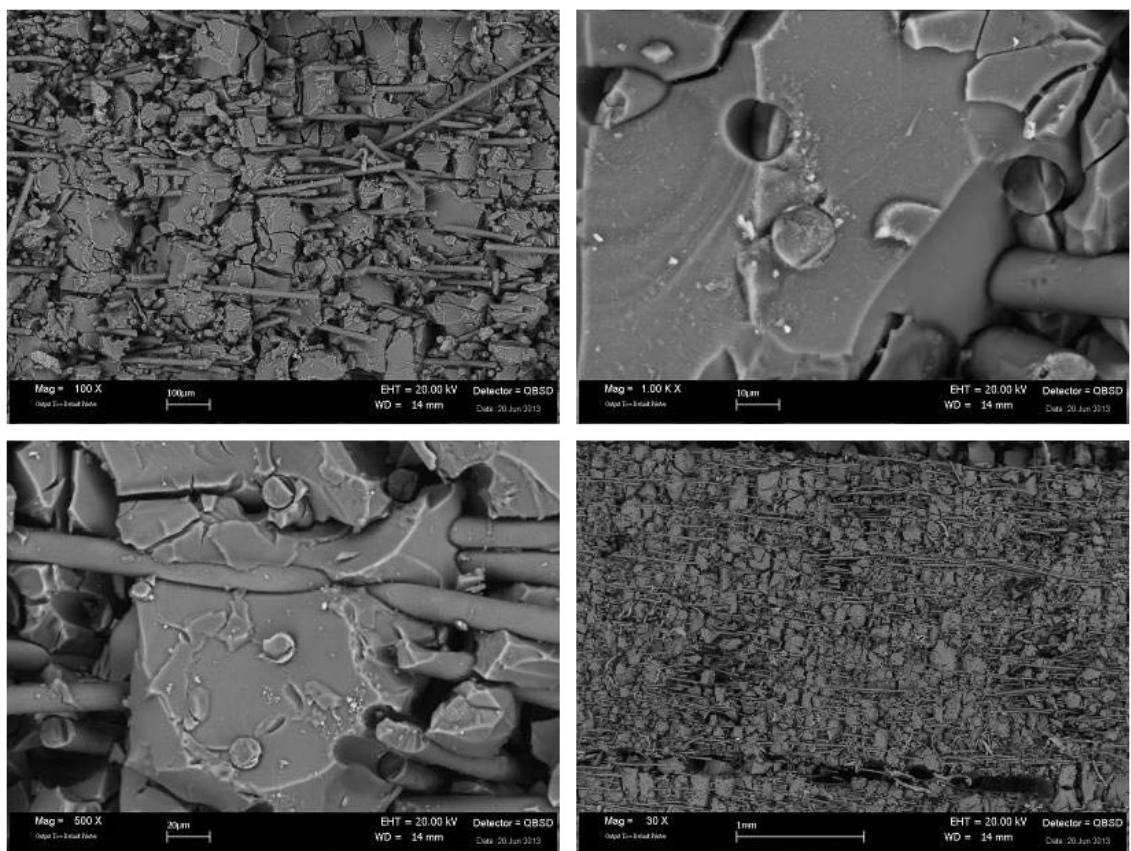


Figure 4.3.6 - Microstructure obtained by 2 PIP steps at 900°C, on 6 pressed felts.

As a comparison, PIP process with poly-methylsiloxane has been also performed on one unpressed felt. In this case the procedure was the following:

- the felt was impregnated with UBE PCS precursor and pyrolysed at 900°C to obtain a low density sponge of SiC fibers;
- then 4 infiltration and pyrolysis at 900°C with poly-methylsiloxane were done;
- and finally a consolidation step at 1350°C for 3 hours was applied.

The first step was aimed both at stabilizing the fiber preform in the form of an open sponge, 4 mm high, and at protecting the CVD Py-C interphase from the reaction with SiCO. The results of the microstructural observations are shown in figures 4.3.7 and 4.3.8, from which porosity can be qualitatively evaluated. As seen before, with a single felt the fiber density is very low, but the mechanical performances could be measured, both at room and at higher temperatures, up to 1000°C. The MOR value decrease between room temperature and 1000°C (figure 4.3.8) is an interesting datum to project possible applications.

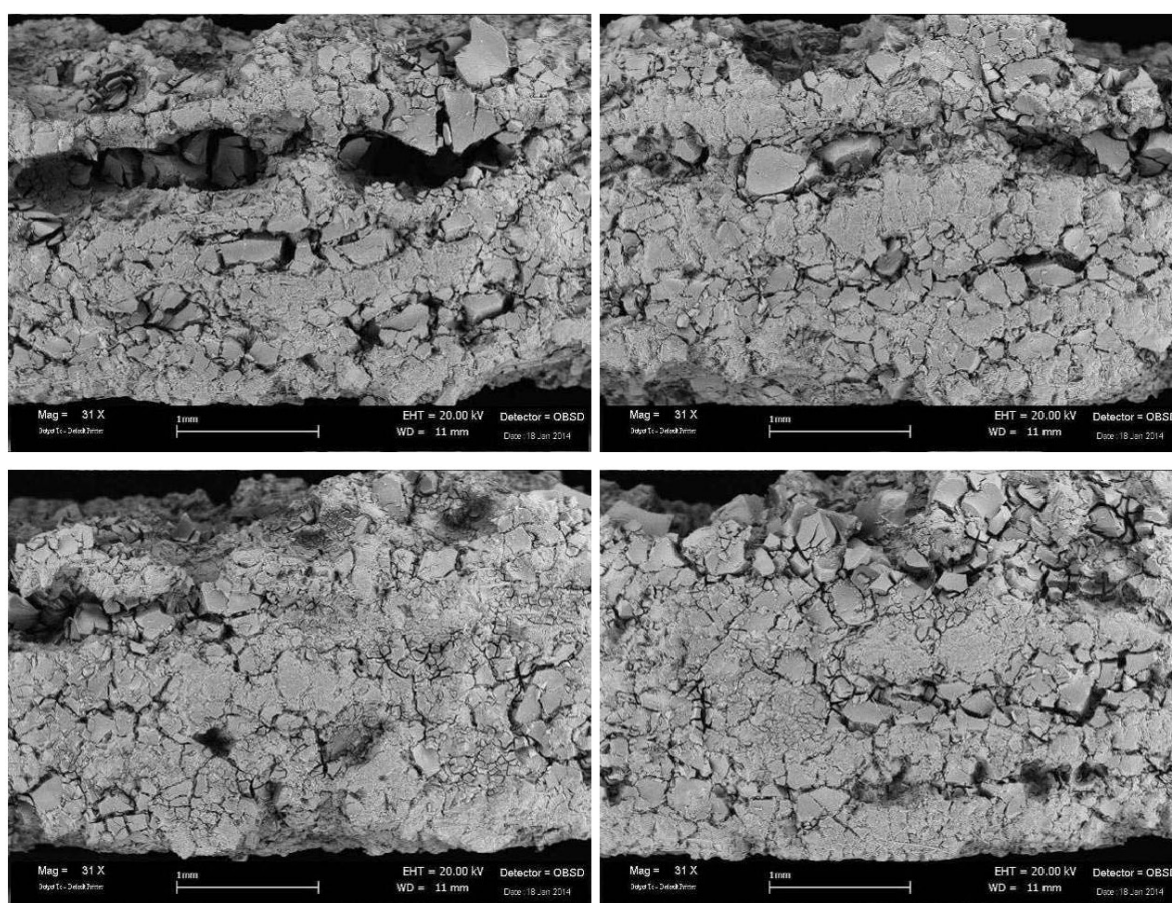


Figure 4.3.7a - Microstructure obtained by 4 PIP steps at 900°C, on unpressed SiC felts.

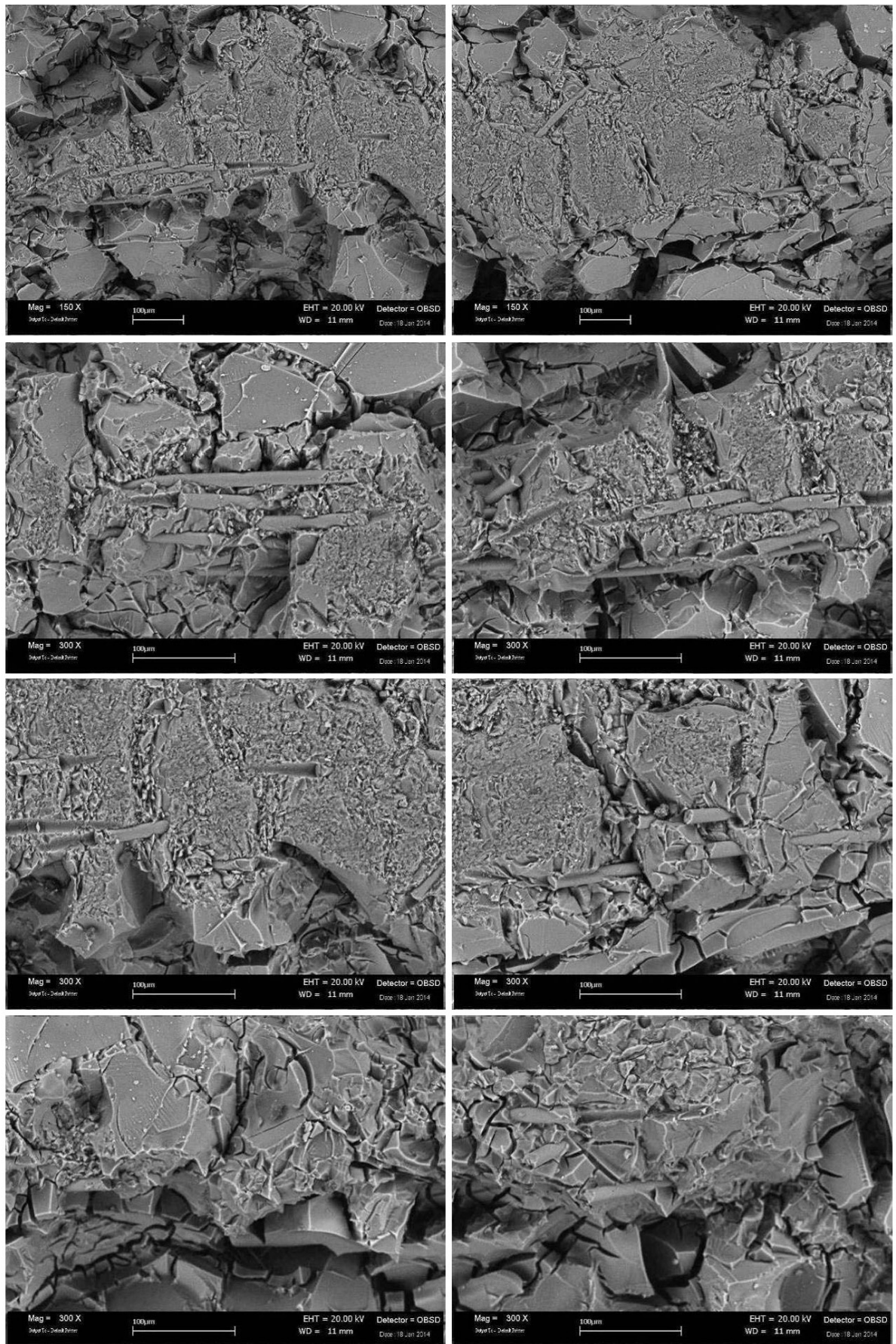


Figure 4.3.7b - Microstructure obtained by 4 PIP steps at 900°C, on unpressed SiC felts.

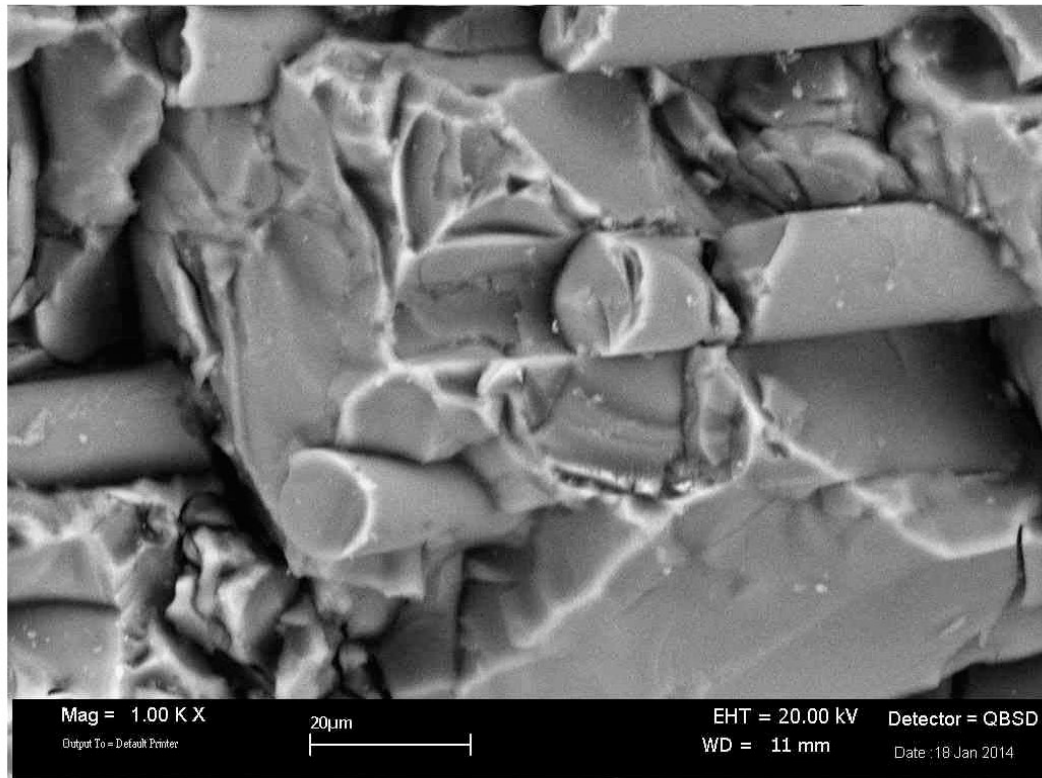


Figure 4.3.7c - Microstructure obtained by 4 PIP steps at 900°C, on unpressed SiC felts.

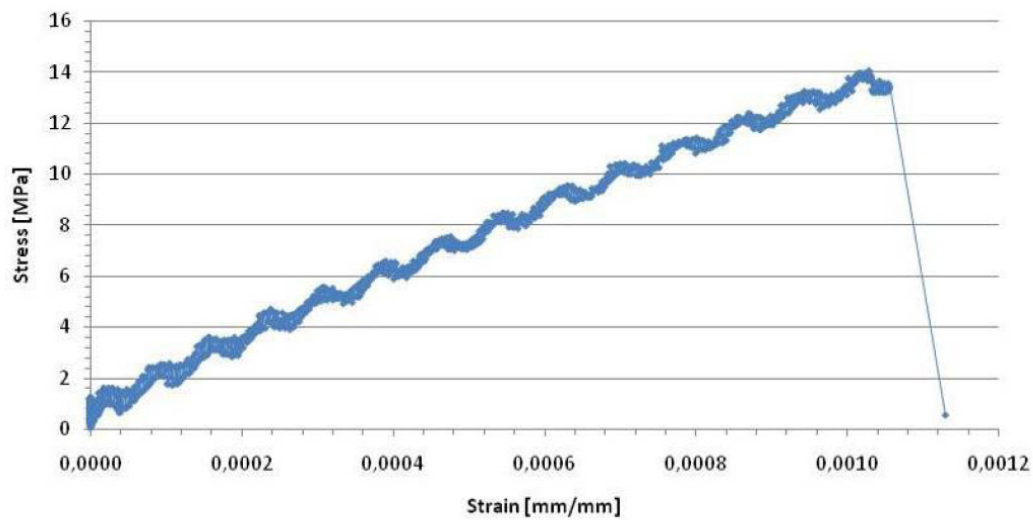


Figure 4.3.8 - Stress-strain curve at 1000°C on the unpressed SiC felt, after 4 PIPs [135].

[135] Regarding the noise in the above stress strain curve, it is due to an electronic interference from the furnace power system, which becomes less evident for higher loads but is always present.

4.3.2 PIP process of poly-methylsiloxane on unidirectional SiC plies

Since SiC 2D-fabric may be very expensive, the first attempt to improve the previous data on $\text{SiC}_f / \text{SiCO}$ were made by employing unidirectional fabric. It is not easy or cheap to buy SiC fabrics even in small quantities. The only SiC fabric we managed to get and test was unidirectional SCS-6. It is generally used for metal matrix composites [136], but it seemed rather interesting also for an association with SiCO because it is modified with metal fibers (of titanium and niobium) which could react with the SiCO matrix, with potential interesting effects [137-138], by reacting with a part of the oxygen to give SiC. As a first attempt it was not applied a Py-C interphase, even it is believed it would be beneficial on the thermomechanical behaviour, since otherwise the CVI plant would be necessary for the processing, making it too expensive for most industrial applications.

The employed unidirectional SiC fabric was SCS-6 SiC, is shown in the figure below. The CFCCs were prepared by using six plies 0-90° and the steel moulds for the first PIP step.

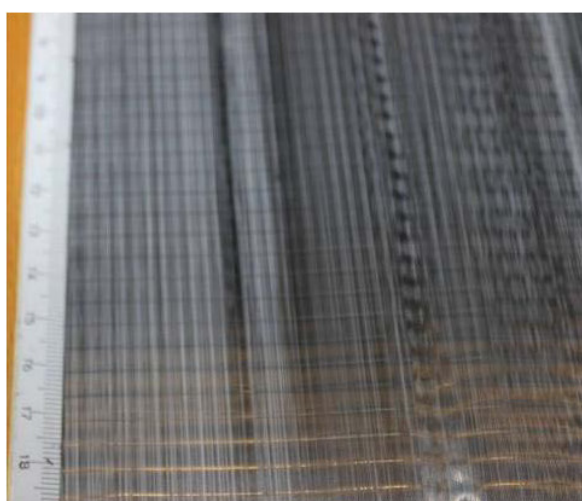


Figure 4.3.9 - Macroscopic morfology of SCS-6 SiC unidirectional fabric.

[136] Y.Q. Yang, H.J. Dudek, J. Kumpfert, " Interfacial reaction and stability of SCS-6 SiC:Ti-25Al-10Nb-3V-1Mo composites "Materials Science and Engineering, A246 (1998) 213-220.

[137] 10S. H. Yu, "Net-Shape Formation of Bulk Composite Materials via the Pyrolysis of Poly(siloxane) Filled Chemically Active Titanium and Inactive Silicon Carbide Fillers" Ph.D. Thesis. Rutgers University, Piscataway, NJ, 1996.

[138] Sung Hun Yu, Richard E. Riman, Stephen C. Danforth, Roger Y. Leung "Pyrolysis of titanium metal filled poly-siloxane preceramic polymers: Effect of Atmosphere on Pyrolysis Product Chemistry", Journal of the American Ceramic Society, 78, 7 (2005) 1818-1824.

Vacuum impregnation was obtained by dipping the preform into the polymer solution and by degassing it under vacuum. Drying of the xylene was carried out by heating at temperature between 60°C and 90°C, as before. Pyrolysis was performed, under nitrogen flow, at 700 °C for 900 min. After two PIP steps, the mechanical characteristics were judged too low to go on with a consolidation thermal treatment. This final step generally aim at completing the ceramic phase formation, but in this particular case, in presence of metallic fibers, it would also have aimed at the creation of new ceramic phases, by a thermally activated reaction. Anyway this step require a rather dense structure as a starting point, since major defects cannot be repaired by sintering, not even by reactive sintering. As usual SEM observations were used to establish the microstructure of the composite. The SiC fibers can be clearly seen, with a diameter of around 150 μm . In some cases the space between the SiC fibers is filled with SiCO, but the space appears too big and the matrix is seriously damaged and cracked. This explains the observed low mechanical characteristics and the tendency to delaminate, which made impossible to cut the standard samples for MOR measurements. The SiC fibers appear undamaged and could still give high mechanical performances, but only if the matrix had connected them.

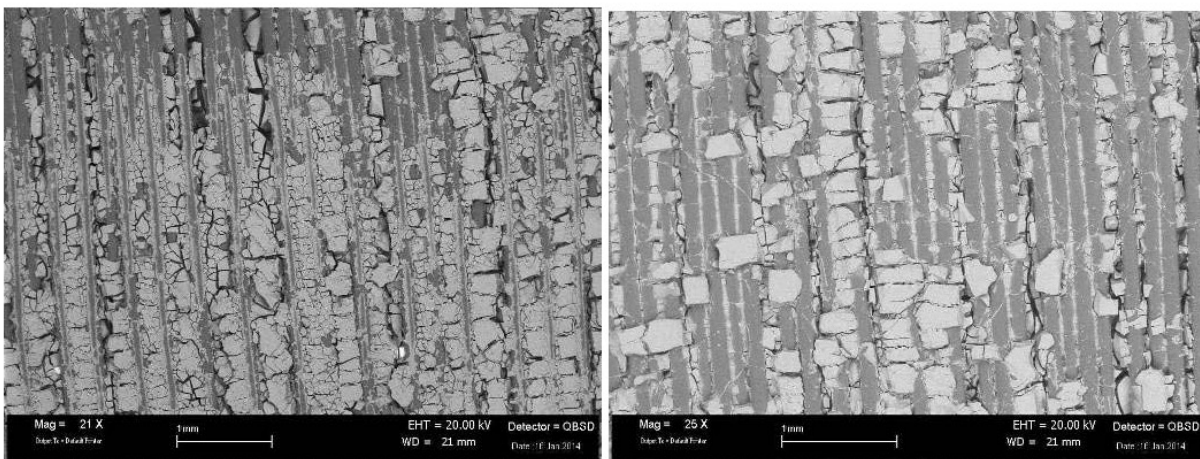


Figure 4.3.10 - SEM of the SiC_f / SiCO composite.

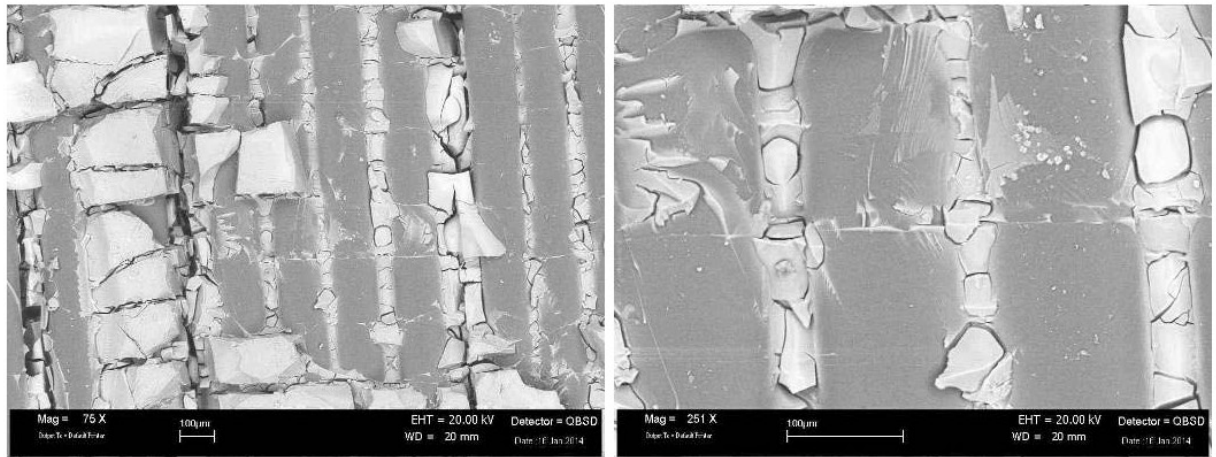


Figure 4.3.11 - SEM of the SiC_f/ SiCO composite.

Regarding the metallic fibers, only one type was visible, and, after the PIP process at 700°C, it appears already partially reacted and seriously cracked, incapable of contributing to the mechanical performance. On the basis of the macroscopic and microscopic observation, this solution was discontinued.

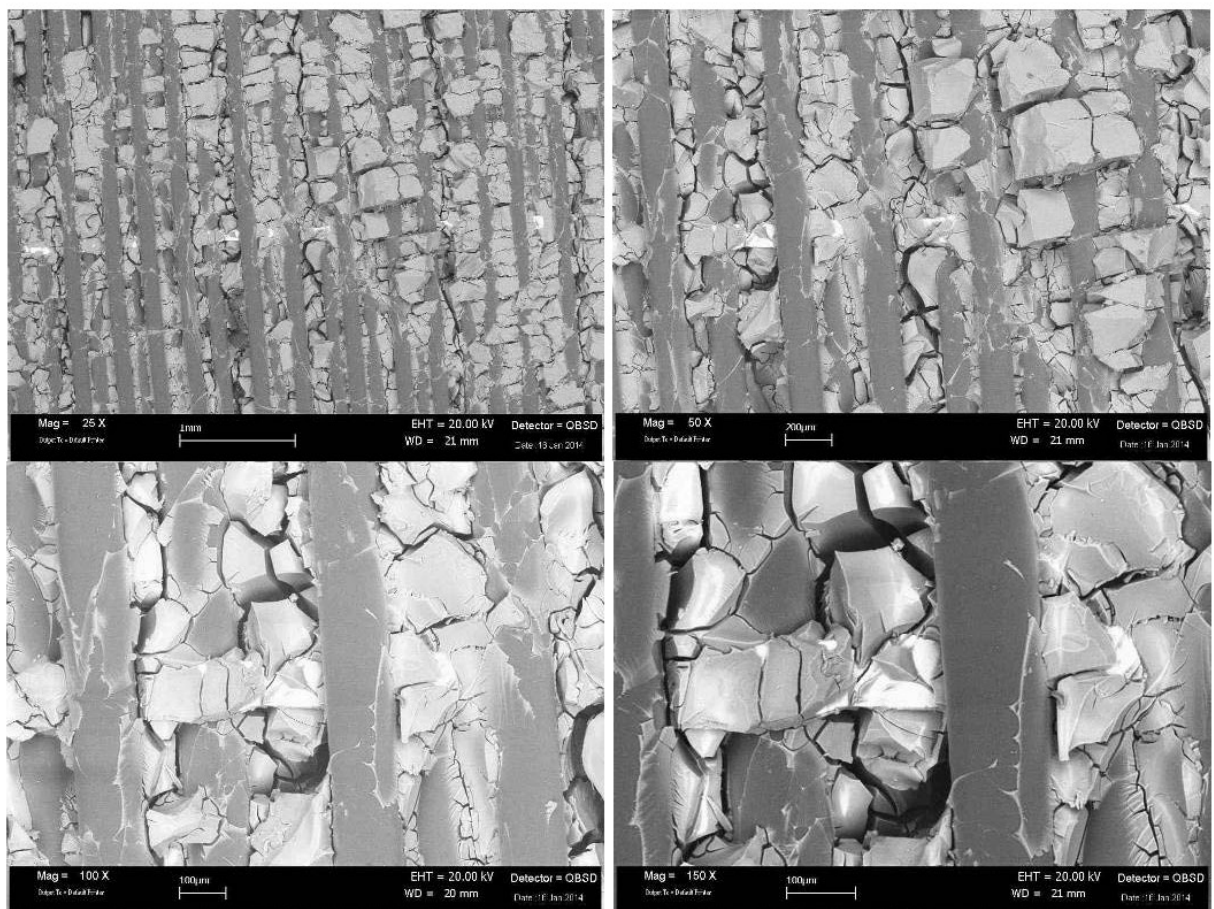


Figure 4.3.12 - Residue of a metallic fiber, originally present.

4.4 Study of the PIP process of poly-methylsiloxane on basalt fibers

Regarding the solution of basalt fibers and poly-methylsiloxane, a comparatively low pyrolysis temperature was chosen (650-700°C) in order to avoid the thermo mechanical degradation of the basalt fibers, which has been reported in literature, in previous cited Černý works. Even if produced at much higher temperature, above 750°C basalt fibers crystallize, starting to show XRD with sharp diffraction patterns [139] corresponding to spinel and sometimes other phases. One or two PIP steps were applied, in order to further reduce production times to the minimum. In order to reduce production costs, pyrolysis in inert atmosphere was compared to pyrolysis under vacuum. No interphase was deposited on fibers, even if in the future sol-gel interfaces could be considered, as it is generally made for oxide CMCs, for obtaining more "pull-out" reinforcement. Also for this case, poly-methylsiloxane on basalt fibers, several combinations were considered and tested:

- One PIP step with poly-siloxane on 0-90° orthogonal yarns (paragraph 4.4.1)
- Two PIP steps with poly-siloxane, in N₂ flow on four bidirectional orthogonal fabric plies (paragraph 4.4.2);
- Two PIP steps with poly-siloxane, in vacuum, on four bidirectional orthogonal fabric plies (paragraph 4.4.3);
- Two PIP steps with poly-siloxane, 2D-twill fabric plies (paragraph 4.4.4);
- One PIP step, in vacuum or under nitrogen, on eight unidirectional orthogonal plies (paragraph 4.4.5);
- PIP with poly-siloxane on rock wool and other oxide fibers (paragraph 4.4.6).

For the first solution, a pyrolysis temperature of 650°C was chosen, but the pyrolysed material resulted unstable to oxidation, and from that point two processing variables were changed:

- active carbon was put into the pyrolysis chamber;
- the pyrolysis temperature was increased to 700°C.

[139] Černý, M., Glogar, P., Goliáš, V., Hruška, J., Jakeš, P., Sucharda, Z. and Vávrová, I, "Comparison of mechanical properties and structural changes of continuous basalt and glass fibres at elevated temperatures", *Ceramics - Silikáty*, 51, 2 (2007) 82–88.

Regarding the pyrolysis temperature cycle, after several attempts and comparisons with literature data, a curing step at 250°C of 5 hours and a pyrolysis isothermal step at 700°C of 15 hours were chosen. Ramp rates up to 250°C were chosen as 30°/h, and 60°/h up to 700°C. Active carbon proved to be effective to ensure reducing environment and oxygen free environment, acting as an "oxygen getter", to trap trace amount of oxygen, both under nitrogen flux and under vacuum. Regarding the pyrolysis temperature, according to Cerny's works, 700°C represents the best compromise between the degradation of basalt fibers and the ceramic SiCO phase formation. The pyrolysis parameter analysed were the pyrolysis environment (vacuum or nitrogen flow), the number of PIP steps and the fiber preform structure. The parameters were optimised aiming at a low cost industrial production of thermostructural components.

4.4.1 One PIP step with poly-methylsiloxane

In this case yarns were extracted from calcinated Mapegrid B 250, a basalt net distributed from MAPEI for the construction field (250 g/m²; 6x6 mm open squares). They were put orthogonally and impregnated with a wet lay-up procedure, before being squeezed in the steel clenched mould.

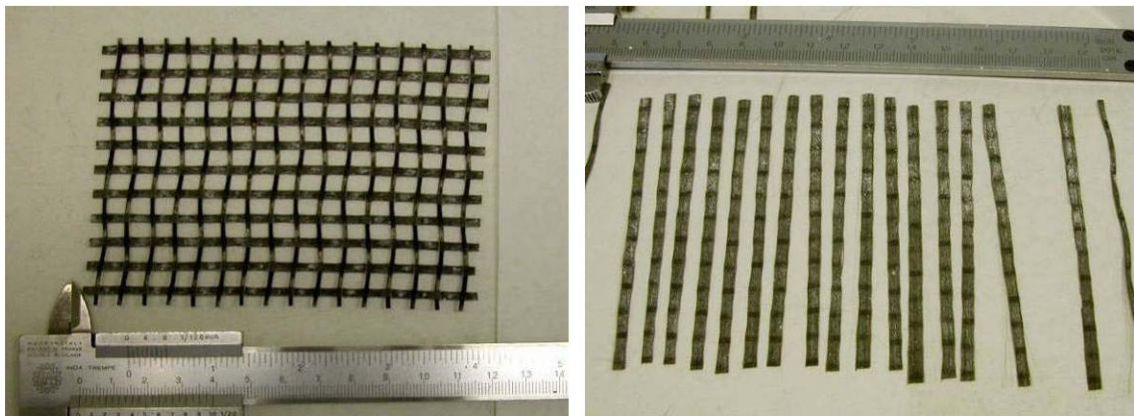


Figure 4.4.1 - Preparation of the uniaxial basal fibers for the PIP experiments.

The fabric yarns (tows) are still visible after the pyrolysis (figure 4.4.3), connected together thanks to the ceramic matrix, formed after the unique PIP step. The volume change of the poly-siloxane-to-silicon oxycarbide is compensated both by shrinkage and porosity formation, but overall result still have interesting structural characteristics and MOR values (figures 4.4.4 and 4.4.5).



Figure 4.4.2 - Basalt reinforced composite after one PIP step with poly-methylsiloxane.

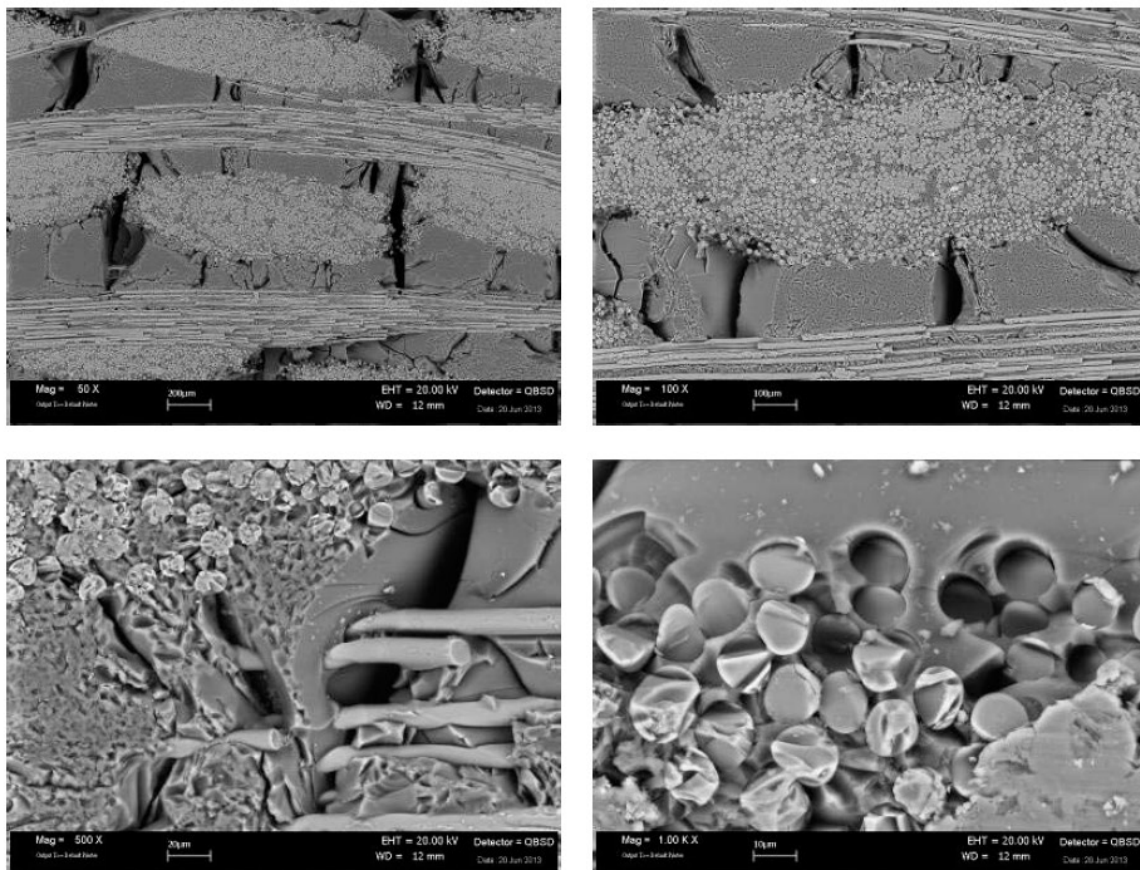


Figure 4.4.3 - Microstructure obtained after one PIP step at 650°C.

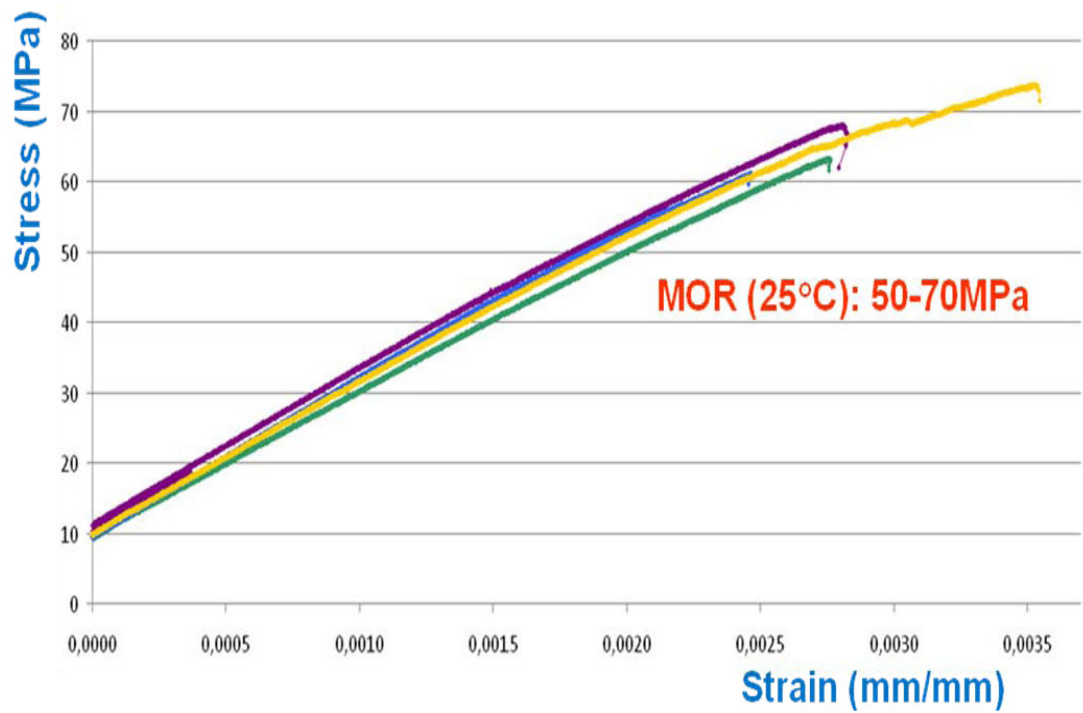


Figure 4.4.4 - MOR values at 25°C on the basalt reinforced composite, after one PIP step.

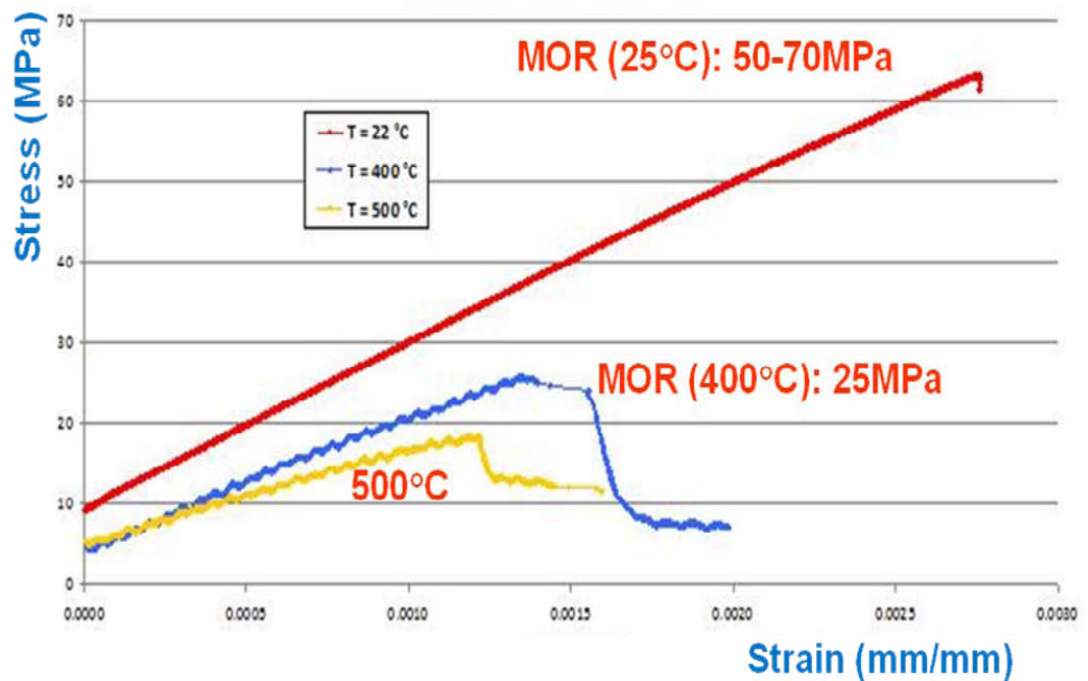


Figure 4.4.5 - MOR values (vs T) on the basalt reinforced composite, after one PIP step.

The preliminary thermomechanical results are interesting establishing that:

- good mechanical properties can be achieved even if the reinforcement fibers were non weaved, nor optimized and only one PIP step was applied;
- these mechanical properties can be retained in temperature, at least up to 400°C, that can be considered a suitable result for applications in the automotive field.

The obtained relative density was around 69%. The value of relative it was calculated as the ratio of the theoretical density, measured with the pycnometer, 2.44 g/cm³, and the geometrical density, 1.68 g/cm³. The weight fiber density in the CFCC was around 57% w/w.

The pycnometer density is used as an approximation of the theoretical density (a rather acceptable approximation because the high porosity and the production process both contribute to make rather improbable the occurrence of significant closed porosity) which could also be calculated from the fiber density (2.66 g/cm³) and the matrix density (2.22 g/cm³).

4.4.2 Two PIP steps on four bidirectional plies

The second solution considered corresponds to the use of bidirectional orthogonal fabrics consolidated using two PIP steps with poly-siloxane. Fabrics were cut in pieces of the mould size, as shown in the subsequent figures. The preforms were produced by using HG-GBF bidirectional basalt fabrics, being made of two orthogonal unweaved unidirectional layers (figure 4.4.7, 800 g/m²). To produce a composite sample of an approximate thickness between 2.5 and 3 mm, 4 plies of bidirectional were used. The fabric cutting is rather difficult, being the fabric stability obtained thanks to weaving with some rare cotton fibers, between flat basalt yarn 2.5 mm wide. It is not the optimal solution, since these cotton yarns produce some amorphous carbon during the pyrolysis step which probably react with the forming SiOC, producing C-rich SiCO, but the real problem is low fabric stability, so later (see paragraph 4.4.5) a solution based on 8 orthogonal plies of a more stable unidirectional fabric with half gsm, gram per square meter, (400 g/m²) was also tested, considering it more interesting for practical applications. The fiber density of the bidirectional fabric was measured by helium picnometry as 2.66 g/cm³ while SiCO density (produced by PIP at 700°C) was measured as 1.81 g/cm³, a value that is to be compared to the density of 2.0 g/cm³ reported in

literature for the same precursor polymer, pyrolysed at 1000°C (table 4.1.1). The difference is due to the different pyrolysis temperature, as the measures performed in ENEA showed. From the density of the basalt fibers, the density of the matrix and the volume percentages of fibers, the theoretical density of the composite was calculated, as essential data to evaluate relative density and porosity.



Figure 4.4.6 - HG-GBF bidirectional basalt fabric (800 g/m²).

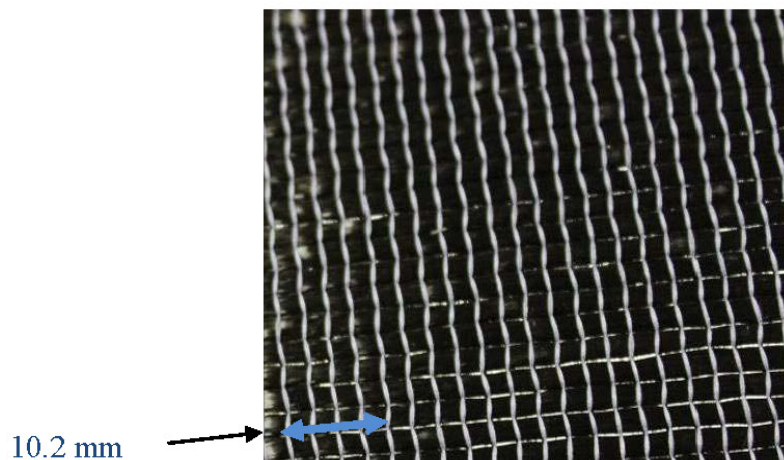


Figure 4.4.7 - Morphology of HG-GBF bidirectional basalt fabric.

The results of the thermomechanical characterization on the material (after cutting standard samples as before) were quite interesting: indeed mean MOR value reached values around 130 MPa at room temperature and 100 MPa at 400°C. These results were considered very promising, being expected significant improvements by employing 2D fabrics.

The mechanical behavior is also quite interesting, since the composites can be considerably deformed before reaching the failure, showing pseudo-plastic behavior both at room temperature (figure 4.4.9, three different samples reported) and at high temperature (figure 4.4.11). The obtained relative density in this case was around 70%. The value of relative density was calculated as the ratio of the calculated theoretical density, measured with the pycnometer, 2.42 g/cm^3 , and the geometrical density, 1.72 g/cm^3 . The fiber density in the CFCC was around 82% w/w. The intermediate geometrical density after one PIP step was 1.68 g/cm^3 , so the opportunity to make two PIP steps instead of one should be carefully evaluated.

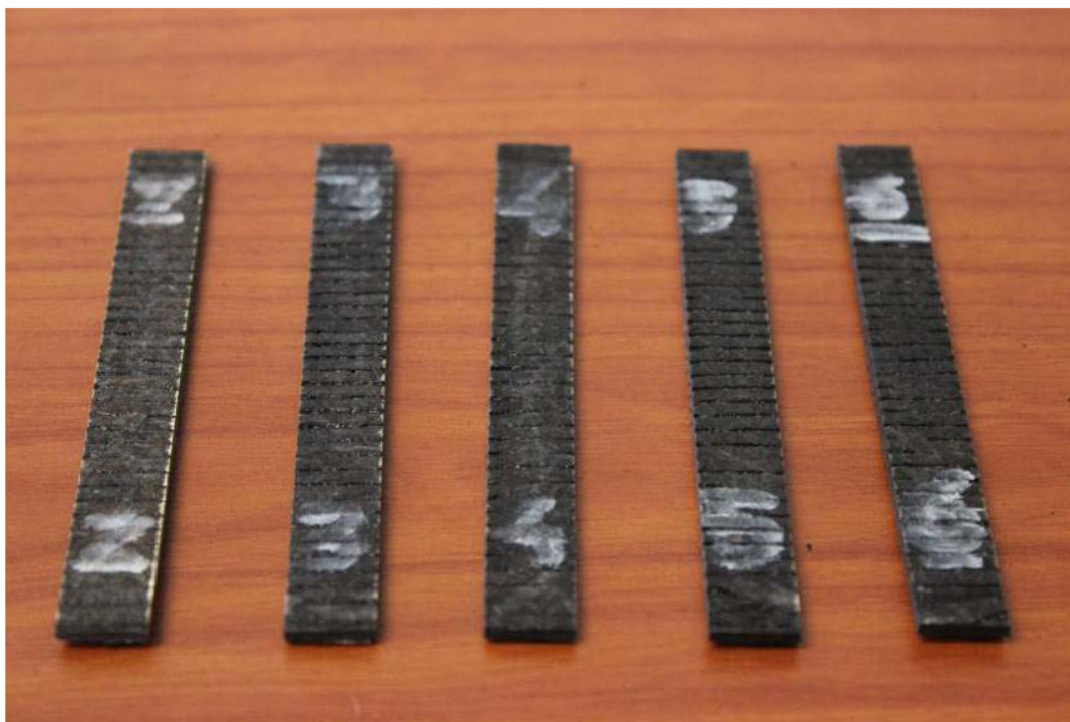


Figure 4.4.8 - Standard samples for the thermomechanical characterization.

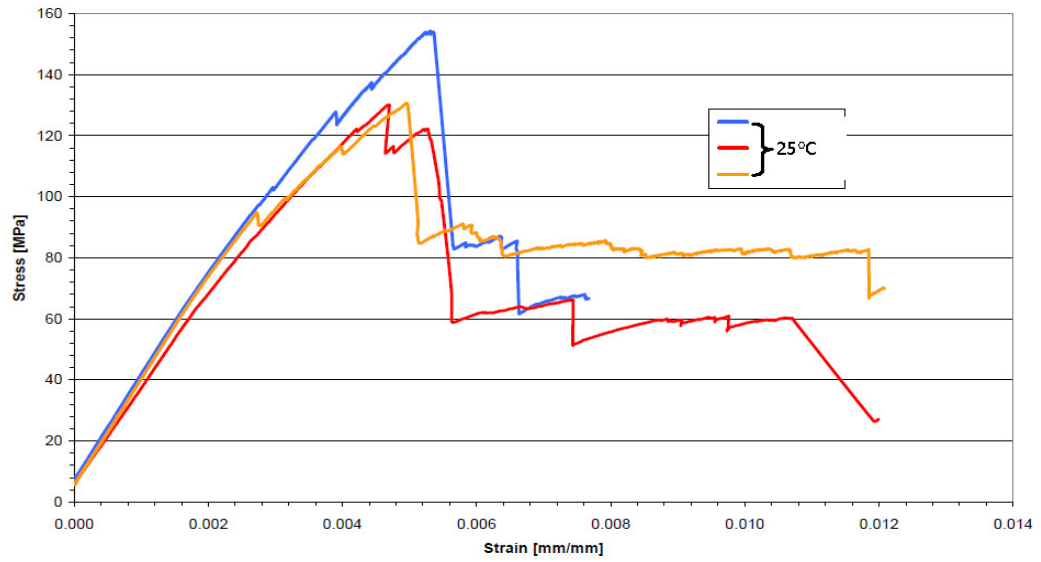


Figure 4.4.9 - Stress strain curves at 25°C (4 bidirectional basalt fabric plies, 2PIP steps).

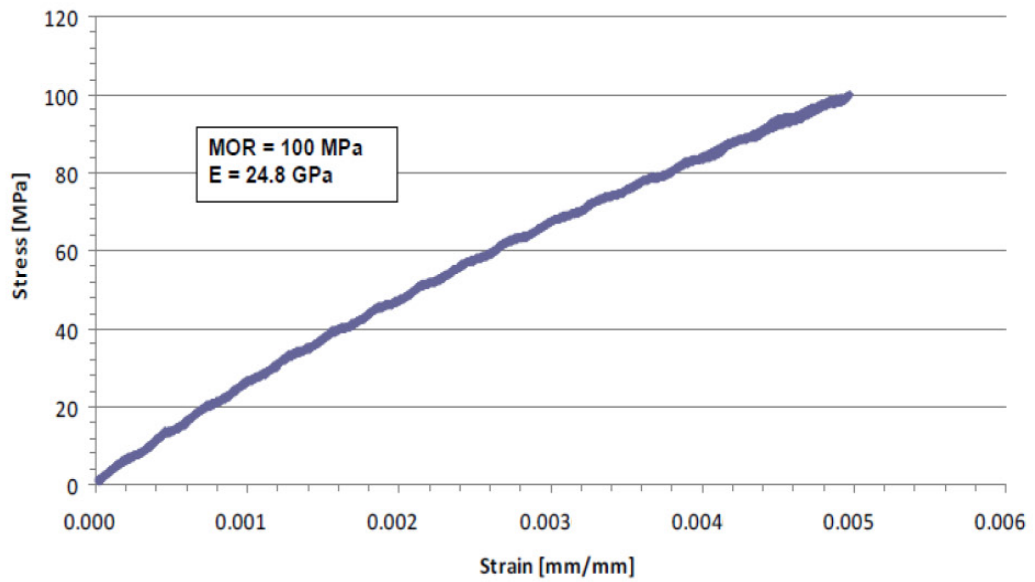


Figure 4.4.10 - MOR and E values at 400°C (4 bidirectional basalt plies, 2PIPs).

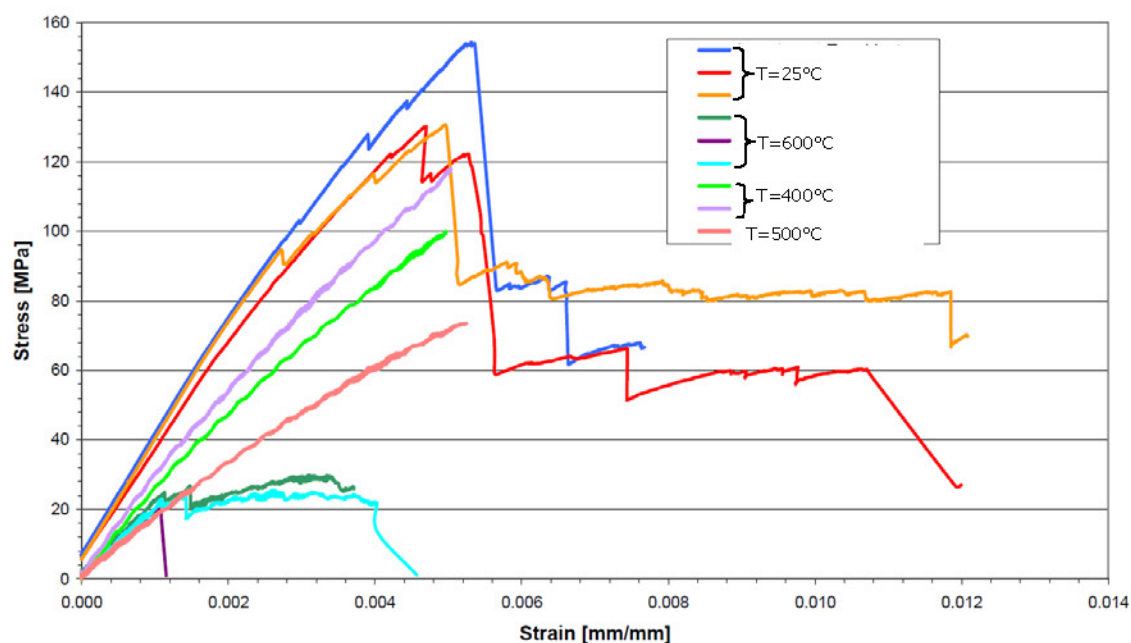


Figure 4.4.11 - Stress strain curves at 25, 400, 500 and 600°C (4 bidirectional basalt plies, 2 PIPs).

The following table reports all the measures done (each result on a different standard sample of the same type).

Two PIP steps on 4 bidirectional plies - PIP in nitrogen			
Temperature	MOR (MPa)	E (GPa)	Failure type
25°C	130-131	34.0-31.7	Shear failure
400°C	100-118	24.8-27.8	unbroken
500°C	74	16.2	unbroken
600°C	20.3-18.2-19.1	29.8-21.0-25.5	unbroken

Table 4.4.1 - Mechanical parameters for PIP derived CFCC at various T.

It should be noted that in the case of "unbroken" samples, the LVDT used for measuring the strain reached the limit of the range of measure before the sample broke. All tests have been done "in control of displacement".

4.4.3 Two PIP steps with poly-methylsiloxane, in vacuum

The subsequent investigation was aimed at establishing if there is a decrease in mechanical performances, by making pyrolysis under vacuum, instead of flowing nitrogen. The preliminary result (table 4.4.2 and figure 4.4.12, two standard

samples for each pyrolysis condition) were encouraging, since the decrease in the flexural strength was around 15-20%, which could be an acceptable performance compromise, considering the potential economical advantages in using vacuum instead of a flowing inert gas [140,141,142].

Two PIP steps on 4 bidirectional plies			
Temperature	MOR (MPa)	E (GPa)	Pyrolysis conditions
400°C	89-96	23.0-23.3	700°C-vacuum
400°C	100-120	24.8-27.8	700°C-nitrogen

Table 4.4.2 - Mechanical parameters for PIP derived CFCC in vacuum and N₂.

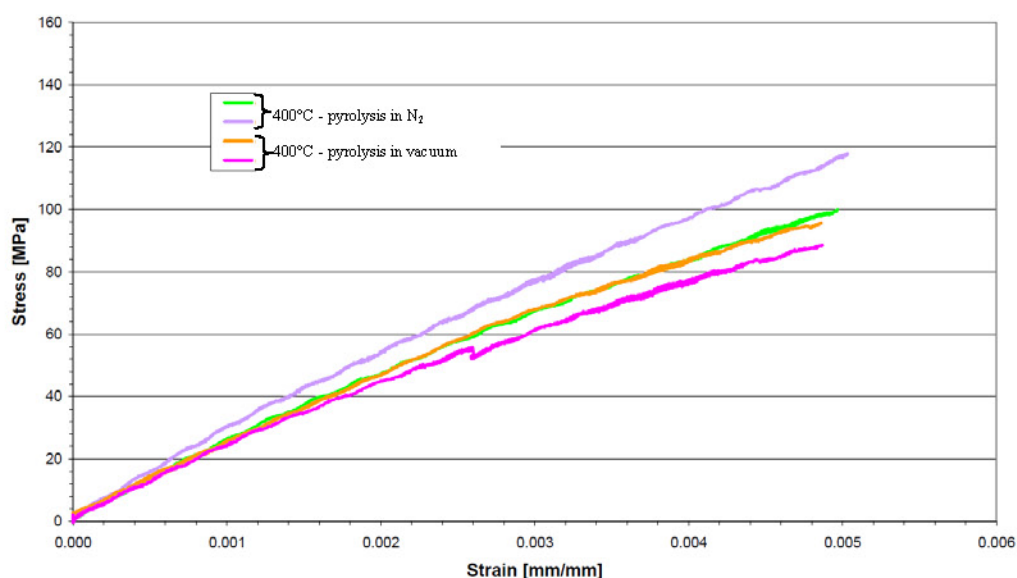


Figure 4.4.12 - Stress-strain curves at 400°C (from PIP in vacuum and N₂).

In the following table, all the measures done are reported, confirming that, performing the pyrolysis under vacuum instead of nitrogen flow, a slight decrease

[140] C. Mingazzini, TECNPOLO TALKS "Il Tecnopolo della provincia di Ravenna si racconta" Ravenna, 26 settembre 2013, Oral presentation about Thermostructural Composites developed within the MITAI technopole.

[141] C. Mingazzini, "I Materiali del futuro: Technology Dating", Faenza, 25 novembre 2013. Oral intervention about Thermostructural Composites developed within the MITAI technopole.

[142] C. Mingazzini, M. Scafè, A. Brentari E. Buresi, D. Caretti and D. Nanni, "Poly-siloxane Impregnation Pyrolysis for the cost-effective production of basalt fibers CFCCs" accepted as an oral contribution at CIMTEC 2014.

of mechanical performance occurs, considering both stiffness (measured by the Young modulus) and strength (measured by the MOR values).

Two PIP steps on 4 bidirectional plies - PIP in vacuum			
Temperature	MOR (MPa)	E (GPa)	Failure type
25°C	83-79-67-79-90	21.7-22.3-19.4- 27.7-31.9	strain
400°C	89-96	23.0-23.3	unbroken
600°C	58-47	15.4-22.6	unbroken

Table 4.4.3 - Mechanical parameters for PIP derived CFCC in vacuum.

Moreover, also the weight fiber density in the CFCC was almost the same for vacuum pyrolysis (around 80% w/w) like for pyrolysis in nitrogen flow. Besides the thermomechanical properties, the microstructure and the mean values of the relative density in the case of vacuum pyrolysis were also compared. The relative density in the case of vacuum processing was similar to that obtained in the case of PIP under nitrogen. The microstructures are reported in the following figures. A certain variability between the samples is inevitable, but anyway it appears evident that the matrix fills only the areas where there is a good density of fibers. Even if from the micrographs vacuum pyrolysis would seem having produced more porosity defects (figures 4.4.13 and 4.4.14), that is not the conclusion from the porosity measurements, which are expected to give the most accurate result regarding this macroscopic characteristic on a material characterized by a high variability. Especially in the areas filled with fibers, there are no evident differences between the material produced by vacuum and nitrogen pyrolysis: in these areas, porosity cannot be appreciated and pull-out mechanisms occurs (figures 4.4.15 and 4.4.16), limited only by the strength of the fibers, which is not as high as for ceramic fibers. It was almost impossible to find works on "vacuum pyrolysis" for PIP [143], anyway our results in this case of one or two PIP steps suggest that, considering industrial production costs, vacuum pyrolysis really appears an alternative to be considered.

[143] Shyankay Jou, Chao Ken Hsu, "Preparation of carbon nanotubes from vacuum pyrolysis of polycarbosilane", *Materials Science & Engineering B*, 106, 3 (2004) 275-281.

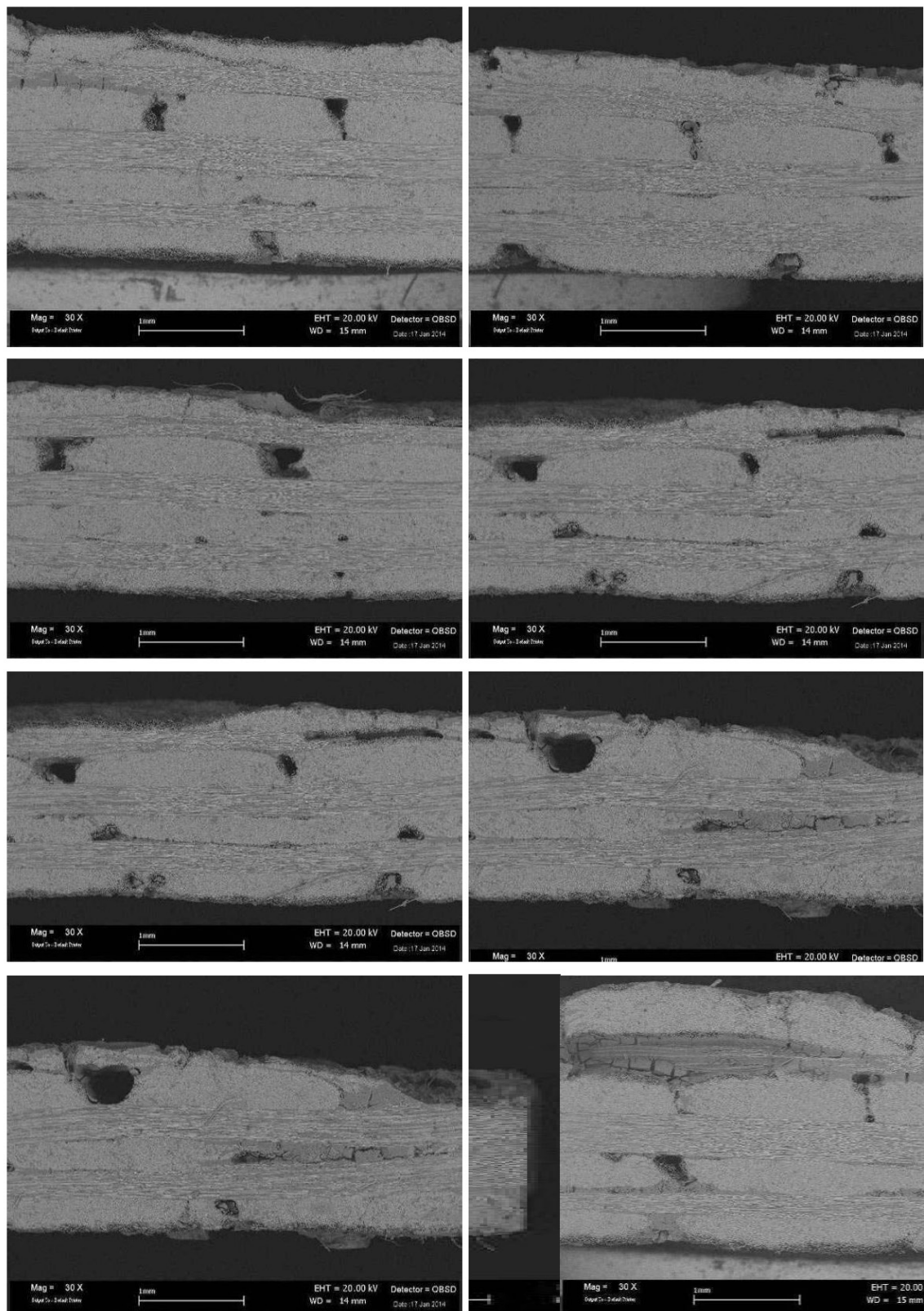


Figure 4.4.13 - SiCO-basalt composites produces at 700°C under vacuum.

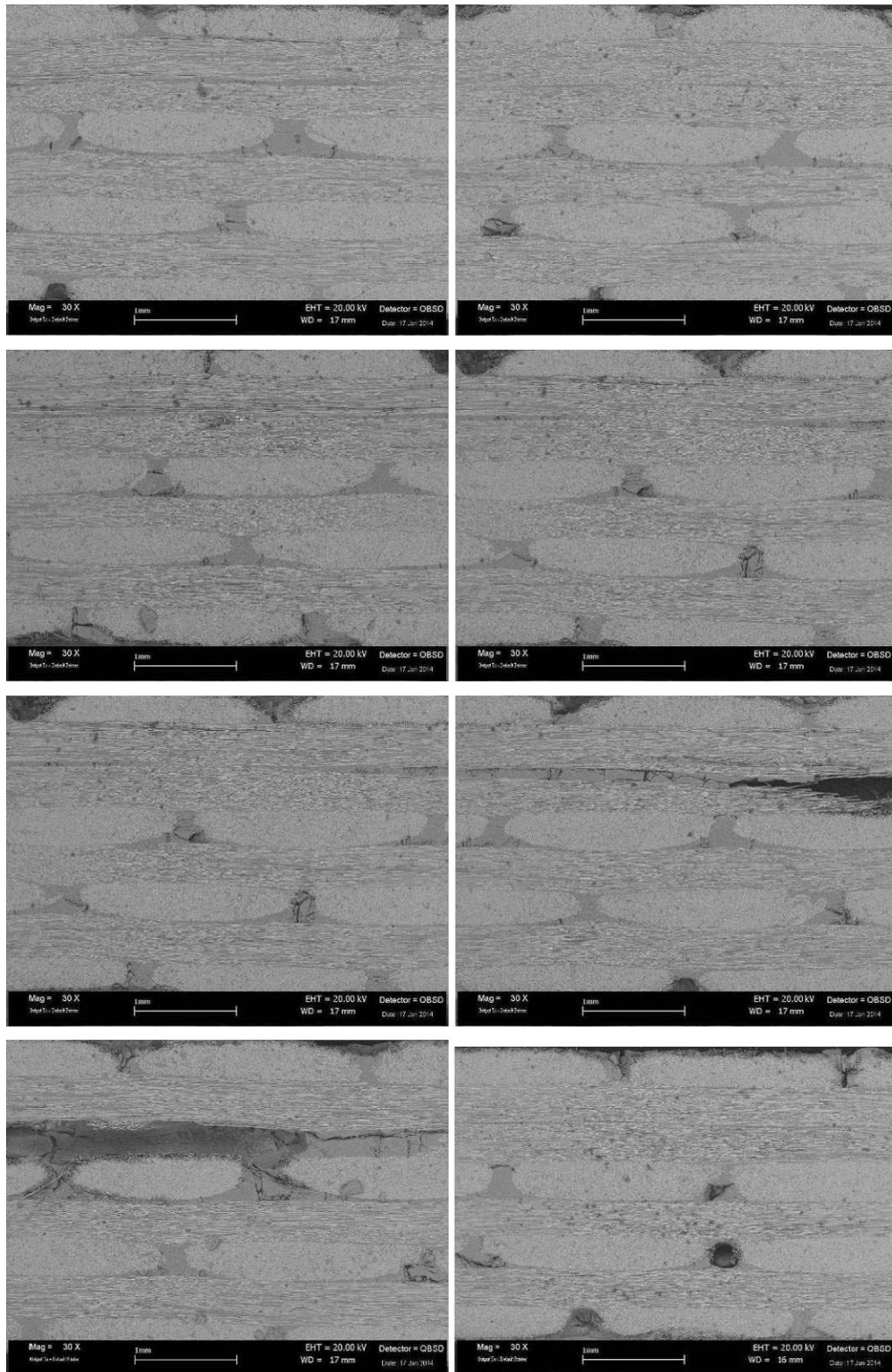


Figure 4.4.14 - SiCO produced at 700°C under nitrogen flow.

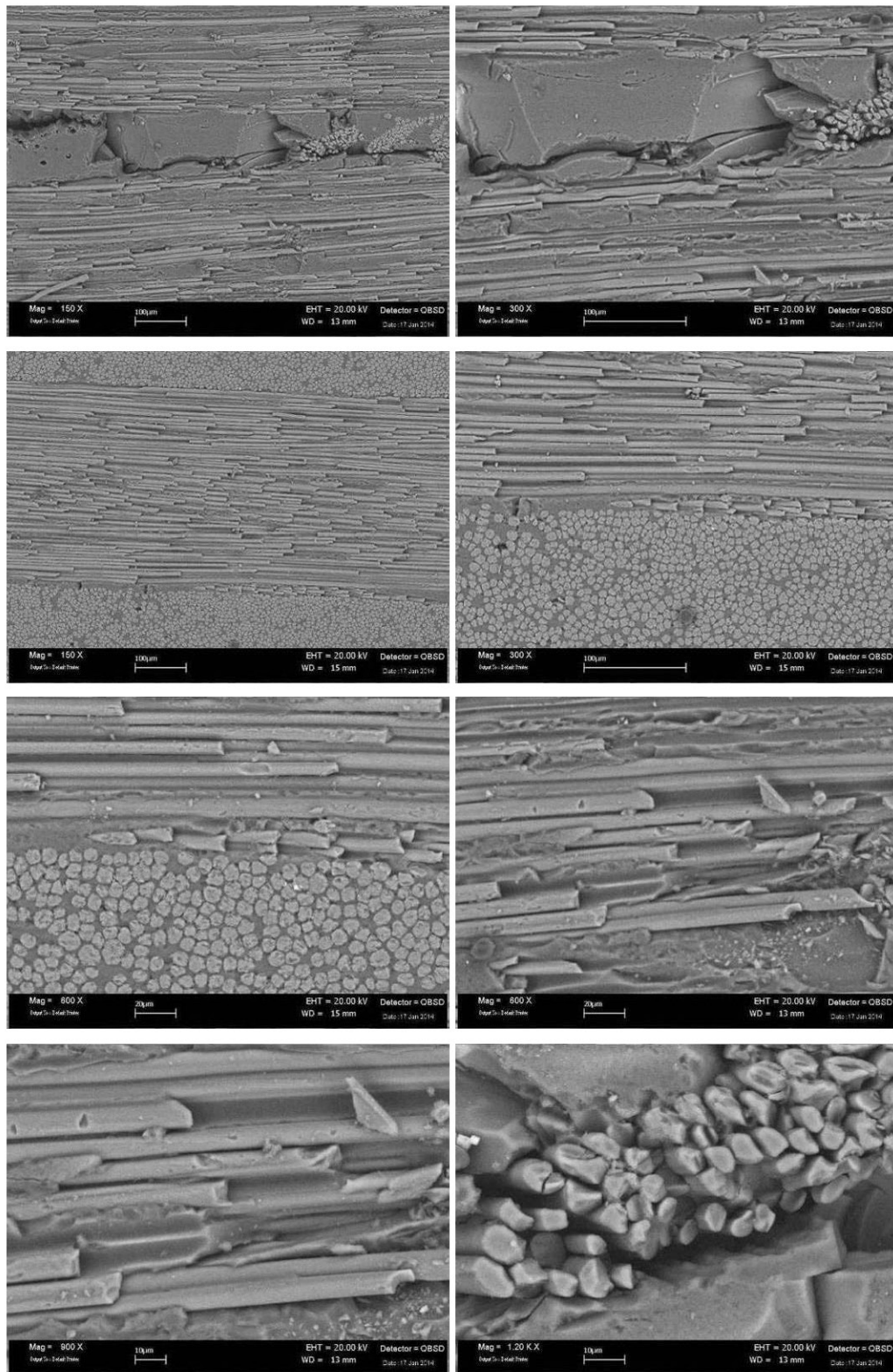


Figure 4.4.15 - SiCO-basalt microstructure obtained under vacuum.

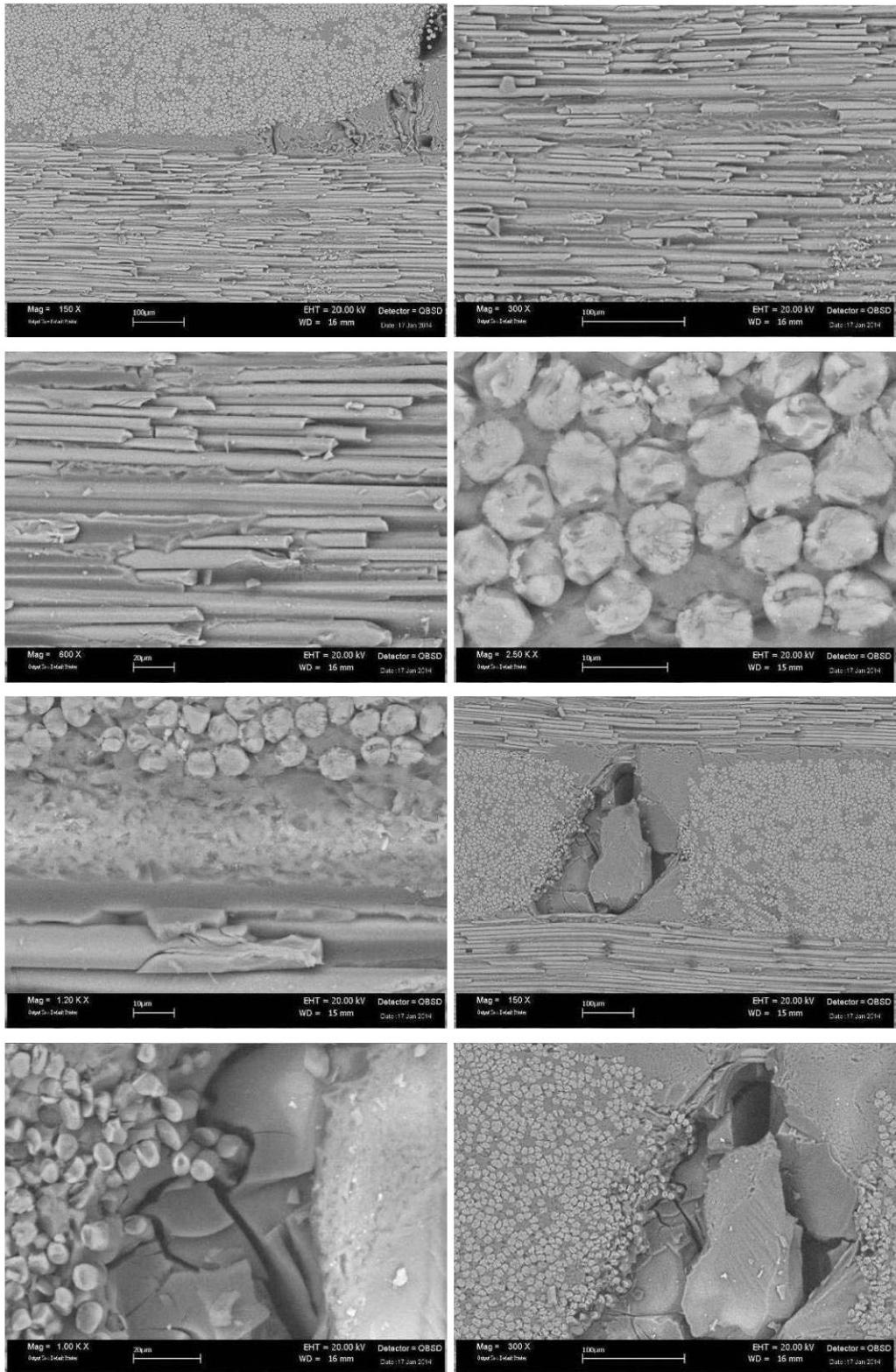


Figure 4.4.16 - SiCO-basalt microstructure obtained under nitrogen flow.

4.4.4 Two PIP steps with poly-methylsiloxane, 2D fabric plies

As discussed in the introduction, one of the traditional approach for increasing CFCCs mechanical performances is to use of 2D plies, or 3D preforms, in order to ensure a more isotropic fiber reinforcement. As a first attempt, it was tested a fiber preform prepared by the wet lay-up of four 2D twill-weave basalt fabric plies, but the first results were not good and are shown below. The 2D fabrics was derived from preregs (580 g/m², after calcination). The composite broke, during the second PIP step, breaking along the two orthogonal directions of the fibers (figure 4.4.18).

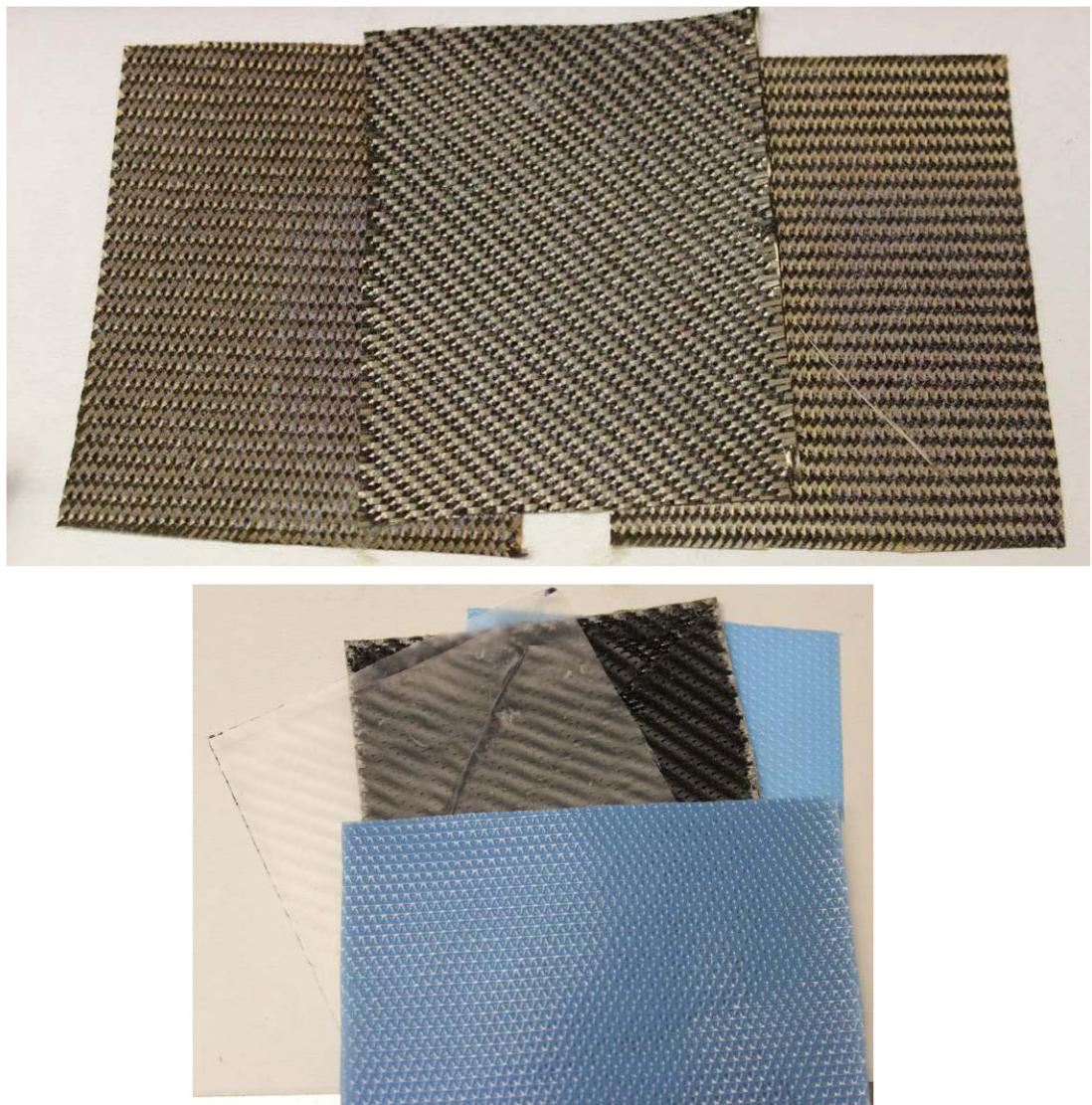


Figure 4.4.17 - 2D basalt fabrics (9x11 cm²) derived from preregs.

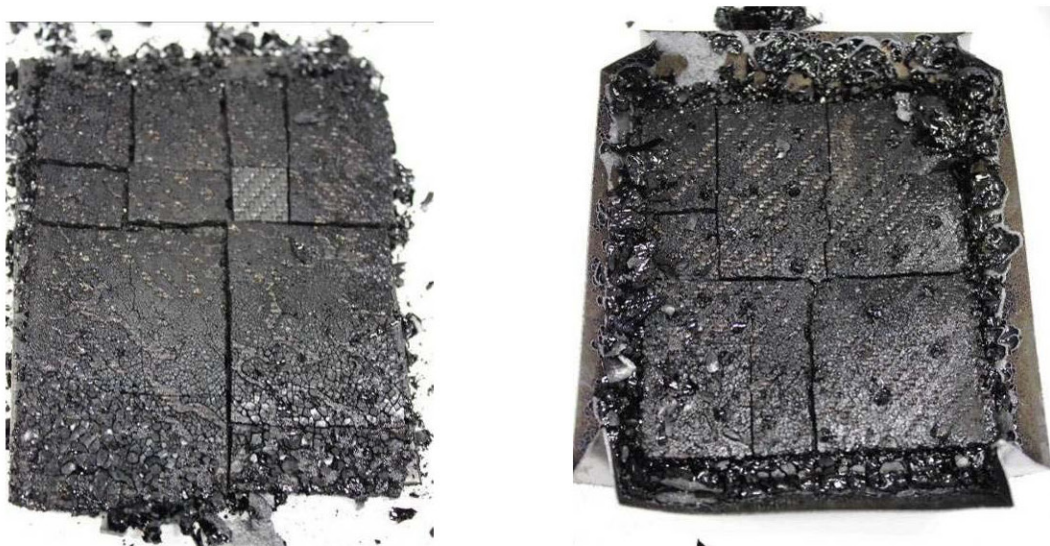


Figure 4.4.18 - Morphology of the CFCCs obtained using 2D basalt fabric plies.

This kind of "orthogonal" rupture during the second PIP step was initially attributed to the mechanical stress linked to a difference in the coefficient of thermal expansion. In order to better study this problem other preparations were attempted, using higher fiber density (6 plies in the same volume) in a way to achieve the same fiber density which had given satisfying results using bidirectional plies. Moreover, differently from before, the thickness of the CFCC samples was fixed using a spacer, and the orientation of the plies was changed in order to have a $0\text{-}45^\circ$ fiber orientation, with parallel twill orientation. Another solution considered was to keep parallel fiber orientation and orthogonal twill orientation. The results was that increasing the fiber density is enough to solve the problem of cracking, so it was not a problem of different thermal expansion. In this way, after 2 PIP steps, high densification was obtained (relative density of about 80%, to be compared to a value of about 75% in the case of bidirectional fabrics) but nevertheless the fiber density was still low compared to that obtained with bidirectional fabrics (about 63%, versus about 80% in the case of bidirectional fabrics) and, maybe as a consequence, MOR values were much lower (e.g. figure 4.4.23). The microstructural observations on the sample surface and sections are shown in the following figures. The solution with $0\text{-}45^\circ$ fiber orientation seems more compact, but the porosity measurements gave similar mean value in both cases. An important result that could be taken from the SEM investigations is that the fiber "pull-out" occurs also in the case of prepreg-derived 2D fabrics by calcinations, as in the case of the fibers bought from HG-GBF.

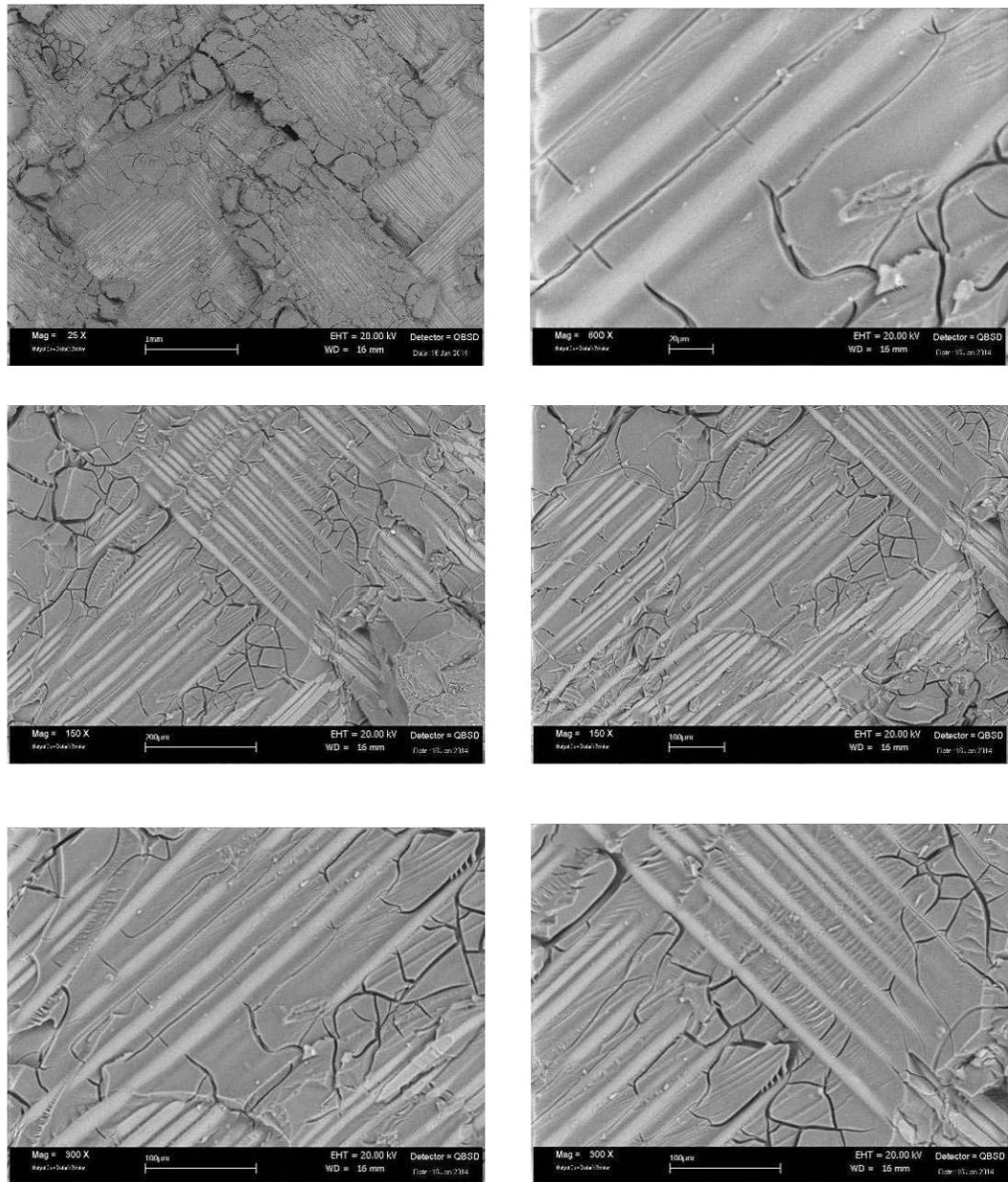


Figure 4.4.19 - Microstructure of the CFCCs obtained using 2D basalt fabric plies.

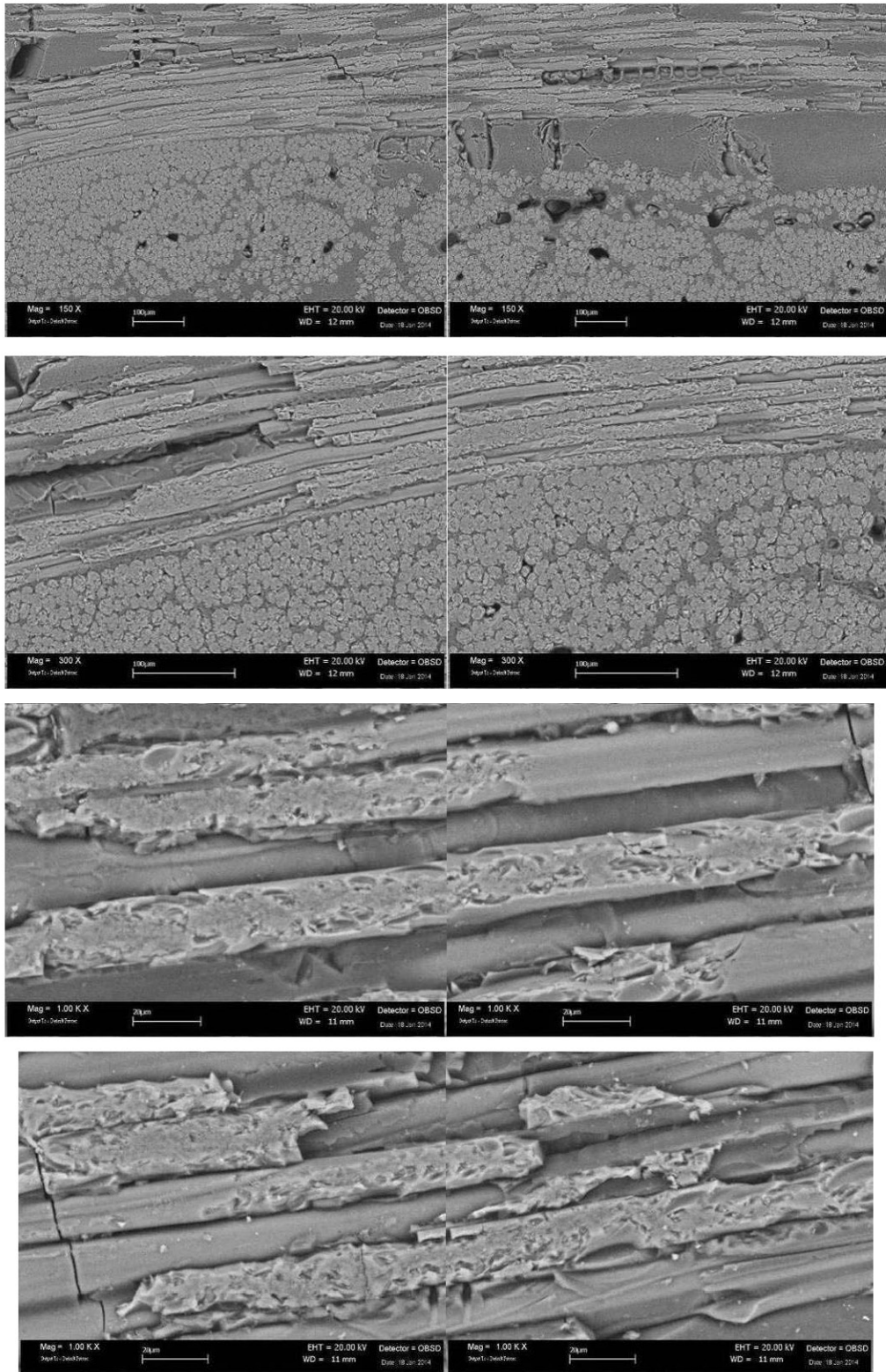


Figure 4.4.20 - Microstructure obtained using 2D-ply with 0 - 90° twill orientation.

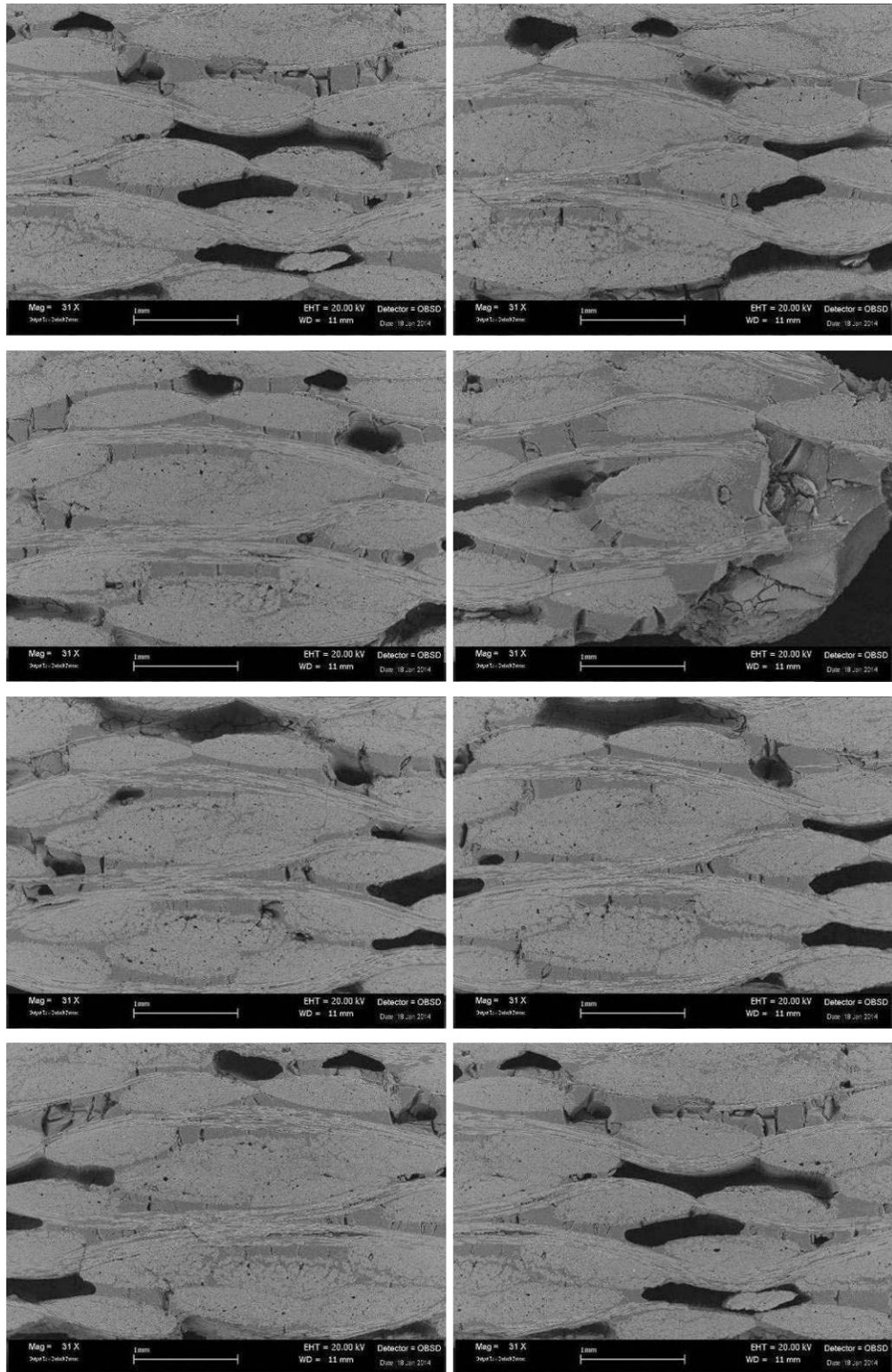


Figure 4.4.21 - Microstructure obtained using 2D-plyies with 0 - 90° twill orientation.

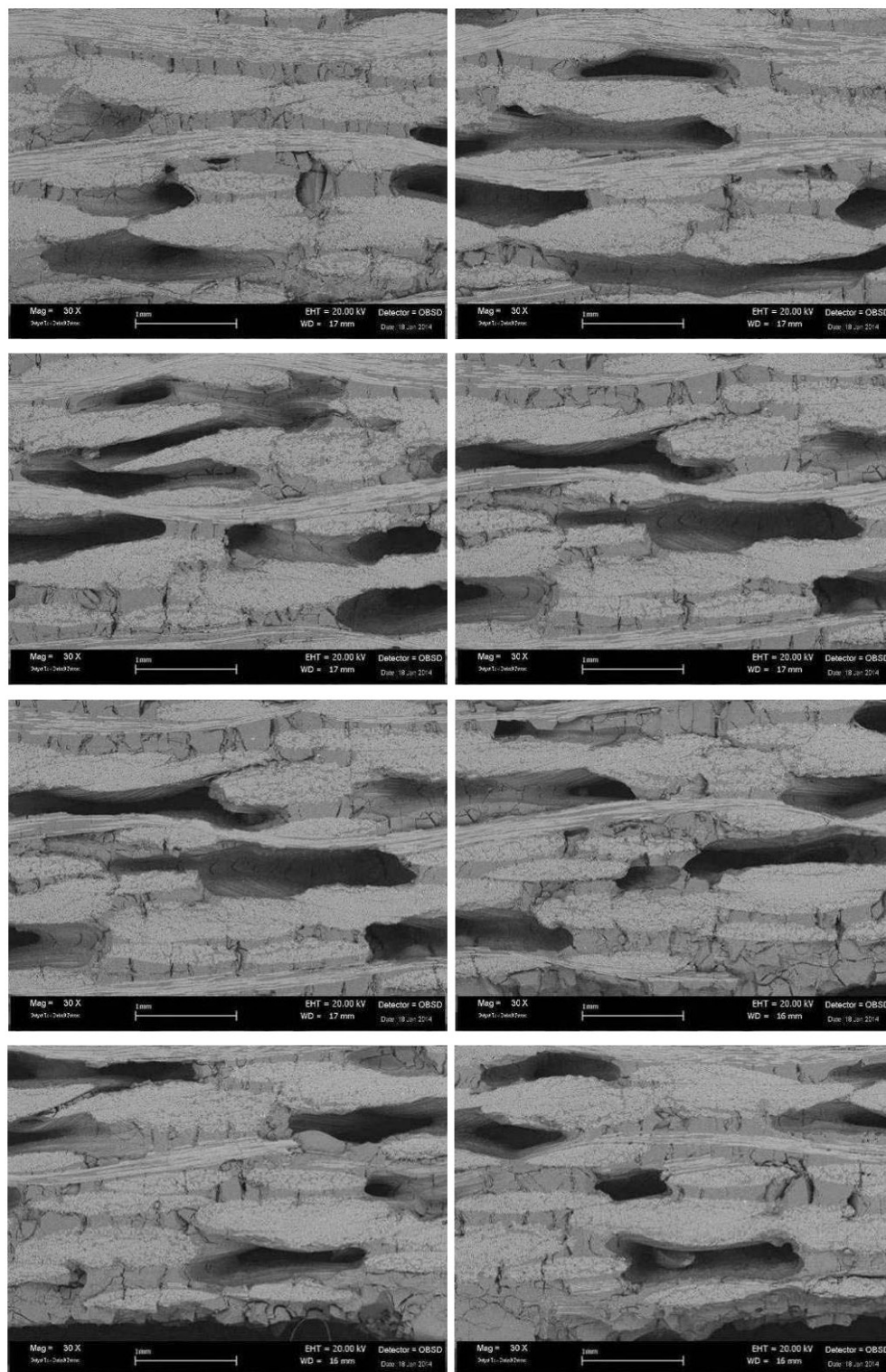


Figure 4.4.22 - Microstructure obtained using 2D-plyes with 0 - 45° fiber orientation.

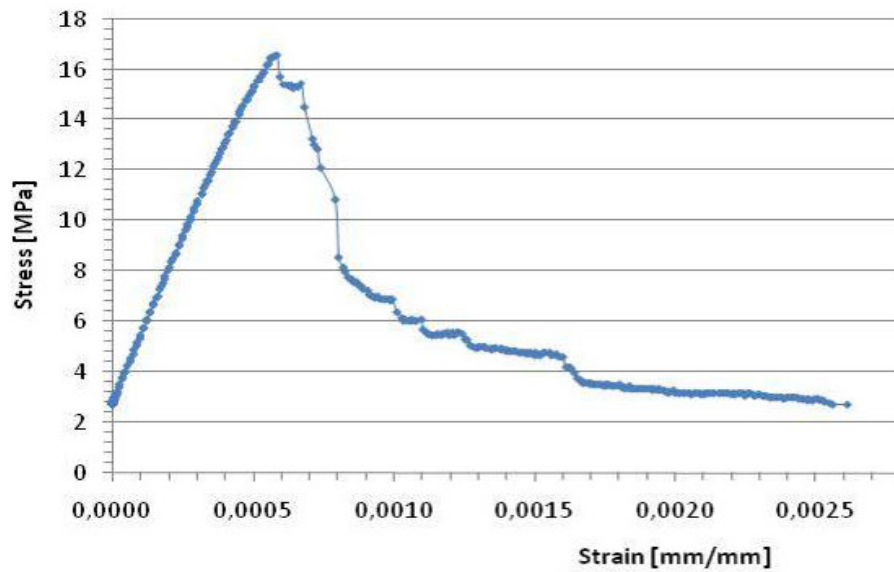


Figure 4.4.23 - Stress strain curves at room temperature (6 2D-basalt plies, 2 PIPs).

Summarizing, as stated before and as shown by the stress strain curve above using these 2D fabrics obtained by calcination, it was not possible to obtain MOR values as high as before, possibly because of the damages during the calcination step or because of a low tensile strength of these particular basalt fibers, so the experimental work continued with bidirectional and unidirectional fabrics.

4.4.5 Densification data for the various solutions

Even if the main property to be checked for thermostructural applications is the flexural strength at different temperatures, after considering many different solutions it is also important to summarize the densification data, which is made in the following table.

Fiber type	Pyr. condit.	Fiber weight	After 1st PIP	After 2nd PIP	% w/w fibers	% w/w fibers	Absolute & relative density	Theor. Density (pycnom.)
		(g)	(g) and (100*w/w)	(g) and (100*w/w)	1° PIP	2° PIP	g/cm ³ ; % 2° PIP	g/cm ³
4 bidir bas. plies	700°C N ₂	33.8	41.0(121)	42.1(124)	n.d.	80%	1.72 (71%)	2.42
		34.2	39.7(116)	40.6(119)		84%		
4 bidir bas. plies	700°C Vacuum	33.2	38,2 (115)	39.3 (118)	87%	84%	1.84 (77%)	2.39
		31.3	36.7 (117)	38.5 (123)	85%	81%		
2D basalt 4 plies	700°C Vacuum	22.9	34.3 (149)	Broken				
		23.2	35.7 (153)					
2D basalt 6 plies	700°C N ₂	36.9	57.3(155)	58.9 (160)	64%	63%	1.79 (76%)	2.36
		36.4	56.5(155)	57.9 (159)	64%	63%	1.95(82%)	2.39
15 plies 2D carbon	700°C N ₂	40.1	57.5(143)	66.8(166)	n.d.	60%	n.d.	n.d.
		39.9	59.0 (147)	68.8(172)		58%		
unpressed SiC felt	900°C N ₂	1.98	32.3 (I)	43.9 (III)	n.d.	5%-2°PIP	(1.26-2°PIP)	2.48
			39.1 (II)	46.1 (IV)		4%-4°PIP	(1.48-4°PIP)	
Pressed SiC felts	900°C N ₂	22.2	119.5	145.69	19%	15%	1.35	2.48
		21.1	113.9	152.13	19%	14%		

Table 4.4.4 - Densification data on the various solution considered.

The main considerations that can be made are the following:

- On 2D fabrics and pressed and unpressed felts, the possibility to infiltrate matrix with the first PIP step is considerably increased, as it was observed both on basalt, SiC and carbon fabric. In the case of the tested 2D basalt fabric high infiltration (which can be measured from the weight ratio between the composite and the

fibers) was anyway associated to a low mechanical performance. The reason however could also be a difference in fiber properties, which could have been damaged in calcination from the prepreg state. Some other work should be done on other types of 2D basalt fabrics (when available).

- The enhanced possibility to infiltrate matrix in the case of 2D fabrics/felts is higher than in the case of bidirectional fabrics (actually coupled unidirectional, as discussed earlier) also for the PIP steps which follows the first infiltration.

- On basalt bidirectional fabric, the densification after the first step is moderate, really it doesn't appear useful to go on with other steps. The unidirectional SiC fabric (that is SCS 6) behaves differently, but in this case the fiber diameter and the space between the fibers are higher of one order of magnitude: consequently the infiltration behavior is completely different. Anyway thick fibers doesn't appear promising for achieving good mechanical properties, since the matrix cracks if the space between the fibers is too large. In the case of pressed SiC felts, it was obtained a non regular geometric shape, which made it difficult to calculate geometrical density. Anyway the most significant result was the fragility of the obtained composite, even at room temperature. This observation suggested that this solution could not have any practical application. A MOR of at least 100 MPa at room temperature was chosen as the minimal acceptable strength for application to transports and construction, and the only system, among those considered, which managed to achieve these MOR values appears to be the basalt_f/ SiCO.

- The difference in the densification behavior between vacuum and nitrogen flow pyrolysis was studied in the case of bidirectional basalt fabrics. The differences are found to be moderate, and this was confirmed also by the mechanical data (table 4.4.5). The higher performance of vacuum pyrolysed samples at 600°C is difficult to understand and other measurements are needed.

Fiber type	Pyrolysis conditions & n° PIP	% w/w fibers	Absolute & relative density	MOR 25°C	MOR 400°C	MOR 600°C	MOR 1000°C
			g/cm ³ (%)	MPa	MPa	MPa	MPa
4 bidir bas. plies	700°C 2PIP N ₂	80-84%	1.72 (71%)	130-150	100-120	20-30	-
4 bidir bas. plies	700°C, 2PIP Vacuum	81-84%	1.84 (77%)	70-90	90-95	50-60	-
2D basalt 6 plies	700°C, 2PIP N ₂	63%	1.79-1.95 (76-82%)	23;35;32	18	-	-
unpressed SiC felt	900°C 4PIP, N ₂	4%-4°PIP	1.48-4°PIP	10-12	n.d.	12.5	14
pressed SiC felts	900°C 2PIP, N ₂	15% 14%	55%	15-18			8-9

Table 4.4.5 - MOR values for the various solution considered after 2 PIP steps (except otherwise specified).

It should be noted here that pressed fibers (without matrix) would have a comparatively high relative density, and 100% w/w fiber content but, obviously, no flexural properties, so the comparison of systems significantly different from each other would require considering other parameters, the choice of which is not so obvious, also because there is a change of volume during the PIP composite production. However, relative density and the fiber content (%w/w and %v/v) seem good enough parameters to compare similar systems, or check the reproducibility of the same solution. Fiber content in volume percent is also needed since a significant variability in sample thickness was observed.

Regarding the Young modulus, the values generally follow the same trends (e.g. vs temperature, or vs processing condition, pyrolysis in vacuum or nitrogen) of the MOR values. Certainly rigidity is one of the important characteristic of the composite and is determined by the efficiency of infiltration process, but a minimal value can not be chosen without having decided which is the application and which thickness is of interest.

4.4.6 Further optimization of the process

On the basis of the previous results, some other parameters were tested and corrections to the procedure were made. In particular, from the previous results, the second PIP, in the case of unidirectional/bidirectional fabrics, seems useless and time consuming, because it contributes very little to densification, with the problem that the samples tend to deform during the second PIP, if it is performed out of the steel mould. So, as a rule, the optimization of a procedure with a single PIP step was attempted. Regarding the mould, two new configuration were considered:

- a)- a more rigid steel mould, with holes only on the upper side as before, using spacers to control the volume percent fiber content;
- b)- a more rigid steel mould, with holes on both sides and spacers (mould 2).

Applying solution a) it was obtained significant improvements in the MOR values. For example, with 1 PIP at 700°C in nitrogen, the stress-strain curve at 400°C is reported in figure 4.4.24. With the process introduced the MOR after one PIP step are higher than the previous values after 2 PIPs, which is quite a good result. In figure 4.4.25 the stress vs the "piston stroke" was plotted, since this measure was performed without LVDT, in order to have an higher geometrical span available to reach rupture.

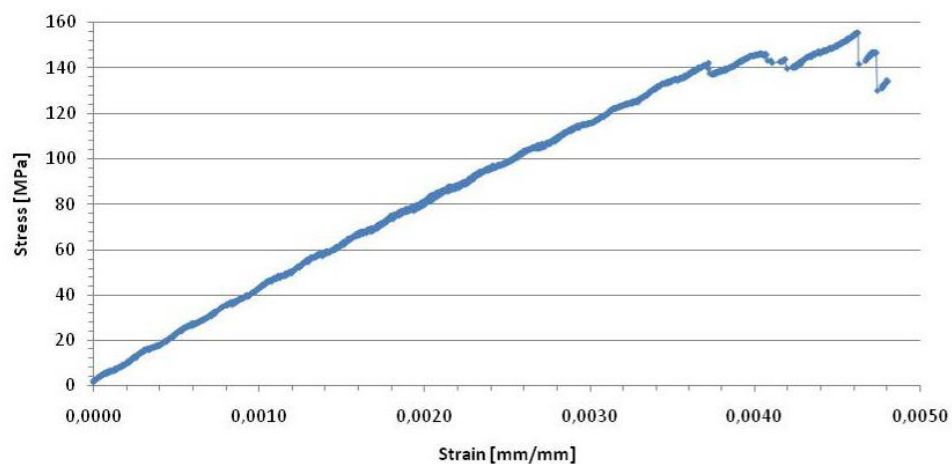


Figure 4.4.24 - Stress strain curve at 400°C after one PIP at 700°C (N₂).

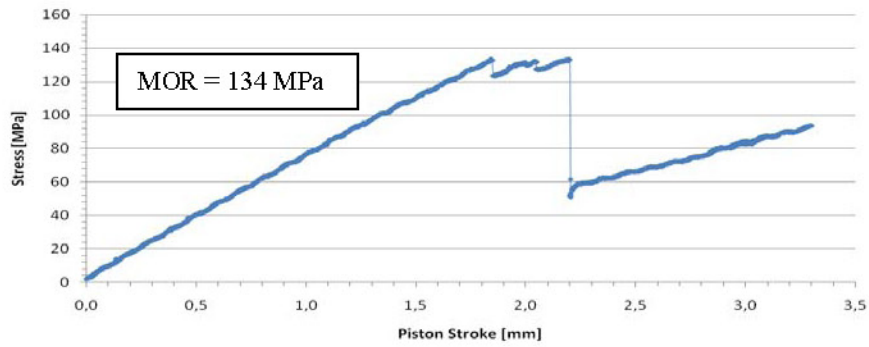


Figure 4.4.25 - Stress vs piston stroke at 400°C up to rupture (one PIP, 700°C, N₂).

On the other hand, even if more measures are needed, the mould with holes on both sides seems to give lower MOR results, due to a less efficient infiltration. For example, after 1 PIP step at 700°C in nitrogen, the MOR value at 400°C was around 100 MPa (instead of 150 MPa). The microstructure reveals an high porosity, and some more matrix would be beneficial to increase mechanical performance, especially in the case of pyrolysis at 700°C in vacuum. In figure 4.4.26, stress strain curve at 400°C is reported on a sample produced in vacuum ($d = 1.62 \text{ g/cm}^3$; relative density 71%; fiber = 64%w/w; theoretical density 2.27 g/cm^3) and in nitrogen flow ($d = 1.89 \text{ g/cm}^3$; relative density 81%; fiber = 71%w/w; theoretical density 2.33 g/cm^3). In figure 4.4.27 a measures without LVDT to reach rupture in the case of pyrolysis performed in nitrogen.

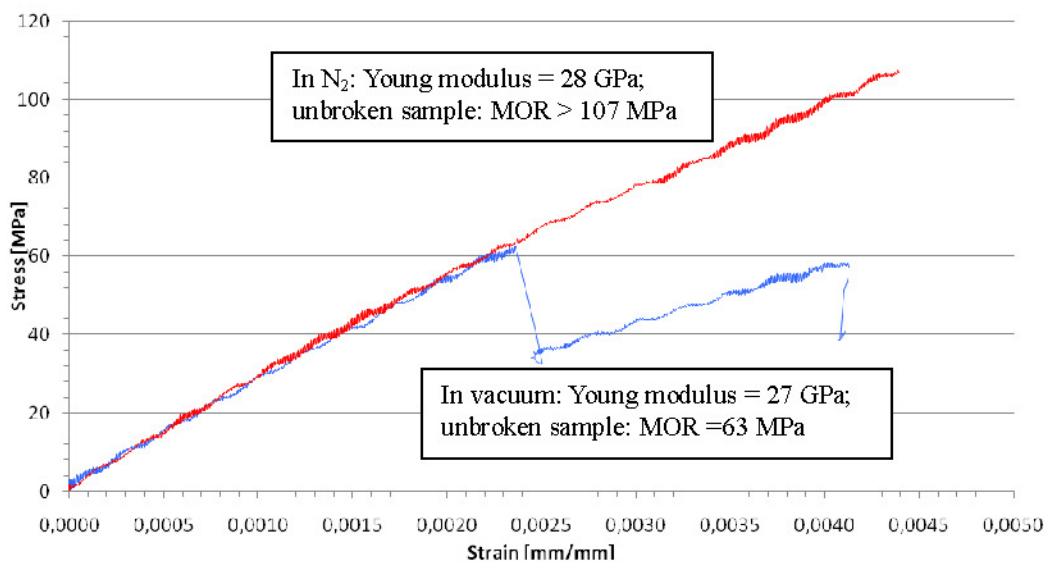


Figure 4.4.26 - Stress strain curve at 400°C on composites produced with 4 bidirectional basalt plies: pyrolysis at 700°C-N₂ (red) and 700°C-vacuum (blu).

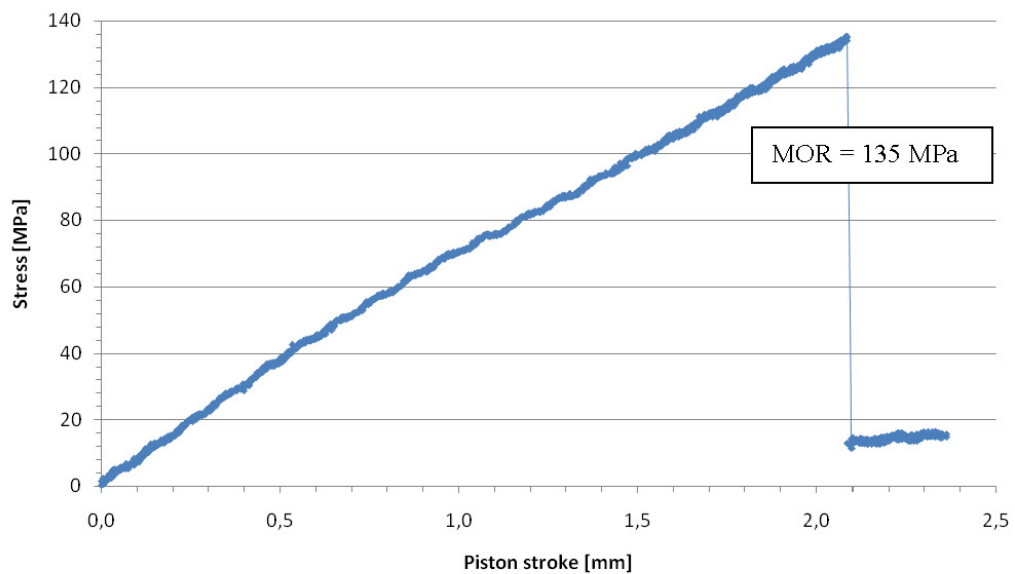


Figure 4.4.27 - Stress vs the piston stroke on composites produced with 4 bidirectional plies: at 700°C-N₂.

Another important parameter which was changed aiming at the industrial scaling up was choosing a basalt fabric more stable and without cotton fibers, which possibly reduce performances and are not fully effective in ensuring stability of the fabric. Since we did not find cheap 2D basalt fabrics, it was tested another unidirectional fabric from HG-GBF, shown in the figure 4.4.28.

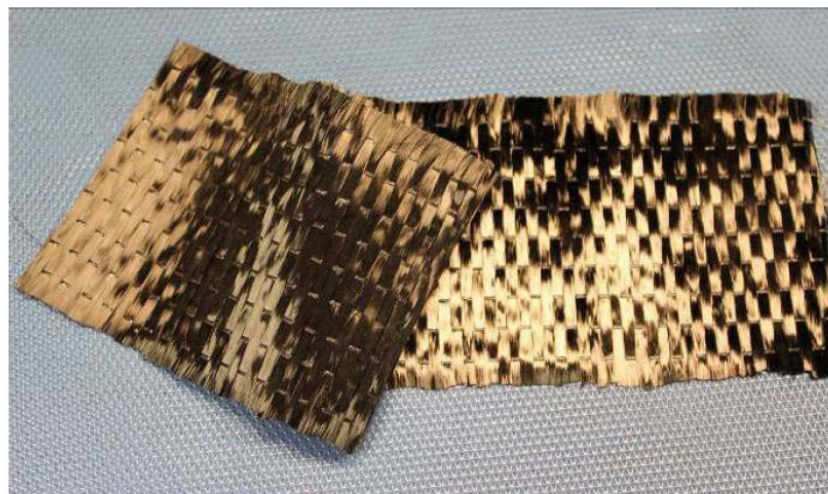


Figure 4.4.28 - HG-GBF unidirectional basalt fabric (400 g/m²).

In this case, the unidirectional basalt fabric is kept into position by glued glass fibers (figure 4.4.29). These glass fibers tows can be individuated by SEM-EDS in

the composite after PIP process (figure 4.4.30) because of thinner diameter and a different chemical composition. EDS semiquantitative results in both cases are reported in figures 4.4.31 and 4.4.32. Eight orthogonal plies of this fabrics (400 g/m^2) correspond perfectly to the 4 plies of bidirectional plies used before, which was characterised by 800 g/m^2 . The picnometer density was evaluated in 2.51 g/cm^3 , slightly lower than previous 2.66 g/cm^3 , for the fiber without glass.

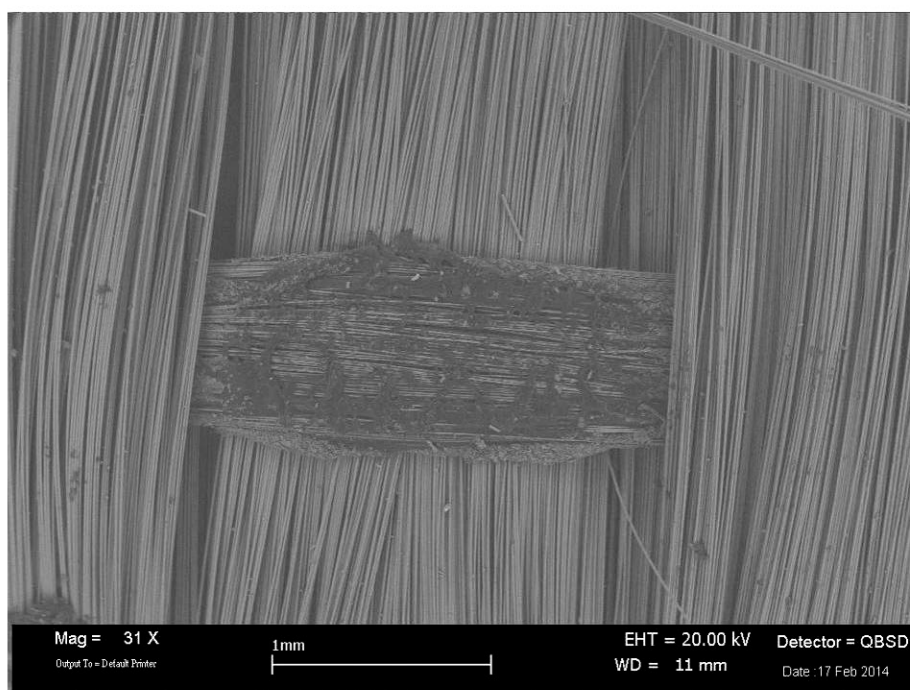


Figure 4.4.29 - Unidirectional basalt fabric, using glued glass fibers as fixers.

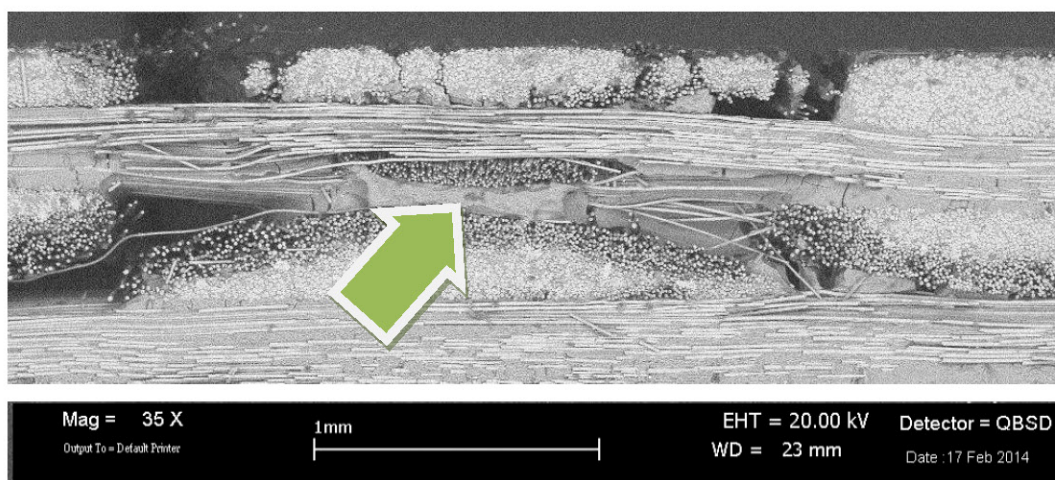


Figure 4.4.30 - Glass tow included in the PIP composite microstructure.

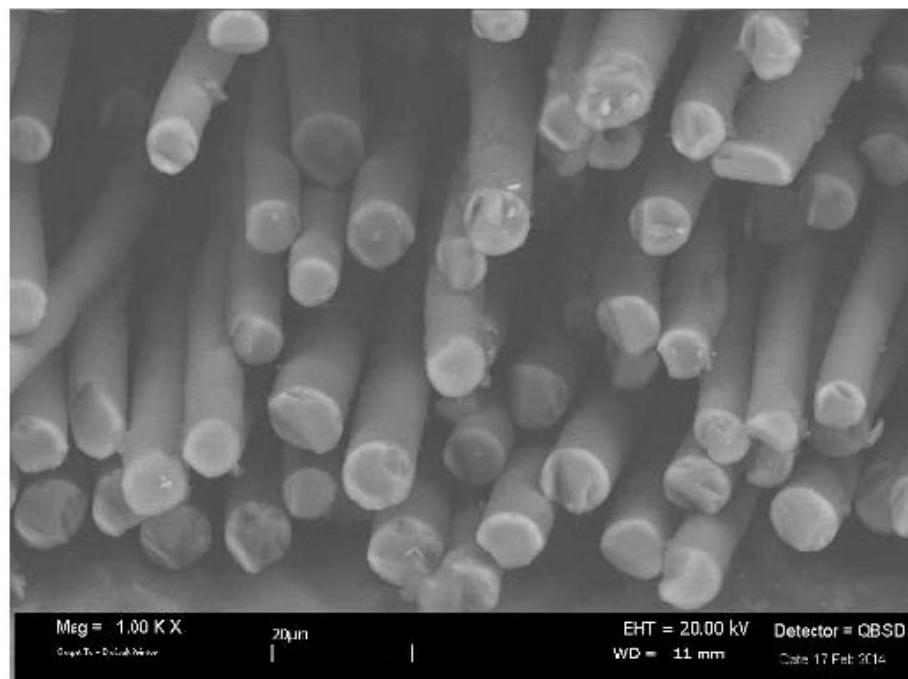
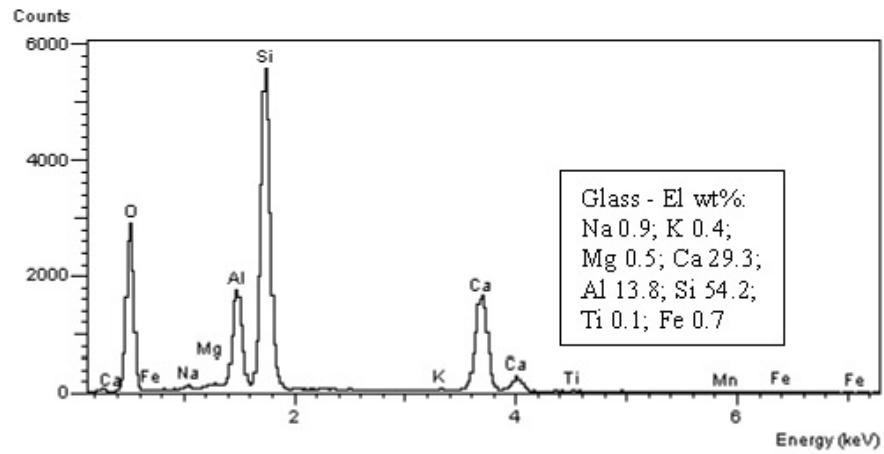


Figure 4.4.31 - EDS spectrum and microstructure of glass fibers in the PIP composites obtained from unidirectional basalt fabric.

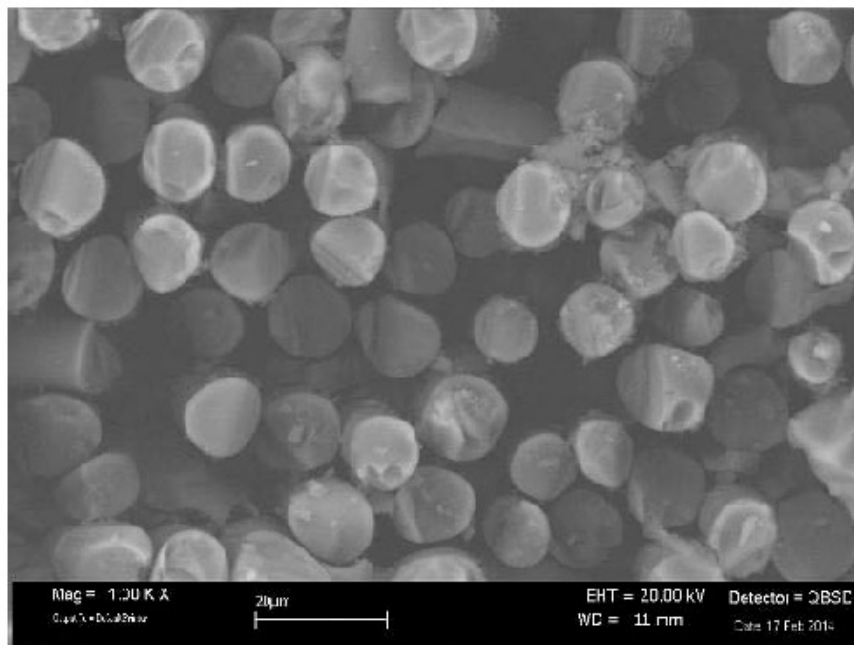
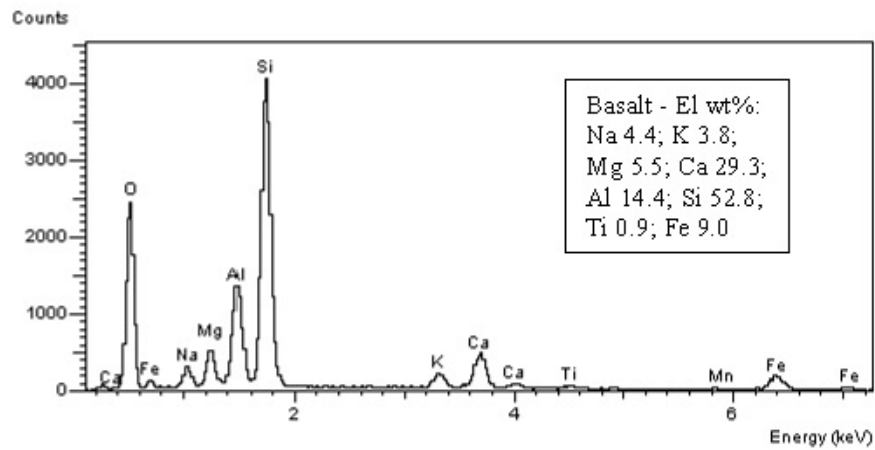


Figure 4.4.32 - EDS spectrum and microstructure of basalt fibers in the PIP composites obtained from unidirectional basalt fabric.

The obtained microstructures are reported in figures 4.4.33 and 4.4.34 (for pyrolysis in vacuum and nitrogen respectively). Especially in figure 4.4.34 there is a certain asymmetry, which it is thought due to the new mould (mould 2), with holes on both sides, which it seems having a negative effect on "matrix infiltration" on one side and which could significantly affect MOR measures. Density values using 8 plies unidirectional fabrics however are higher than those achieved with 4 bidirectional plies, with the same mould type, so the change from bidirectional to unidirectional actually appears as an improvement. In both cases, as was expected, vacuum pyrolysis produces lower densification (higher weight percentages of fiber on the total mass) and, if the other parameters are the same, it negatively affects MOR values. The effect on relative density is less linear, since relative density is also determined by shrinkage, which is not the same in the different cases: same samples shrink and the final thickness is variable and significantly lower (e.g. 2.35 mm) than that of the spacers (2.85 mm). The reason of less effective matrix infiltration is probably that vacuum favors the early production of gaseous products during the pyrolysis, especially if some low molecular weight fraction is present, contributing to the creation of porosity.

Fiber type	Pyrolysis conditions	Fiber weight	After 1st PIP	Density of MOR samples	%w/w fibers	MOR 400°C	Rel dens	Thick	Calc. Theor. Density
		(g)	(g)			MPa	%	mm	(g/cm ³)
4 bidir basalt plies	700°C- Vacuum mould 2	55.6	86.6	1.57; 1.62	64%	60-70	73	2.3-2.5	2.20
4 bidir basalt plies	700°C- N ₂ mould 2	36.6	51.8	1.89; 1.90	71%	110-140	84	2.5-2.6	2.25
8 unidir basalt plies	700°C- Vacuum mould 2	48.3	56.1	1.77; 1.73; 1.72	86%	90-90	73	2.3-2.5	2.38
8 unidir basalt plies	700°C-N ₂ mould 2	62.1	47.8	1.68; 1.73	77%		74	2.2-2.3	2.30
8 unidir basalt plies	700°C-N ₂ mould 1	76.1	52.6	1.94; 1.92	69%	>120	87	2.8-2.9	2.24

Mould 1: holes only on the upper side

Mould 2: holes on both sides

Table 4.4.6 - Density and MOR values for the new solutions.

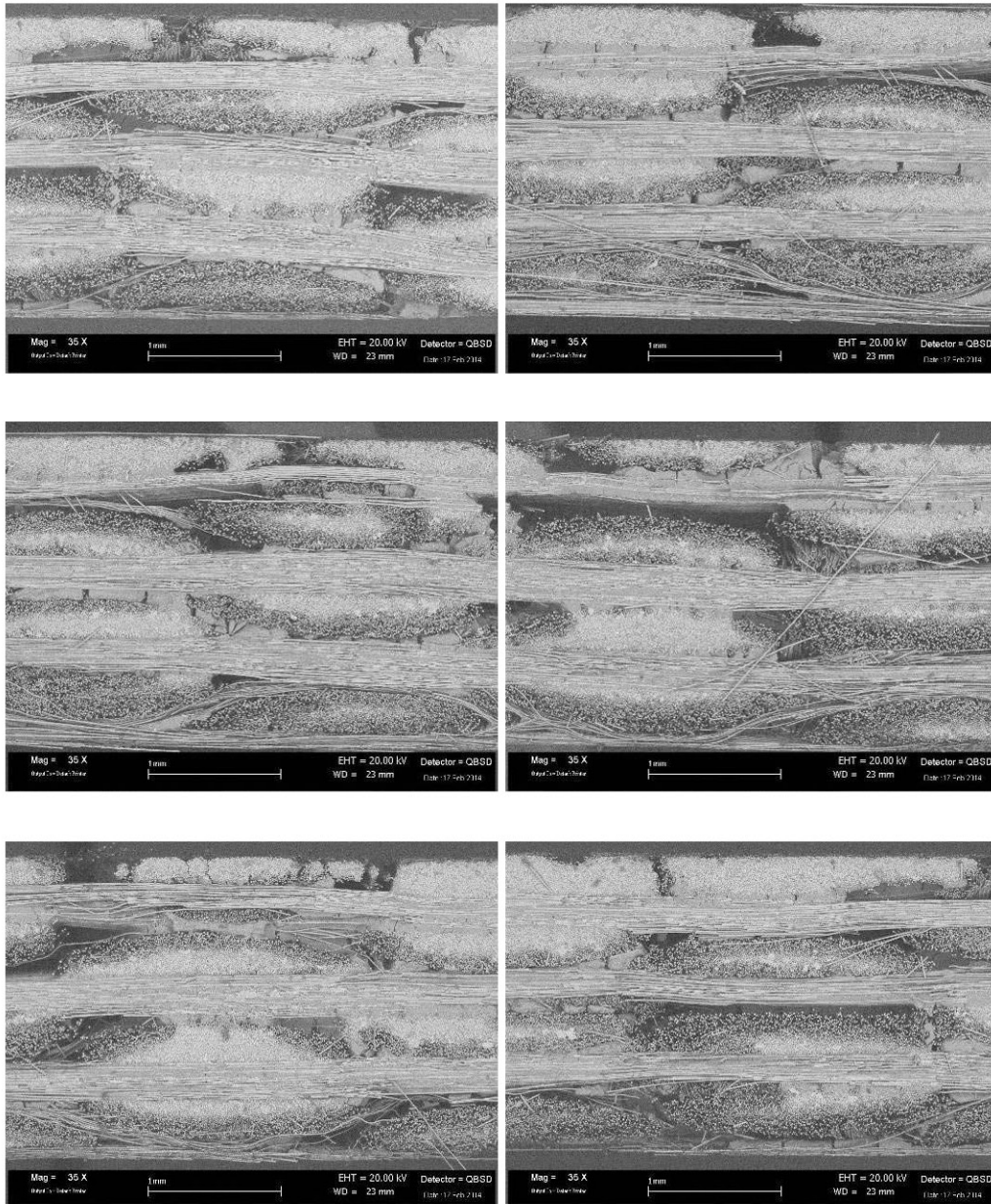


Figure 4.4.33 - Microstructure obtained using unidirectional basalt fabric.
Pyrolysis at 700°C in vacuum; mould 2.

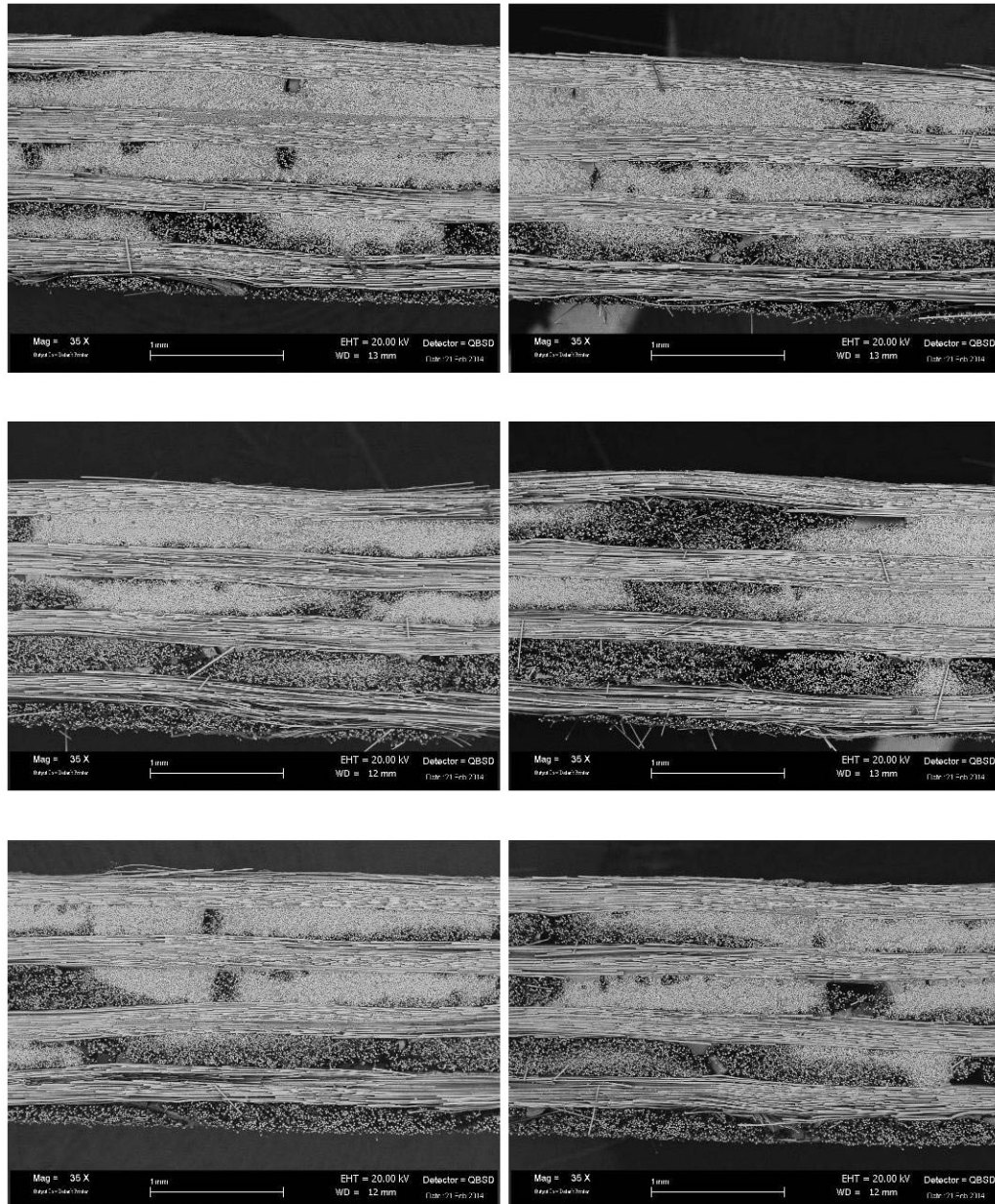


Figure 4.4.34 - Microstructure obtained using unidirectional basalt fabric.
Pyrolysis at 700°C in nitrogen; mould 2.

Regarding the nature of the new basalt fibers and its interaction with the SiCO matrix, figure 4.4.35 suggests a fiber pull-out behavior similar to that registered before. The less effective matrix infiltration implies a lower mechanical performance, which was confirmed by measures (figures 4.4.36 and 4.4.37). However, with the new variables (new fiber type, new mould and new fabric type) a MOR value at 400°C around 90 MPa was measured for a sample prepared by pyrolysis in vacuum, which is indeed a rather satisfying and promising result.

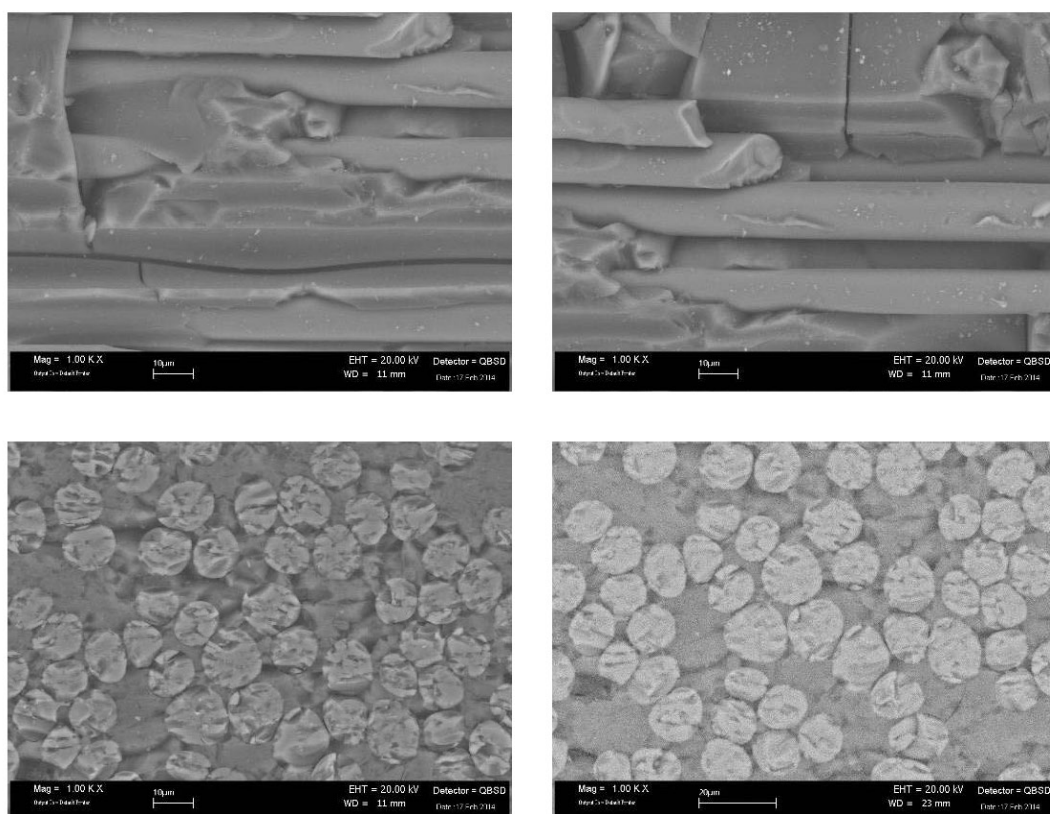


Figure 4.4.35 - Microstructure obtained using unidirectional basalt fabric. Pyrolysis at 700°C in vacuum; mould 2.

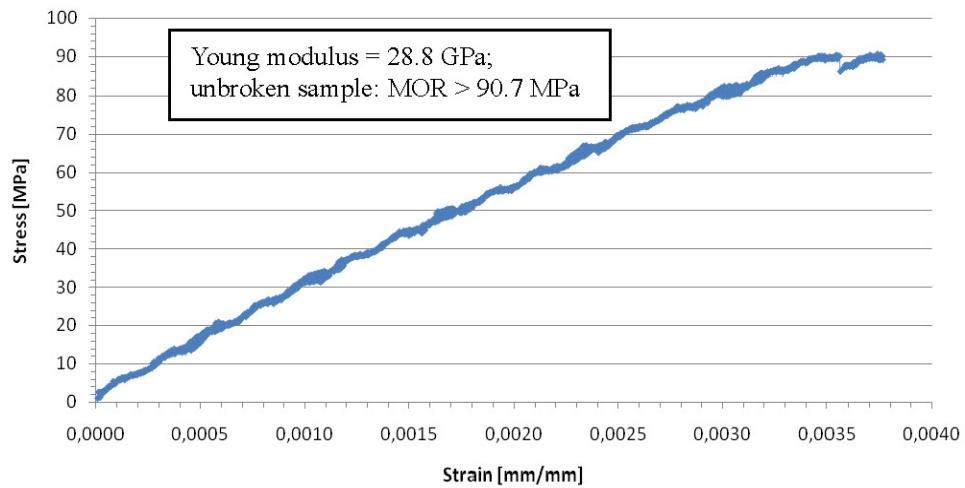


Figure 4.4.36 - Stress strain curve on composites produced with 8 unidirectional basalt plies.
Pyrolysis at 700°C in vacuum.

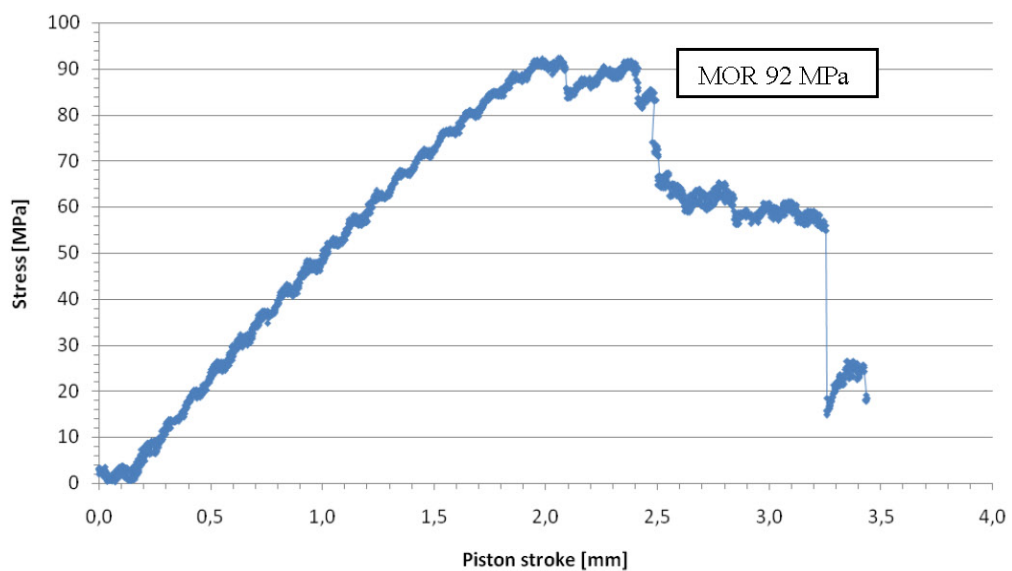


Figure 4.4.37 - Stress vs the piston stroke on composites produced with 8 unidirectional basalt plies. Pyrolysis at 700°C in vacuum.

The effect of the mould was checked by stepping back to the mould 1, with holes only on the upper side (last row of table 4.4.6). An increase in the densification efficiency was verified, as it is also shown by microstructure (figure 4.4.38 and 4.4.39) and stress strain curves (figure 4.4.40).

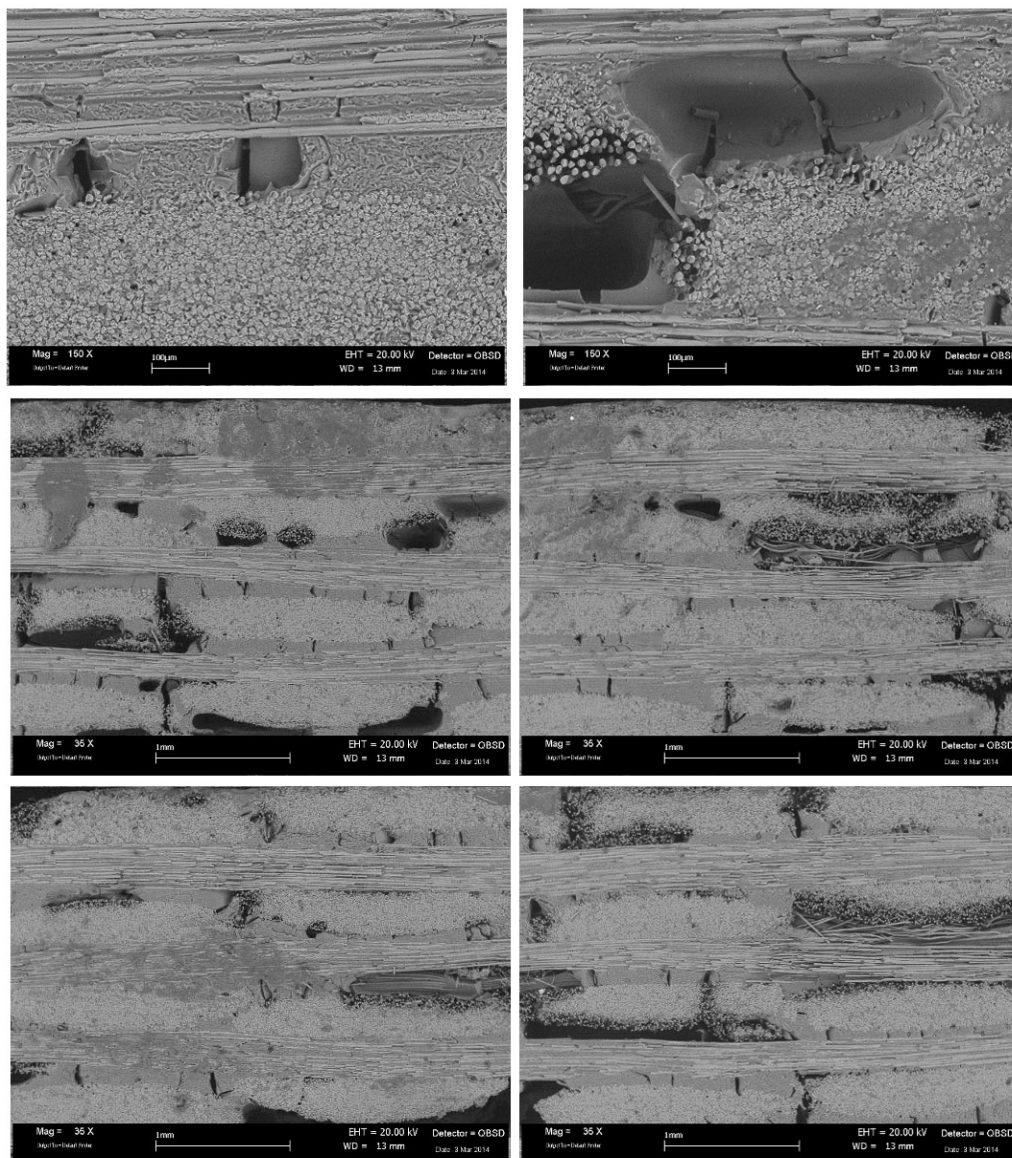


Figure 4.4.38 - Microstructure obtained using unidirectional basalt fabric.

Pyrolysis at 700°C in nitrogen; mould 1.

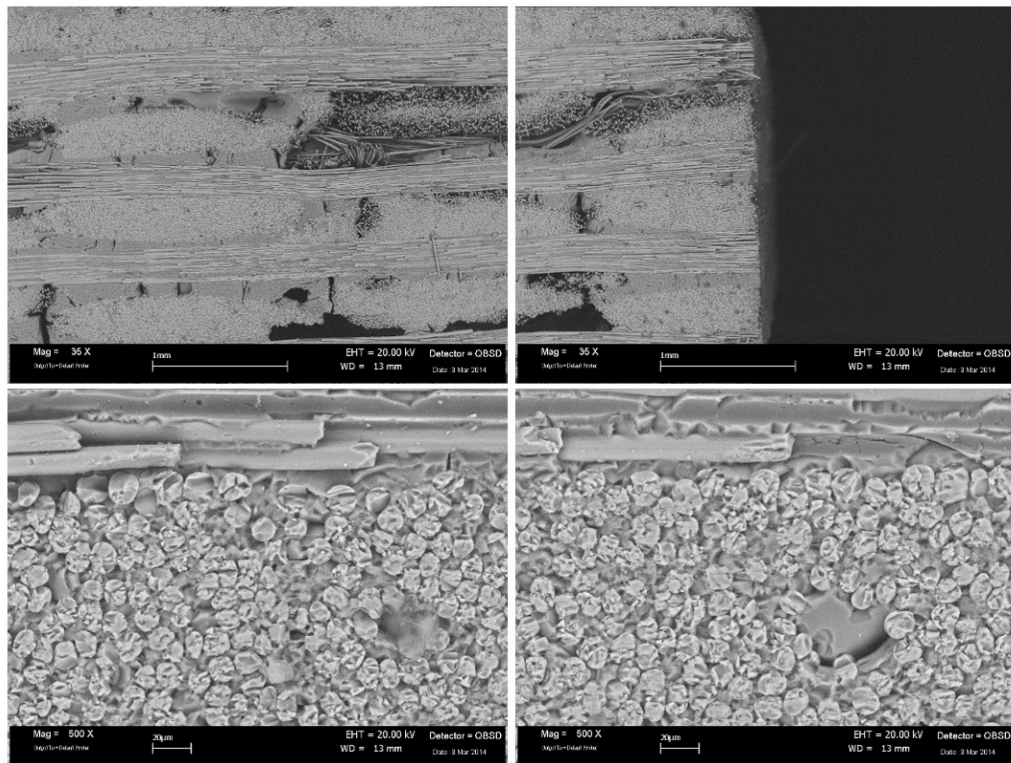


Figure 4.4.39 - Microstructure obtained using unidirectional basalt fabric.
Pyrolysis at 700°C in nitrogen; mould 1.

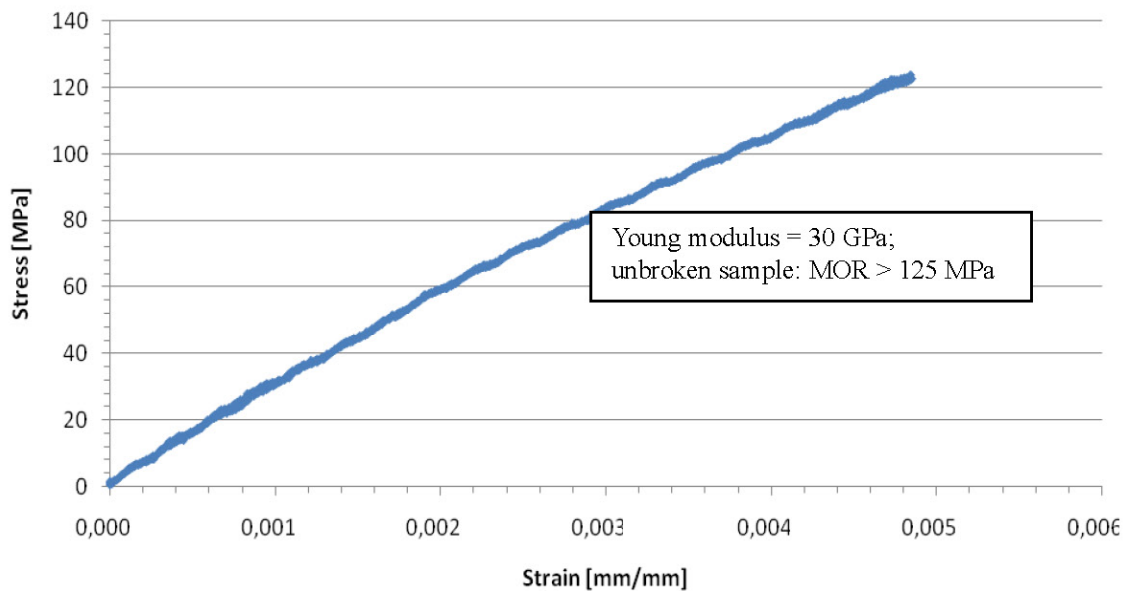


Figure 4.4.40 - Stress strain curve on composites produced with 8 unidirectional basalt plies.
Pyrolysis at 700°C in nitrogen. Mould 1 (with holes on the upper side only).

4.4.7 Stability towards oxidation and completion of pyrolysis

Even if, in the case of basalt fibers, pyrolysis cannot be performed at temperature higher than 700°C, it is important to establish pyrolysis completeness and oxidation resistance of the SiCO produced. During the developing of the process, it had been performed a check on the macro scale about oxidation resistance, finding that SiCO prepared at 700°C doesn't change colour and weight after 5 hours at 650°C in fluent air. However a specific thermogravimetical study was necessary to understand the involved phenomena, since oxidation and pyrolysis could compensate each other.

Regarding pyrolysis completeness, the SiCO produced in vacuum at 700°C in our pilot plant was heated in argon flow up to 1350°C (10°C/min up to 1350°C, followed by a 30 min of isothermal step) with the result that the weight loss after 700°C is below 2.5%. The weight loss (figure 4.4.41) is concentrated around 890°C but there is also weight loss before 500°C. As shown from the plot against time, plot which includes the isothermal step, the weight loss during the isothermal step at 1350°C is rather small (0.1%) and tends to zero with time. The DTG peaks can be identified if the same TG (except the isothermal step) is plotted against temperature.

The weight loss at temperature below 500°C (figure 4.4.41) was not expected, being the material produced at 700°C, and required a specific investigation. It resulted that the material could absorb moisture from air. Initially the position of DTG peaks above 160°C suggested the formation of some sort of hydroxides, a phenomenon which could have been of fundamental importance in determining the thermomechanical behaviour, so a specific investigation was done. Upon boiling with water and subsequent drying under vacuum at 125°C for two hours, it was found an added weight loss, still suggesting hydroxides formation (figure 4.4.42). This experiment was performed on samples without milling, possessing a granulometry (measured as the maximum linear size of the pieces) comprised between 0.5 and 4 mm, produced by cracking occurring spontaneously during the pyrolysis, considering this state more similar to the working condition of the

matrix into the composite (thickness around 2-4 mm). Further TG measures on powdered samples demonstrated that this weight loss is not due to hydroxides formation, but due to the slow kinetics of drying of SiCO, which is probably highly porous as a consequence of pyrolysis.

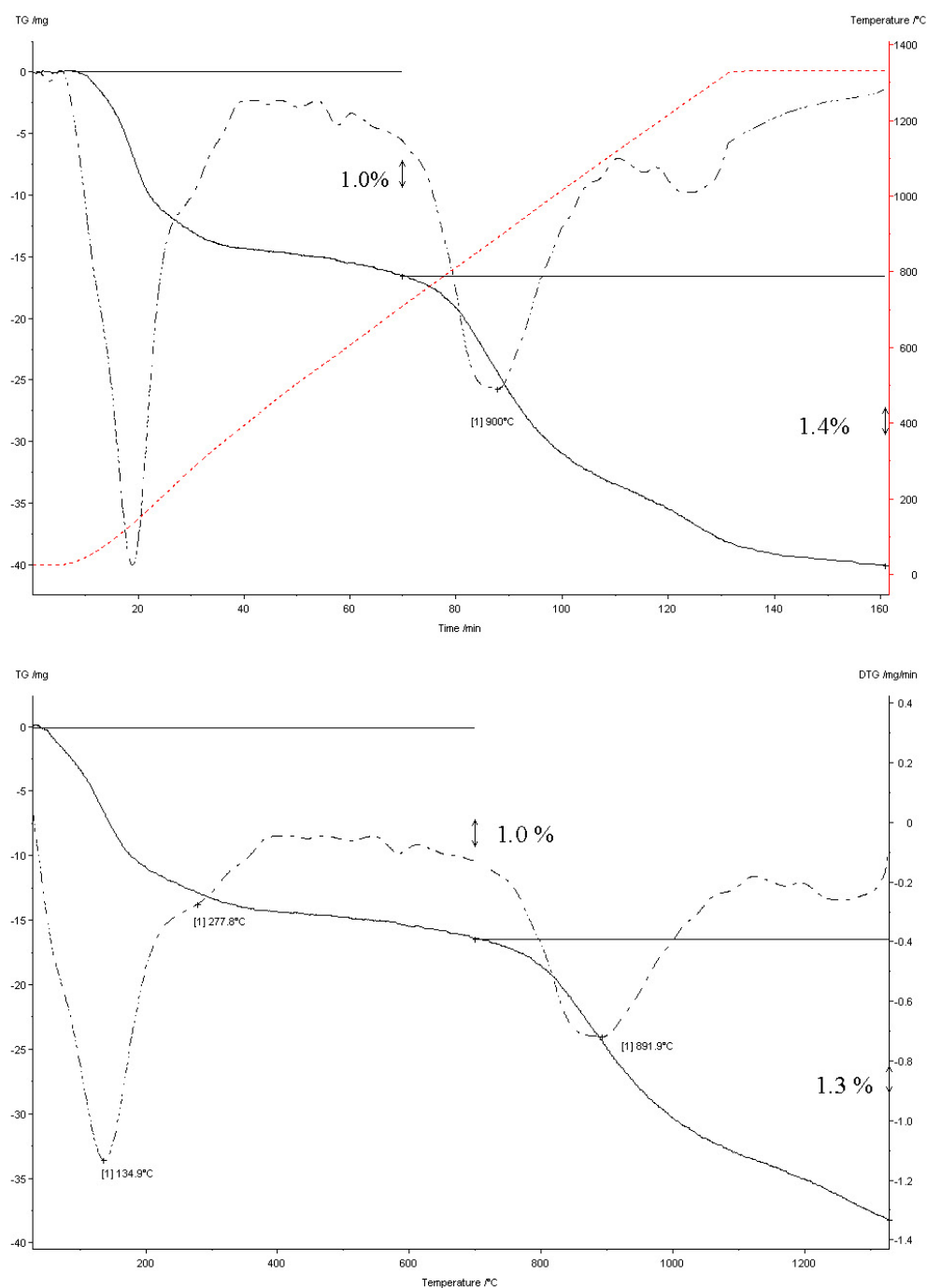


Figure 4.4.41 - TG in argon (10°C/min up to 1350°C) on SiCO (produced in vacuum, 700°C, 15h).

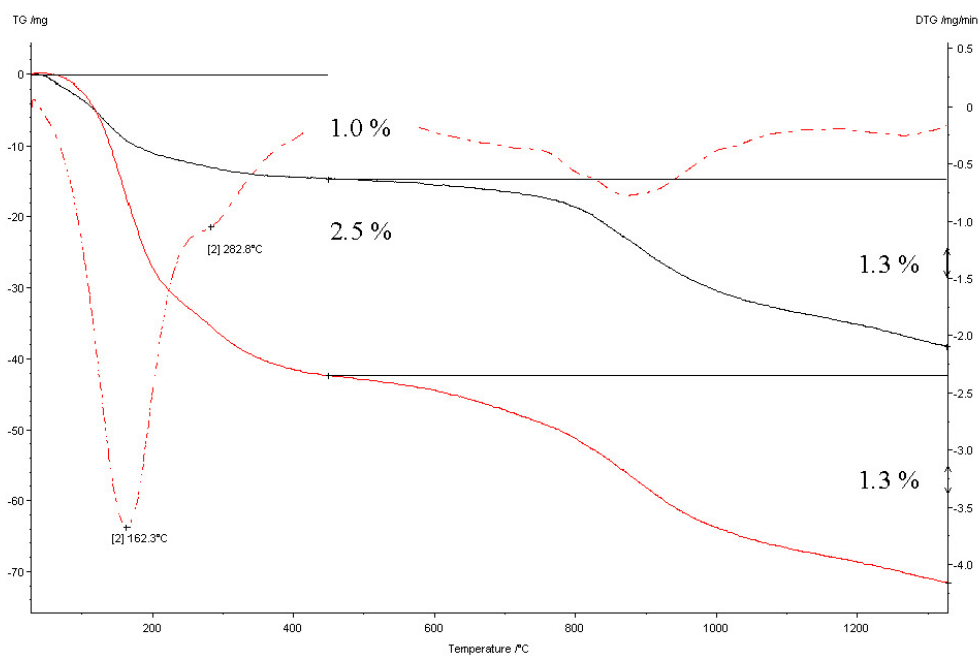
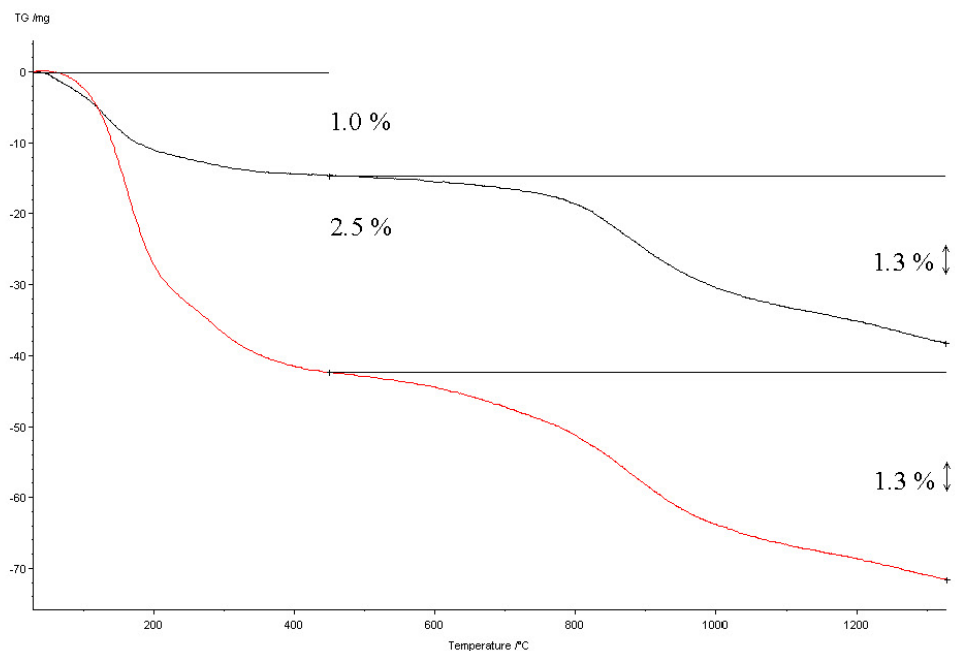


Figure 4.4.42 - TG in Ar (10°C/min) on SiCO (produced in vacuum, 700°C, 15h) before (green) and after (red) boiling with water.

On the other hand, to establish the resistance to oxidation, another fraction of the SiCO produced at 700°C in vacuum in the pilot plant was analysed with the same cycle, by employing air instead of argon. The previous curve in argon was subtracted as a blank, to consider and correct for the weight loss (due to incomplete pyrolysis) which would occur also under inert atmosphere, and that could hinder completely the oxidation process. The result is that SiCO produced in vacuum at 700°C oxides in a negligible amount (1%) between 650 and 850°C (DTG peak a 740°C), and then it is stable up to 1350°C (figure 4.4.43).

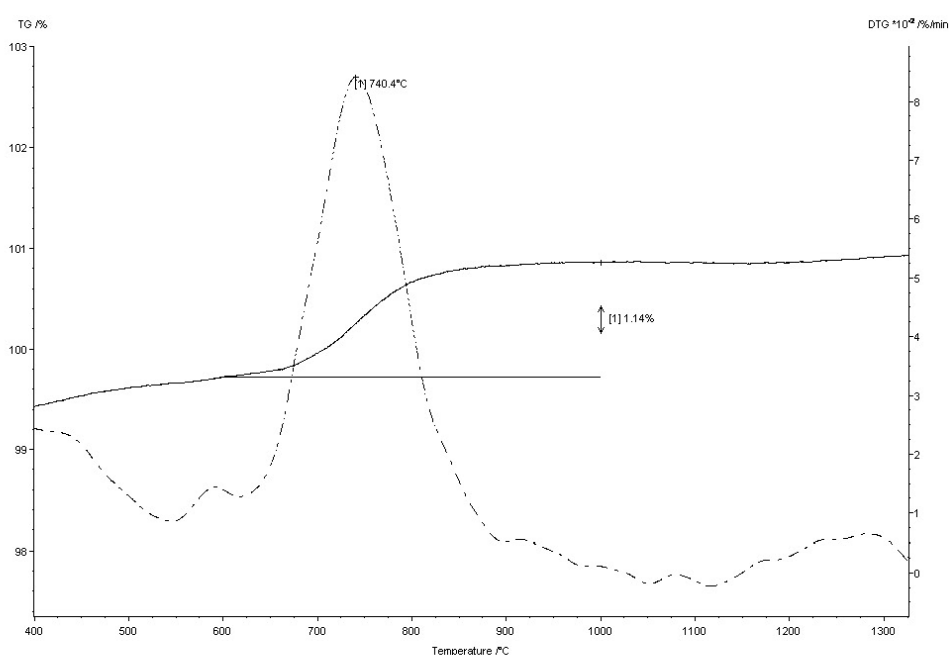


Figure 4.4.43 - TG in air (10°C/min up to 1350°C) on SiCO (produced in vacuum, 700°C, 15h).

The same curves were also registered on SiCO produced by pyrolysis at 900°C under vacuum and at 700 and 900°C in N₂. The results established that:

- the pyrolysis for 15h at 900°C, both in vacuum and inert atmosphere is complete: no significant weight change (<0.3 % weight gain) occurs during the subsequent pyrolysis up to 1350°C in argon;
- the pyrolysis for 15h at 700°C, both in vacuum and inert atmosphere is almost complete: weight loss during the subsequent pyrolysis up to 1350°C in argon is below 2 %;
- SiCO is very igroscopic, easily adsorbing atmospheric humidity;

- regarding oxidation stability the material pyrolysed at 700°C is fairly enough oxidation resistant (<3% weight gain upon oxidation up at 1350°C) and the oxidation occurs mainly between 800 and 1000°C;
- oxidation stability of the material produced at 900°C is higher than that produced at 700°C (<1% weight gain upon oxidation up at 1350°C);
- regarding the comparison between vacuum and N₂ processing, the differences are always not significant or very moderate.

A crucial step in determining the pyrolysis result was demonstrated to be the drying step. Because of a problem in the drying system, some sample were unintentionally dried at higher temperature. The difference in the pyrolysis result was dramatic. In the figure 4.4.44, the TG in argon of the SiCO, obtained at 700°C after a drying at 60-90°C and at 120-140°C are reported. In the latter case the ceramic phase is much less stable to heating above 700°C, even in argon. The density of the ceramic phase in the two cases was measured on the powdered material and resulted 1.80 g/cm³ in the case of a correct drying procedure and 1.49 g/cm³ in the case of drying a higher temperature. There is also a difference in colour, black in the first case, brown-red in the second case, which makes easier avoiding this possible mistake.

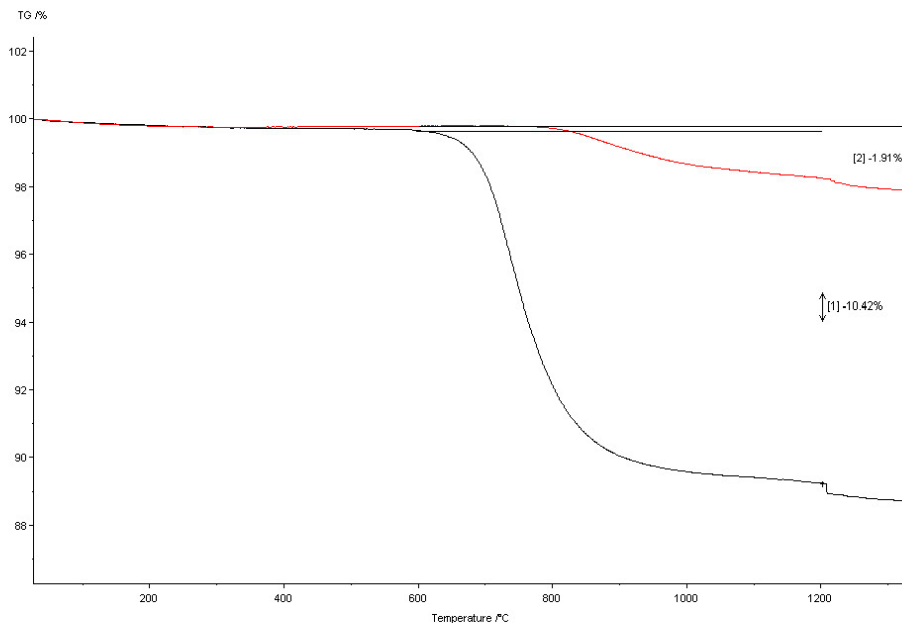


Figure 4.4.44 - TG in Argon on SiCO produced by pyrolysis at 700°C under vacuum, after drying at 60-90°C (red line) and at 120-140°C (green line).

The difference for a thermal treatment in air is even more important: the ceramic phase that forms after an incorrect xylene drying undergoes oxidation much more easily, changing its colour to white. The overall balance between SiCO oxidation to SiO₂, a phase change which implies a weight increase, and the pyrolysis completion is reported in the following figure 4.4.45, although the XRD spectra is much more significant in demonstrating the conversion of partially formed SiCO to SiO₂, which happens only in the case of incorrect xylene drying (see subsequent figure 4.4.51).

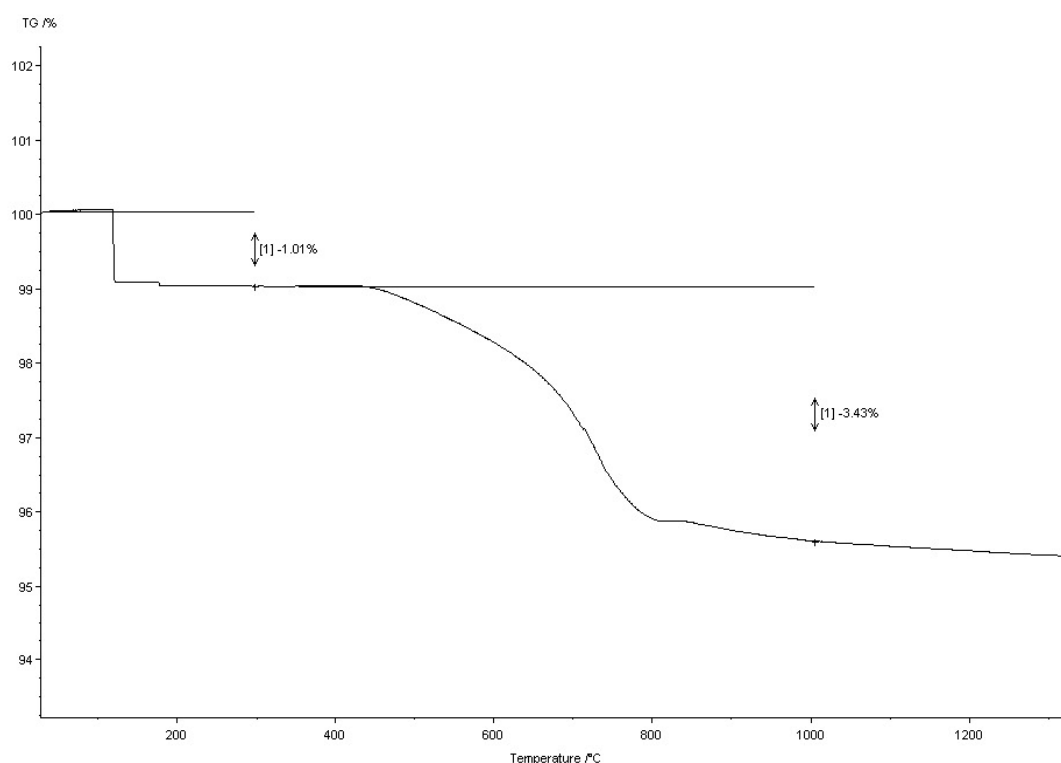


Figure 4.4.45 - TG in air on SiCO produced by pyrolysis at 700°C under vacuum, after drying at 100-120°C (green line).

The XRD characterization of the material produced in the pilot plant at 700 and 900°C, before and after the TG (10°C/h up to 1350°C followed by 30 minutes at 1350°C) was also recorded. It was used to establish if there is a correlation between the pyrolysis parameters and the ceramic phase evolution in argon and in air. As a preliminary step, it was verified that the crystallographic phase evolution during pyrolysis at 700°C is identical under vacuum and under nitrogen (figure 4.4.46) and that the presence of the basalt fibers doesn't produce new crystallographic phases (e.g. figure 4.4.47, under nitrogen, at 700°C).

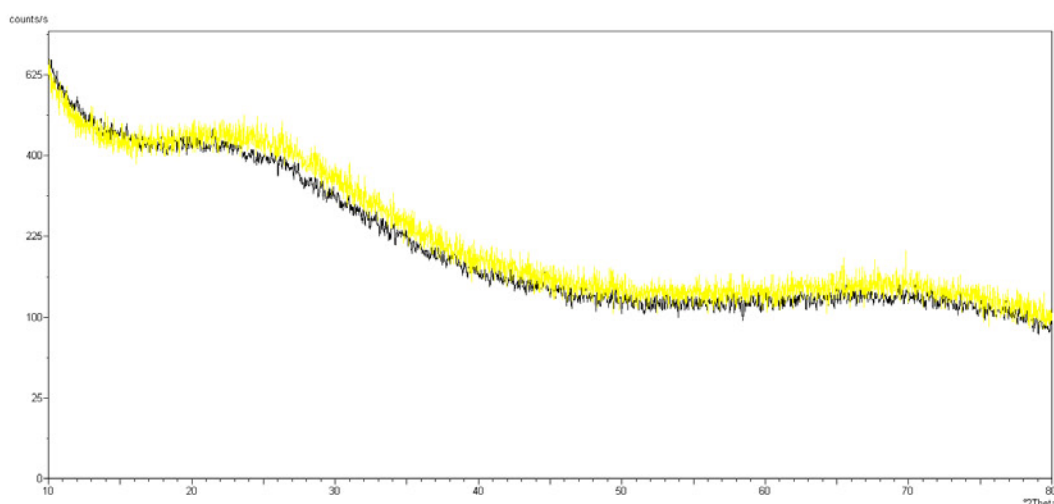


Figure 4.4.46 - XRD on SiCO produced by pyrolysis at 700°C under N₂ (black line) and under vacuum (yellow line).

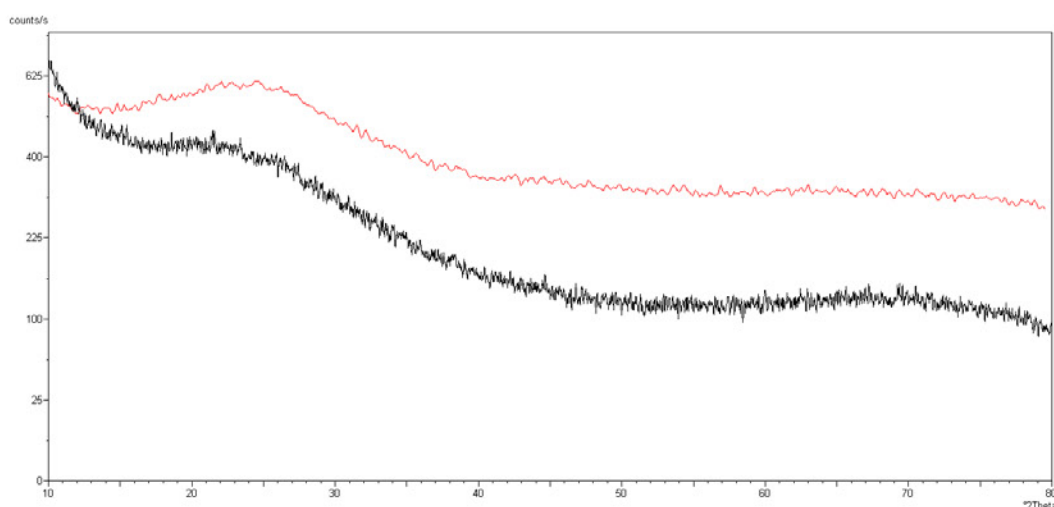


Figure 4.4.47 - XRD on SiCO produced by pyrolysis at 700°C under N₂, with (red line) and without (black) basalt fibers.

After the TGs, SiCO develops two broad peak between 15 and 40° of 2 θ . Quite interestingly, this peak evolution is nearly identical in air and argon, so it is not due to oxidation, and does not depend on pyrolysis temperature (700 or 900°C) but only on the final temperature. Also the dependence on the time length of the isothermal step is moderate. The oxidation resistance upon treatment at 1350°C in air is good, unless some change in the pyrolysis procedure is made, in particular a too fast drying or an incorrect curing of the polymer before pyrolysis produces SiCO which is unstable to oxidation to cristobalite, an allotropic form of SiO₂.

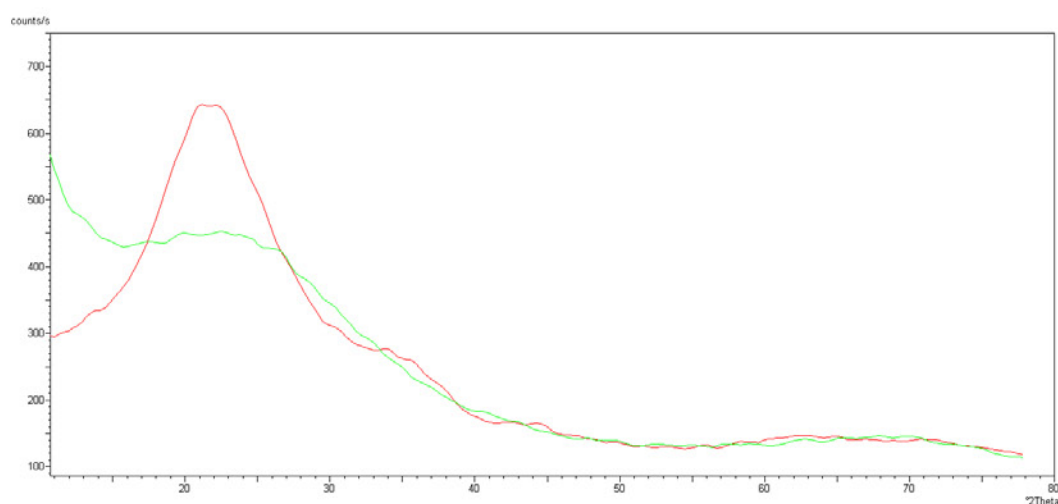


Figure 4.4.48 - XRD on SiCO produced by pyrolysis at 700°C under vacuum, before (green) and after (red) the TG in air (with final 30 min at 1350°C).

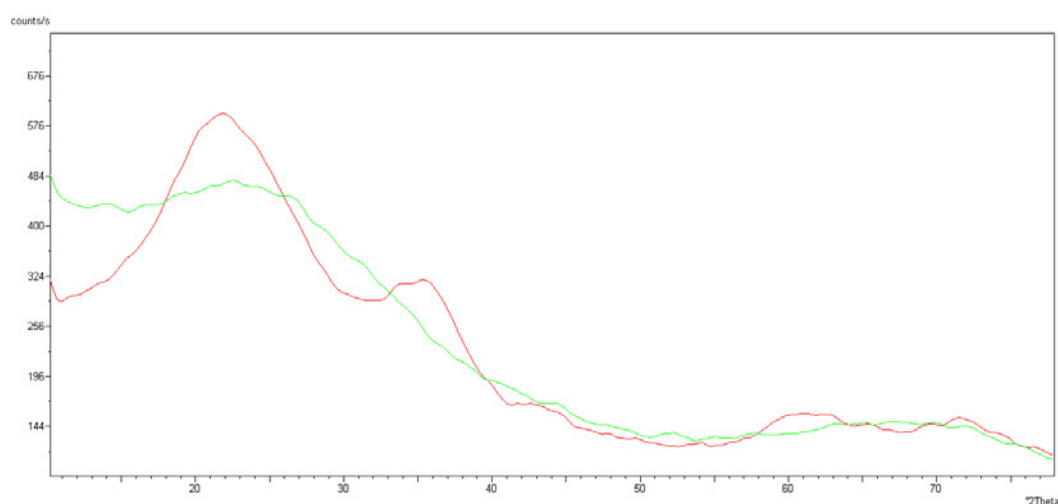


Figure 4.4.49 - XRD on SiCO produced by pyrolysis at 900°C under N₂, before (green) and after (red) the TG in air (with final 30 min at 1350°C).

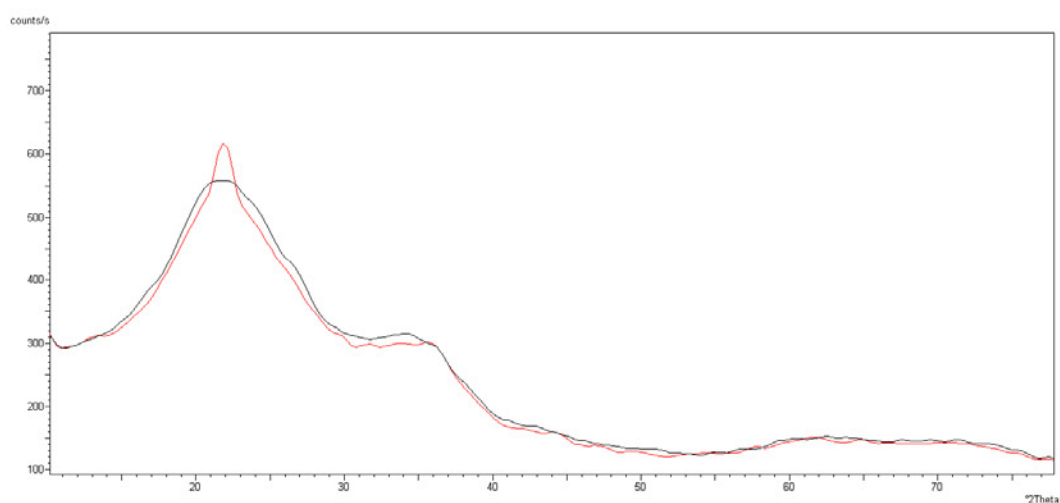


Figure 4.4.50 - XRD on SiCO produced by pyrolysis at 900°C under vacuum, after TG (with final 30 min at 1350°C), in air (red) and in argon (black).

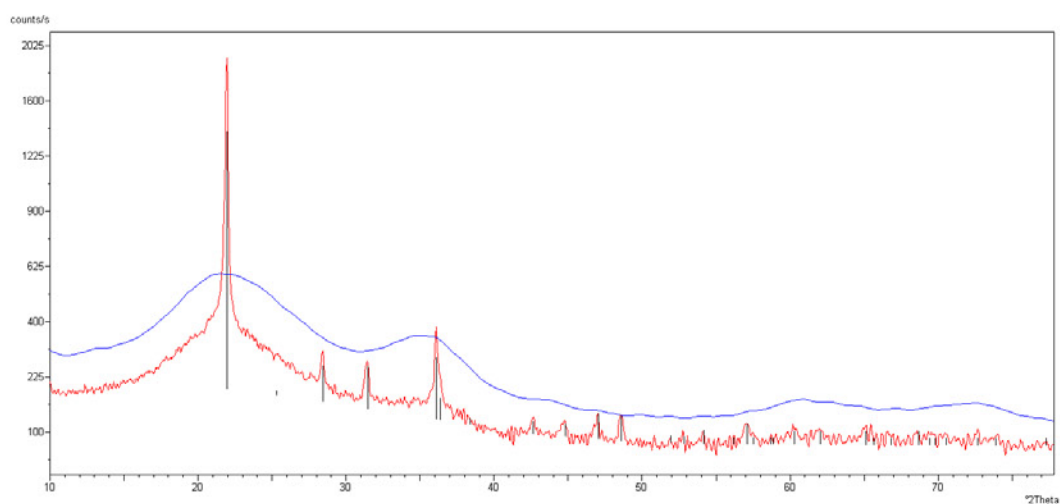


Figure 4.4.51 - XRD on SiCO produced by incorrect drying (pyrolysis at 700°C under nitrogen), after TG in air (red line), showing crystallite formation. In blu the corresponding spectrum after TG in argon.

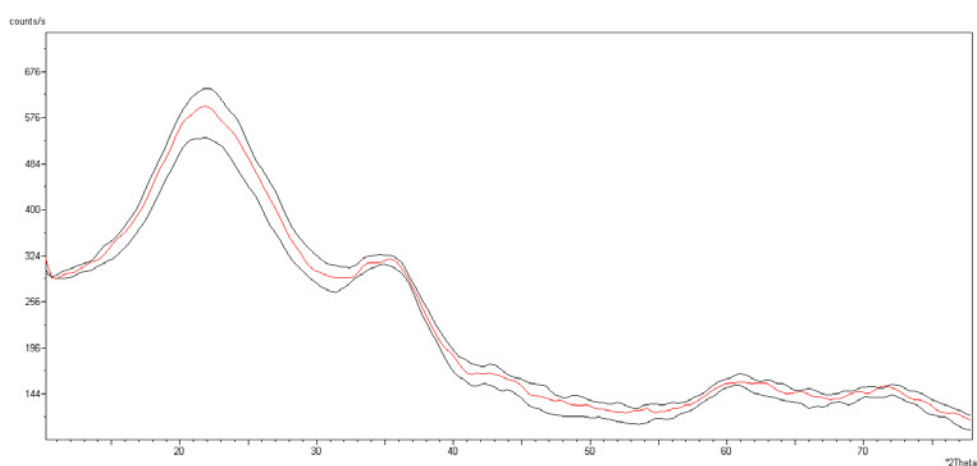


Figure 4.4.52 - XRD on SiCO produced by pyrolysis at 900°C under N₂, after TG (with final 30 min at 1350°C), in air (red) and in argon (black) and after two TG in argon (green).

Since the produced SiCO is highly hygroscopic, and somehow difficult to dry, probably due to its high porosity, it was also verified that hydrated SiCO develops the same ceramic phases upon thermal treatment in air or argon (figure 4.4.53).

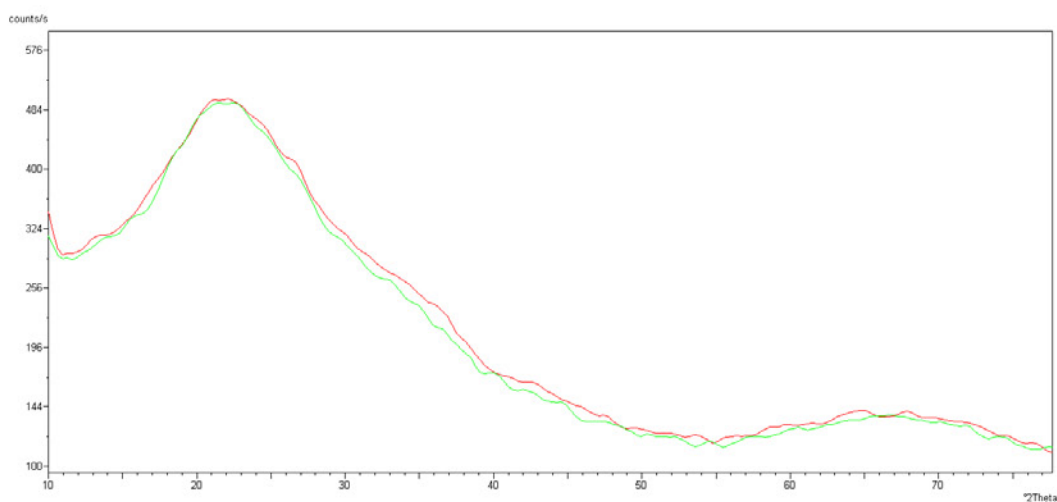


Figure 4.4.53 - XRD on SiCO produced by pyrolysis at 900°C under vacuum, (red) and after pyrolysis at 700°C under vacuum (green) after milling, treatment with boiling water, drying and TG in argon up to 1350°C.

4.4.8 Fracture toughness optimization

Besides strength, measured by MOR values, the other fundamental mechanical parameter for a CMC is fracture toughness, which measures the material opposition to crack propagation. According to already cited Cerny works on basalt_f / SiCO composites, to get good results it is essential to avoid basalt crystallization. The best way to check this phenomenon is by making optical microscopy. In the following figure it is shown the appearance of the fiber. Crystallization would present as white spots within the fiber [106], which were not found after pyrolysis at 700°C.

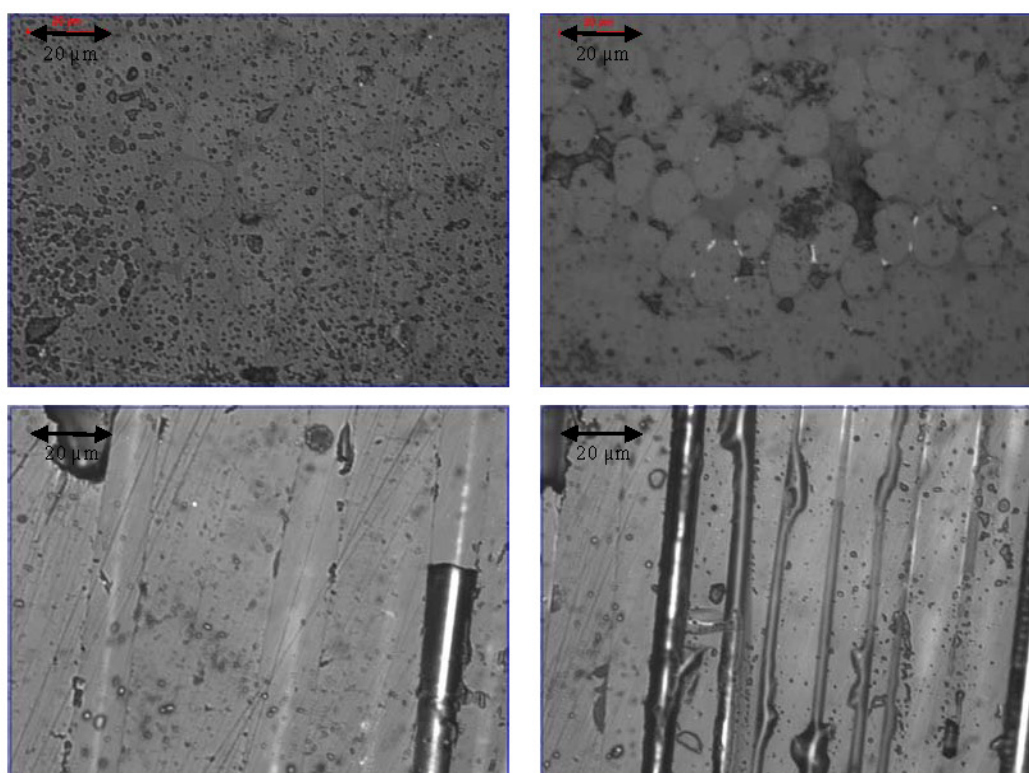


Figure 4.4.54 - Optical microscopy observations on basalt_f/SiCO produced at 700°C.

According to literature, fracture toughness is to be determined using the chevron notch technique on sub-sized specimens, based on the standard procedure [144]. The value, however, is less critical than MOR for practical applications, and these measures were postponed.

[144] EN 14425-3, "Advanced Technical Ceramics - Test method for determination of fracture toughness of monolithic ceramics - part 3: Chevron notched beam (CNB) method, 2010.

4.4.9 PIP with poly-methylsiloxane on oxide fibers

Similarly to the infiltration of SiC pressed felts, also the impregnation of oxide rock wool (normally employed as a thermally insulating material) and low quality quartz fibers (Carlo Erba, cod 457471, generally used for analytical purposes, as a selective ion retention media) was tested, but the resulting composite was brittle and useless, due to both the low tensile strength of the used fibers and the lack of an interphase between the matrix and the fibers. For improving the performances, changing the fibers (e.g. using the Nextel fibers, or high performance quartz fibers) would be certainly necessary, but this activity goes over the scope of the present Doctorate.



Figure 4.4.55 - CFCC obtained using oxide rock wool.

CHAPTER 5. CBC COMPOSITES

5.1 Introduction

Other possible inorganic matrixes currently under study are CBC ceramics (Chemically Bonded Ceramics), for example geopolymers. Thank to the low costs of the raw materials and of the process, they are particularly interesting for the automotive and construction field, in association with various types of low cost fibres, basalt in particular [145- 148]. A good review about the use of basalt fibers in strengthening the reinforced concrete beams is cited below [149], but the research is still ongoing. Geopolymers are obtained by the reaction of an aluminosilicate powder, with a highly concentrated alkali hydroxide (KOH, NaOH) and/or silicate (Na_2SiO_3 or K_2SiO_3). This aqueous slurry produces a synthetic amorphous to semi-crystalline solid material, with interesting mechanical properties.

Basalt reinforced geopolymers can be prepared using a wet lay-up process, similarly to PIP composites. Geopolymers are fire resistant, however, for a continuous thermostructural application of a basalt-fiber reinforced geopolymer, it is necessary to study the compatibility of CTE (Coefficient of Thermal Expansion) between the fibers and the matrix and controlling the kinetic of the drying and the shrinkage that occurs on drying and on sintering. In order to tailor matrix characteristics like CTE, and reduce the shrinkage, the CBC may need to be added with suitable inorganic fillers. All these problems are far from having been solved, together with the necessary reliability studies, so there's still need an important research work before thinking about a technology transfer.

Generally geopolymers are materials with low specific strength, not suitable for

[145] Weimin Li, Jinyu Xua, " Mechanical properties of basalt fiber reinforced geopolymeric concrete under impact loading", *Materials Science and Engineering A*, 505 (2009) 178–186.

[146] A. Natali, S. Manzi, M. C. Bignozzi, "Novel fiber-reinforced composite materials based on sustainable geopolymer matrix", presented at the 2011 International Conference on Green Buildings and Sustainable Cities, *Procedia Engineering*, 21 (2011) 1124-1131.

[147] Aaron Richard Sakulich, "Reinforced geopolymer composites for enhanced material greenness and durability", *Sustainable Cities and Society*, 1 (2011) 195-210.

[148] C. Mingazzini, "New materials for the Ideal City", Convegno sulle Smart Cities organizzato dalla "Unione dei Comuni della Romagna Faentina". "Unione delle idee per un territorio smart: 16 maggio 2013", oral intervention.

[149] Andreea Serbescu, Kypros Pilakoutas, N. Taranu, "The efficiency of basalt fibers in strengthening the reinforced concrete beams" *Buletinul Institutului Politehnic din Iasi*, vol LII (LVI), f.3-4 (2006) 47-57.

automotive. However quite recently Pyromeral Systems SA, with a strong background on geopolymers, developed PyroSic[®] an alkali bonded glass ceramic composite, probably a poly-sialate, $M-(Si-O-Al-O-)$ with $Si/Al=1$ [150] reinforced with SiC fabrics, e.g. Nicalon type, for operation up to 1000°C in oxidative environments [151]. PyroSic[®] offers indeed good performances for continuous operation, generally up to 500-600°C, in F1 racing cars and aims at filling the gap between Carbon Fiber Reinforced Plastics (CFRP) and Ceramic Matrix Composites (CMC). It can be processed at low temperature (<150°C) at very low thicknesses (e.g. 0.2 mm) with high specific strength, and can be effectively used to build components like the car exhaust systems. It has also several drawback, in particular it has to be protected from rain since water could be adsorbed and cause defects, when fast released at the next heating.



Figure 5.1.1 - Pyrosic[®] "Formula 1" racing car exhaust systems.

[150] Joseph Davidovits, et al "Alkaline aluminosilicate geopolymeric matrix for composite materials with fiber reinforcement and method for obtaining same" US5798307A, 1998 (and related WO9628398 and FR 2731697).

[151] <http://www.pyromeral.com/doc/jec-magazine-nb53-dec-2009.pdf>

Property	Value
Density	1.8 to 2.2 g/cm ³
Coefficient of thermal expansion	3 x 10 ⁻⁶ /K
Thermal conductivity (through thickness)	0.90 w/m.K
Thermal conductivity (in-plane)	0.95 w/m.K

Table 5.1.1 - Typical PyroSic[®] properties.

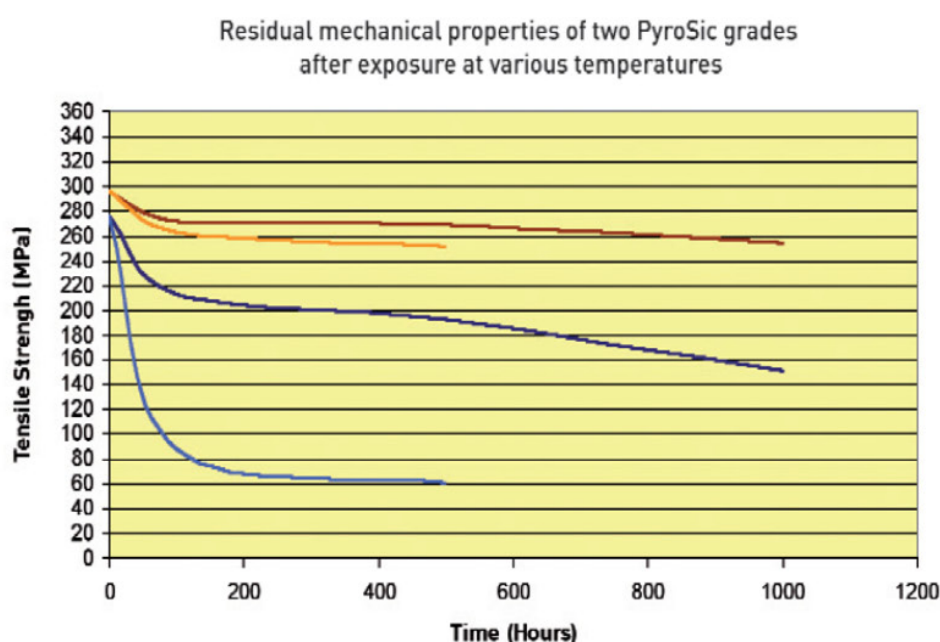


Figure 5.1.2 - PyroSic[®] main characteristics and thermomechanical properties.

Pyromeral is continuously going on working on the development of these technologies for new applications and possesses several patents [152-155]. Quite recently we managed to get a free sample of a basalt-reinforced version, probably developed by Pyromeral for the construction field. The sample was too small for thermomechanical characterizations, but it was possible a SEM-EDS microstructural investigation (figures 5.1.3 and 5.1.4).

-
- [152] WO2011 128521 - Matrix based on nanocrystalline cristobalite for a thermostructural fibrous composite material (and related US2013130886A1, EP 2558430 A1, FR 295934 A1)
- [153] FR2901786 (2007) - Method of manufacturing an exhaust line element of a motor vehicle, and corresponding exhaust element (and related WO2007 141455A3).
- [154] FR2782713 - Heat insulating composite sleeve or cylinder, for flat glass transport and cooling rollers, comprises high temperature stable fibers impregnated with a hardenable ceramic matrix especially of thermosetting ceramic resin.
- [155] FR 2659319 - Process for obtaining a geopolymeric alumino silicate and products thus obtained (WO9113830).

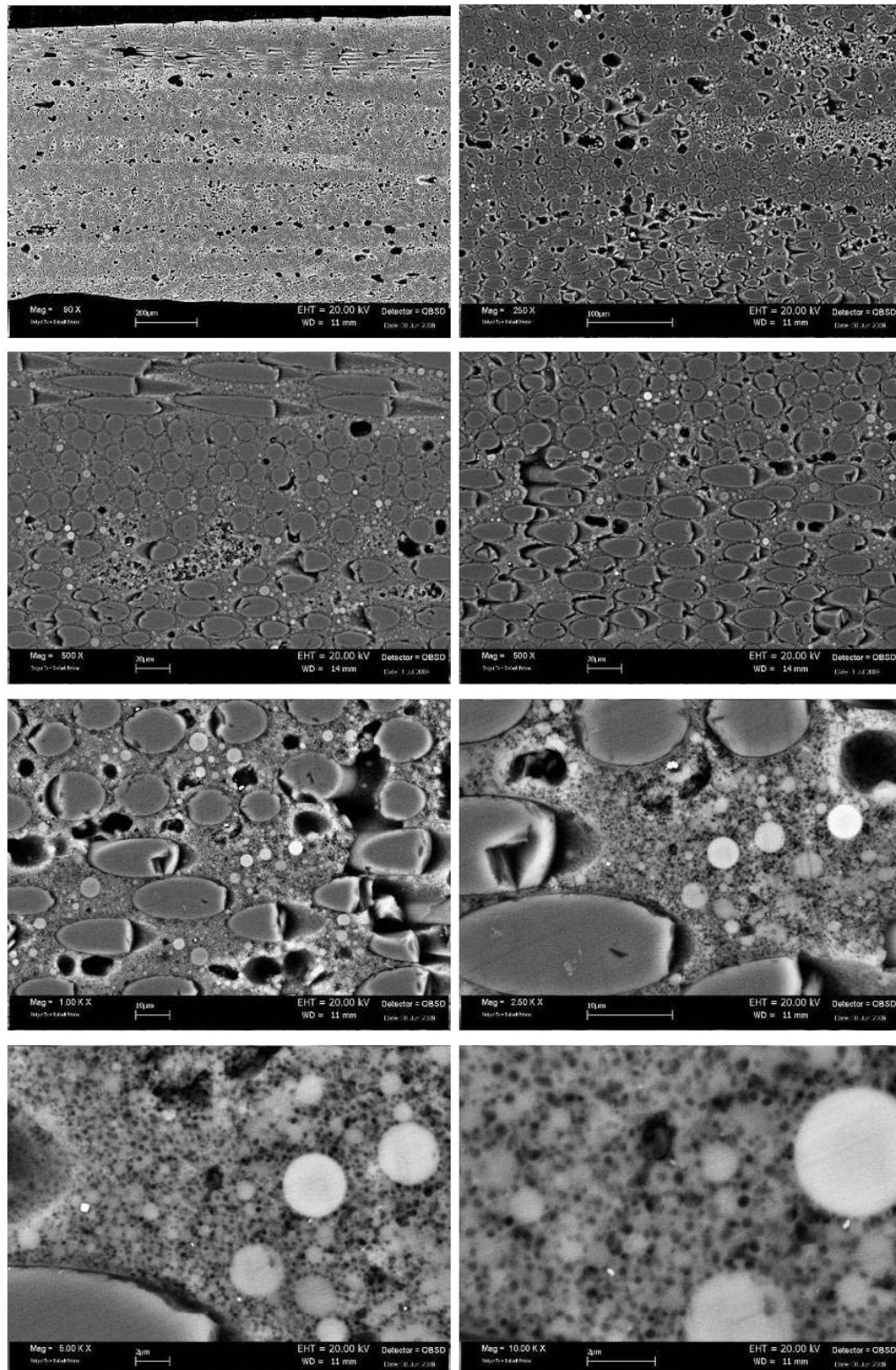


Figure 5.1.3 - Microstructure of a basalt reinforced Pyromeral composite.

The microstructure suggests a CBC synthesized starting from glass microspheres, on basalt fibers, and so the idea it should be a Pyromeral composite. In the table 5.1.2 the results of the chemical analysis on the fibers, the matrix and the mean composition are reported.

%w/w	Mean composition (500 X area)	Fibers		Microspheres					
Na ₂ O	0.4	0.2	0.1	0.7	1.2	0.4	0.6	0.5	1.0
Al ₂ O ₃	0.6	-	-	6.5	1.6	5.7	4.2	4.6	3.0
SiO ₂	93.9	96.5	96.4	74.3	76.0	77.0	75.0	79.5	76.4
K ₂ O	3.3	1.1	1.0	18.5	21.2	16.9	19.9	15.4	19.6
TiO ₂	1.8	2.2	2.5	-	-	-	-	-	-

%w/w	Matrix						Matrix on the outer layer	Matrix without microspheres
Na ₂ O	2.1	1.0	1.1	1.0	1.2	1.1	0.9	0.6
Al ₂ O ₃	0.0	1.6	2.0	2.7	1.8	1.6	1.8	1.7
SiO ₂	86.0	88.6	87.3	88.0	88.1	88.8	81.1	90.3
K ₂ O	9.6	8.5	9.6	8.3	8.9	8.5	16.2	6.5
TiO ₂	2.3	0.3	-	-	-	-	0	0.9

Table 5.1.2 - EDS chemical analysis on a basalt reinforced composite: mean composition, matrix, basalt fibers and residual glass microspheres.

The microstructure together with the chemical data clearly suggest the application of the Pyromeral process, how it is presented in their patents, to a basalt fabric fiber preform. However these composites are still not being proposed on their web site, so maybe they are not satisfied by their performances. One problem that they probably did not managed to solve is avoiding the creation of a strong bond between basalt fiber and the glass microspheres in alkaline medium, so probably the MOR value and the fracture toughness are low, making the solution based on SiC fibers much more interesting, even for the construction field. SiC fibers cost much more, but their tensile strength is indeed much higher, and this fact, together with the development of a weak bond with the glass matrix, could fully make them the preferred choice.

5.2 New Phosphate Cements

Over the last few years, researchers in the Vrije Universiteit Brussel (VUB) have been developing a chemically bonded Inorganic Phosphate Cement (IPC) for construction and industrial applications. In particular they developed Vubonite (which is now commercially available) as an ecological, inorganic, non-alkaline resin that is prepared by mixing a powder and a liquid, consisting of a calcium silicate powder and a phosphoric acid based solution of metal oxides. The processing time can be adjusted and varies from a few minutes to approximately one hour. After hardening, the material's properties are similar to those of cement based materials. The resulting material is a ceramic material with a three dimensional network structure that should be strong, durable and fire-resistant. Since all components are inorganic, no toxic gases are released upon heating, that could imply a fire hazard. The reference IPC post curing procedure involves wrapping the material in plastic foil (after curing it for 24 hours at RT) and then heating it for another 24 hours at 60 °C, but there are also versions which do not require heating [156,157,158], which seem perfect to build fire resistant Textile Reinforced Cement (TRC) structures [159, 160].

One of the most important features of IPC should be that ordinary E-glass fibers are not attacked by the IPC matrix and can be used as reinforcement without losing post-cracking stiffness and strength. However literature also reports that glass reinforced Vubonite tolerates very well freezing–thawing but shows some

[156] H. Cuypers, "Analysis and design of sandwich panels with brittle matrix composite faces for building applications", PhD thesis, Vrije Universiteit Brussel (VUB), Belgium 2002

[157] M. Alshaaer H. Cuypers G. Mosselmans H. Rahier J. Wastiels, " Evaluation of a low temperature hardening Inorganic Phosphate Cement for high-temperature applications", *Cement and Concrete Research*, 41(1) (2011) 38-45.

[158] E. De Bolster, H. Cuypers, P. Van Itterbeeck, J. Wastiels, W.P. De Wilde, " Use of hypar-shell structures with textile reinforced cement matrix composites in lightweight constructions", *Composites Science and Technology*, 69 (2009) 1341–1347.

[159] J. Van Ackeren, J. Blom, D. Kakogiannis, J. Wastiels, D. Van Hemelrijck, "Impact study of textile reinforced cementitious materials: test method and preliminary results" *Proc. Int. Symp. "Brittle Matrix Composites 9"* A.M. Brandt, J. Olek and I. H. Marshall, eds., Warsaw, October 25-28, 2009.

[160] Alsaar M (2006), Optimization of properties of inorganic phosphate cement (IPC) for construction and high-temperature applications. PhD thesis, Vrije Universiteit Brussel.

problems in wetting/drying cycles [161] because of mismatch between matrix and fibers deformations.

Particularly interesting is the patented Self Compacting Impregnator (SCI), developed from the same group of the Vrije Universiteit (Brussel, Belgium) [162,163] to enable the continuous industrial production of well impregnated textiles, which can be processed and shaped further. The penetration of the matrix into the fabrics is induced by system of rollers, which squeezes the matrix through two layers of fabrics. A pretty remarkable result claimed by the inventors of the SCI is that glass fiber volume fractions of more than 20% can be obtained in an automatic way, like in the hand lay-up method. Tensile specimens showed a remarkable strain hardening behavior with a strength of 45 to 50 MPa. Moreover, tensile fatigue testing was performed on a hydraulic MTS test bench with a capacity of 100 kN, applying a sinusoidal cyclic load that was imposed with a frequency of 10 Hz, up to a total number of one million cycles. Repeated cyclic loading results show that specimens subjected to a maximum cycling stress of 22 MPa can withstand one million cycles. This stress was about 50% of the static strength, and well beyond the cracking load of the matrix. Further tests under environmental conditions (humidity and freezing) are on the way to assess the durability and serviceability limit state of this kind of composites.

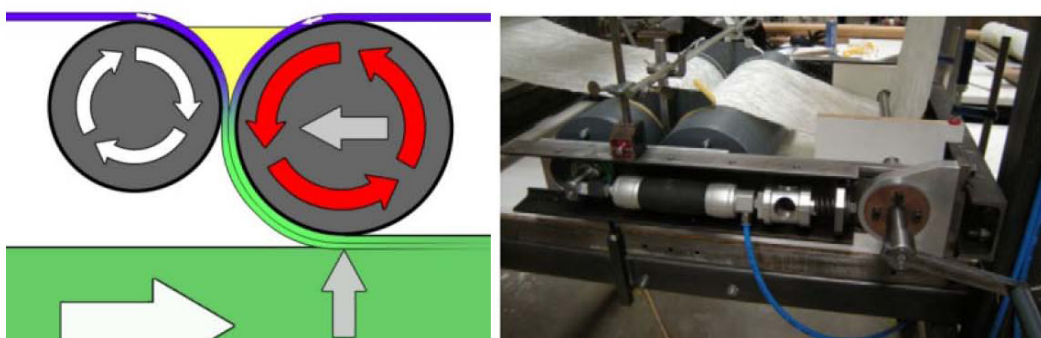


Figure 5.2.1 - Working principle and prototype of the Self Compacting Impregnator (SCI).

[161] H. Cuypersa,, J. Wastielsa, P. Van Itterbeecka, E. De Bolstera, J. Orlowskyb, M. Raupachb, Durability of glass fibre reinforced composites experimental methods and results" Composites: Part A, 37 (2006) 207–215.

[162] Vanherck, J., Wastiels, J., Remy, O., Dannau, M.: Impregnation method. WO 2009/030710.

[163] J. Wastiels and O. Remy "Industrial Processing Technique for Textile Reinforced Cement Composites with Structural Use", HPFRCC 6, pages 511–518.

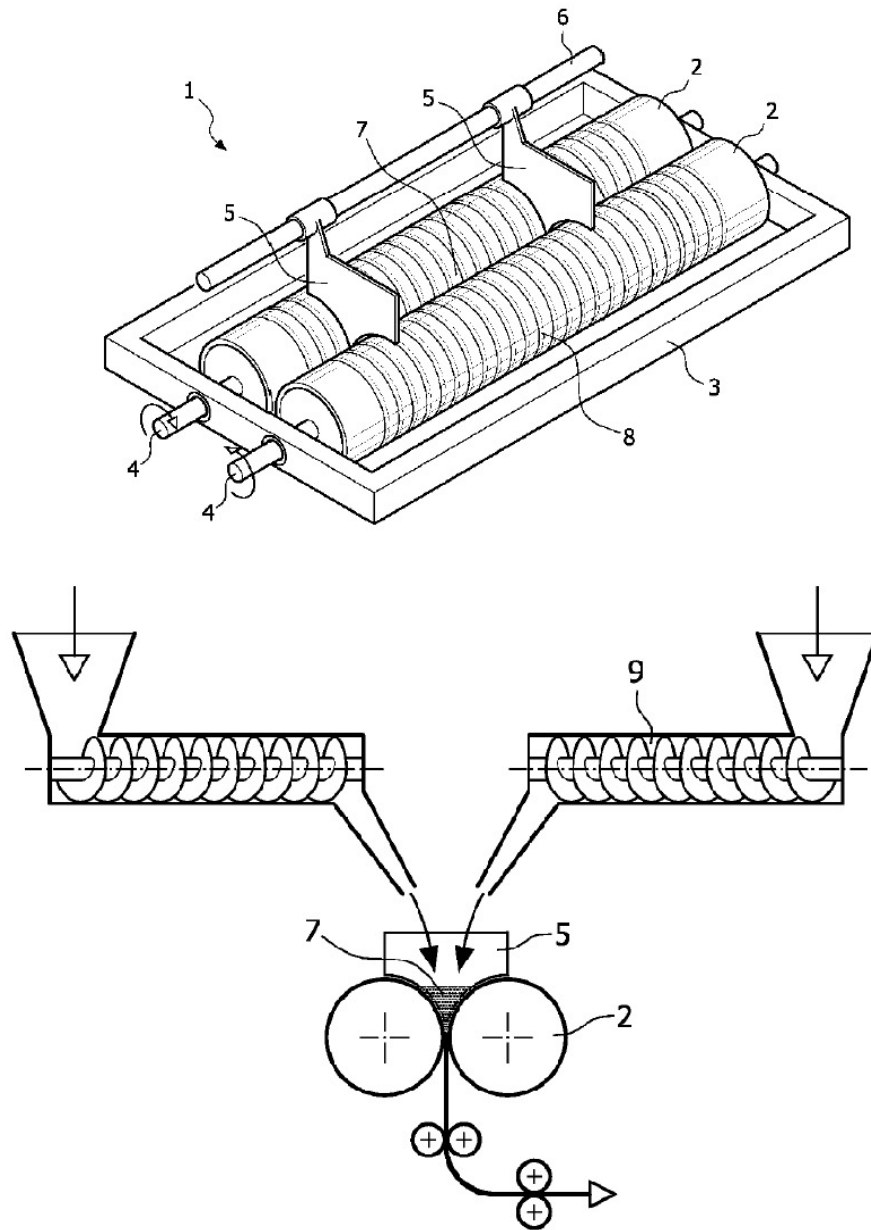


Figure 5.2.2 - Working principle of the Self Compacting Impregnator, from WO 2009/030710.

However, the correct evaluation (and comparison) of durability in new GRC (Glass Fiber Reinforced Composites) require an ageing performed with care and that sufficient temperatures, acceleration, times and specimens are studied. If these precautions are not taken, the long term durability cannot be correctly assessed, since new material combinations might be subjected to different degradation mechanisms at different temperatures [164].

[164] P. Van Itterbeeck, H. Cuyper, J. Orlowsky, J. Wastiels "Evaluation of the strand in cement (SIC) test for GRCs with improved durability" *Materials and Structures*, 41 (2008) 1109–1116.

5.3 Characterization of a commercially available phosphate cement: Grancrete

The production of geo-polymeric composites was tested, using conventional sodium silicate - based formulations developed previously in ENEA, finding that they are affected by several drawbacks:

- most formulations requires a thermal treatment at 60-90°C to set completely;
- they tend to crack on rapid heating (because of water release, shrinkage and CTE differences with the fibers) especially at high heating ramp rates.

As an alternative matrix material, we considered a commercial phosphate cement, GrancreteTM [165] with several advantages over geopolymers, in particular it is already commercially available at low price (1 €/kg) and it is easier to process. Like geopolymers, Grancrete possesses fire-resistant characteristics. The setting occurs rapidly (20 minutes) at room temperature, by simply adding water (16% w/w) to a precursor powder, and is based on the exothermic reaction:



Generally the mixture is poured into plastic or rubber containers, since, on setting, the adhesion on metals is generally quite strong. The formulation was developed at the Argonne National Laboratory (ANL), by Aaron Wagh [166]. It belongs to "Acid-base cements" which are formed at room temperature but exhibit properties similar to those of ceramics. An acidic and an alkaline component neutralize each other, and the resulting paste sets rapidly into a product with neutral pH. Many of the "Acid-base cements" were developed while looking for suitable dental cements.

Compared to traditional cementitious materials Grancrete is superior in terms of :

- chemical and thermal stability (pH between 2 and 13 and temperatures up to 1100°C);
- improved flexural strength (at least 15% higher than traditional cements);
- neutral pH formulation, more suitable for including glass fibers, which could be degraded by alkaline environments.

[165] www.grancrete.net

[166] Arun S. Wagh "CHEMICALLY BONDED PHOSPHATE CERAMICS", Elsevier, New York, 2004, ISBN: 0-08-044505-5

In order to evaluate the material for thermostructural application it was preliminarily necessary to study:

- the mineralogical composition before and after the setting;
- the mineralogical, volume and weight changes on drying and on firing;
- the mechanical and thermomechanical compression and flexural strength;
- the thermal conductivity;
- the freeze-thaw resistance.

Regarding freeze thaw resistance, grancrete samples demonstrated to be able to withstand the standard cycles required to bricks, corresponding to accelerated ageing induced by alternate wetting and freezing.

Regarding thermal conductivity, a value, at room temperature, of 0.9 W / m·K was experimentally measured using a thermofluximeter (Anter Corporation, model 2022).

The other characteristics will be discussed in the following paragraphs, with the aid of TG and XRD results. All the test, but the mechanical measurement in particular, were performed after a "maturation time" of the cement of at least 20 days.

5.3.1 Mineralogical investigations on the setting reaction

The mineralogical composition change during the setting reaction was studied by XRD. Before the setting, Grancrete is a fine precursor powder, which consolidated on addition of a suggested percentage of water of 16-20 % w/w. After setting (figure 5.3.1) the material was crushed in order to make the XRD investigation possible on the bulk material.

Before the setting Grancrete reveals the following phases (figure 5.3.2):

MgO	ICDD 01-089-4248 (43-1022)
CaSiO ₃	ICDD 01-073-1110 (43-1460) - wollastonite
KH ₂ PO ₄	ICDD 01-079-0585 (35-807)

After the setting the phase composition is the following (figures 5.3.3 and 5.3.4):

CaSiO ₃	ICDD: 01-073-1110 (43-1460) - wollastonite
MgKPO ₄ ·6H ₂ O	ICDD: 01-075-1076 (35-812)
MgO	ICDD: 01-089-7746 (43-1022)

The mineralogical investigation on Grancrrete reveals that wollastonite is added as inert to a phosphate cement and that MgO is in stoichiometric excess.



Figure 5.3.1 - Grancrrete after molding into various shapes into silicone rubber moulds.

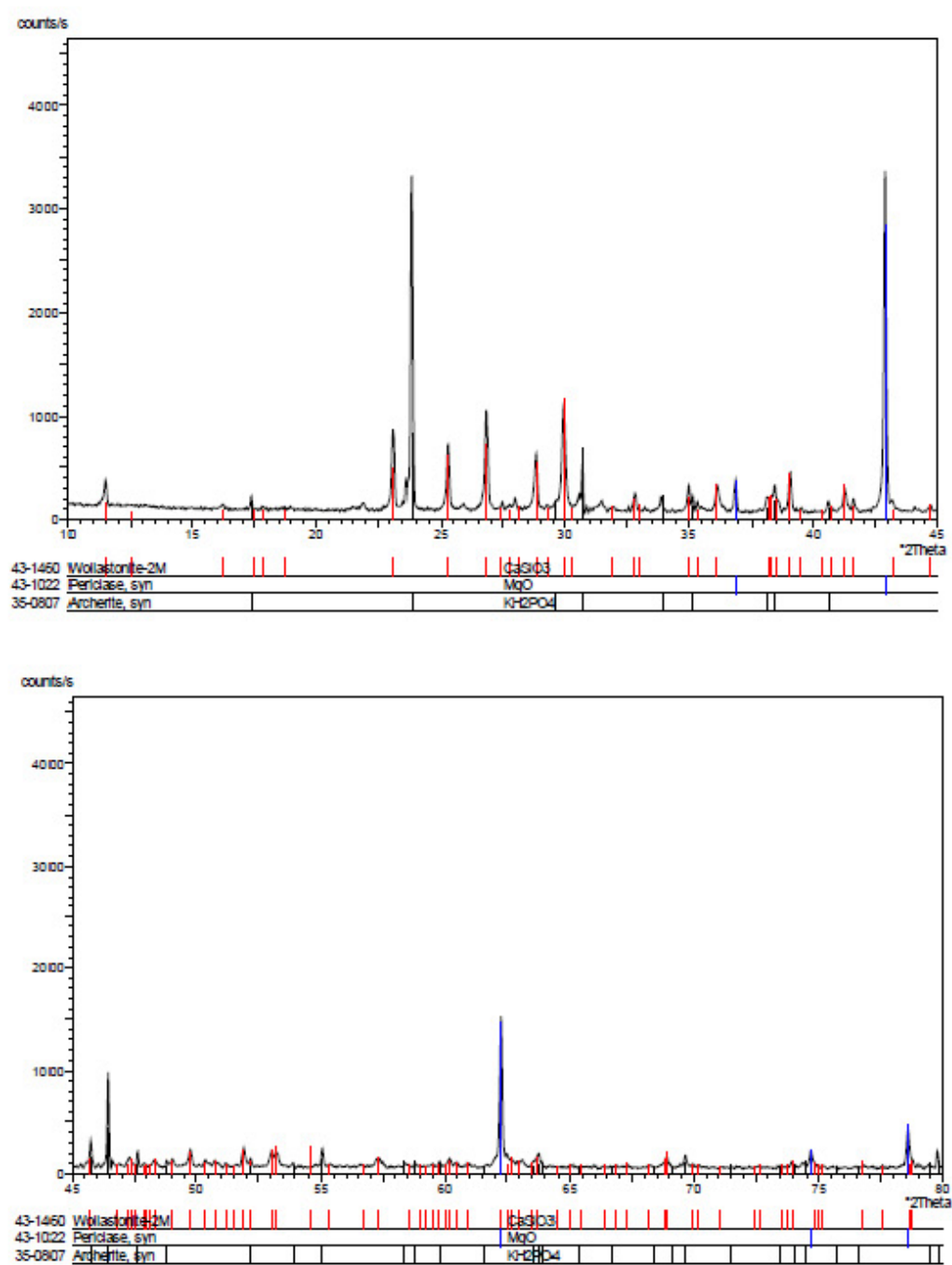


Figure 5.3.2 - XRD on Grancrete starting powder.

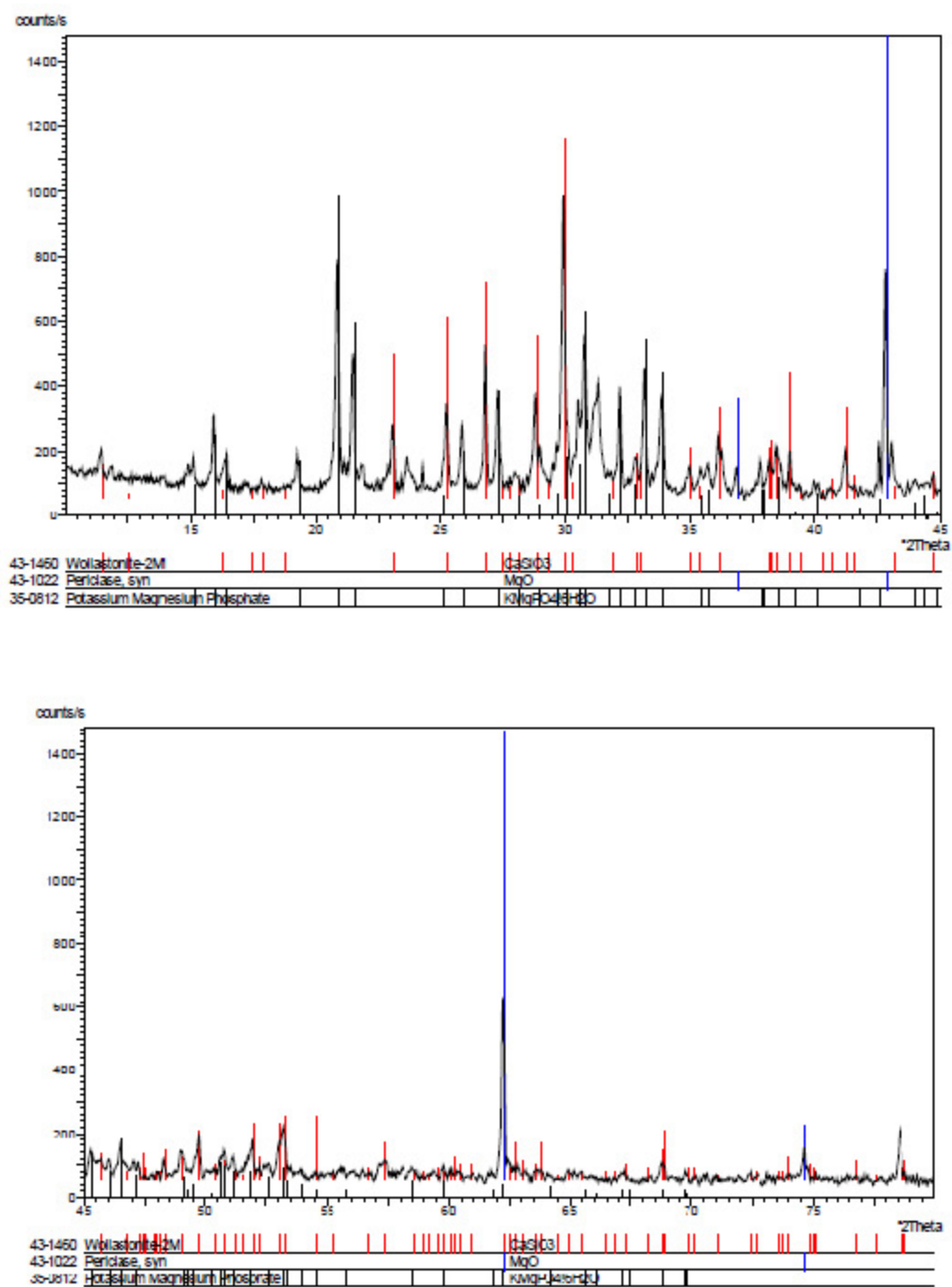


Figure 5.3.3 - Mineralogical composition of Grancrete after the setting.

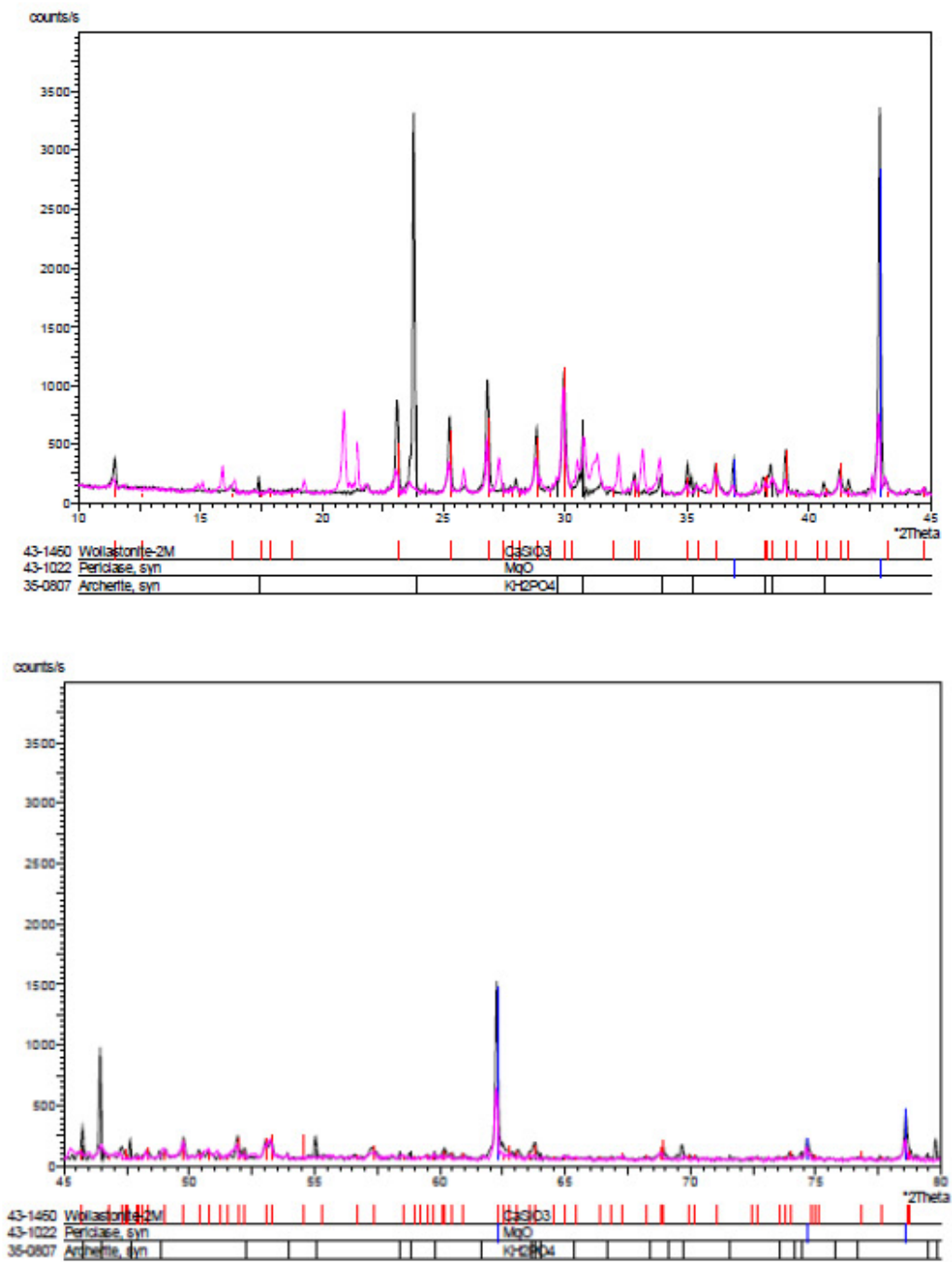


Figure 5.3.4 - XRD on Grancrete before and after (magenta) the setting.

By applying the RIR method for semi-quantitative evaluations, the results were the following:

On the precursor powder:

MgO	ICDD 01-089-4248	- 31 %
CaSiO ₃	ICDD 01-073-1110	- 49 %
KH ₂ PO ₄	ICDD 01-079-0585	- 20 %

On the set material:

MgO	ICDD: 01-089-7746	- 12 %
CaSiO ₃	ICDD: 01-073-1110	- 46 %
MgKPO ₄ .6H ₂ O	ICDD: 01-075-1076	- 42 %

From the above results, it can be easily demonstrated that unreacted MgO was in stoichiometric excess, which is discussed in literature to be favorable for getting better mechanical properties.

It was decided to study also the XRD spectra on the white efflorescences. In figure 5.3.5 it is reported the comparison of the spectrum on the set Grancrète (black line) and the white efflorescences (red line) revealing that the mineralogical phases are the same, but there is a reduced quantity of wollastonite and residual MgO. Applying the RIR method as before:

MgO	ICDD: 01-089-7746	- 7 %
CaSiO ₃	ICDD: 01-073-1110	- 33 %
MgKPO ₄ .6H ₂ O	ICDD: 01-075-1076	- 60 %

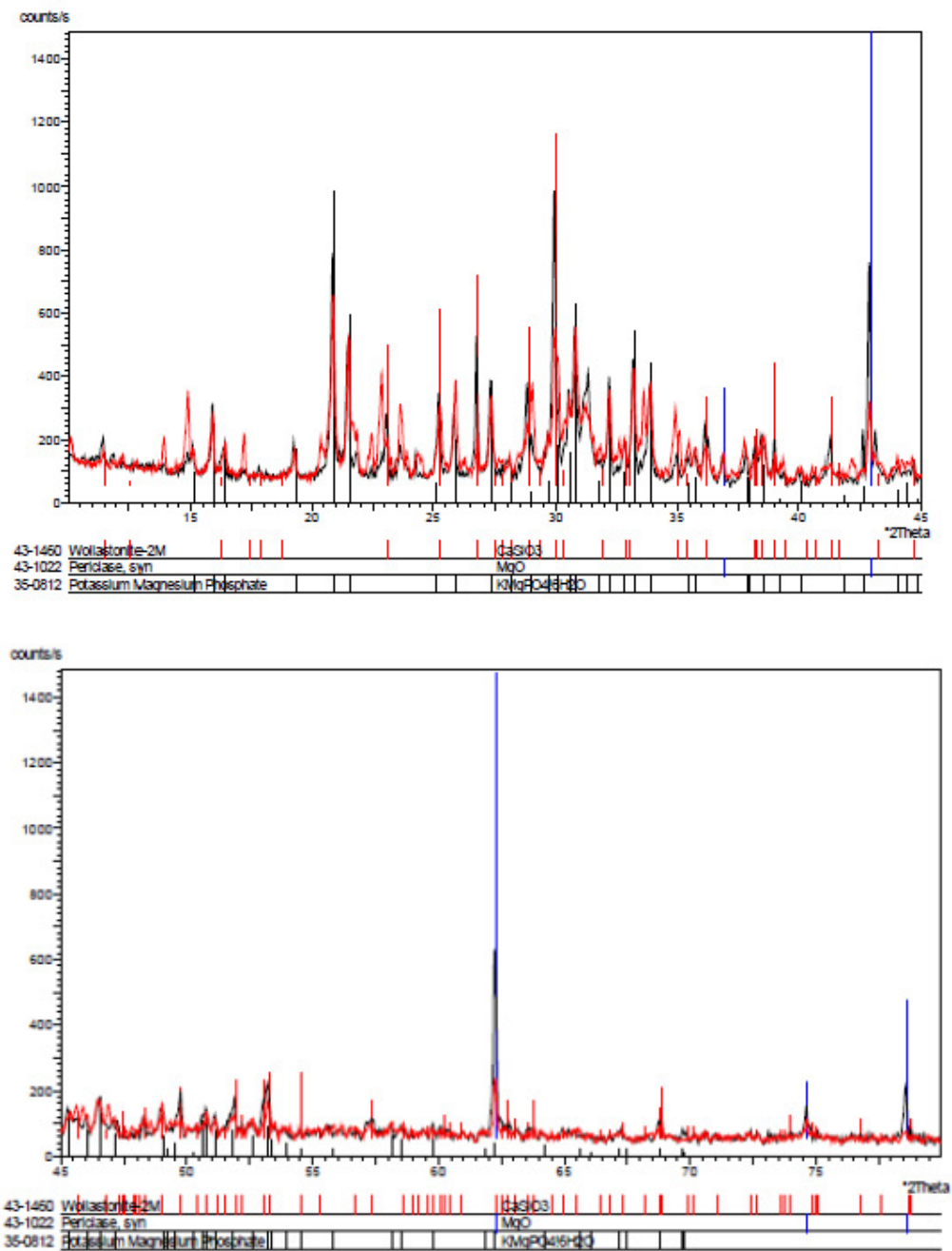


Figure 5.3.5 - XRD on set Grancrrete (black line) and white efflorescences (red line).

5.3.2 Thermogravimetric and thermomechanical investigations

Since for its forming and setting Grancrete is added of a considerable amount of water, for thermostructural application it is necessary to understand what happens to this water, since a too fast water release could create cracks, as it happens to traditional Portland cements.

The thermogravimetric investigation was performed in flowing air, with the following ramp rates:

- 1 °C/min, between 30 and 200 °C;
- 10 °C/min, between 200 and 1400 °C.

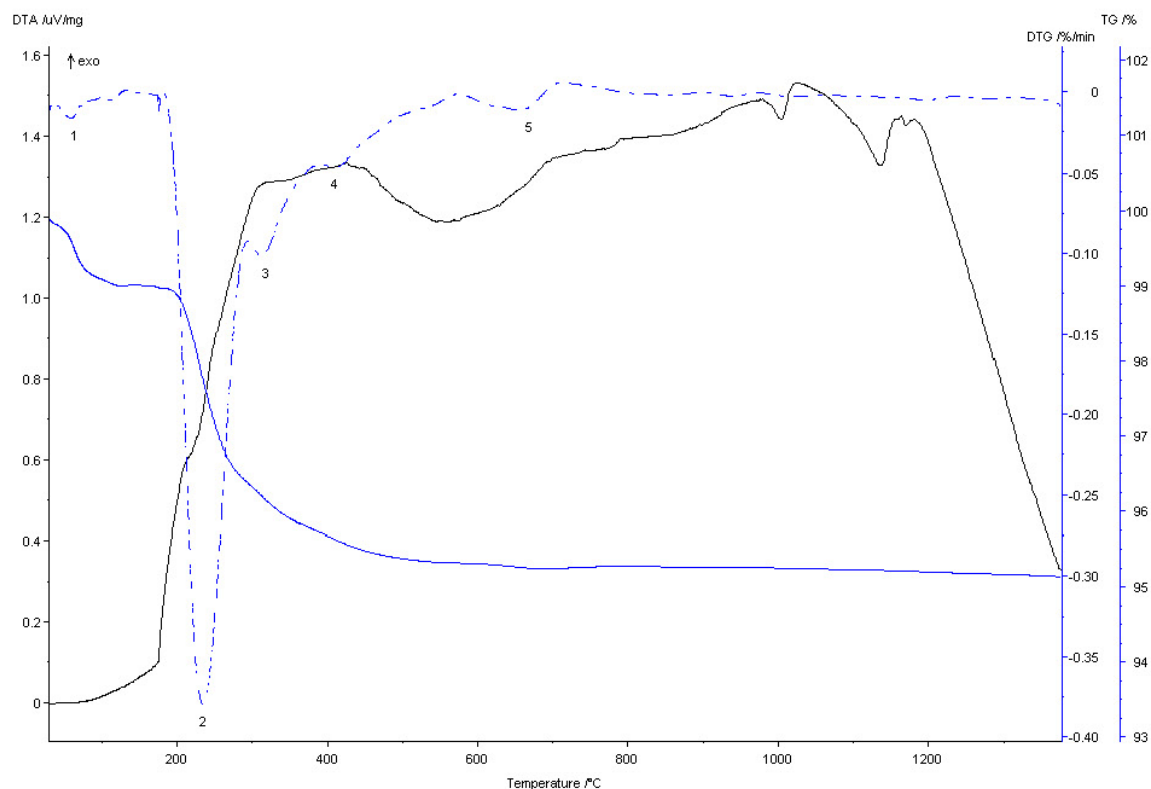


Figure 5.3.6 - TG-DTA on Grancrete precursor.

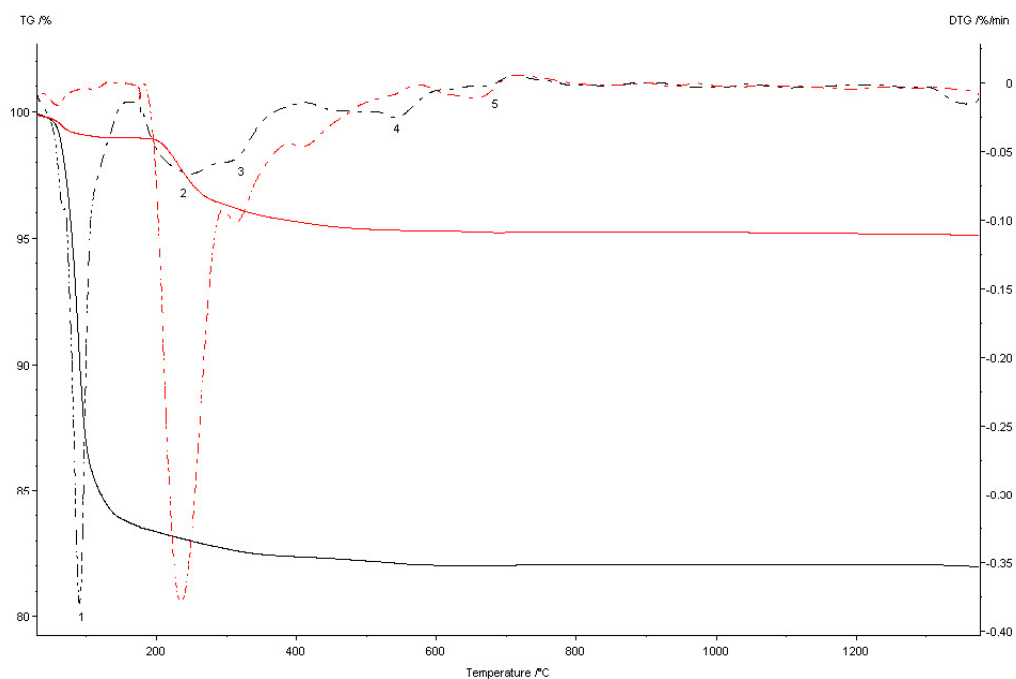


Figure 5.3.7 - TG-DTA on set Grancrète (compared to precursor).

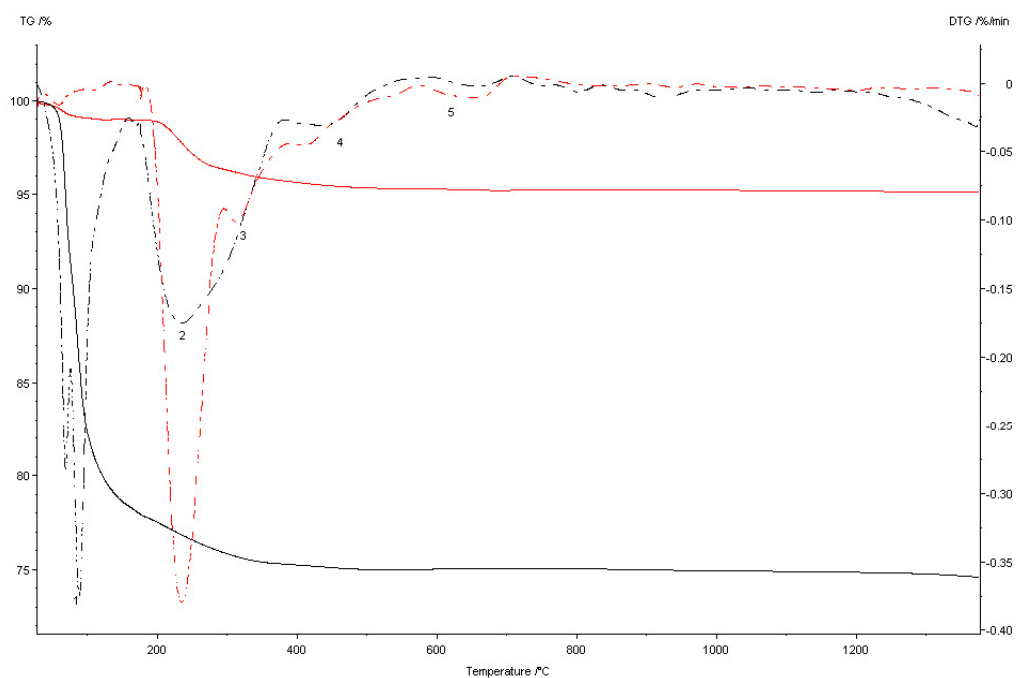


Figure 5.3.8 - TG-DTA on "white efflorescences" (compared to precursor and set Grancrète).

The results may be discussed using the following table. On set Grancrete there are three main DTG peaks, the first corresponding to the unreacted water and the water contained in the phase $\text{MgKPO}_4 \cdot 6\text{H}_2\text{O}$. The efflorescences are richer in this phase, as discussed before.

DTG peaks	DTG 1 T (°C)	Mass Loss 1	DTG 2 T (°C)	Mass Loss 2	DTG 3 T (°C)	Mass Loss 3
Grancrete precursor	60	1 %	234	2.6 %	310	0.4 %
Set Grancrete	90	16.2 %	250	1.0 %	310	0.4 %
Efflorescences	88	21.6 %	230	3.1 %	-	--

Table 5.3.1 - DTG peaks and the corresponding mass losses.

Upon heating, the crystallization water of $\text{MgKPO}_4 \cdot 6\text{H}_2\text{O}$ is expected to be lost: the corresponding molecular weight changes from 266.47 to 158.37, with an expected weight loss of 16-17%, which is in very good accordance with the above data, suggesting that this phenomenon is complete for an isothermal step at 150°C. Thermal treatments for 10 hours at 600 and 1000°C was also tested, weight stability is reached after less than 100 minutes (see figure 5.3.9).

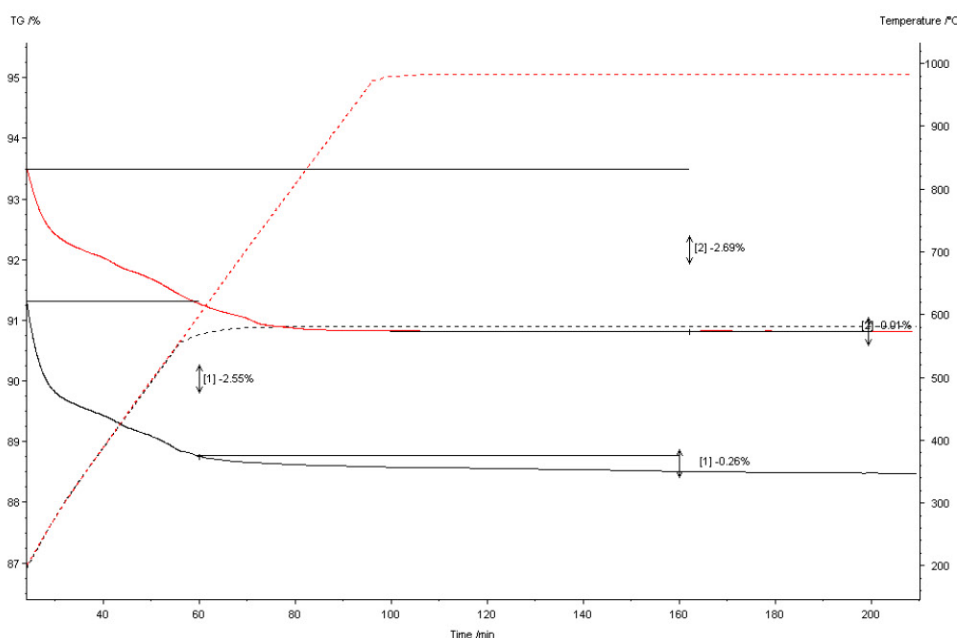


Figure 5.3.9 - TG on set Grancrete in fluent air, up to 600°C (green) and up to 1000°C (red).

At 600°C the three phases present do not react with each other, while at 1000°C

some wollastonite (black, 43-1460) and some KMgPO_4 (50-0151, not reported in figure below) are consumed and new phases are formed: KCaPO_4 (cyan, 33-1002), Magnesium silicate (cyan, 34-0189). The sample were kept dry, otherwise KMgPO_4 would easily rehydrate. According to our observations, this phenomenon can not be avoided even by heating at 60°C , due to the high stability of the hydrated phase.

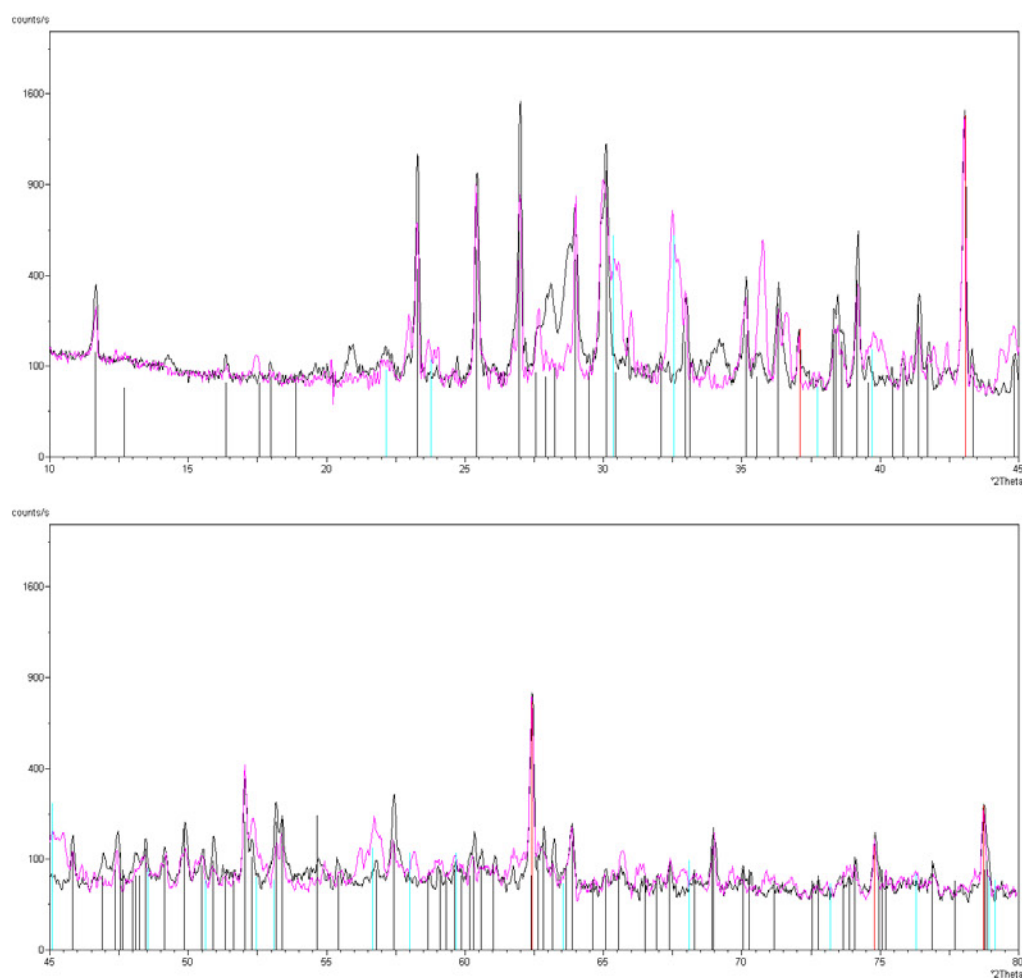


Figure 5.3.10 - XRD on Grancrète calcinated 10 hours at 1000°C (magenta) and at 600°C (black line).

5.3.3 Mechanical and thermomechanical compression tests

The diffractometric study has demonstrated the main phases changes upon heating, and in particular $\text{MgKPO}_4 \cdot 6\text{H}_2\text{O}$ dehydrates. Correspondingly a change in mechanical properties were expected. Another problem is expected from the cracks that water evolution could make upon thermal shock or fast heating.

The compressive tests were performed on a four-column frame, MTS electro-hydraulic testing machine, 1000 kN full range; the machine, managed by a digital controller and PC software TESTSTAR II, is equipped respectively by a 500 kN load cell, a 150 mm stroke piston and an MTS extensometer (25 mm gage length, model 632.41-02). The machine sensors are periodically calibrated by a national recognised external body, achieving a SIT certificate. The compressive tests were performed by moving the Grancrete specimen against the upper plate endowed with a ball joint (figure 5.3.11) at a constant displacement rate of 0,25 mm/s, according to the European Standard UNI EN 12390-3:2003. In figure 5.3.11, a Grancrete specimen mounted on the MTS 500 kN testing machine with extensometer. The oven for high-temperature tests can be seen around the specimen.



Figure 5.3.11 - Compressive test assembly.

The tests were performed on the following two types of specimens:

- type A, without stiffening aggregates
- type B, with stiffening aggregates.

The following summary table 5.3.2 reports, for each specimen, diameter, height, maximum stress (σ_{\max}), Young's modulus (E) and preliminary thermal treatment. In one case E was not measured, due to an instrument malfunction.

Specimen	Diameter [mm]	Height [mm]	σ_{\max} [MPa]	E [GPa]	Thermal treatment
A1	104	202	45	-	No
A2	104	201	41	16	No
B1	103	199	32	11	No
B3	103	200	18	5	dried at 150°C

Table 5.3.2 - Summary table of Grancrrete specimens tested at 25°C.

From table 5.3.2 it can be deduced that even simply drying the compressive strength reduces at room temperature to 50% of the original value. It was also attempted of performing compressive tests at high temperature (600 °C) with an increasing rate temperature of about 8 °C/min, but during the heating, the release of large quantities of water vapour caused a drift in the load-cell signal and a subsequent loose of the machine load-controlling. To avoid further problems with the instrumentation, thermomechanical tests have been stopped.

In figure 5.3.12 are reported the plots of Stress vs. Apparent Strain for Grancrrete specimens A1 and B1 for the compression tests at room temperature. The apparent strain was calculated as the ratio between the piston displacement and the initial height of the specimen. As stated before, the results suggest that set grancrrete-based concrete have mechanical properties slightly superior to conventional concrete, and that upon drying the values are lowered to about 50% of the initial value.

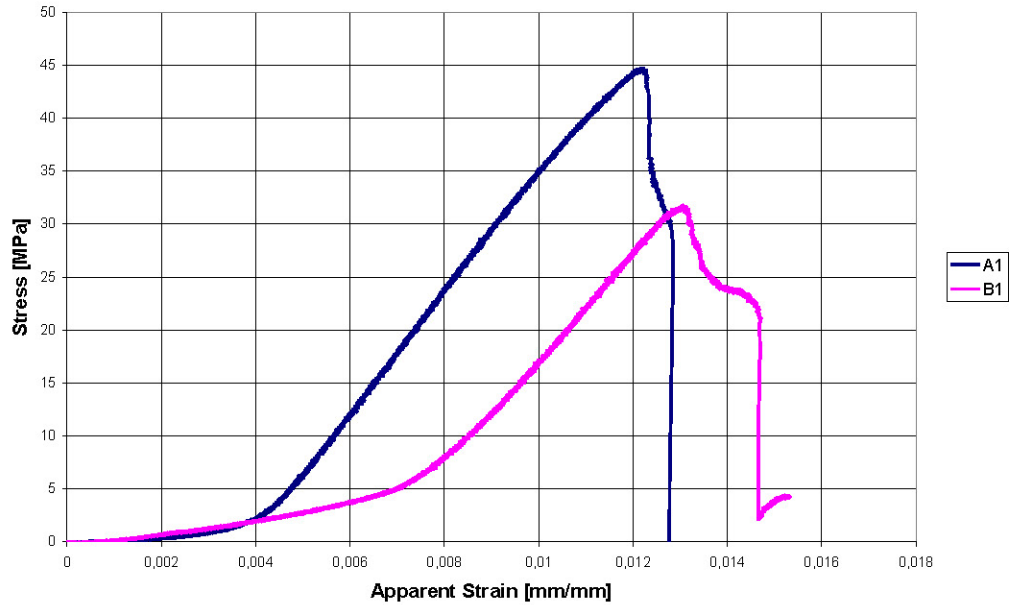


Figure 5.3.12 - Stress vs Apparent Strain: compressive tests at room temperature.

5.3.4 Mechanical bending tests

Flexural strength (σ) and Young modulus (E) measurements were obtained through 4 point bending tests on samples 80x10x2 mm. The measurements were performed on:

- as-set grancrete;
- dried grancrete (in vacuum, at 80°C);
- grancrete after one hour thermal treatment at 500°C (heating ramp rate 100°C/h).

The results are reported in the following tables 5.3.4, 5.3.5 and 5.3.6, and figures 5.3.13, 5.3.14 and 5.3.15, where the stress strain curves on the different samples are reported. Vacuum drying was adopted after it was found that fast drying may involve the sample damage (deformation and, sometimes, cracking). Also slow drying produces a sharp decrease in the Young modulus (from 14.7 to 3.6 GPa) and flexural strength (from 12.1 to 5.6 MPa). Upon fast drying and firing at 500°C, the strength and Young modulus maintain approximatively the same value measured on dried grancrete. The problem with fast drying and firing is deformation and possible cracks formation, so that the bending test was possible only on two of the samples. The rupture type was a strain failure in all cases.

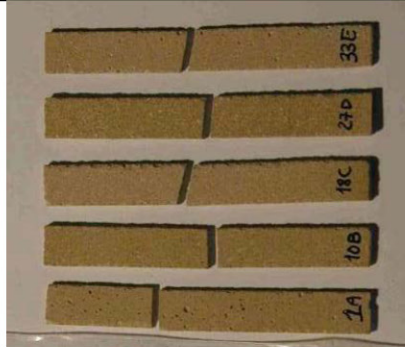
Sample number	F_m	σ	E	
	(N)	(MPa)	(GPa)	
1	11.08	16.28	17.09	
2	10.61	13.14	18.69	
3	9.09	9.23	12.09	
4	10.66	10.05	12.18	
5	9.13	11.56	13.36	
Mean	10.1	12.1	14.7	
Δ		3.5	3.3	

Table 5.3.4 - Flexural strength and Young modulus, at 25°C, of as-set grancrete.

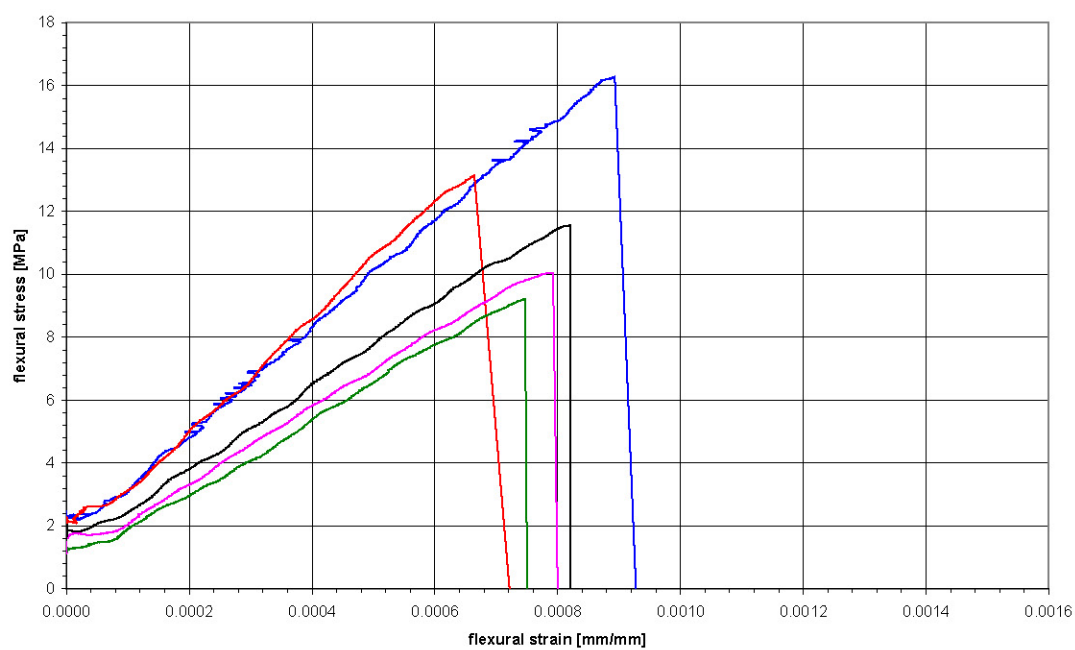


Figure 5.3.13 - Stress strain curves, at 25°C, on as-set grancrete.

Sample number	F_m	σ	E
	(N)	(MPa)	(GPa)
1	4.10	7.26	3.28
2	4.74	7.04	4.87
3	3.51	4.62	2.15
4	3.65	4.82	4.06
5	2.77	4.76	3.43
Mean	3.8	5.7	3.6
Δ		1.3	1.4

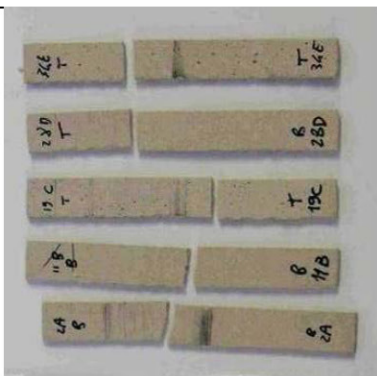


Table 5.3.5 - Flexural strength and Young modulus, at 25°C, of vacuum dried grancrete.

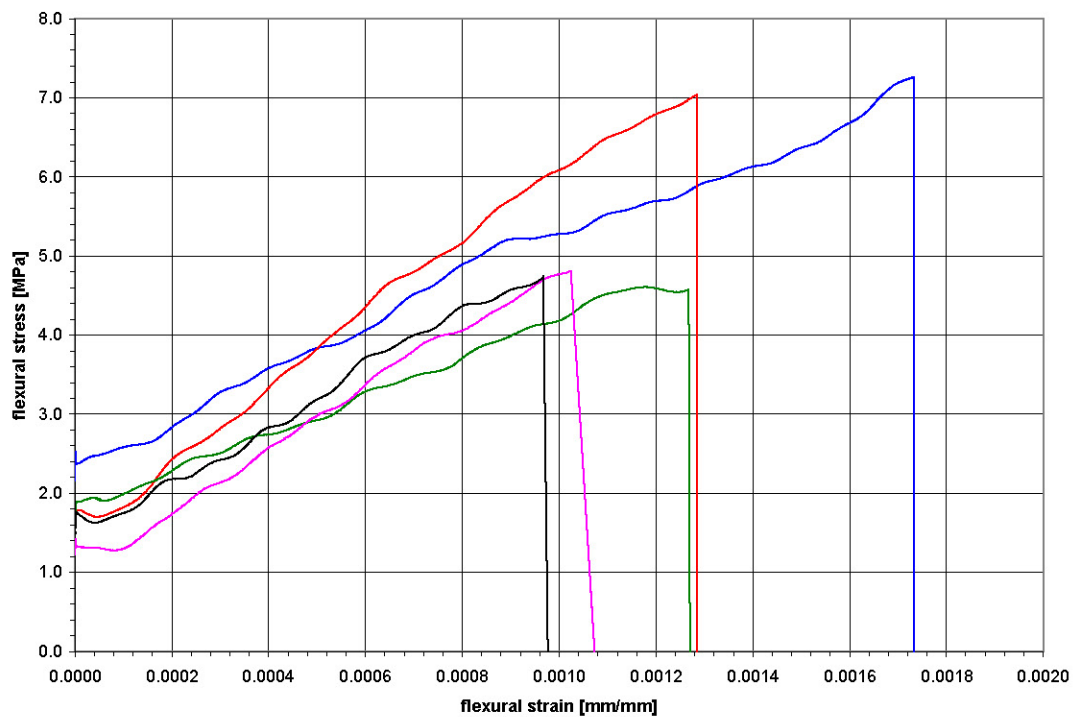


Figure 5.3.14 - Stress strain curves, at 25°C, on as-set grancrete.

Sample number	F_m	σ	E	Status upon firing
	(N)	(MPa)	(GPa)	
1				deformed
2				deformed
3	3.60	4.21	3.89	
4				broken
5	3.72	6.31	4.98	
Mean	3.7	5.3	4.4	
Δ		1.1	0.5	

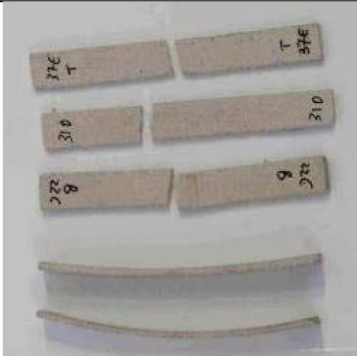


Table 5.3.6 - Flexural strength and Young modulus, at 25°C, of grancrete fired at 500°C.

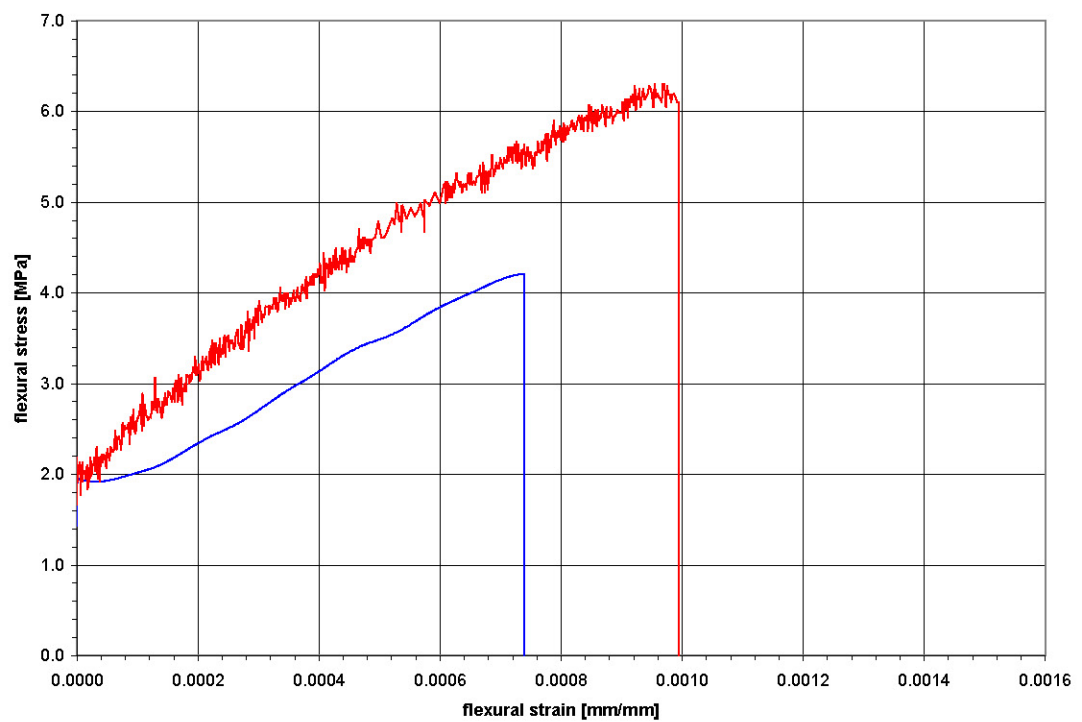


Figure 5.3.15 - Stress strain curves, at 25°C, on grancrete fired at 500°C.

5.3.5 Evaluation of suitable maturation time

For a conventional cement, mechanical properties reach their maximum value in about 40 days. In the case of grancrete, the setting reaction is much faster and a shorter maturation time was expected.

The evaluation was made by measuring the Young modulus with the so called "Impact excitation method" [167] using a Grindo-Sonic System Mk5 (JW Lemmens NV, Belgium). This equipment (figure 5.3.16) makes possible much easier and faster determinations of E than bending tests. It is based on a microphone and a frequency analyzer (the Grindo-sonic) and evaluate the vibrational frequencies produced upon hitting the sample with a suitable "hammer". The results in the case of grancrete are reported in figure 5.3.17, suggesting that the chosen maturation time of 20 days can certainly be considered high enough.

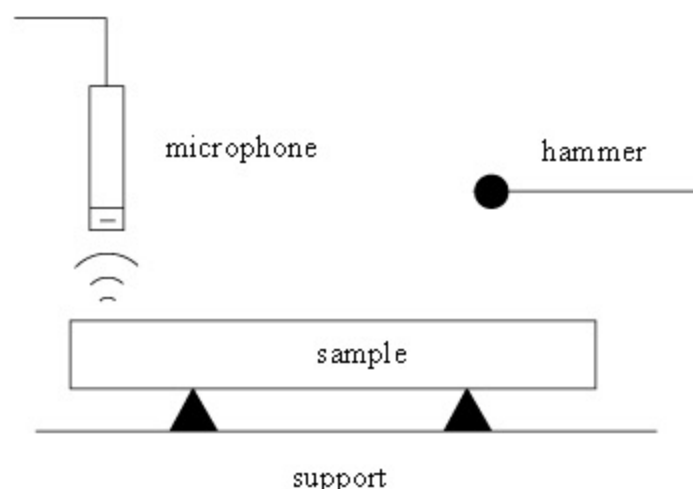


Figure 5.3.16 - Schematic representation of "impact excitation technique".

[167] EN 843-2:2006 Annex A. Impact excitation method applied to disc test pieces.

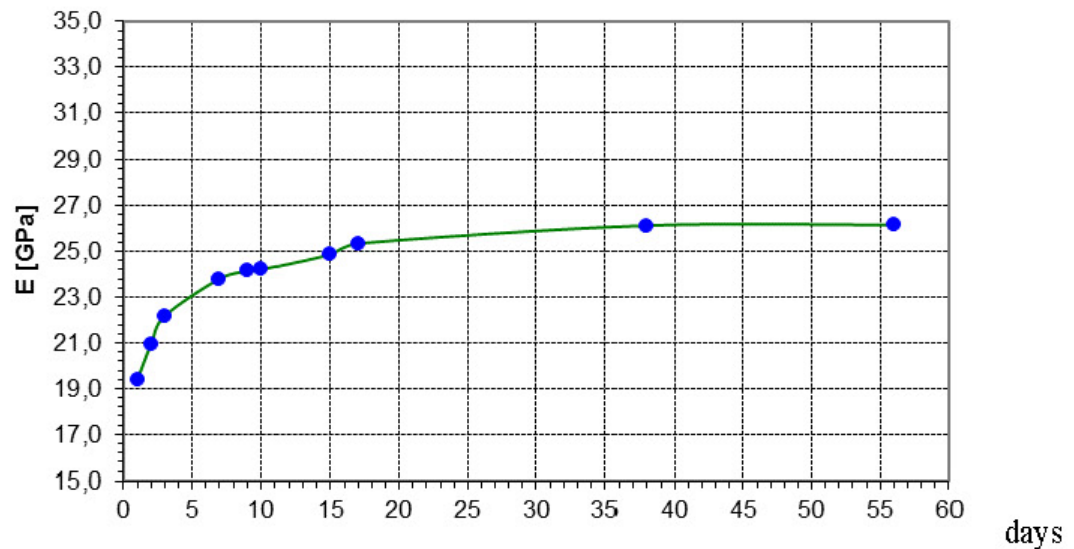


Figure 5.3.17 - Young modulus vs maturation time (days) at 25°C.

5.4 Development of fibre-reinforced phosphate material

The strength of Grancrrete appear far too low to be considered for producing CFCC. Moreover the material cracks easily during drying even at very moderate speed. Anyway some basalt reinforced composites were produced, in order to test the wet lay-up procedure, as it is shown in the following figures 5.4.1 and 5.4.2. As usual standard samples for MOR measurements were then cut (figure 5.4.3).



Figure 5.4.1 - Example of basalt reinforced CBC composite that was produced.

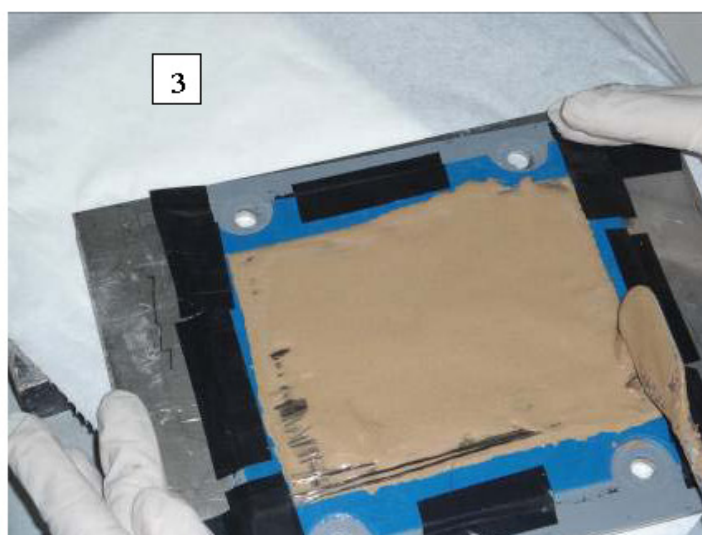
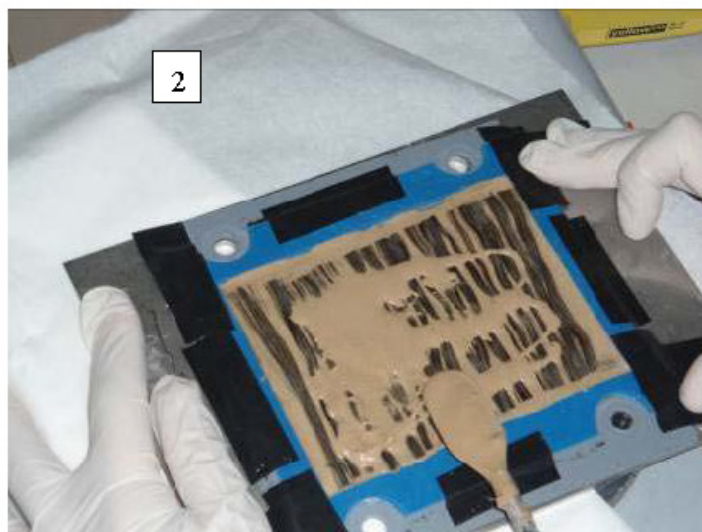
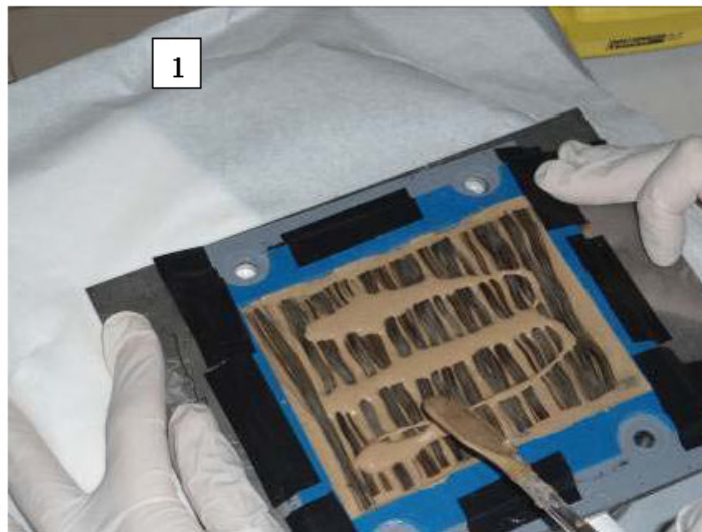


Figure 5.4.2 - Three steps of the wet lay-up procedure for the CBCC composite.

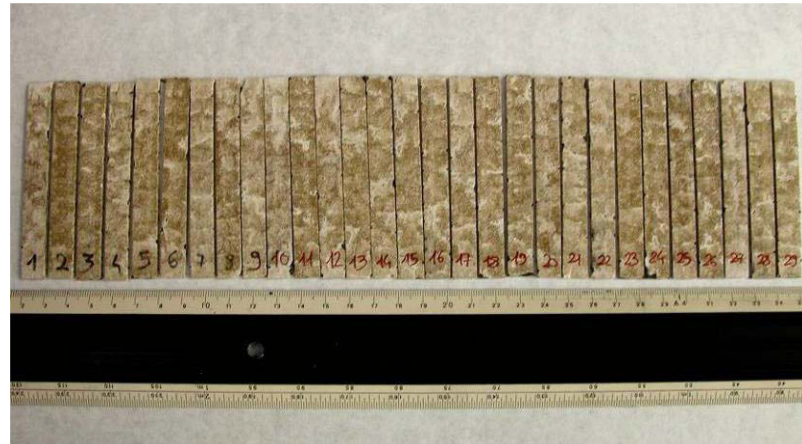


Figure 5.4.3 - Fiber reinforced CBC for MOR measurements.

In the following table some preliminary MOR results are reported, using MAPEI polymer painted basalt fibers. Compared to the data of corresponding unreinforced matrix in the same conditions, the conclusion is that basalt fiber reinforcement is effective in increasing flexural strength. Moreover, the sample don't break, being the fibers effective in bridging the fracture. However, the MOR values, compared to those obtained on basalt reinforced SiCO obtained by PIP are low for practical applications. Moreover, for thermostructural applications, this material would be affected by all the problems linked to the drying (which may cause cracks and bending) and the dynamic moisture equilibrium with the environment. To study these effects, other fiber reinforced material was prepared, using MAPEI basalt fibers after heat treatment, to remove the polymer paint.

Sample	Length (mm)	width (mm)	Thickness (mm)	Weight (g)	Density (g/cm ³)	F max-totale N	σ max MPa
1	85.10	10.63	2.45	3.9519	1.78	20.1	23.6
2	84.74	10.82	2.31	3.7717	1.78	19.9	25.9
3	84.73	10.23	2.37	3.615	1.76	19.3	25.1
4	85.10	10.86	2.24	3.7811	1.83	25.3	34.8

Table 5.4.1 - MOR results on basalt-reinforced grancrete at 25°C (test speed 0.5 mm/min).

In figures 5.4.4a, figure 5.4.5a and figure 5.4.6a are reported the stress-strain curves recorded at room temperature for fiber reinforced grancrete before any treatment, after vacuum drying (60°C, 10⁻³ mbar) and after an heating ramp up to 500°C (100°/h). In the tables 5.4.3, 5.4.4 and 5.4.5 the MOR and E values are

reported, together with the photo of the samples after the measurements. The name of the standard samples were arbitrarily chosen, in order not to influence the measures. All the samples showed pseudoplastic strain failure and, as expect for the samples after heat treatment at 500°C, they did not break into separate pieces (figures 5.4.4b, 5.4.5b and 5.4.6b). As can be noted from figure 5.4.4b, the samples present colour differences, indicating that the "maturation" and drying was not complete when these tests were made, so all measures underestimate the true values. The results are summarized in table 5.4.2 and demonstrate that basalt-reinforced grancrete MOR values decrease upon drying and heat treatment significantly lower than those for grancrete alone. Moreover the difference between dried and heat treated sample is moderate, indicating CTE compatibility between basalt fibers and grancrete matrix. The heat treatment on the basalt fibers lowered the mechanical performances, maybe due to a partial crystallization.

MOR (MPa)	No treatment	Vacuum drying at 60°C	After heating at 500°C, 1h (ramp 100°/h)
Grancrete	12.1	5.7 (-53%)	5.3 (-56%)
Fiber reinforced Grancrete	19.6	15.1 (-23%)	12.1 (-38%)

Table 5.4.2 - MOR results (at 25°C) for grancrete samples after drying and after heat treatment.

The data also demonstrate that vacuum drying at 60°C can be used to avoid cracks formation and bending during drying, however after that the samples easily rehydrate with exposure to environmental humidity, interfering with thermostructural applications. In order to avoid rehydration, some sort of impermeabilization should be done. It was subsequently found that this can be achieved using a ceramic glaze, at 600°C, a temperature which do not change the mineralogical phases of dried grancrete. However the solution of drying, impermeabilization appears far too complicated for industrial application of the process, so maybe the only possible applications that could be found for such a material is in the construction field, were high T exposition may occur only in incidental conditions (like fire) and so a dynamic equilibrium with environmental moisture is acceptable.

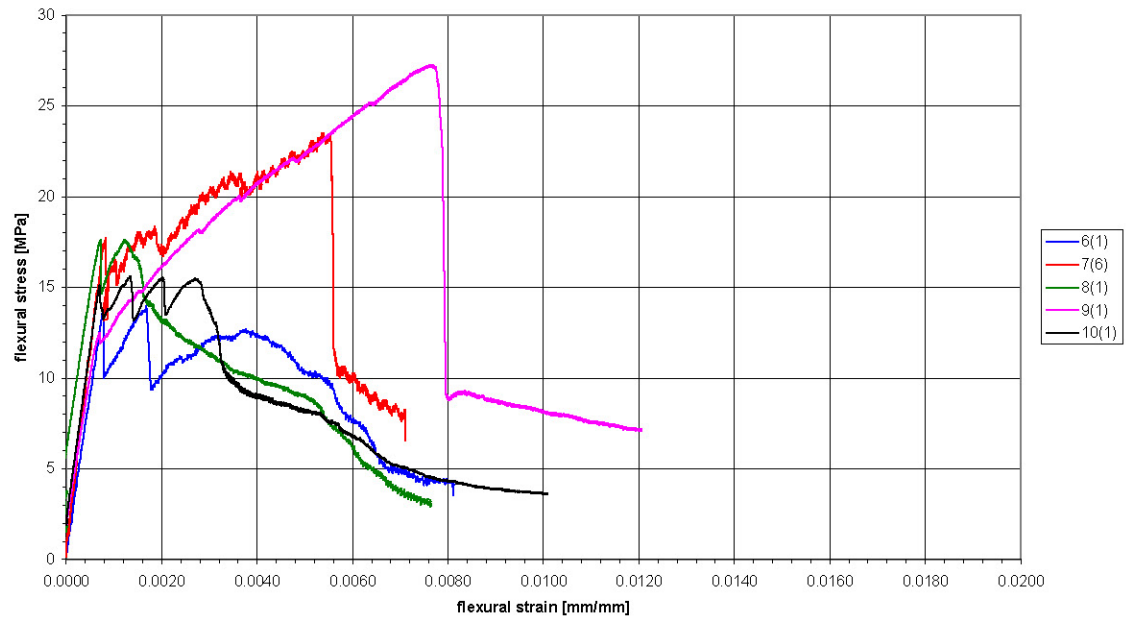


Figure 5.4.4a - Stress strain curves (at 25°C) on basalt-reinforced grancrete.



Figure 5.4.4b - Basalt-reinforced grancrete samples after the bending tests (at 25°C) [168].

Samples	F_m	$\sigma_{f,m}$	E	Failure type and notes
	N	MPa	GPa	
6 (1)	41.0	14.0	17.6	Strain failure-unbroken sample
7 (6)	52.6	23.5	22.0	Strain failure-unbroken sample
8 (1)	67.8	17.6	17.5	Strain failure-unbroken sample
9 (1)	85.8	27.3	16.5	Strain failure-unbroken sample
10 (1)	49.0	15.6	19.0	Strain failure-unbroken sample
Mean value	59.3	19.6	18.5	
Δ		6.7	2.7	

Table 5.4.3 - MOR and E values (at 25°C) on basalt-reinforced grancrete.

[168] The numbers 1 and 6, between brackets identify, the "slab" which was cut to obtain the standard samples.

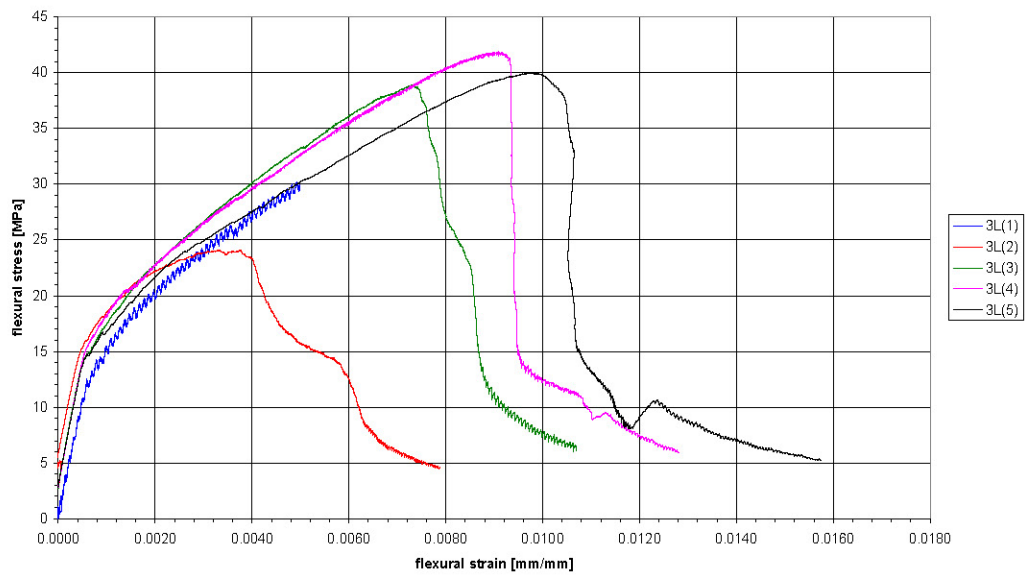


Figure 5.4.5a - Stress strain curves (at 25°C) on basalt-reinforced grancrete after vacuum drying.

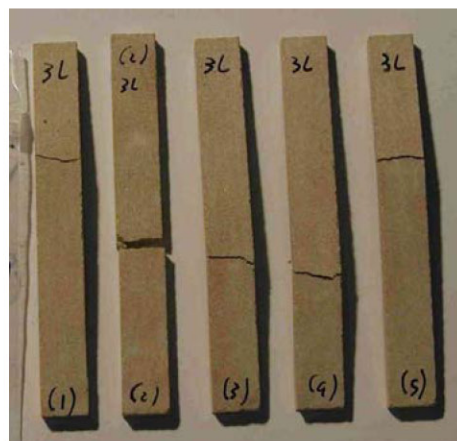


Figure 5.4.5b - Vacuum dried basalt-reinforced grancrete samples after the bending tests (at 25°C)
[169].

Samples	F_m	$\sigma_{f,m}$	E	Failure type and notes
	N	MPa	GPa	
3L(1)	77.5	35.2	20.3	Strain failure-unbroken sample
3L(2)	52.3	24.1	20.7	Strain failure-broken sample
3L(3)	83.7	38.9	22.8	Strain failure-unbroken sample
3L(4)	88.4	41.9	22.9	Strain failure-unbroken sample
3L(5)	84.2	40.0	22.0	Strain failure-unbroken sample
Mean value	77.2	36.0	21.8	
Δ		8.9	1.3	

Table 5.4.4 - MOR and E values (at 25°C) on basalt-reinforced grancrete after vacuum drying.

[169] The name "3L" identifies the "slab" from which the standard samples 1,2,3,4 and 5 were cut.

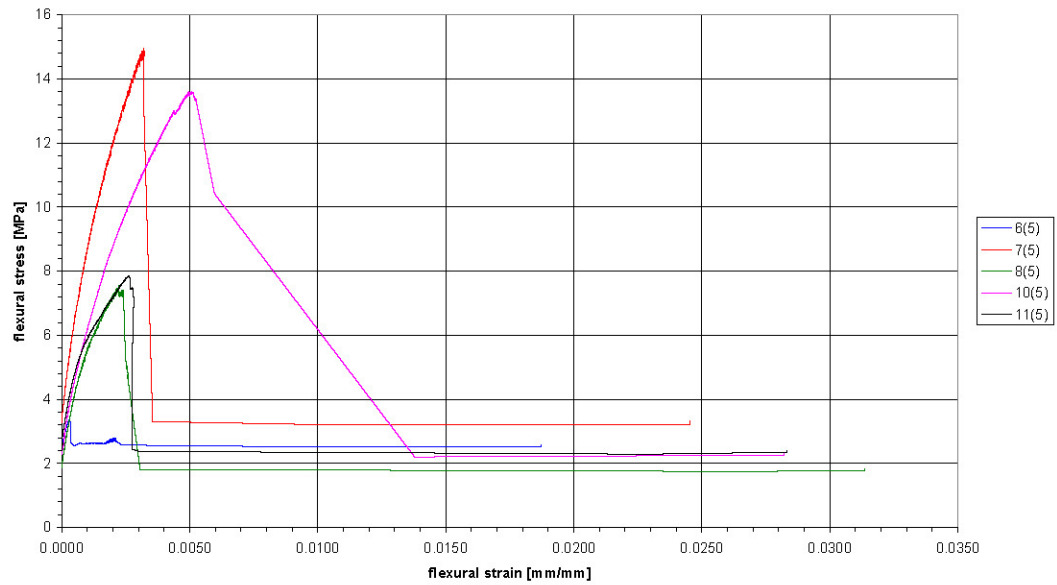


Figure 5.4.6a - Stress strain curves (at 25°C) on basalt-reinforced grancrete after heating at 500°C [170].



Figure 5.4.6b - Heat treated (at 500°C) basalt-reinforced grancrete samples after the bending tests (at 25°C).

Samples	F_m	$\sigma_{f,m}$	E	Failure type and notes
	N	MPa	GPa	
7(5)	27.5	15.0	6.4	Strain failure-broken sample
8(5)	23.6	7.6	4.5	Strain failure-broken sample
10(5)	35.5	13.6	4.2	Strain failure-broken sample
6(5)	8.0	(3.4)	(3.5)	Samples that broke outside the inner span: not considered
11(5)	19.6	(7.9)	(3.9)	
Mean value	28.9	12.1	5.0	
Δ		3.7	1.1	

Table 5.4.5 - MOR and E values (at 25°C) on basalt-reinforced grancrete after heating at 500°C.

[170] The number 5, between brackets, identifies the "slab" which was cut to obtain the standard samples.

Another system which was developed to produce composites were Teflon and plastic moulds, following the principle illustrated below (figure 5.4.7). This system proved to be particularly effective to produce thin samples with no fibers, or short fibers, or to process materials which require a thermal curing treatment. The sample thickness is established by using spacers between the mould parts, while the holes are used to take out air and squeeze out material in excess, while applying a pressure.

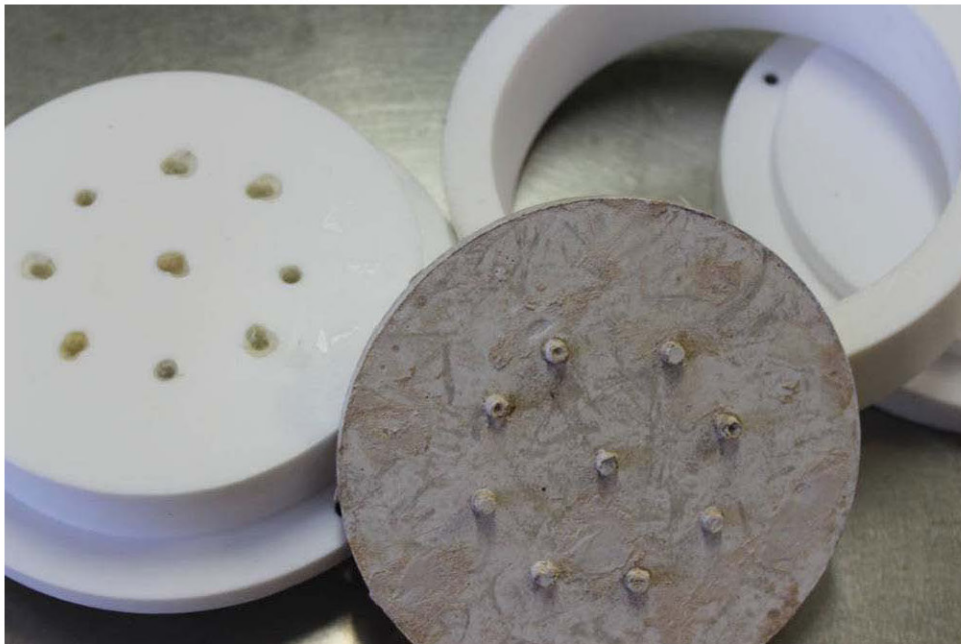


Figure 5.4.7 - Teflon mould used to produce thin CBC samples.

6. CONCLUSIONS

Several CFCC (Continuous Fiber Composite Ceramics) production processes were tested, concluding that PIP (Polymer Impregnation, or Infiltration, Pyrolysis) and CBC (Chemically Bonded Ceramics) based procedures have interesting potential applications in the construction and transportation fields, thanks to low costs to get potentially useful thermomechanical performances.

One of the first activity during the present Doctorate was developing a PIP pilot plant, necessary for the subsequent development of ceramic composites, starting from preceramic polymers and fibers. The combination of fairly original characteristics of the developed pilot plant are that:

- it can work also in vacuum (ensuring up to 4×10^{-1} mbar during the pyrolysis);
- it is made of austenitic steel, AISI 310S.

This kind of furnace is considerably cheaper than the graphite furnaces normally used for PIP and, moreover, it can be periodically cleaned with a heating step in fluent air. These characteristics were specifically chosen to facilitate a rapid technology transfer to an industrial mass production.

Our results indicate that a cleaning cycle in air at 900°C every 3-4 months is enough to keep the furnace fully operational. When not done for over 6 months, the formation of pyrolysis residues over the heating elements may originate a short circuit between them and the AISI internal parts, event which actually happened once, but that was easily solved with an heating cycle in air. This periodic oxidation is important also to preserve the Kanthal[®] SiC based heating elements, with the restoration of a self generating protection coating.

At first the synthesis of new ceramic polymeric precursors was attempted, but it was immediately clear that it would not be possible to produce the polymer quantities needed for the production of composites for a thermomechanical characterization, being the minimum quantity necessary at least 10 kg of preceramic. So it was decided to use only commercial polymeric precursors, choosing the cheapest available, poly-carbosilanes and poly-siloxanes, for producing SiC and SiCO matrixes respectively.

Regarding the combination of fibers and matrixes, several systems were tested and developed by PIP:

- $\text{SiC}_f / \text{SiC}$
- $\text{SiC}_f / \text{SiOC}$
- C_f / SiOC
- $\text{Basalt}_f / \text{SiOC}$

The first solution, $\text{SiC}_f / \text{SiC}$, would actually be too expensive for any application for transports and construction, being a rough estimate of the SiC produced by a polymeric precursor maybe 100 times of the SiC produced by sintering. However, being this solution widely studied for producing CFCCs, it was tested preliminarily, in order to make it possible a comparison with previous data and validate our furnace and our way of operating.

The second solution, $\text{SiC}_f / \text{SiOC}$, may be considered only is rather cheap SiC fabrics could be found. It was tested that it is virtually impossible obtaining good results with electrospun SiC felts, which is the cheapest form of SiC fibers which can be found. The problems found with this solution were that the tested SiC felts were difficult to be manipulated, difficult to be pressed in a preform and also the final mechanical performances at room temperature were low. Even with low specific strength, this is the only possible combination of fiber and matrix we found suitable for a continuous application at 1000°C.

The third solution, C_f / SiOC , produce high densification and high mechanical performances even with one PIP step only, but has two disadvantages:

- the chemical reaction between the matrix and the fiber results in a rigid mechanical behavior;
- thermomechanical performance in air is limited by the oxidation of the carbon fibers, so approximately below 300°C.

Based on the previous considerations, the entire third year was devoted to the third solution only, $\text{basalt}_f / \text{SiOC}$, i.e. the combination of the cheapest fibers and the cheapest preceramic, being poly-siloxanes already mass-produced for different applications. The basalt fiber reinforcement gave interesting thermomechanical performances up to 400-600°C, which is well over any polymeric matrix composite and could be a solution for exhaust pipes and other thermomechanical parts in the transports field. In the construction this solution could be interesting for fire resistant panels, since the material do not produce harmful gases and do not undergoes chemical transformations up to 1200°C. The aim of the experimental work on $\text{Basalt}_f / \text{SiOC}$ was aimed to optimize the process in order

to obtain good thermomechanical properties in the minimum processing time. One of the most original results was found testing vacuum pyrolysis, which could significantly reduce industrial processing costs, and gave only a small reduction of mechanical performance ($< 20\%$) compared to pyrolysis in nitrogen flow. The other processing parameters that were studied were:

- preform characteristics;
- number of PIP steps.

Regarding preform characteristics, several basalt fabric types were compared, unidirectional and coupled unidirectional in particular, finally orientating the tests towards a unidirectional fabric which was the best compromise between cost, fabric stability, fiber characteristics and final mechanical performances. The mechanical characterization was performed on composites produced by putting 8 orthogonal plies of this fabric (which weights 400 g/m^2) in a steel mould fixed with screws. The final composite is about 2.8 mm thick, with a density below 2 g/cm^3 , which are considered acceptable data for application in the automotive field. Regarding the number of PIP steps, the solution with one PIP only appear the best, being the effort in performing the second PIP step, with the considered raw materials, not fully repaid in term of mechanical performances. This also is a pretty remarkable results, being most literature data about PIP related to a number of PIP steps between 6 and 10, which means approximately one month of continuous processing time

Summarizing, among the different processes considered during the Doctorate (from the synthesis of new preceramic polymers, to the PIP of $\text{SiC}_f / \text{SiC}$) the more promising results for high mechanical performances useful for the transports field came from the PIP process with poly-siloxanes on basalt fabrics. Low processing time and costs, together with fairly good thermomechanical properties were demonstrated, even after only one or two PIP steps in nitrogen flow. In alternative, pyrolysis in vacuum was also tested, a procedure still not discussed in literature, but which could originate an interesting reduction of production costs, with only a moderate detrimental effect on the mechanical properties. The resulting CFCC is a $\text{basalt}_f / \text{SiCO}$ composite that can be applied for continuous operation up to 600°C , also in oxidant environment, as TG and XRD demonstrated. The failure upon loading is generally pseudo-plastic, being interlaminar delamination the most probable rupture mechanism. The strength

depends on several different factors (microstructure, polymer curing and subsequent ceramic phase evolution, fiber pull-out, fiber strength, fiber percentage) and can only be optimized empirically. At 400°C a MOR value of about 130 MPa can be obtained, even with an overall production time of only 2 days. Future and further work on basalt_f/ SiCO composites should aim at:

- determining and optimizing tensile strength (also in temperature);
- determining and optimizing fracture toughness;
- fatigue and creep tests;
- testing high performing fibers and fabrics;
- optimizing the stacking and the fiber preform characteristics;
- testing active and passive fillers;
- developing hybrid procedures.

Regarding the first point, in ENEA Faenza laboratories it is being prepared the instrumental apparatus, keeping in mind that tensile strength is non trivial to measure, but also that is the most significant characteristic in order to develop and engineer new applications. Fracture toughness, fatigue and creep tests are more specific and should aim at specific applications. In order to go over the temperature of 400°C, different fibers should be considered, which could be a significant element in determining the final production cost. There are several products potentially interesting, being both SiC, quartz and alumina-based fibers and fabrics suitable solutions for applications in oxidant conditions up to 1000°C, however none of this product are cheap or easy to get, being their use generally limited to the military and aerospace field.

One research activity which can be performed investing less money is optimizing the stacking and fiber preform structure, a study which should be done having chosen the geometry of the component, as the final study before starting with an industrial production.

Active fillers, as already discussed, represent an easy way to improve characteristics, with little or no impact on the production costs, so are particularly interesting for developing new formulations. For example, poly-siloxanes added with titanium and zirconium alcoxides can be used to introduce Ti and Zr in the SiCO matrix, originating a wide range of potential products, with customizable characteristics. Passive fillers may help in reducing matrix volume reduction, potentially contributing to densification and mechanical performances. Their use

is limited by the negative effect they may have on rheological properties of the preceramics, keeping in mind that the starting polymers must infiltrate, in the liquid or solution state, a rather dense fiber preform.

Hybrid procedure generally imply the use of techniques that require the use of other plants (like CVI or a furnace dedicated to Liquid Silicon Infiltration) in combination with the PIP plant. In Faenza there is already a CVI, while a LSI furnace is currently being developed, in order to offer a complete technological capability in the field of thermostructural composites.

In order to be "open minded" in selecting the best technology, during this Doctorate also CBC matrixes were considered, making some preliminary investigations on a fire-resistant phosphate cements. Unfortunately the costs of PyroSic[®] components are far too high for being of any interest for the traditional automotive but targeting the same (or similar) characteristics with significantly cheaper products would certainly find a wide potential market, especially in the constructions field. That could be possible to be achieved with other CBC systems, based on basalt fibers, like apparently also Pyromeral Systems SA, the well-known company which developed PyroSic[®], is working at.

Our results on Grancrete phosphate cement however evidenced some interesting thermomechanical capabilities. In particular the most interesting results are:

- the verified compatibility between the thermal expansion coefficient (CTE) of Grancrete and basalt fibers;
- the phase stability of dried Grancrete up to 600°C;
- flexural strength of about 20 MPa at 25°C, even after thermal treatments.

However the experiments showed also some serious limitations. In particular:

- flexural strength about ten times less PIP basalt composites;
- phase change and possible cracking and deformations on drying at 130°C;
- strength reduction also on slow drying (about minus 20%)
- easy rehydration upon exposure to environmental humidity.

The necessity of a slow drying step and subsequent impermeabilization makes difficult to think the overall process as interesting for the automotive sector, although some applications in the construction and fire protection could be considered, since an heating at 1000°C is possible without creep, and up to 1200°C without production of toxic gases.

In conclusion, in the following table the currently available solution and the still

to be developed solution are compared. In the construction and transports field, there could be a potentially huge market for cheap thermostructural composites which can work up to 1000°C in continuous. In this case PIP and CBC based solution, like those studied in the present Doctorate, are probably the more suitable technologies. For space, aeronautics and energy production, more performing composites are required, and PIP should be considered only in combination with other infiltration techniques, like CVI, and suitable coatings.

Technology Max temperature Applications	POSSIBLE COMPOSITES AND SOLUTIONS TO BE DEVELOPED
CBC infiltration T<1000°C constructions, automotive	Mineral resins (e.g.: Vubonite) on basalt fabric; PyroSic [®] (mineral resin on SiC fabric) To be developed: - cheaper and more performing material solutions; - forming techniques for complex geometries.
PIP with silicones T <1200°C automotive, fire-resistance, anti-ballistic	C _f / SiCO SiC _f / SiCO Basalt _f / SiCO To be developed: - cheaper (e.g. vacuum pyrolysis) and more performing processes; - other cheap preceramic polymers, besides silicones; - forming techniques for complex geometries.
PIP/CVI T 1000-1600°C aerospace, energy demanding productions (power production, gasification plants, etc)	High performing CFCC (e.g.: SiC _f / SiC, C _f / SiC) with Environmental Barrier Coatings (EBC) and/or Thermal Barrier Coatings (TBC) To be developed: - PIP - CVI hybrid processes, exploiting the benefits of both techniques; - oxidation resistant interphases on fibers or oxidation resistant fibers (e.g. SiBCN _f / SiBCN); - self-healing CFCCs; - more performing coatings (both EBC and TBC).

Table 6.1.1 - Conclusions and perspectives of CFCCs.

ABSTRACT

Several CFCC (Continuous Fiber Composite Ceramics) production processes were tested, concluding that PIP (Polymer Impregnation, or Infiltration, Pyrolysis) and CBC (Chemically Bonded Ceramics) based procedures have interesting potential applications in the construction and transportation fields, thanks to low costs to get potentially useful thermomechanical performances.

Among the different processes considered during the Doctorate (from the synthesis of new preceramic polymers, to the PIP production of SiC / SiC composites) the more promising results came from the PIP process with polysiloxanes on basalt fabrics preforms. Low processing time and costs, together with fairly good thermomechanical properties were demonstrated, even after only one or two PIP steps in nitrogen flow. In alternative, pyrolysis in vacuum was also tested, a procedure still not discussed in literature, but which could originate an interesting reduction of production costs, with only a moderate detrimental effect on the mechanical properties. The resulting CFCC is a basalt / SiCO composite that can be applied for continuous operation up to 600°C, also in oxidant environment, as TG and XRD demonstrated. The failure upon loading is generally pseudo-plastic, being interlaminar delamination the most probable rupture mechanism. . The strength depends on several different factors (microstructure, polymer curing and subsequent ceramic phase evolution, fiber pull-out, fiber strength, fiber percentage) and can only be optimized empirically.

In order to be open minded in selecting the best technology, also CBC (Chemically Bonded Ceramics) matrixes were considered during this Doctorate, making some preliminary investigations on fire-resistant phosphate cements. Our results on a commercial product evidenced some interesting thermomechanical capabilities, even after thermal treatments. However the experiments showed also phase change and possible cracking and deformations even on slow drying (at 130°C) and easy rehydration upon exposure to environmental humidity.

DEDICATION

To my nieces Anna, Ilaria and Chiara.

ACKNOWLEDGEMENTS

I wish to sincerely thank Dr. Eng. Sergio Sangiorgi, head of the ENEA UTTMATF unit to which I belong. I'm working on his directions since 1999 and he has always managed to make things go on in ENEA Faenza laboratories, even when everything seemed to work against.

Other acknowledgements are due to the several ENEA colleagues who contributed to the present work, and in particular Luciano Pilloni, who first introduced me to PIP technologies, Federica Burgio, Emiliano Burrelli, Paride Fabbri, Giancarlo Raiteri, Elena Salernitano and Matteo Scafè. Most of all I'd like to thank Alida Brentari, who greatly helped me with the experimental work (she became my right arm, when I broke my own one) and subsequent critical discussion of the results.

Last but not least, sincere thanks to professor Daniele Caretti and professor Daniele Nanni, who were really kind and helpful during all the Doctorate.